Positioning Algorithms for RFID-Based Multi-Sensor Indoor/Outdoor Positioning Techniques

Ming Zhu

Bachelor of Science (Beijing Normal University, China)

Thesis submitted for the fulfilment of the degree of Doctor of Philosophy

School of Mathematical and Geospatial Sciences

RMIT University

GPO Box 2476V

Melbourne, Victoria 3001

Australia

10 Feb 2011

Declaration by the Candidate

This thesis contains no material that has been accepted for the award of any other higher degree or graduate diploma in any tertiary institution. This thesis contains work of mine alone and the best of my knowledge and belief contains no material previously published or written by another person, except where due reference is made in the text. Furthermore, the work presented has been carried out after the official starting date of the program.

Ming Zhu

Acknowledgements

First of all, I would like to thank my supervisors Professor Kefei Zhang and Professor William E. Cartwright for providing guidance and many thoughtful suggestions regarding the content and direction of my research program. I would also like to thank all the staff in the School of Mathematical and Geospatial Sciences and the International Scholarship Office for their help and support throughout my education, you are a credit to the University.

I would like to acknowledge Dr. Falin Wu, Dr. Guenther Retscher and Ms Qing Fu for their constructive inputs with regard to the technical side of this thesis, Mr. Rodney Deakin, Ms Jing Peng and Dr. Suqin Wu for their help in the algorithm developments and Dr. Huqiang Zhang, Dr Sue Choy, Dr. Robert Norman and Mr. Lucas Holden for proofreading the thesis.

To all of my fellow postgraduate students who have made my time in the department so enjoyable, thanks for providing the fantastic memories, especially to Dr. Jianhong Xia, Mr. Bobby Wong, Mr. Erjiang Fu and Ms. Yanxi Zhou.

I would like to offer my sincere thanks to my parents for their encouragement and support throughout my education. Finally, I would like to thank my wife, Xueyan, for her continuous support and encouragement throughout this research project. Your understanding and support has made this possible.

To my grandmother

Table of Contents

List of Figures

List of Tables

List of Acronyms

1-D	One Dimensional
2-D	Two Dimensional
3-D	Three Dimensional
A-GPS	Assisted Global Positioning System
AGRF	Australian Geomagnetic Reference Field
AoA	Angle of Arrival
CoO	Cell of Origin
DCM	Direction Cosine Matrix
DOP	Dilution of Precision
DR	Dead Reckoning
DTG	Dynamically-Tuned Gyroscope
EKF	Extended Kalman Filter
FOG	Fiber-optic Gyroscope
GIS	Geospatial Information System
GNSS	Global Navigation Satellite Systems
GPS	Global Positioning System
HRG	'Hemispherical Resonator' Vibratory Gyroscope
IGRF	International Geomagnetic Reference Field
INS	Inertial Navigation System
KF	Kalman Filter
LBS	Location Based Services
MEMS	Micro-Electro-Mechanical Systems
NMR	Nuclear Magnetic Resonance
PDOP	Position Dilution of Precision
PDR	Personal/Pedestrian Dead Reckoning
RF	Radio Frequency

RFID	Radio Frequency Identification
RLG	Ring Laser Gyroscope
RMSE	Root Mean Square Error
RSPKF	Reduced Sigma Point Kalman Filter
RSS	Received Signal Strength
RTK	Real Time Kinematic
SISP	Site Specific Model
SPKF	Sigma Point Kalman Filter
TDoA	Time Difference of Arrival
ToA	Time of Arrival
UWB	Ultra-wide Band
WiFi	Wireless Local Area Network
ZOI	Zone of Influence

List of Notations

f	Acceleration
G	Antenna gain
h	Antenna height
$\approx$	Approximately equal to
$\bullet^b$	Body frame
$\mathrm{cholupdate}\{\bullet\}$	Cholesky updates
c	Constant
$Cov(\bullet)$	Covariance function
$\underset{\sim}{R}$	Covariance matrix of measurement uncertainty
$\underset{\sim}{Q}$	Covariance matrix of process noise
$\underset{\sim}{P}$	Covariance matrix of state estimation uncertainty
$\phi(\bullet)$	Density function of Gaussian distribution
$\delta(\bullet)$	Difference
DN	Digital outputs
N	Dimension
$\underset{\sim}{C}$	Direction cosine matrix
d	Distance
$\|\bullet\|$	Distance between vectors
$=$	Equal to
$\tilde{\bullet}$	Error
$\hat{\bullet}$	Estimation
$[\phi, \theta, \psi]^T$	Euler angles
$E(\bullet)$	Expectation
$\exp[\bullet]$	Exponential term of a matrix

H	Free space transfer function
g	Gravity
$\equiv$	Identical to
j	Imaginary unit
$[\bullet]^{-1}$	Inverse of matrix
$\underset{\sim}{J}$	Jacobian matrix
$\underset{\sim}{\bar{K}}$	Kalman gain matrix
L	Latitude
l	Length
$\mathrm{qr}\{\bullet\}$	Lower-triangular part resulted from a QR decomposition of the matrix
m	Magnetic vector
$\lvert\bullet\rvert$	Magnitude
$\underset{\sim}{\bullet}$	Matrix
μ	Mean of the observations
$\underset{\sim}{H}$	Measurement sensitivity matrix
v	Measurement uncertainty
z	Measurement vector
$\bullet^{n}$	Navigation frame
ε	Noise
$\bullet^{nom}$	Nominal value
n	Number of step
PL	Path loss
γ	Path loss exponent
p	Position
$\bullet^{+}$	Posteriori estimation

α	Primary scaling factor
$\bullet^{-}$	Priori estimation
$P(\bullet)$	Probability
w	Process noise
ρ	Pseudorange
R	Radius of the Earth
r	Ratio
$\bullet_r$	Receiver
Γ	Reflection coefficient
ζ	Scalar scaling factor
e'	Second eccentricity of ellipse
β	Secondary scaling factor
a	Semi-major axis of ellipse
D	Set of locations
Z	Set of observations
$\mathbf{X}_i^x$	Sigma-point
s	Signal
S	Signal strength / power
$\sigma\times$	Skew symmetric matrix
$\underset{\sim}{\Phi}$	State transition matrix
x	State vector
κ	Tertiary scaling factor
t	Time
D_a	The largest physical linear dimension of the antenna
$[\bullet]^T$	Transpose of matrix
$\bullet_t$	Transmitter

σ^2	Variance
v	Velocity
λ	Wave length
$\underset{\sim}{W}$	Weight matrix
δ	Zero-mean stochastic process of the observations

Abstract

Position information has been very important. People need this information almost everywhere all the time. However, it is a challenging task to provide precise positions indoor/outdoor seamlessly. Outdoor positioning has been widely studied and accurate positions can usually be achieved by well developed GPS techniques. However, these techniques are difficult to be used indoor since GPS signals are too weak to be received. The alternative techniques, such as inertial sensors and radio-based pseudolites, can be used for indoor positioning but have limitations. For example, the inertial sensors suffer from drifting problems caused by the accumulating errors of measured acceleration and velocity and the radio-based techniques are prone to the obstructions and multipath effects of the transmitted signals. It is therefore necessary to develop improved methods for minimising the limitations of the current indoor positioning techniques and providing an adequately precise solution of the indoor positioning and seamless indoor/outdoor positioning.

The main objectives of this research are to investigate and develop algorithms for the low-cost and portable indoor personal positioning system using Radio Frequency Identification (RFID) based multi-sensor techniques, such as integrating with Micro-Electro-Mechanical Systems (MEMS) Inertial Navigation System (INS) and/or GPS. A RFID probabilistic Cell of Origin (CoO) algorithm is developed, which is superior to the conventional CoO positioning algorithm in its positioning accuracy and continuity. Integration algorithms are also developed for RFID-based multi-sensor positioning techniques, which can provide metre-level positioning accuracy for dynamic personal positioning indoors. In addition, indoor/outdoor seamless positioning algorithms are investigated based on the iterated Reduced Sigma Point Kalman Filter (RSPKF) for RFID/MEMS INS/low-cost GPS integrated technique, which can provide metre-level positioning accuracy for personal positioning. 3-D GIS assisted personal positioning algorithms are also developed, including the map matching algorithm based on the probabilistic maps for personal positioning and the Site Specific (SISP) propagation model for efficiently generating the RFID signal strength distributions in location fingerprinting algorithms.

Both static and dynamic indoor positioning experiments have been conducted using the RFID and RFID/MEMS INS integrated techniques. Metre-level positioning accuracy is achieved (e.g. 3.5m in rooms and 1.5m in stairways for static position,

4m for dynamic positioning and 1.7m using the GIS assisted positioning algorithms). Various indoor/outdoor experiments have been conducted using the RFID/MEMS INS/low-cost GPS integrated technique. It indicates that the techniques selected in this study, integrated with the low-cost GPS, can be used to provide continuous indoor/outdoor positions in approximately 4m accuracy with the iterated RSPKF.

The results from the above experiments have demonstrated the improvements of integrating multiple sensors with RFID and utilizing the 3-D GIS data for personal positioning. The algorithms developed can be used in a portable RFID based multi-sensor positioning system to achieve metre-level accuracy in the indoor/outdoor environments. The proposed system has the potential applications, such as tracking miners underground, monitoring athletes, locating first responders, guiding the disabled and providing other general location based services (LBS).

Chapter 1 Introduction

Precise positioning is a challenging task in surveying and mapping, robotic control and personal guidance and tracking. To date, geodetic grade GPS systems such as the *Trimble* R8, can provide centimetre level accuracy in real time over a large area using real-time kinematic (RTK) or network-based RTK techniques. However, the major drawbacks of high accuracy GPS systems are that they are either too expensive, too heavy or too clumsy (e.g. large volume). An essential requirement for GPS positioning is its direct reception of GPS signals, without which proper use in indoor and signal-obstructed areas containing major human activities is not possible.

Some alternative techniques, including Micro-Electro-Mechanical Systems (MEMS), Inertial Navigation System (INS) and the radio frequency identification (RFID) positioning technique have recently become the focus of interest from the positioning community. This is because they satisfy the requirements of personal guidance and indoor tracking applications due to their indoor positioning capability, simple infrastructure, portable device size and relatively low cost (Zhu *et al.*, 2009).

1.1 Applications of Indoor Positioning Techniques

The potential applications of indoor positioning techniques, when using MEMS INS and RFID include:

(a) Tracking miners underground;

(b) Monitoring athletes;

(c) Locating first responders;

(d) Guiding the disabled; and

(e) Providing other general location based services (LBS).

For the mining industry, it is very important to know the positions of the miners underground, in order to prevent them from moving into hazardous environments, as well as rescuing them from dangerous situations should this situation arise. One remarkable attempt to track and visualise miners underground was conducted by RMIT University in cooperation with China University of Mining and Technology (Zhang et al., 2009). A prototype of an intelligent response and rescue system was developed based on the RFID/INS positioning and 3-D visualisation techniques.

Other relevant research of indoor positioning techniques involves a MEMS INS/low-cost GPS-based motion capturing device for assisting with athlete training programmes (Wu *et al.*, 2008; Wu, Zhu *et al.*, 2007) and an RFID/Pedestrian Dead Reckoning (PDR) integration system for locating first responders in hazardous environments (Miller *et al.*, 2006). For general LBS, mobile phone positioning has been recently extensively investigated by, for example, Retscher *et al.* (2005) for positioning in the metropolitan area of Hong Kong and Chen *et al.* (2009) for the Shanghai EXPO 2010 through a 3-D personal navigation system. Besides the numerous potential applications, there are extraordinary challenges for developing and refining indoor positioning techniques.

1.2 Current Challenges in Indoor Positioning

Even though outdoor positioning problems have been generally solved by the application of Global Navigation Satellite Systems (GNSS), there are still a number of challenges in indoor positioning. The main challenges are positioning accuracy, system simplicity, device portability and cost reduction.

1.2.1 Positioning Accuracy

The first challenge for the indoor positioning is accuracy. Most indoor positioning applications require very high accuracy (e.g. metre-level or higher). This is determined by the dimensions of indoor environments. For example, considering the normal width of a corridor which is about 2 to 3m, a positioning system with 10m accuracy is most likely to locate a mobile user in the corridor to wrong adjacent rooms. Most of the stand-alone low-cost indoor positioning techniques do not provide high accuracy. For instance, the MEMS INS, which is less prone to environmental effects, can provide relative accurate positions in a short term (a few seconds) but it drifts quickly (about 100m in 30sec). Other techniques, such as radio frequency based positioning techniques, are highly affected by complex indoor environment layouts.

1.2.2 System Simplicity

The challenge of simplicity includes both infrastructures and algorithms. In indoor positioning, the obstruction from surrounding objects in complex environments is a major problem for signal-based positioning techniques, such as ultrasonic, infrared

and radio frequency positioning techniques. In order to overcome this limitation and cover the positioning area seamlessly, either high transmission power or a large number of transmitters is required. Consequently, the simplicity of the devices and the simplicity of the systems in these instances are not satisfactory.

1.2.3 Device Portability

A major area of indoor positioning applications is personal positioning. The size and weight of the device for mobile users is a critical issue. Unlike vehicle or robot mounted devices, personal positioning devices must be small in size and light in weight. However, small size always requires increased device sophistication. The accuracy and the cost need to be compromised with the device portability, which is a challenge when selecting a technique that can satisfy all the requirements for personal indoor positioning.

1.2.4 Cost Reduction

The last challenge for indoor positioning is cost. Even though there are some techniques that can provide an accurate (centimetre-level or higher) positioning capability, such as Ultra-wide Band (UWB) positioning techniques, the tremendous cost (tens of thousand Australian dollars) is a major challenge for wide-spread uses of the techniques and delivering them into the marketplace.

1.3 Objectives of the Research

The aim of this research is to develop algorithms for RFID-based multi-sensor personal positioning techniques. The algorithms developed considered factors that would compensate for the limitations of low-cost sensors, such as RFID, MEMS INS and low-cost GPS. Metre-level accuracy was sought by applying these algorithms to the test bed for personal positioning applications.

Based on this aim, the following hypothesis was formulated:

Positioning algorithms can be developed to achieve metre-level accuracy indoor/outdoor in low-cost RFID-based multi-sensor personal positioning platforms.

In order to test this hypothesis, the following research objectives were set:

(a) To investigate the techniques which can be used for low-cost personal positioning;

(b) To investigate and develop the algorithms for RFID positioning techniques;

(c) To develop algorithms for RFID-based multi-sensor integrated techniques in order to improve positioning accuracy and reliability;

(d) To investigate the feasibility of applying algorithms developed to RFID-based test platforms for indoor/outdoor seamless positioning applications; and

(e) To provide the means of using geospatial information to improve the positioning accuracy of RFID-based test platforms that are specific to personal positioning applications.

The associated research questions are:

(a) Which techniques can be used in low-cost RFID-based multi-sensor personal positioning platforms?

(b) What are the pros and cons of the existing received signal strength (RSS) based algorithms?

(c) What algorithm/algorithms based on RSS are suitable for RFID positioning techniques?

(d) How can multi-sensor integration compensate for the limitations in RFID-based positioning techniques?

(e) Is it feasible to use the RFID-based multi-sensor personal positioning techniques developed for indoor/outdoor seamless applications? And, what algorithms can be used in these applications?

(f) What are the performance differences when using geospatial information to aid positioning performance in conventional vehicle and personal applications? What can be improved when using geospatial information to aid positioning performance that is specific to personal applications?

(g) Can geospatial information be used to improve other aspects of RFID-based positioning techniques, such as generating a database for location fingerprinting algorithms?

1.4 Contributions of the Research

The specific contributions of this research are:

(a) Intensive reviews and comparisons of current indoor and personal positioning techniques;

(b) Optimal selection and integration of the techniques (e.g. RFID, MEMS INS and low-cost GPS) for a low-cost personal positioning system;

(c) Evaluations of Kalman Filters (KF), such as KF, linearized KF, extended KF and sigma point KF, for data fusion;

(d) Evaluations of RSS based positioning algorithms, including the Cell of Origin (CoO), trilateration and location fingerprinting algorithms;

(e) Evaluations of RFID signal propagation characteristics, such as path loss, directional patterns and multipath effects; and

(f) Development of RFID-based multi-sensor indoor/outdoor positioning algorithms, such as the probabilistic CoO algorithm, the integrated INS/RFID location fingerprinting algorithm, the integrated GPS/RFID/INS seamless positioning algorithm and the probabilistic map based map matching algorithm for personal positioning.

1.5 Overview of the Thesis

This thesis comprises of eight chapters.

The first chapter outlines key research question and provides a brief introduction to the research objectives and a general overview of this thesis.

Chapter 2 describes the current techniques used in indoor and personal positioning and comprehensive comparisons of these techniques are made. A discussion of the feasibility of using an RFID-based multi-sensor technique for personal positioning is also provided, according to reviews and evaluations of current techniques.

Chapter 3 concentrates on the algorithms related to RFID positioning techniques, including KF and RSS-based positioning algorithms (CoO, trilateration and location fingerprinting).

Chapter 4 discusses the key aspects of RFID positioning techniques, such as path loss models, directional patterns of the signal strength and multipath effects. This

chapter also provides evaluations of RSS-based positioning algorithms used for stand-alone RFID positioning techniques.

Chapter 5 concentrates on the improvements to RFID-based positioning techniques using multi-sensor integrated methods, like probabilistic CoO algorithms and INS/RFID location fingerprinting algorithms.

Chapter 6 provides information on the development of the iterated reduced Sigma Point Kalman Filter (SPKF) and its applications for RFID-based multi-sensor seamless positioning techniques.

Chapter 7 discusses the utilization of 3-D indoor Geographical Information Systems (GIS) for the RFID-based positioning techniques, including map matching algorithms for personal positioning and a site specific propagation (SISP) model for RFID location fingerprinting.

Chapter 8 presents results and conclusions from this research, and provides areas that need further investigation in future.

Chapter 2 Indoor Personal Positioning Techniques – an Overview

The demand for providing positional information has grown rapidly. With the advent of geolocation-empowered consumer electronics there is common consensus that the addition of location information has significantly enriched the information provided to the end-users. This has been especially true for indoor and personal applications of electronically-provided position. Tremendous research has been conducted related to developing methods and techniques for these applications. For example, The Olivetti Research Laboratory (Want *et al.*, 1992) developed the *Active Badge* system using the infrared CoO technique for locating staff in a building. Judd (1997) introduced a dead reckoning module for enhancing the tracking capability of personnel when GPS signals are blocked or unavailable. *AT&T* (Harter *et al.*, 1999) produced a centimetre-level accuracy ultrasonic positioning system, *Active Bat*, for indoor applications based on the 'Time of Arrival' (ToA) technique. Krumm *et al.* (2000) used the vision-based positioning technique to locate people. *Arc Second* (2002) produced the *Indoor GPS* system using the 'Angle of Arrival' (AoA) technique by infrared laser beams to achieve a millimetre-level of accuracy. Unlike GNSS, such as GPS, GLONASS and GALILEO that are widely used for outdoor positioning applications, there is no mature technique suitable for the majority of indoor positioning applications to date. This is because of the cost, accuracy required and the harsh indoor environment for implementing positioning techniques.

This chapter will provide a brief review of existing techniques for both indoor and personal positioning. An RFID-based multi-sensor integrated technique for personal positioning is also proposed.

2.1 Review of Indoor Positioning Techniques

Broadly speaking the mainstream techniques used for indoor positioning include (Zhu, Zhang, Wu and Cartwright, 2007):

(a) Assisted GPS (A-GPS) techniques;

(b) Inertial navigation techniques;

(c) Infrared positioning techniques;

(d) Radio-based positioning techniques;

(e) Ultrasonic positioning techniques; and

(f) Vision-based positioning techniques.

All these techniques, developed for indoor or personal positioning applications, have their own pros and cons. The following provides an outline over each of these techniques.

2.1.1 Assisted GPS Techniques

One of the pioneering developments is to calculate positions by processing weak GPS signals indoors using the A-GPS technique implemented in the receivers used. The first receiver using this technique was developed in the late 1990s (Moeglein and Krasner, 1998). This technique uses satellite ephemeris, a priori position and/or a priori time through an alternative communication channel (e.g. cell phone) to enhance the positioning performance. It makes the receiver capable of finding the correct frequency and code-delay in a smaller search space than other receivers without assistance. Consequently, the A-GPS receivers receive and process satellite signals more easily and quickly than the conventional GPS receivers (Diggelen, 2009). It also makes the A-GPS more sensitive to weak GPS signals so that the receivers can be used for indoor positioning using existing GPS infrastructures and conducting indoor/outdoor seamless positioning using a single device for end users.

However, the major limitations of this technique are multipath effects and cross correlation problems in high-sensitive signal processing process. Firstly, due to high sensitivity of GPS signals, A-GPS can not only receive GPS signals from line of sight but also the signals penetrated through and/or reflected from the surrounding environments. These multipath effects can sometimes degrade the positioning accuracy into 100m level or even worse in complex indoor environments (Larson *et al.*, 2008). Secondly, the signal strength from satellites received by A-GPS can be various between -160dBm and -123dBm depending on the complexity of the environments. This large difference in signal strength may lead to a false peak in correlation (a cross-correlation peak rather than an autocorrelation peak) for the satellites with a low signal strength and consequently degrade the positioning accuracy to several kilometres (Misra and Enge, 2006). Accordingly, A-GPS is not

suitable for accurate indoor positioning even though it is relatively low-cost and simple.

2.1.2 Inertial Navigation Techniques

Two well known inertial navigation techniques are INS and Dead Reckoning (DR), where the current position is calculated from a known previous position with inertial measurements, such as velocity and rotation rate in INS or distance and orientation in DR. In the early stages of navigation system's development, DR was widely used due to its simplicity in distance calculation but it was limited by its kinematic accessibility and accuracy for vehicle navigation. Another limitation is that it can only deal with one dimensional rotation and two dimensional translations. In order to achieve high accuracy in a highly kinematic environment, INS was introduced in the end of the 19th Century (see Table 2.1) (King, 1998). However, traditional INS with a high cost and large volumes were impractical for personal positioning. These techniques were introduced into personal positioning only after the development of MEMS when the cost and size of these instruments were dramatically reduced over the past decade. Table 2.1 provides a synopsis of milestones in INS developments.

This newly introduced technology, MEMS, provides sensors with physical dimensions of millimetre-level by using silicon or quartz to build up the mechanical structures (Titterton and Weston, 2004). However, the current limitation of the MEMS INS for personal positioning is its accuracy. The stabilities of the scale factor and bias are normally two and five orders lower than the highly accurate mechanical ones respectively. It always causes rapid and extremely high positioning errors in applications within a short timeframe (e.g. drifting over 100m in 60 seconds).

Some research (Judd, 1997; Mezentsev *et al.*, 2005) indicates that DR can achieve better precision than INS for personal positioning since it represents distance by the product of the number of steps and step length. In this case, the errors are largely related to the estimation of step length rather than the double integration of the acceleration. Consequently, the drifts of estimated position become slow.

In addition, Mezentsev *et al.* (2005) state that these errors in both INS and DR are hard to detect and are even harder to correct without any external corrections. Consequently, most positioning systems developed with these technologies are often coupled with other positioning technologies, such as the infrared technique (Lee and

Mase, 2001), GPS (Retscher and Thienelt, 2004) and RFID (Miller *et al.*, 2006), allowing frequent corrections to be made.

Table 2.1 The milestones of INS developments
(King, 1998; Schmidt, 2009)

Time	Developments	Scale factor stability (ppm)	Bias stability (deg/hr)	Parts
end of the 19th Century	simple gyro-assisted magnetic compasses	N/A	N/A	N/A
early 20th Century	stand-alone gyro compasses	N/A	N/A	N/A
1940s	advanced inertial instrument technology for missile guidance (Germany)	N/A	N/A	N/A
early 1950s	first Schuler-tuned INS by MIT	N/A	N/A	N/A
	development of the floated-rate integration gyro	0.1-10	0.00001-0.01	125
mid-1960s	development of the dynamically-tuned gyro (DTG)	1-over 1000	0.0001-100	70
	research on high-accuracy 'Hemispherical Resonator' vibratory gyro (HRG)	N/A	N/A	N/A
	research on the Ring Laser Gyro (RLG)	0.1-1000	0.0001-10	44
1970s	strapdown systems became practicable	N/A	N/A	N/A
	research on nuclear magnetic resonance (NMR) gyros	N/A	N/A	N/A
	development of fiber-optic gyro (FOG)	0.1-1000	0.0001-10	30
late 1980s	integration with GPS	N/A	N/A	N/A
1990s	development of MEMS gyro	10-over 1000	0.1-10000	3

2.1.3 Infrared Positioning Techniques

The infrared technique, which was first used in indoor positioning in the Olivetti Research Laboratory's *Active Badge* in 1992, has been well advanced since it has a relatively inexpensive unit cost. It also makes the most of these positioning systems easy to be installed in a defined area with adequate placements and density of infrared sensors (Want *et al.*, 1992). According to the transmitting power and the propagation characteristics of conventional infrared signals, the most popular method used in infrared positioning systems is CoO, which can only provide an approximate position within the sensors' detectable area or cell. This method does not usually provide continuous position due to two main reasons. First, the discontinuous coverage of the cells can eliminate the conflict of receiving signals caused by overlapped cells. Secondly, the small cell size is always applied to increase the

precision of the retrieved positions from cells. However, the smaller the cell size, the larger the number of sensors that is needed to cover the entire area. Consequently, the CoO infrared positioning technique is always used as active landmarks, providing accurate positions when particular transmitters are detected (Lee and Mase, 2001; Tenmoku *et al.*, 2003a, 2004, 2003b, 2003c).

Between 2003 and 2004, two different groups of researchers improved the CoO infrared positioning techniques' accuracy and continuity by retrieving the positions from overlapped transmission coverage via different approaches. Hallaway *et al.* (2003) used eight directional receivers placed at 45° in each plane to receive signals from different transmitters simultaneously. Jung and Woo (Jung and Woo, 2004; Jung and Woo, 2005a, 2005b) grouped the transmitters and made them emit signals group-by-group in a high frequency to avoid conflicts. Both approaches obtained continuous positions at metre-level accuracy by analysing a combination of the received signals. These new methods were recognised as zones of influence (ZOI) and are discussed in details in Chapter 3.

The most accurate and continuous infrared positioning technique used so far is *Arc Second Indoor GPS* which increases accuracy by completely changing the transmitted signals. Instead of the conventional omni or directional signals, two fan-shaped rotational infrared laser beams and a strobe light are transmitted to implement the AoA method (Arc Second, 2002). The vertical angle is calculated from the time between receiving two tilted laser beams and the horizontal angle was estimated by the time between the strobe light and laser beams. The experiments show that this technique can achieve 5-arcsecond accuracy within a range of 50m. That is equal to approximately 7 centimetres at the most in linear measurement error (Arc Second, 2004). However, the cost of achieving this accuracy is considerable. In addition, as one of the infrared positioning techniques, the *Arc Second Indoor GPS* still requires line of sight observations and is also affected by sunlight and other sources of infrared radiations (Hightower and Borriello, 2001).

2.1.4 Radio-based Positioning Techniques

Radio-based positioning techniques, such as those employed by cell phones (Trevisani and Vitaletti, 2004), WiFi (Li *et al.*, 2005), Zigbee (Mok and Retscher, 2008) and pseudolites (Barnes *et al.*, 2003), are some of the most commonly used positioning techniques due to their relatively high transmission power and the

requirements of dedicated devices (Christ and Lavigne, 2000). The positioning methods used in radio-based techniques include:

(a) CoO;

(b) AoA;

(c) ToA and time difference of arrival (TDoA);

(d) RSS-based trilateration; and

(e) Location fingerprinting.

2.1.4.1 Cell of Origin

CoO is the method that is usually used in low-cost radio-based techniques. It can neither provide accurate time measurements nor stable and long-range signal strengths. Some pioneer implementations, such as the European *E112* mandate, were applied to cell phone positioning. Trevisani and Vitaletti (2004) evaluated the performances of CoO and claimed that even though the accuracy was not impressive, it (CoO) was still superior, due to its low-cost and simplicity.

2.1.4.2 Angle of Arrival

The directional patterns of RF signals have been also investigated for positioning purposes. Researchers tried to implement this method in cell phone positioning with the directional antennae (Drane *et al.*, 1998; Li, 2006). Kim *et al.* (2004) proposed a method that uses a three-orthogonal-antennae array to measure the relative angles for positioning. They conducted simulations in a defined area (5m×5m) and average centimetre-accuracy was achieved. But in some particular directions errors could be up to 1 metre. Yet no real-world implementations have been done. Li *et al.* (2007) identified that the orientation of mobile users and environmental dynamics can be the major influences on the variation of direction patterns. In addition, multipath effects can also cause the patterns to be unpredictable. All the negative effects make the implementation of positioning based on direction patterns difficult in a real-world situation.

2.1.4.3 Time of Arrival and Time Difference of Arrival

High performance radio-based positioning techniques can use modulated information on carrier frequencies to calculate ToA or TDoA for positioning purposes, such as the case in cell phone positioning (Krasner *et al.*, 2002). Both methods require extremely accurate synchronisations in all base stations in order to achieve accurate time delay for distance measurements. For example, one microsecond in time is equal to hundreds meters in distance due to the fact that signals travel at the speed of light. A later method, the TDoA, is superior to the ToA because it eliminates the mobile users' clock errors by differencing ToA between base stations and mobile users.

Positioning pseudolites - devices that mimic positioning satellites' functionalities - is another radio-based technique that uses ToA or TDoA for positioning. These techniques are more specific to measurement times than cell phones, but are usually more complex and more expensive as well, for example, the systems of *HAPPI* (Ford *et al.*, 1996), *asynchronous pseudolite navigation system* (Yun and Kee, 2002), *LOCATA* (Barnes *et al.*, 2003) and *WASP* (Sathyan *et al.*, 2009). Each of these systems claims sub-meter-level accuracy for indoor positioning. However, the general technical problems for pseudolite systems include system synchronisation, near/far problems and multipath effects which impose further challenges and, apparently, the cost of developing a system also degrades the positioning accuracy in harsh environments.

One superior radio-based positioning technique using TDoA, which is not prone to multipath effects, is UWB. It was originally developed between the 1960s and 1970s for land mine detection and ground penetrating radar and it has been used for communication applications since the late 1990s. Due to its unique characteristics it has also been investigated for positioning applications over recent decades (Bellusci *et al.*, 2009; Opshaug and Enge, 2001; Parikh and Michalson, 2008; Yan and Bellusci, 2009). According to the literature, multipath effects can be minimised using the leading edge detection method in UWB. The idea is that UWB transmits short discrete pulses instead of continuously modulated signals and detects the leading edge of the first returned signal. According to the geometry of paths, this leading edge will not be corrupted, even though the rest of the first returned signals are corrupted by multipath effects (Fontana, 2002). In Opshaug and Enge's simulations (2001), the performance of UWB was proved to be ten times better than using GPS

in the same multipath-affected environments. The limitation of UWB is its extremely wide bandwidth, which is over 500MHz. This makes UWB signals significantly raise the noise levels for other radio systems (Dafesh *et al.*, 2004), such as GPS. This eventually makes UWB hard to be integrated with other positioning techniques. In addition, some extra work is required to avoid signal jams (Chiu and O'Keefe, 2008; MacGougan and Klukas, 2009).

2.1.4.4 RSS-based Trilateration

Where precise distances cannot be measured using ToA or TDoA, the RSS-based trilateration can be used according to the relationship between the signal strength and the distance from the transmitter to the receiver. In general, physical or statistical models are used to estimate distances and then trilateration is used to determine mobile users' positions according to distance and known transmitter coordinates. Details of this method are discussed in Chapter 3. The typical applications of this method include positioning using cell phone (Zhu, 2006) and WiFi (Li B *et al.*, 2008). The key challenge of this method is to accurately model the relationship between the RSS and distance in complex environments.

2.1.4.5 Location Fingerprinting

This method is designed to overcome the difficulties of modelling the relationships between the RSS and distance for RSS-based positioning techniques such as WiFi positioning (Frank *et al.*, 2009; Li *et al.*, 2005; Wayn *et al.*, 2009). Positions are retrieved by matching the real-time collected RSS with the values in previous measured databases. According to the literature (also see Chapter 3), various matching methods have been developed, including deterministic methods and probabilistic methods.

2.1.4.6 Limitations of Radio-Based Positioning Techniques

Radio-based positioning techniques are superior due to their relatively high transmition power and indoor coverage range. These techniques do, however, have limitations. For RSS-based systems, the instability of RSS caused by environment dynamics is one of the main drawbacks. For timing systems that use ToA or TDoA, synchronising different components in the system is a major concern. Usually, highly accurate clocks or networks are engaged to maintain synchronisation and

consequently accurate time measurements. Other problems that occur in the timing systems are near/far problems (Cobb, 1997), weak signal acquisition and multipath effects (Dedes and Dempster, 2005). All of these detrimental effects degrade the positional accuracy, especially in indoor environments. Lehner and Steingaß (2003) identified that by increasing the bandwidth of the spread spectrum multipath effects can be reduced. This idea has been proven to be effective in the developments of UWB positioning techniques. However, the cost of this improvement and the side-effects, such as interference due to the wide band, are tremendous.

2.1.5 Ultrasonic Positioning Techniques

The ultrasound technique used in *AT&T Active Bat* (Harter *et al.*, 1999) and MIT *Cricket* (Priyantha, 2005) which measures ToA through ultrasound pulses, can achieve much higher accuracy with low-cost devices than the systems that use radio frequency signals (Priyantha, 2005). In addition, the ultrasound technique can overcome some drawbacks of the radio-based positioning technologies, such as multipath effects (ibid.).

Active Bat works in a base station mode. This suggests that the positioning information is processed and displayed in the central computer rather than on the user's handset. The central base station sends radio signals to let the user's transmitter emit an ultrasonic pulse which is in turn received by a receiver matrix. The distances between the transmitter (on the user side) and the receiver matrix (in the defined area) are then calculated and the position of the mobile user is determined (Harter *et al.*, 1999). After a distance-measuring pulse has been emitted from a user, the base station waits for reverberations of the pulse to die out before triggering another user to avoid the collision of multiple users' ultrasonic pulses. This time interval is usually up to 20ms, implying that there may be up to 50 time slots per second per base station. In this case, the system cannot provide frequent positioning information to users when the number of users becomes large.

Cricket is superior to *Active Bat*. It works in a handset mode. In this case positions are calculated in the user's handset by measuring the distances between the handset and beacons that periodically transmits RF messages and ultrasonic pulses at the same time. This active-beacon passive-listener architecture has advantages in the areas of system scalability and user privacy protection (Priyantha, 2005).

The advantage of the ultrasonic positioning technique is the ultrasound's relatively slow propagation speed which can increase the measuring accuracy of signal propagating durations and eliminate the multipath effects. It is due to the fact that ultrasound travels at the speed of sound (340.29m/s at sea level). The duration of a wide pulse caused by multipath effects will be no more than a few milliseconds, which is less than 1mm in distance with respect to the speed of sound. Both *Active Bat* and *Cricket* claim centimetre-level accuracy (Harter *et al.*, 1999). However, most of these systems always need to establish a complex infrastructure in a large defined area. In most cases the level of transmitting power of ultrasound is set to a low-level so that a low power consumption and a long life circle can be achieved. This leads to an affective range of a single beacon of only a few metres. To cover a floor level of a building as big as 20×50 m^2, dozens of beacons need to be established. In addition, indoor objects will cast a shadow from the ultrasonic signals emitted by the transmitters and thus degrade accuracy (Harter *et al.*, 1999).

2.1.6 Vision-based Positioning Techniques

There are two categories of vision-based positioning techniques - passive and active. The former uses the multiple fixed imaging sensors to detect and locate mobile users in environments, such as *pFinder* (Wren *et al.*, 1997), *EasyLiving* (Krumm *et al.*, 2000) and *ADVISOR* (Siebel, 2003). In contrast, the active technique uses imaging sensor or sensors mounted on mobile users to identify their locations according to the images of surrounding environments. One example of active technique is the 3-D map matching technique proposed by Olesk and Wang (2009).

Both techniques are based on computer vision algorithms and are not prone to problems like sensor drift errors in the inertial navigation systems and multipath effects in radio-based positioning methods. In addition, the sensors used in these techniques usually have longer effective ranges than that of infrared and ultrasonic positioning techniques. Nevertheless, the following two major drawbacks limit the wide usage of these techniques - reliability and computational complexity. One of the major problems affecting reliability is the need to identify the target object or background objects. Siebel (2003) identified that background instability and the low contrast between the targets and the background could generate challenges in vision-based tracking. For example, in the case of outdoor personal tracking, trees waving in the wind and moving vehicles could make it difficult to separate people

being tracked from a background, since most solutions assume static backgrounds. Another challenging situation is tracking people in a poorly illuminated room. The dark environment will degrade the contrast between the targets and the background and consequently make the extraction of the targets difficult. Even though much research (Siebel, 2003; Wren *et al.*, 1997) has focussed on overcoming these limitations in vision-based tracking and positioning by introducing accurate statistical and physical models into the target extracting areas. The subsequent computational burden associated with complex models limits the use of those accurate methods in real applications.

2.2 Comparisons of Indoor Positioning Techniques

Table 2.2 shows the comparisons of the RFID positioning technique and other popular indoor positioning techniques using MEMS INS, DR, infrared, ultrasound, pseudolite, UWB, WiFi and vision-based techniques.

According to the above comparisons, the radio-based, infrared and ultrasonic positioning techniques generally suffer from similar problems, such as multipath effects, obstructions and interferences. This is due to the fact that they use similar positioning methodologies. Radio-based positioning techniques are superior to the other two techniques due to their high transmission power, leading to a large coverage and high-penetration capabilities (Zhu, Zhang, Wu and Cartwright, 2007). The positioning methods used by various radio-based techniques have also been compared in the literature. Mok *et al.* (2007) in their primary tests indicate that the UWB techniques can achieve decimetre-level accuracy, which is ten times better than the other radio-based ToA techniques, which are prone to multipath effects. However, this improvement results in a tremendous cost burden due to the fact that the state-of-art technologies are used. For low-cost radio-based devices, Li *et al.* (2006) identified that location fingerprinting methods are superior to trilateration methods. This is because it is difficult to establish an accurate model for signal propagation methods due to the complexities and dynamics in the surrounding environments. Gallagher *et al.* (Gallagher, Li *et al.*, 2009; Gallagher, Tan *et al.*, 2009) showed that metre-level accuracy can be obtained indoors in static environments using the WiFi location fingerprinting method, which is suitable for personal positioning applications.

Table 2.2 The comparisons of various indoor positioning techniques

Positioning Methods		Examples	Effective Range	Complexity of Instruments	Positioning Accuracy
Assisted GPS		*Snap Track*	• Global	• Portable device	Hundreds of metres
Inertial navigation techniques		MEMS INS	• Unlimited range	• Portable device	Accuracy degrades with time
		PDR	• Unlimited range	• Portable device	Accuracy degrades in steps
Infrared positioning techniques	CoO	*Active Badge*	• Line of sight	• Few number of transmitters required	Locating people in a room
	ZOI	*UbiTrack*	• Line of sight	• Few number of transmitters required • Specific methods required to avoid conflicts	Metre-level
	AoA	*Indoor GPS*	• Line of sight	• Few number of transmitters required	Millimetre-level
Ultrasonic positioning techniques	ToA	*Active Bat* & *Cricket*	• About 5 metres for a single transmitter • Line of sight	• A large number of devices required	Centimetre-level
Radio-based positioning techniques	CoO	Cell phone	• A few kilometres • Non-line of sight	• Few number of cells required	Hundreds of metres
		Passive RFID	• Less than 5 metres • Discrete cells	• A large number of devices required	Metre-level
	ToA / TDoA	*LOCATA*	• Over 20 metres for a single transmitter indoor • Non-line of sight	• Few number of transmitters required, hard to synchronize the system	Metre-level
		UWB	• Over 20 metres for a single transmitter indoor • Non-line of sight	• Large device • Few number of transmitters required • Hard to synchronize the system	Decimetre-level
	RSS	WiFi	• Over 20 metres for single transmitter indoor • Non-line of sight	• Few number of transmitters required • Existing access points can be used • Require external power supply	Metre-level
		Active RFID	• Over 20 metres for single transmitter indoor • Non-line of sight	• Few number of transmitters required • No external power supply required for tags	Metre-level
Vision-based positioning techniques		*pFinder*	• Line of sight	• Complex algorithms based on computer vision	Sub-metre-level

In contrast, the inertial navigation and vision-based positioning techniques are two unique techniques which are almost unaffected by the signal propagation problems that occur in radio-based, infrared and ultrasonic positioning systems. However, the inertial sensors contain significant drifts. The accumulated errors quickly increase, either with time in INS or with moving steps in DR (Judd, 1997; Mezentsev *et al.*, 2005). Vision based positioning techniques do not have these accumulated errors, but their applications are limited by the complex computer vision algorithms and expensive vision sensors required. In these circumstances, these two techniques, inertial navigation techniques and vision-based positioning techniques are not widely used as stand-alone solutions.

2.3 RFID-Based Multi-sensor Positioning Techniques

As a result of the comparisons, multi-sensor integration was selected for developing a metre-level accuracy personal navigation technique in this research. RFID was used as the fundamental component of this indoor/outdoor personal positioning technique. It was an essential element for providing positions using RSS-based algorithms.

2.3.1 Using RFID for Positioning

The RFID technique was originally designed as a contactless and low energy consumption device to replace conventional smart card systems which were prone to problems of wear and damage by frequent contacts (Finkenzeller, 2003). Previously, the major application of this technique was for transferring object identification to monitoring sensors in logistic industries. Since RFID techniques use a radio frequency (RF) interface to implement the contactless functionality, it provides not only the ability to identify, but also to locate the targeting objects by analysing the signals received. From the literatures (Finkenzeller, 2003; Retscher *et al.*, 2006), typical applications of RFID are listed below.

(a) Security/access control;

(b) Asset management;

(c) Transportation;

(d) Supply chain management;

(e) Point of sale;

(f) Rental item tracking;

(g) Toll collection;

(h) Automobile immobilisers;

(i) Baggage handling;

(j) Animal tracking;

(k) Real time location systems; and

(l) Many other applications.

These applications have already shown the changes of the RFID usages from a stand-alone identification system (its original design) into a system that can be used for tracking and positioning, such as those listed in items (f), (j) and (k) above. The benefits using RFID in indoor/outdoor personal positioning include:

(a) Simplicity (of the system);

(b) Low-cost (of the device);

(c) High portability;

(d) Ease of maintenance (battery free for passive tags and built-in battery for active tags);

(e) Capability of providing both identification and location;

(f) A long effective range (up to 100m for a single transmitter in free space); and

(g) RF signals - which have the capability of penetrating a few obstacles.

Despite of its limitations of one-way communication links and unstable RSS, RFID offers the potential for the provision of personal positioning. This is due to its ever-decreasing cost and size of the device.

2.3.2 Advantages of Integrated Positioning Techniques

In personal positioning research, one of the main topics was the trade-off between the simplicity of the technique used and the accuracy and reliability it can provide. Higher accuracy device is usually more complicated and involved in a higher cost – this is “you get what you pay for” (keynote speech “Beyond GPS”, of the IGNSS 2009 conference). Techniques like RFID, which are low-cost and small in size, cannot

always provide accurate solutions. In contrast, accurate positioning techniques are usually more expensive and more complex.

One emerging solution is to use a hybrid system - integrating multiple sensors to compensate for the limitations in each single technique. In the Pedestrian Navigation Systems in Combined Indoor/Outdoor Environments (NAVIO) research project (Retscher, 2007a, 2007b) an integrated low-cost GPS, DR module, digital compass, biometric pressure sensor and WiFi positioning system was developed for seamless pedestrian positioning applications. Every sensor or sub-system played a unique role in situations where the rest sensors became less reliable. For example, the low-cost GPS was for outdoor horizontal positioning, the biometric pressure sensor was for vertical measurements, the digital compass was for measuring orientations and the WiFi was for indoor positioning. The information collected was fused together by Kalman filtering and metre-level accuracy could be obtained in both indoor and outdoor applications.

In this research, an integrated low-cost GPS and MEMS INS device (Wu, Zhang *et al.*, 2007), *MinimaxX* (see Figure 2.1), was combined with RFID to enhance the accuracy and reliability of the RFID positioning indoors. The proposed roles of sensors in personal positioning systems are listed below (Table 2.3).

Figure 2.1 The front view and back view of minimaxX
(It contains a low-cost GPS, a tri-axis accelerometer, a tri-axis gyroscope and a tri-axis magnetometer. The dimension of the module is approximately 8×5×2 cm)

Table 2.3 Roles of sensors used in the proposed personal positioning system.

	RFID	MEMS INS	Low-cost GPS
indoor	• To provide continuous positions using RSS-based algorithms.	• To provide high sampling rate orientations, velocities and relative positions; and • To provide constraints for RFID solutions.	• N/A.
outdoor	• To provide instant positioning corrections as active landmarks; or • To provide ranging information using RSS-based algorithms	• To provide high sampling rate orientations, velocities and relative positions	• To provide continuous absolute positions.

2.4 Summary

This chapter has presented an overview of and made a comprehensive comparison of typical indoor positioning techniques, including assisted GPS, inertial navigation systems, infrared positioning, radio-based positioning, ultrasound positioning and vision-based positioning. Each of these techniques have their own pros and cons. Inertial sensors are less prone to the effects from surrounding environments, but contain significant drifts. The infrared positioning technique is low-cost but is limited by the accuracy achievable. Radio-based techniques provide a relatively large coverage using a small number of devices, but they have serious multipath effects. Ultrasound positioning technology is superior in cost and is less affected by multipath effects, but restricted by its effective transmission ranges. Vision-based positioning does not need user-mounted mobile devices; however, complex algorithms are required.

This chapter has also shown the need to study the RFID-based multi-sensor techniques for personal positioning due to their unique advantages. The key advantages of using RFID are its powerful RF signals, low-cost and small size. The limitations of its unstable RSS can be compensated by developing algorithms for integrating other sensors, such as MEMS INS.

A general understanding of the positioning algorithms for the RFID-based multi-sensor positioning technique will be provided in the next chapter.

Chapter 3 Positioning Algorithms

Mobile users' positions can be displayed on the screens of personal digital devices or the contrail monitors when an appropriate positioning technique is applied to them. Positioning algorithms are the initial part of the positioning techniques behind the screen, which convert the measurements of positioning device into positions.

The first section of this chapter will provide an overview and evaluations of the algorithms used for state estimation of the system and multi-sensor integration. These algorithms were implemented using different forms of KF in this research. KF, least square adjustment, Extended KF (EKF) and linearised KF are also compared in this section. The RSS-based positioning algorithms, including CoO, RSS-based trilateration and location fingerprinting are introduced in the second part of this chapter and their characteristics are compared.

3.1 Kalman Filter

An initial task in positioning is to estimate the system states, such as positions, velocities and orientations based on noisy observations. One solution is to predict a state and its uncertainty then make corrections according to the observations. This is done to separate the signals from noises based on the theories of least square adjustment, probability and dynamic systems. This is a recursive system and its solution to the discrete linear filtering problem was developed by and hence named after R.E. Kalman (1960). This technique is now widely used in the areas of automation and navigations in its original form and further developed forms (e.g. EKF or SPKF) (Grewal and Andrews, 2001).

The core components of KF are two mathematical models, the dynamic model and the measurement model. The dynamic model describes the changes of the estimated states in a stochastic process and the later one represents the relationship between the states and the measurements. In general, the dynamic model and the measurement model are listed as Equation (3.1) and (3.2) respectively.

$$x_k = f_{k-1}(x_{k-1}) + w_{k-1},\ w_k \sim N(0, \underset{\sim}{Q}_k) \qquad (3.1)$$

$$z_k = h_k(x_k) + v_k,\ v_k \sim N(0, \underset{\sim}{R}_k) \qquad (3.2)$$

where,

x_k is the state vector at epoch k;

w_k is the zero-mean white Gaussian process noise with process noise covariance $\underset{\sim}{Q}_k$ at epoch k;

$f_k(\bullet)$ is the state transition function at epoch k;

z_k is the measurement vector at epoch k;

v_k is the zero-mean white Gaussian measurement uncertainty with measurement uncertainty covariance $\underset{\sim}{R}_k$ at epoch k; and

$h_k(\bullet)$ is the measurement function at epoch k.

In a linear system, the dynamic model and measurement model can be written as:

$$x_k = \underset{\sim}{\Phi}_{k-1} \cdot x_{k-1} + w_{k-1},\ w_k \sim N(0, \underset{\sim}{Q}_k) \qquad (3.3)$$

$$z_k = \underset{\sim}{H}_k \cdot x_k + v_k,\ v_k \sim N(0, \underset{\sim}{R}_k) \qquad (3.4)$$

Where the state transition function and measurement function are replaced by the state transition matrix $\underset{\sim}{\Phi}_k$, and measurement sensitivity matrix $\underset{\sim}{H}_k$, respectively.

The goal of KF is to obtain an optimal linear estimate based on the observation, z_k (see Equation (3.5)) as follows (Grewal and Andrews, 2001).

$$\hat{x}_k^+ = \underset{\sim}{K}_k^1 \cdot \hat{x}_k^- + \underset{\sim}{\overline{K}}_k \cdot z_k \qquad (3.5)$$

where,

$\hat{x}_k^+$ and $\hat{x}_k^-$ are the posterior and priori estimates of the state vector, x_k, respectively;

$\underset{\sim}{K}_k^1$ and $\underset{\sim}{\overline{K}}_k$ are the weights of $\hat{x}_k^-$ and the observation, z_k, respectively.

This estimate should satisfy the orthogonality condition that the products of the estimation error, $x_k - \hat{x}_k^+$, and measurement vector z_i, $i = 1, \ldots, k$ are zero-mean (see Equation (3.6)).

$$E[(x_k - \hat{x}_k^+) \cdot z_i^T] = 0,\ i = 1, \ldots, k \qquad (3.6)$$

Eventually, it yields that:

$$\underset{\sim}{K}_k^1 = \underset{\sim}{I} - \underset{\sim}{\bar{K}}_k \cdot \underset{\sim}{H}_k \qquad (3.7)$$

The coefficient, $\underset{\sim}{\bar{K}}_k$, specifically, is called Kalman gain.

Accordingly, KF can be implemented via two steps: the measurement update; and the time update, with a set of five equations (Welch and Bishop, 2006) (see Equations (3.8) - (3.12)).

The measurement update equations are:

$$\underset{\sim}{\bar{K}}_k = \underset{\sim}{P}_k^- \cdot \underset{\sim}{H}_k^T \cdot [\underset{\sim}{H}_k \cdot \underset{\sim}{P}_k^- \cdot \underset{\sim}{H}_k^T + \underset{\sim}{R}_k]^{-1} \qquad (3.8)$$

$$\hat{x}_k^+ = \hat{x}_k^- + \underset{\sim}{\bar{K}}_k \cdot [z_k - \underset{\sim}{H}_k \cdot \hat{x}_k^-] \qquad (3.9)$$

$$\underset{\sim}{P}_k^+ = [\underset{\sim}{I} - \underset{\sim}{\bar{K}}_k \cdot \underset{\sim}{H}_k] \cdot \underset{\sim}{P}_k^- \qquad (3.10)$$

The time update equations are defined as:

$$\hat{x}_k^- = \underset{\sim}{\Phi}_{k-1} \cdot \hat{x}_{k-1}^+ \qquad (3.11)$$

$$\underset{\sim}{P}_k^- = \underset{\sim}{\Phi}_{k-1} \cdot \underset{\sim}{P}_{k-1}^+ \cdot \underset{\sim}{\Phi}_{k-1}^T + \underset{\sim}{Q}_{k-1} \qquad (3.12)$$

where,

$\underset{\sim}{P}_k$ is defined as the error covariance matrix of the state vector x_k (see Equation (3.13)).

$$\underset{\sim}{P}_k \equiv E(\tilde{x}_k \cdot \tilde{x}_k^T) \qquad (3.13)$$

$$\tilde{x}_k \equiv x_k - \hat{x}_k \qquad (3.14)$$

3.1.1 Comparisons of KF and Least Square Adjustment

As well as KF, Least Square adjustment is a conventional and widely used technique for state estimation. It was first described by Gauss in 1794. The idea is to find the optimal estimation $\hat{x}$ to minimise the sum of the squared residuals, $\sum_{i=1}^{k} (z_i - \hat{z}_i)^2$ (Ghilani and Wolf, 2006). Consequently, the solution comes out as Equation (3.15).

$$\hat{x} = (\underset{\sim}{H}^T \cdot \underset{\sim}{H})^{-1} \cdot \underset{\sim}{H}^T \cdot \underset{\sim}{Z} \qquad (3.15)$$

where,

z_i is the measurement;

$z_i - \hat{z}_i$ is the residual;

$\underset{\sim}{Z}$ is a set of measurements, z_i; and

$\underset{\sim}{H}$ is the measurement sensitivity matrix.

Sorenson (1970) proved that the KF is equivalent to the least square adjustment when the state is constant and there is no error in the dynamic model. The following derivations describe this statement in detail and show the relationship between KF and the weighted least square adjustment in the case of the constant state.

In the KF, substituting Equation (3.8) into Equation (3.9) yields:

$$\hat{x}_k^+ = \hat{x}_k^- + [\underset{\sim}{P}_k^- \cdot \underset{\sim}{H}_k^T \cdot [\underset{\sim}{H}_k \cdot \underset{\sim}{P}_k^- \cdot \underset{\sim}{H}_k^T + \underset{\sim}{R}]^{-1}] \cdot [z_k - \underset{\sim}{H}_k \cdot \hat{x}_k^-] \tag{3.16}$$

Multiplying $\underset{\sim}{H}_k$ on both sides of Equation (3.16) and rearranging it gives:

$$\underset{\sim}{H}_k \cdot \hat{x}_k^+ = [\underset{\sim}{R} \cdot [\underset{\sim}{H}_k \cdot \underset{\sim}{P}_k^- \cdot \underset{\sim}{H}_k^T + \underset{\sim}{R}]^{-1}] \cdot [\underset{\sim}{H}_k \cdot \hat{x}_k^-] + [\underset{\sim}{H}_k \cdot \underset{\sim}{P}_k^- \cdot \underset{\sim}{H}_k^T \cdot [\underset{\sim}{H}_k \cdot \underset{\sim}{P}_k^- \cdot \underset{\sim}{H}_k^T + \underset{\sim}{R}]^{-1}] \cdot z_k \tag{3.17}$$

Defining $\underset{\sim}{W}_{1,k}$ and $\underset{\sim}{W}_{2,k}$ as coefficients of the terms $[\underset{\sim}{H}_k \cdot \hat{x}_k^-]$ and z_k respectively gives:

$$\underset{\sim}{W}_{1,k} \equiv \underset{\sim}{R} \cdot [\underset{\sim}{H}_k \cdot \underset{\sim}{P}_k^- \cdot \underset{\sim}{H}_k^T + \underset{\sim}{R}]^{-1} \tag{3.18}$$

$$\underset{\sim}{W}_{2,k} \equiv \underset{\sim}{H}_k \cdot \underset{\sim}{P}_k^- \cdot \underset{\sim}{H}_k^T \cdot [\underset{\sim}{H}_k \cdot \underset{\sim}{P}_k^- \cdot \underset{\sim}{H}_k^T + \underset{\sim}{R}]^{-1} \tag{3.19}$$

where,

$$\underset{\sim}{W}_{1,k} + \underset{\sim}{W}_{2,k} = \underset{\sim}{I} \tag{3.20}$$

Substituting Equations (3.18) and (3.19) into Equation (3.17) yields:

$$\underset{\sim}{H}_k \cdot \hat{x}_k^+ = \underset{\sim}{W}_{1,k} \cdot [\underset{\sim}{H}_k \cdot \hat{x}_k^-] + \underset{\sim}{W}_{2,k} \cdot z_k \tag{3.21}$$

Substituting Equation (3.11) into Equation (3.21) yields:

$$\underset{\sim}{H}_k \cdot \hat{x}_k^+ = \underset{\sim}{W}_{1,k} \cdot [\underset{\sim}{H}_k \cdot \underset{\sim}{\Phi}_{k-1} \cdot \hat{x}_{k-1}^+] + \underset{\sim}{W}_{2,k} \cdot z_k \tag{3.22}$$

Substituting Equation (3.21) into Equation (3.22) yields:

$$\underset{\sim}{H}_k \cdot \hat{x}_k^+ = \underset{\sim}{W}_{1,k} \cdot [\underset{\sim}{H}_k \cdot \underset{\sim}{\Phi}_{k-1} \cdot (\underset{\sim}{H}_{k-1}^T \cdot \underset{\sim}{H}_{k-1})^{-1} \cdot \underset{\sim}{H}_{k-1}^T \cdot [\underset{\sim}{W}_{1,k-1} \cdot [\underset{\sim}{H}_{k-1} \cdot \hat{x}_{k-1}^-] + \underset{\sim}{W}_{2,k-1} \cdot z_{k-1}]] + \underset{\sim}{W}_{2,k} \cdot z_k \tag{3.23}$$

Rearranging Equation (3.23) yields:

$$\begin{aligned} \underset{\sim}{H}_k \cdot \hat{x}_k^+ = & \underset{\sim}{W}_{1,k} \cdot \underset{\sim}{H}_k \cdot \underset{\sim}{\Phi}_{k-1} \cdot (\underset{\sim}{H}_{k-1}^T \cdot \underset{\sim}{H}_{k-1})^{-1} \cdot \underset{\sim}{H}_{k-1}^T \cdot [\underset{\sim}{W}_{1,k-1} \cdot \underset{\sim}{H}_{k-1} \cdot \hat{x}_{k-1}^-] \\ & + \underset{\sim}{W}_{1,k} \cdot \underset{\sim}{H}_k \cdot \underset{\sim}{\Phi}_{k-1} \cdot (\underset{\sim}{H}_{k-1}^T \cdot \underset{\sim}{H}_{k-1})^{-1} \cdot \underset{\sim}{H}_{k-1}^T \cdot \underset{\sim}{W}_{2,k-1} \cdot z_{k-1} + \underset{\sim}{W}_{2,k} \cdot z_k \end{aligned} \tag{3.24}$$

Substituting Equations (3.11) and (3.21) into Equation (3.24) and rearranging yields:

$$\begin{aligned} \underset{\sim}{H}_k \cdot \hat{x}_k^+ = & [\underset{\sim}{W}_{1,k} \cdot \underset{\sim}{H}_k \cdot \underset{\sim}{\Phi}_{k-1} \cdot (\underset{\sim}{H}_{k-1}^T \cdot \underset{\sim}{H}_{k-1})^{-1} \cdot \underset{\sim}{H}_{k-1}^T] \cdots [\underset{\sim}{W}_{1,2} \cdot \underset{\sim}{H}_2 \cdot \underset{\sim}{\Phi}_1 \cdot (\underset{\sim}{H}_1^T \cdot \underset{\sim}{H}_1)^{-1} \cdot \underset{\sim}{H}_1^T \cdot] \cdot \underset{\sim}{W}_{1,1} \cdot [H_1 \cdot \underset{\sim}{\Phi}_0 \cdot \hat{x}_0] \\ & + [\underset{\sim}{W}_{1,k} \cdot \underset{\sim}{H}_k \cdot \underset{\sim}{\Phi}_{k-1} \cdot (\underset{\sim}{H}_{k-1}^T \cdot \underset{\sim}{H}_{k-1})^{-1} \cdot \underset{\sim}{H}_{k-1}^T] \cdots [\underset{\sim}{W}_{1,2} \cdot \underset{\sim}{H}_2 \cdot \underset{\sim}{\Phi}_1 \cdot (\underset{\sim}{H}_1^T \cdot \underset{\sim}{H}_1)^{-1} \cdot \underset{\sim}{H}_1^T] \cdot \underset{\sim}{W}_{2,1} \cdot z_1 \\ & + [\underset{\sim}{W}_{1,k} \cdot \underset{\sim}{H}_k \cdot \underset{\sim}{\Phi}_{k-1} \cdot (\underset{\sim}{H}_{k-1}^T \cdot \underset{\sim}{H}_{k-1})^{-1} \cdot \underset{\sim}{H}_{k-1}^T] \cdots [\underset{\sim}{W}_{1,3} \cdot \underset{\sim}{H}_3 \cdot \underset{\sim}{\Phi}_2 \cdot (\underset{\sim}{H}_2^T \cdot \underset{\sim}{H}_2)^{-1} \cdot \underset{\sim}{H}_2^T] \cdot \underset{\sim}{W}_{2,2} \cdot z_2 \\ & + \cdots \\ & + [\underset{\sim}{W}_{1,k} \cdot \underset{\sim}{H}_k \cdot \underset{\sim}{\Phi}_{k-1} \cdot (\underset{\sim}{H}_{k-1}^T \cdot \underset{\sim}{H}_{k-1})^{-1} \cdot \underset{\sim}{H}_{k-1}^T] \cdot \underset{\sim}{W}_{2,k-1} \cdot z_{k-1} \\ & + \underset{\sim}{W}_{2,k} \cdot z_k \end{aligned} \tag{3.25}$$

Rearranging Equation (3.25) yields:

$$\begin{aligned} \underset{\sim}{H}_k \cdot \hat{x}_k^+ = & (\prod_{i=1}^{k-1} [\underset{\sim}{W}_{1,k-i+1} \cdot \underset{\sim}{H}_{k-i+1} \cdot \underset{\sim}{\Phi}_{k-i} \cdot (\underset{\sim}{H}_{k-i}^T \cdot \underset{\sim}{H}_{k-i})^{-1} \cdot \underset{\sim}{H}_{k-i}^T]) \cdot \underset{\sim}{W}_{1,1} \cdot [\underset{\sim}{H}_1 \cdot \underset{\sim}{\Phi}_0 \cdot \hat{x}_0] \\ & + \sum_{j=1}^{k-1} ((\prod_{i=1}^{k-j} [\underset{\sim}{W}_{1,k-i+1} \cdot \underset{\sim}{H}_{k-i+1} \cdot \underset{\sim}{\Phi}_{k-i} \cdot (\underset{\sim}{H}_{k-i}^T \cdot \underset{\sim}{H}_{k-i})^{-1} \cdot \underset{\sim}{H}_{k-i}^T]) \cdot \underset{\sim}{W}_{2,j} \cdot z_j) \\ & + \underset{\sim}{W}_{2,k} \cdot z_k \end{aligned} \tag{3.26}$$

where,

$\hat{x}_0$ is the vector of the initial state;

$\underset{\sim}{\Phi}_0$ is the state transition matrix for the initial state;

the first term refers to the initial state;

the last term refers to the last measurement; and

the terms in between are the rest of the measurements.

Given the condition of the state, vector x is a constant, the state transition matrices become identity matrices and the measurement sensitive matrices at every epoch become constants (see Equations (3.27) and (3.28)).

$$\underset{\sim}{\Phi}_i = \underset{\sim}{I}, \; i = 0,1,\ldots,k \tag{3.27}$$

$$\underset{\sim}{H}_i = \underset{\sim}{H}, \; i = 1,\ldots,k \tag{3.28}$$

Consequently,

$$\underset{\sim}{H}_{k-i+1} \cdot (\underset{\sim}{H}_{k-i}^T \cdot \underset{\sim}{H}_{k-i})^{-1} \cdot \underset{\sim}{H}_{k-i}^T = \underset{\sim}{I} \tag{3.29}$$

Equation (3.26) can be written as:

$$\begin{aligned} \underset{\sim}{H} \cdot \hat{x}_k^+ = & (\prod_{i=1}^{k} \underset{\sim}{W}_{1,k}) \cdot [\underset{\sim}{H} \cdot \hat{x}_0] \\ & + \sum_{j=1}^{k-1} ((\prod_{i=1}^{k-j} [\underset{\sim}{W}_{1,k-i+1}) \cdot \underset{\sim}{W}_{2,j} \cdot z_j) \\ & + \underset{\sim}{W}_{2,k} \cdot z_k \end{aligned} \tag{3.30}$$

Defining $\underset{\sim}{Z}$ as a vector of measurements as well as the term for the initial state on the right side of Equation (3.30) and $\underset{\sim}{W}$ as the coefficients of each term (see Equation (3.31) and (3.32)), we have

$$\underset{\sim}{W} \equiv \begin{bmatrix} \prod_{i=1}^{k} \underset{\sim}{W}_{1,k} \\ (\prod_{i=1}^{k-1} [\underset{\sim}{W}_{1,k-i+1}) \cdot \underset{\sim}{W}_{2,1} \\ \vdots \\ (\prod_{i=1}^{1} [\underset{\sim}{W}_{1,k-i+1}) \cdot \underset{\sim}{W}_{2,k-1} \\ \underset{\sim}{W}_{2,k} \end{bmatrix} \tag{3.31}$$

$$\underset{\sim}{Z} \equiv \begin{bmatrix} \underset{\sim}{H} \cdot \hat{x}_0 \\ z_1 \\ \vdots \\ z_k \end{bmatrix} \tag{3.32}$$

Equation (3.30) can be written as:

$$\underset{\sim}{H} \cdot \hat{x}_k^+ = \underset{\sim}{W}^T \cdot \underset{\sim}{Z} \tag{3.33}$$

Its solution is:

$$\hat{x}_k^+ = (\underset{\sim}{H}^T \cdot \underset{\sim}{H})^{-1} \cdot \underset{\sim}{H}^T \cdot (\underset{\sim}{W}^T \cdot \underset{\sim}{Z}) \tag{3.34}$$

This solution is similar to the solution of a least square adjustment except that the observations are weighted by the matrix $\underset{\sim}{W}$. Experiments are designed to validate this outcome.

In the experiments, a KF was defined to calibrate the accelerometers in INS. According to the calibration, a linear relationship was established between the accelerometer's digital outputs and the accelerations measured in $m \cdot s^{-2}$ (see Equation (3.35)). The vertical component of the gravity was used as a reference in this calibration. The KF was used to determine the scale factors and offsets in this

relationship in real time. 1000 samples were taken, half of which were aligned with the direction of the gravity and the other half were aligned with the opposite direction of the gravity.

$$DN = \alpha \cdot f + \beta \tag{3.35}$$

where,

DN is the accelerometer's digital output;

f is the acceleration in $m \cdot s^{-2}$;

α is a scale factor; and

β is an offset.

The state vector of KF is:

$$x = \begin{bmatrix} \alpha \\ \beta \end{bmatrix} \tag{3.36}$$

The observation vector is:

$$z = [DN] \tag{3.37}$$

The dynamic model of KF is:

$$x_k = x_{k-1} + w_{k-1}, \; w_k \sim N(0, \underset{\sim}{Q}_k) \tag{3.38}$$

$$\underset{\sim}{Q}_k = \begin{bmatrix} \sigma_\alpha^2 & 0 \\ 0 & \sigma_\beta^2 \end{bmatrix} \tag{3.39}$$

where,

σ_α^2 and σ_β^2 are the variances of the scale factor and the offset respectively, both are in the order of 10^{-4}.

The measurement model is:

$$z_k = f_k^{REF} \cdot \alpha + \beta + v_k, \; v_k \sim N(0, \underset{\sim}{R}_k) \tag{3.40}$$

$$\underset{\sim}{R}_k = \left[\sigma_{DN}^2 \right] \tag{3.41}$$

where,

f_k^{REF} is the reference acceleration at epoch k; and

σ_{DN}^2 is the variance of accelerometer's outputs in the order of 10^{-1}.

$$f_k^{REF} = \begin{cases} g_z & (k \le k_0) \\ -g_z & (k > k_0) \end{cases} \tag{3.42}$$

where,

g_z is the vertical component of the gravity; and

k_0 is the epoch at which the accelerometer changes from aligning with positive gravity to aligning with negative gravity.

Figure 3.1 shows the weights on the observations changed with respect to time in KF.

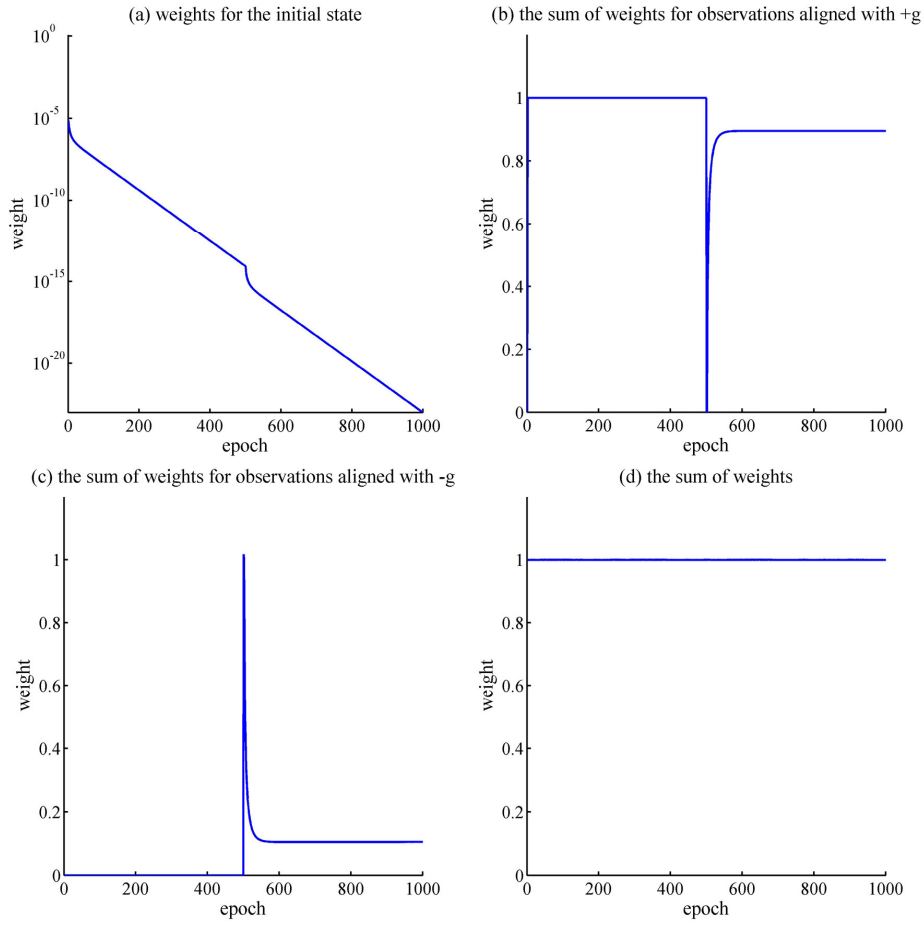

Figure 3.1 Weights of the observations in KF and the sum of the weights ((a) The weight of the initial state falls rapidly to the level of 10^{-5} within a few epochs; (b) The sum of weights for observations aligned with +g which converges to a new level when the observations aligned with –g are included; (c) The sum of weights for observations aligned with –g; (d) The sum of weights for all the terms in KF equals to one constantly.)

The weight of the initial state drops quickly to the order of 10^{-5} and can be ignored with the increase of the number of observations (see Figure 3.1 (a)). This means that the initial values of KF provide very subtle effects on the results. Figure 3.1 (b) and (c) presents the changes of weights for the observations aligned with the direction of the gravity and aligned with the opposite direction of the gravity respectively. The plots show that the weights are redistributed when the new statues are included and the values of the weights are converged to a new level quickly. According to the Equations (3.18) and (3.19), the values of the newly converged weights are controlled by the covariance matrices, $\underset{\sim}{Q}$ and $\underset{\sim}{R}$. Figure 3.1 (d) indicates that the summary of the weights equals to one constantly. That is to say the weights of the observations, $\underset{\sim}{W}$, are normalized all the time. The parameters were also estimated by the unweighted least square adjustment based on the following function.

$$\hat{x} = (\underset{\sim}{H}^T \cdot \underset{\sim}{H})^{-1} \cdot \underset{\sim}{H}^T \cdot \underset{\sim}{Z} \qquad (3.43)$$

where,

$$\underset{\sim}{H} = \begin{bmatrix} g & 1 \\ \vdots & \vdots \\ g & 1 \\ -g & 1 \\ \vdots & \vdots \\ -g & 1 \end{bmatrix}; \text{ and}$$

$\underset{\sim}{Z}$ is a set of observations.

Figure 3.2 shows the comparison of the results from KF and unweighted least square adjustment. The results from the least square adjustment are very close to those estimated by KF and all fall into the 95% confidence intervals. Accordingly, the result from KF can be similar to the result from the unweighted least square adjustment and can be identical if the same normalised weights are applied to the observations. It indicates that it is feasible to use KF to estimate the constant state in real time.

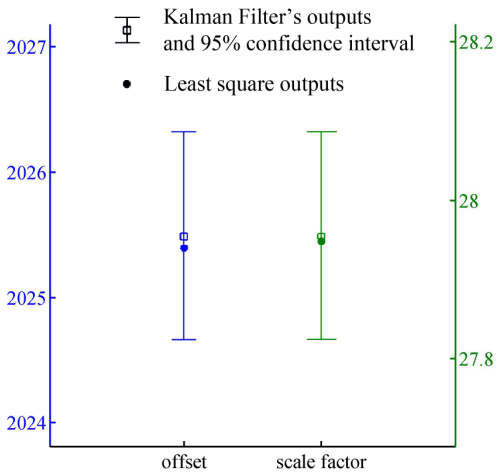

Figure 3.2 The estimated values of the offset and scale factor via KF and least square adjustment respectively
(The error bars show the 95% confidence interval of the outputs from KF according to the error covariance matrix of state vector. All the outputs from least square adjustment (dots) fall into the 95% confidence intervals and they are very close to the outputs from KF (squares).)

One benefit of using KF rather than using least square adjustment in practice is to save computational memories. The KF updates the estimated state only based on the current observations, the Kalman gain and the covariance matrices in real time. In contrast, the least square adjustment estimates the state based on all the observations at once in the post process. Furthermore, the anomalies in KF can be detected in real time since those observations with significant errors will cause the redistribution of the weights and apparently the variance of the estimated states. The operator can determine whether to wait for more good observations or redo the experiment immediately. However, the anomalies will not be detected in the data acquisition stage by using least square adjustment and, sometimes, it will required to repeat the experiments and the data again in order to achieve optimal results.

3.1.2 Comparison of Linearised KF and Extended KF

Many navigation problems are non-linear. Although KF was designed for linear problems, there are two simple approaches to adapt KF for non-linear problems, the linearised KF and the EKF. This section will present a comparison of using linearised

KF and EKF for personal positioning applications. Other complex solutions, such as SPKF, will be discussed in Chapter 6.

In the linearised KF, a nominal state vector, x^{nom}, is used to generate the linearised perturbed dynamic model (see Equation (3.46)) (Grewal and Andrews, 2001).

$$x_k^{nom} = f_{k-1}(x_{k-1}^{nom}) \tag{3.44}$$

$$\delta x \equiv x - x^{nom} \tag{3.45}$$

$$\delta x_k \approx \left.\frac{\partial f_{k-1}}{\partial x}\right|_{x=x_{k-1}^{nom}} \cdot \delta x_{k-1} + w_{k-1}\,,\ w_k \sim N(0, \underset{\sim}{Q}_k) \tag{3.46}$$

where,

δx is defined as the perturbation from the nominal state vector, x^{nom}; and

$\left.\frac{\partial f_{k-1}}{\partial x}\right|_{x=x_{k-1}^{nom}}$ is the Jacobian matrix of partial derivative of the non-linear dynamic model $f(\bullet)$ with respect to the state vector x at the nominal state x^{nom}.

Consequently, the time update and measurement update functions of the linearised KF becomes:

$$\delta \hat{x}_k^- = \underset{\sim}{\Phi}_{k-1} \cdot \delta \hat{x}_{k-1}^+ \tag{3.47}$$

$$\underset{\sim}{\Phi}_k \approx \left.\frac{\partial f_k}{\partial x}\right|_{x=x_k^{nom}} \tag{3.48}$$

$$\delta \hat{x}_k^+ = \delta \hat{x}_k^- + \underset{\sim}{\overline{K}}_k \cdot [z_k - h_k(x_k^{nom}) - \underset{\sim}{H}_k \cdot \hat{x}_k^-] \tag{3.49}$$

$$\underset{\sim}{H}_k \approx \left.\frac{\partial h_k}{\partial x}\right|_{x=x_k^{nom}} \tag{3.50}$$

The state transition matrix, $\underset{\sim}{\Phi}$, and the measurement sensitivity matrix, $\underset{\sim}{H}$, are all replaced by the Jacobian matrix of partial derivatives of the non-linear models with respect to the state vector at the nominal state.

Schmidt (1970) introduced another approach, the EKF, formally called Kalman-Schmidt filter. Instead of using perturbation theory in linearised KF, EKF directly evaluates the partial derivatives at the estimated values of the state variables (see Equations (3.51) - (3.54)).

$$\hat{x}_k^- = f_{k-1}(\hat{x}_{k-1}^+) \tag{3.51}$$

$$\underset{\sim}{\Phi}_k \approx \left.\frac{\partial f_k}{\partial x}\right|_{x=\hat{x}_k^-} \tag{3.52}$$

$$\hat{x}_k^+ = \hat{x}_k^- + \underset{\sim}{\overline{K}}_k \cdot [z_k - \hat{z}_k] \tag{3.53}$$

$$\underset{\sim}{H}_k \approx \left.\frac{\partial h_k}{\partial x}\right|_{x=\hat{x}_k^-} \tag{3.54}$$

where,

$$\hat{z}_k = h_k(\hat{x}_k^-) \tag{3.55}$$

Grewal and Andrews (2001) describe the pros and cons of using a linearised KF and EKF. They state that the EKF is superior to a linearised KF in solving non-linear problems. It is because that the EKF only applies linear approximation over the ranges of state space. In contrast, a linearised KF uses linear approximations over both the range of trajectory perturbations and state estimation errors. Therefore, it always contains larger nonlinear approximation errors than using EKF but the trade-off is the computational efficiency. In a linearised KF, the computations of measurement sensitivities, state transition matrices and Kalman gains respected to nominal states can be precomputed. This feature can reduce a large amount of computational load dealing with big datasets.

Simulations of using two RTK GPS receivers to estimate pedestrian orientations outdoors were designed and a comparison between a linearised KF and EKF was conducted by these simulations (see Figure 3.3). The basic idea is to use RTK GPS receivers to obtain centimetre-level positions of the pedestrian's right and left shoulders then the orientations can be calculated based on the pedestrian's shoulders' positions at the same time. Whereas the problem is that two RTK GPS receivers work individually and do not provide simultaneous positions. Normally, there is a time gap less than one second between the two adjacent outputs from two receivers so KFs for non-linear problems are engaged in fusing the asynchronous data.

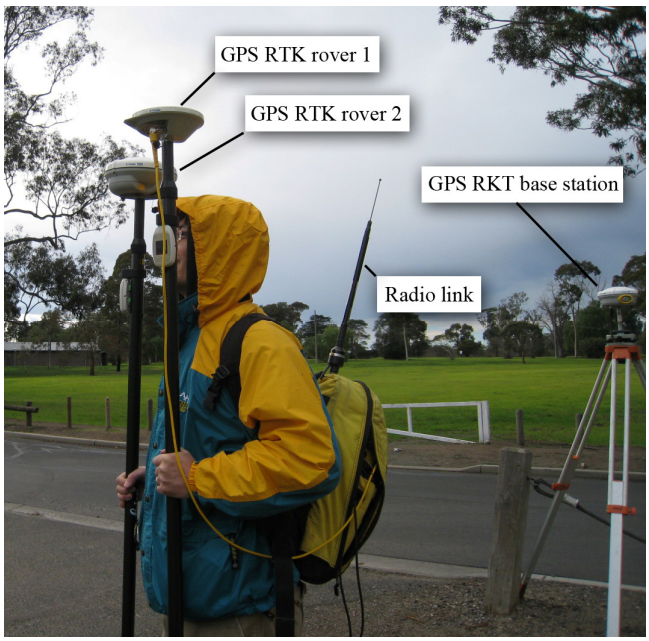

Figure 3.3 Experiments of estimating pedestrian's orientations using two RTK GPS receivers

(Two RTK GPS receivers are used to evaluate the performances of the linearised KF and EKF and also the feasibility of using high accuracy GPS to estimate pedestrian's orientations. Two receivers are mounted on the right-hand-side and left-hand-side of the pedestrian respectively.)

The state vector is:

$$x = \begin{bmatrix} p_x \\ p_y \\ |v| \\ \psi \\ l^L \\ l^R \end{bmatrix} \tag{3.56}$$

where,

p_x and p_y are the horizontal coordinates of the pedestrian in x and y axes respectively;

$|v|$ is the speed of the pedestrian;

ψ is the orientation of the pedestrian; and

l^L and l^R are the widths of the left shoulder and right shoulder of the pedestrian respectively.

The observation vector is:

$$z = \begin{bmatrix} p_x^L \\ p_y^L \\ p_x^R \\ p_y^R \end{bmatrix} \tag{3.57}$$

where,

p_x^L and p_y^L are the x and y coordinates measured by the left RTK GPS; and

p_x^R and p_y^R are the x and y coordinates measured by the right RTK GPS.

It is assumed that the speed and orientation of the pedestrian do not frequently change so the dynamic models are:

$$p_{x,k} = p_{x,k-1} + |v_{k-1}| \cdot \Delta t \cdot \sin(\psi_{k-1}) + w_{px} \tag{3.58}$$

$$p_{y,k} = p_{y,k-1} + |v_{k-1}| \cdot \Delta t \cdot \cos(\psi_{k-1}) + w_{py} \tag{3.59}$$

$$|v_k| = |v_{k-1}| + w_{|v|} \tag{3.60}$$

$$\psi_k = \psi_{k-1} + w_\psi \tag{3.61}$$

$$l_k^L = l_{k-1}^L + w_{l^L} \tag{3.62}$$

$$l_k^R = l_{k-1}^R + w_{l^R} \tag{3.63}$$

where,

Δt is the time interval between two adjacent observations; and

$w_\bullet$ is the zero-mean white Gaussian process noise with respect to each state variable.

The measurement models are:

$$p_x^L = p_x + l^L \cdot \sin(\psi - \frac{\pi}{2}) + v_{p_x^L} \tag{3.64}$$

$$p_y^L = p_y + l^L \cdot \cos(\psi - \frac{\pi}{2}) + v_{p_y^L} \tag{3.65}$$

$$p_x^R = p_x + l^R \cdot \sin(\psi + \frac{\pi}{2}) + v_{p_x^R} \tag{3.66}$$

$$p_y^R = p_y + l^R \cdot \cos(\psi + \frac{\pi}{2}) + v_{p_y^R} \qquad (3.67)$$

where,

$v_{\bullet}$ is the zero-mean white Gaussian process noise with respect to each state variable.

Figure 3.4 shows the simulated pathway and the pedestrian's orientation. The pedestrian walked towards the north about 60m in one minute. Then two slight turns were made, one 15˚ clockwise turn start from 10s and one 15˚ counter clockwise turn start from 30s, and one relatively sharp turn of 30˚ clockwise, start from 45s. The standard deviations in the orders of 10^{-1} ˚ and 10^{-2} m/s respectively were set to the orientation and walking speed of the pedestrian in the simulation.

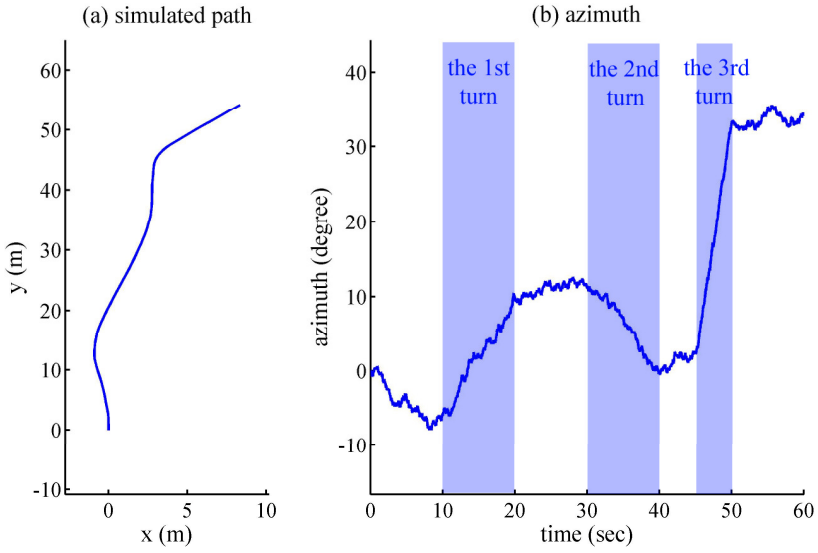

Figure 3.4 The simulated path of the pedestrian and his/her orientation (The simulation lasted one minute. Three turns were made by the pedestrian, two 15˚ turns one from 10s to 20s to the right and one from 30s to 40s to the left respectively and one 30˚ sharp turn from 45s to 50s to the right.)

Figure 3.5 shows the errors in position and orientation estimated by the linearised KF and EKF respectively. The errors in position using both algorithms are similar and acceptable except that the estimations from the linearised KF became slightly large when the pedestrian made the sharp turn. It is because that the nonlinearity between the observations and the estimated positions are not significant. Both the linearised KF and EKF can deal with this simple relationship well. However, EKF provide much better estimation in orientation than using the linearised KF. The Root Mean Square

Error (RMSE) is only 2.6˚ using EKF but the errors are up to 30˚ using the linearised KF. It is because that the nonlinearity becomes significant when establishing the relationship between the observed positions and the estimated orientation (see Equations (3.64) - (3.67)). The estimations from the linearised KF converge much slower than using EKF and eventually lead to large errors. It is concluded that the linearised KF can be used in the situation where the nonlinearity is not significant since it can provide equivalent results with EKF and consumes less computational power. The EKF is required to provide reliable estimations when the nonlinearity becomes significant. In this research, the efficiency was not a primary concern and the EKF was preferred due to the small number of states to be estimated and the significant nonlinearity between the parameters.

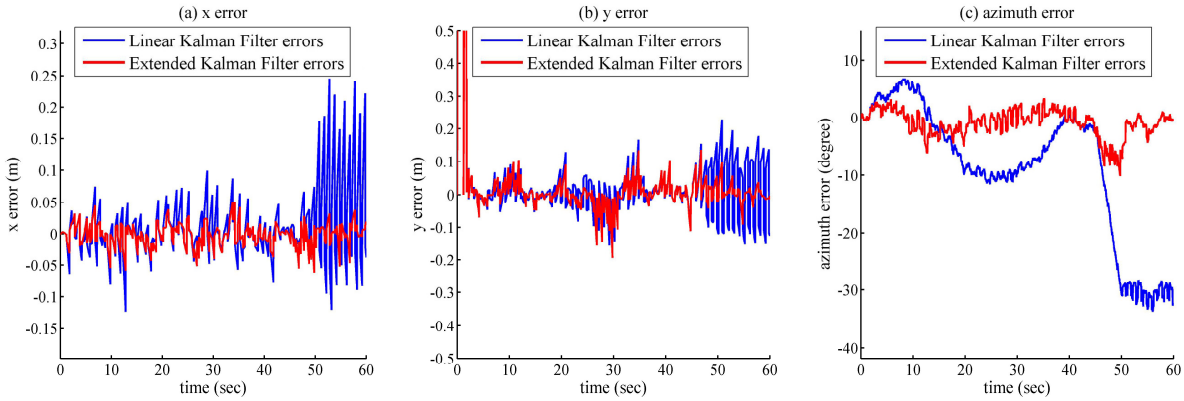

Figure 3.5 Errors in position and orientation estimations by a linearised KF and EKF respectively

(The red lines refer to the EKF errors and the blue lines refer to the linearised KF errors.)

3.1.3 Integration using KF

Previous experiments have also indicated that KF can be used as a tool to integrate the observations. This functionality of KF has been frequently mentioned in literature (Brown and Hwang, 1992; Grewal and Andrews, 2001; Retscher, 2009, 2007b). Retscher (2007b) developed a knowledge-based KF for a multi-sensor personal positioning system to fuse the observations from GPS, PDR, compass and barometer for outdoor positioning and later (Retscher, 2009) included WiFi and RFID for indoor positioning. A positioning accuracy of 1 to 2 metres was achieved by correctly weighted the observations and the state estimations in KF.

The following example shows the integration of gyroscope and magnetometers to estimate pedestrian's orientations using EKF. Both gyroscope and magnetometers

can be used to estimate the orientations and rotation rates stand-alone but each of them has their unique limitations. On one hand, the gyroscope measures the rotation rate according to a series of physical phenomena, such as gyroscopic inertia, angular momentum and precession. This sensor can be treated as a self-contained sensor which is not significantly affected by the surrounding environments so that it can provide reliable rotation rate measurements. However, an integral of the measurements is required when it is used to estimate the orientations. Apparently, the errors from the noise and bias of the gyroscope are accumulated and lead to significant drifts in the orientation estimation. On the other hand, the magnetometers can measure the orientation according to the geomagnetic vector directly. It does not contain the accumulative errors but the geomagnetic vector is not stable and the magnetometers are very sensitive to the metal or electronic devices nearby. These detrimental effects can cause a relatively large noise in the orientation estimation using magnetometers. Accordingly, the integration of gyroscope and magnetometers may decrease the noise level of orientation estimation caused by the noises in magnetometers and constrain the drifts caused by the accumulated errors in the gyroscope.

The EKF used for the integration is described as follows. The state vector is:

$$x = \begin{bmatrix} \psi \\ \dot{\psi} \end{bmatrix} \tag{3.68}$$

where,

ψ is the orientation; and

$\dot{\psi}$ is the horizontal rotation rate.

The dynamic models are:

$$\psi_k = \psi_{k-1} + \Delta t \cdot \dot{\psi}_{k-1} + w_{\psi} \tag{3.69}$$

$$\dot{\psi}_k = \dot{\psi}_{k-1} + w_{\dot{\psi}} \tag{3.70}$$

where,

Δt is the time interval between two adjacent observations; and

$w_{\bullet}$ is the zero-mean white Gaussian process noise with respect to each state variable.

The measurement vector is:

$$z = \begin{bmatrix} m^x \\ m^y \\ \dot{\psi}^z \end{bmatrix} \tag{3.71}$$

where,

m^x and m^y are the measurements from x-axis and y-axis magnetometers respectively; and

$\dot{\psi}^z$ is the horizontal rotation rate measured by the gyroscope.

The measurement models are:

$$m_k^x = m_{AGRF}^N \cdot \sin(\psi_k) + m_{AGRF}^E \cdot \cos(\psi_k) + v_{m^x} \tag{3.72}$$

$$m_k^y = m_{AGRF}^N \cdot \cos(\psi_k) - m_{AGRF}^E \cdot \sin(\psi_k) + v_{m^y} \tag{3.73}$$

$$\dot{\psi}_k^z = \dot{\psi}_k + v_{\dot{\psi}^z} \tag{3.74}$$

where,

m_{AGRF}^N and m_{AGRF}^E are the North and East components of the geomagnetic vector; and

$v_{\bullet}$ is the zero-mean white Gaussian process noise with respect to each measurement variable.

Figure 3.6 shows the results using EKF to integrate the gyroscope and magnetometers. The high-frequency variations in the magnetometers' observations caused by the instability of the geomagnetic vector and the effects from the surrounding environments are filtered and the drifts of the gyroscope are also minimised.

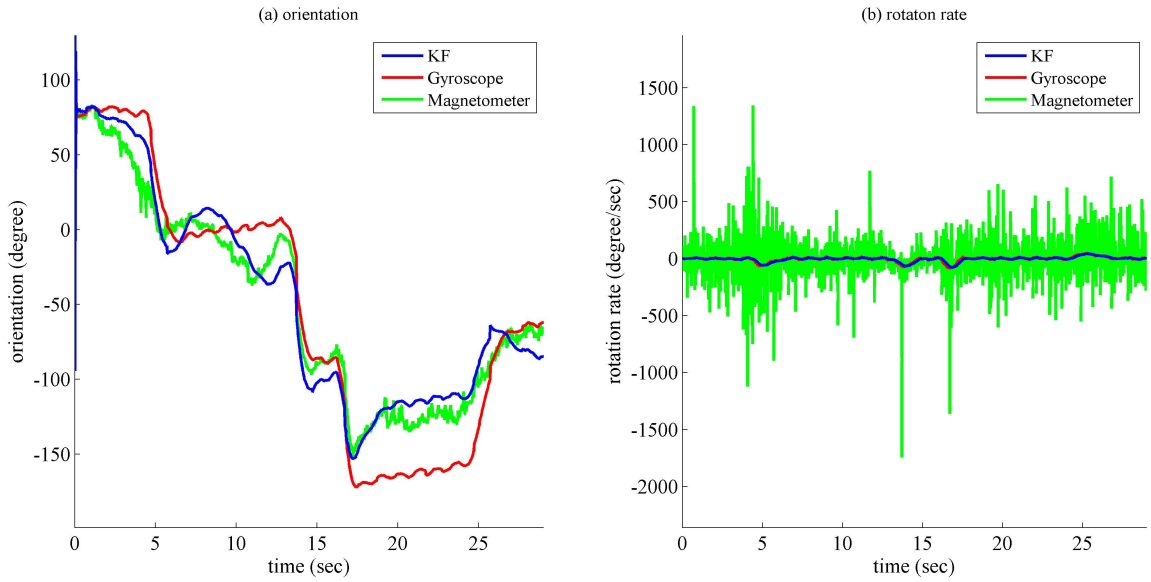

Figure 3.6 Integrated gyroscope and magnetometers' results (Plot (a) shows the estimations of orientation using gyroscope (red), magnetometers (green) and EKF integration (blue) respectively. Plot (b) shows the estimations of rotation rate using gyroscope (red), magnetometers (green) and EKF integration (blue) respectively. The rotation rate estimated by the gyroscope (red) and the integration method (blue) are very close to each other.)

In summary, KF is superior in real-time estimation and data fusion. It provides the optimal estimation by the weighted observations and estimations of the current and previous epochs. It also considered the uncertainties of the measurements and the states based on the covariance matrices. For non-linear problems, EKF, which only applies linear approximation over the ranges of state space, is better than the linearised algorithms. In the following chapters these algorithms will be used for positioning and multi-sensor integrations.

3.2 Positioning Algorithms based on Received Signal Strength

Another category of algorithm included in this research is the positioning algorithm for RFID technique. RFID positioning is a radio-based technique but due to the RFID systems simplicity and limited quality, the accurate time measurements via modulated radio signals or wide band radio pulses are not applicable. RSS becomes the major resource for positioning functionality in RFID systems.

The positioning algorithms used in RSS-based techniques include:

(a) CoO;

(b) RSS-based trilateration; and

(c) Location fingerprinting.

The following sections will provide a brief description and comparison of these algorithms.

3.2.1 Cell of Origin

The simplest algorithm used in RSS-based positioning techniques is CoO. It has been widely used in infrared-based and radio-based techniques, such as *Active Badge* system, cell phone positioning and RFID positioning.

CoO provides the estimated positions of a mobile user, $\hat{p}_0$, bases on the received signal, $Z(p_0)$, using the following formulae.

$$D \equiv \{p_1, \ldots, p_n\} \tag{3.75}$$

$$Z(p_c) \equiv \{s_c\},\ p_c \in D,\ c = 1, \ldots, n \tag{3.76}$$

$$Z(p_0) = Z(p_c) \tag{3.77}$$

$$\hat{p}_0 = p_c \tag{3.78}$$

where,

p_0 is the true position of the mobile user;

p_c is the centre's position of the cell c;

D is a set of cell centres' positions, p, in the defined area; and

$Z(p_c)$ is the signal, s_c, transmitted from the cell c.

When the mobile user's observed signal, $Z(p_0)$, at the position, p_0, aligns with a signal, $Z(p_c)$, from the cell c, the position of the cell centre, p_c, is assigned to the mobile user as its approximated position (see Equation (3.78)).

The conventional CoO can only provide an approximate position within the sensors' detectable area - the cell. This method does not usually provide continuous positions. Firstly, the discontinuous coverage of cells can eliminate conflictions of receiving

signals caused by the overlapped areas. Secondly, the small cell size (normally less than 1m in radius) is always applied in order to increase the precision of positions retrieved from cells. However, the smaller the cell size, the larger the number of sensors to cover the entire area.

Between 2003 and 2004, two different groups of researchers improved the CoO positioning techniques' accuracy and continuity by retrieving the positions from overlapped transmitting coverage via different approaches. Hallaway et al. (2003) used multiple directional transmitters and receivers to avoid the conflictions of receiving the signals from multiple transmitters and detect the overlaps of the transmitting coverage. This method refined the resolution by different combinations of overlapped cells, zones of influence (ZOI). A metre-level accuracy is claimed. (Jung and Woo, 2004; Jung and Woo, 2005a, 2005b) grouped the omni transmitters and let them work in turn to avoid any conflict. The experimental results showed that this method can improve the positioning accuracy by 4 to 9 times comparing with those from the non-overlapped cases.

The approaches based on overlapped transmitting coverage or ZOI can be summarised as follows

$$D \equiv \{p_1, \ldots, p_n\} \tag{3.79}$$

$$Z(p_i) \equiv \{s_{i,1}, \ldots, s_{i,m_i}\},\ i = 1, \ldots, n \tag{3.80}$$

$$Z(p_0) \equiv \{s_{0,1}, \ldots, s_{0,m_0}\} \tag{3.81}$$

$$\left\| Z(p_0) - Z(p_c) \right\| \leq \left\| Z(p_0) - Z(p_i) \right\|,\ p_c \in D,\ \forall p_i \in D \tag{3.82}$$

$$\hat{p}_0 = p_c \tag{3.83}$$

where,

p_c is the position of ZOI's centre;

D is a set of positions of ZOIs' centres, p;

$Z(p_i)$ is a combination of signals, s, which can be received at position p_i; and

$Z(p_0)$ is a combination of signals received by the mobile user at position p_0.

The ultimate goal of this algorithm is to find the most likely combination of signals between the one that is received by the mobile user and the one defined by the

overlapped ZOIs (see Equation (3.82)). The user's estimated position is assigned as the centre of the most likely ZOI (see Equation (3.83)).

Figure 3.7 shows a comparison of different CoO positioning approaches. It includes the conventional CoO methods using both small and large cells and the ZOI method.

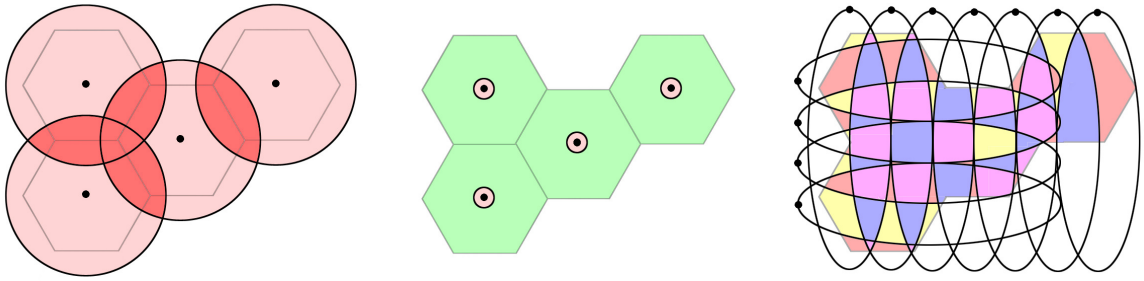

(a) (b) (c)

Figure 3.7 The CoO infrared positioning techniques ((a): overlapped large cells; (b): small cells as active landmarks to provide accurate positioning corrections; (c): directional overlapped cells (the ellipses) which divide the area into over 50 ZOIs (the ZOIs filled with different colours indicate the different combinations of the signals from the transmitters); the black dots refer to the transmitters; the pink areas refer to the cells covered; the dark red areas refer to the overlapped areas of cells; and the green areas refer to the uncovered areas of the system.)

Figure 3.7 (a) simulates the scenario of using high-powered transmitters to establish large cells (with the radius over tens of metres) covering the entire defined area (four adjacent hexagons). Theoretically, this technique can cover a large area with a small number of transmitters. However, it has two major problems. First, large cells generate some overlapped areas along the boundaries of the cells in order to cover the entire area. Complex techniques are required to avoid the conflictions of receiving the signals from multiple transmitters in these overlapped areas when the mobile user uses a single receiver only. Second, the accuracy of this technique is low. It is generally equal to the radius of the cells since the mobile users' position within a cell is determined as the centre position of the cell. Consequently, the smaller the cell the higher the accuracy. Figure 3.7 (b) shows the technique where a small size of cells (normally less than 1m in radius) is used. These small cells can provide sub-metre level positions when a receiver falls into the cell. They usually work as active

landmarks to provide positioning corrections. However, as shown in the figure, it needs more cells to cover the entire area of interest if a small number of cells is used. Other positioning techniques are required when the continuous positioning is needed. Figure 3.7 (c) simulates the directional overlapped cells used in ZOI. The overlapped cells divide the area into over 50 ZOIs with different combinations of 11 elliptical cells. The average size of ZOIs is equivalent to the size of small cells. Instead of discontinuous coverage using small cells, ZOIs can continuously cover the entire area. It improves both accuracy and continuity by only adding a few numbers of transmitters and receivers. The main drawbacks of ZOI are its complexity in receiver designs that are employed to avoid conflicts and the limited scalability of the system.

3.2.2 RSS-based Trilateration

Trilateration is a conventional algorithm used in surveying, as well as in the RSS-based techniques. This algorithm was first introduces by Dutch astronomer and mathematician, Willebrord Snellius, in order to determine the radius of the Earth in the 17th century (Rapp, 1991). It is used to determine the position of the intersection of at least three spherical surfaces given the centres and radii of those spheres.

This algorithm used in the RSS-based techniques is based on the nature of the RSS which varies with the changes of distance between transmitters and receivers. Theoretically, the RSS decreases with the transmitted energy propagating into the space. In physics and radio communication technology, this trend has been well studied (Feuerstein *et al.*, 1994; Rappaport, 1996). A number of models, called path loss models, have been developed to establish the relationship between the RSS and the propagating distance. These models are discussed in Chapter 4 in detail. When the assumptions of the model can be accepted, the distances between transmitters and the receiver can easily be calculated according to the RSS by inverting the model. However, the limitation is that most of these theoretical models are subject to free space propagation or signal propagation in a simple construction with a limited number of reflections and obstacles. In real terms, the environment can be tremendously complex and it is far beyond the assumptions or conditions listed in the physical or theoretical models. For example, in an office building, metal window frames and pipes passing through rooms can be reflectors of RF signals. Cabinets, timber walls and people can cause up to 10dB extra path loss when the signals penetrate through them. These detrimental effects will degrade the accuracy of the

distance estimated using the inversed path loss models. One alternative method is to use regression models based on the previous measured RSS for establishing the relationship between distance and RSS. This method considers the effects on RSS from environments using statistical methods and apparently increases the accuracy of modelling the RSS trend in the specific areas where the RSS data were collected for the regression.

By solving the distances, the mobile user's position can be calculated according to the known transmitters' coordinates and the measurements of ranges between the transmitters and the receiver attached to mobile users. Either the technique of KF or least square can be applied to derive the users' positions. The measurement model is described as the following equations:

$$p_0 \equiv \begin{bmatrix} p_{x,0} \\ p_{y,0} \\ p_{z,0} \end{bmatrix} \tag{3.84}$$

$$p_i \equiv \begin{bmatrix} p_{x,i} \\ p_{y,i} \\ p_{z,i} \end{bmatrix}, \; i = 1, \ldots, n \tag{3.85}$$

$$z \equiv \begin{bmatrix} d_1 \\ \vdots \\ d_n \end{bmatrix} \tag{3.86}$$

$$d_i = \sqrt{(p_{x,i} - p_{x,0})^2 + (p_{y,i} - p_{y,0})^2 + (p_{z,i} - p_{z,0})^2} + \varepsilon_i, \; i = 1, \ldots, n, \; \varepsilon_i \sim N(0, R_i) \tag{3.87}$$

where,

p_0 is the 3-D position of the mobile user;

p_i is the locations of the transmitters with known positions;

z is the estimated distances calculated by ranging models;

R_i is the covariance matrix of measurements; and

ε_i is the associated measurement noise with zero-mean normal distribution.

The major error sources in RSS-based trilateration come from the geometry of the fixed transmitters and the environments which affect signal propagation. The latter error source has been discussed in previous sections, including the reflectors and

obstacles which cause the RSS misalignment with the model's estimations then, subsequently, degrade the positioning accuracy. The former error source is similar to the concept of dilution of precision (DOP), used in GPS positioning. An even distribution of transmitters can provide a small value of DOP and a better estimation of position. In contrast, an odd distribution can cause the anomaly of DOP in some locations and degrade the positioning accuracy in those areas.

3.2.3 Location Fingerprinting

Location fingerprinting was first developed for an indoor RF-based positioning system, RADAR (Bahl and Padmanabhan, 2000). This algorithm can provide continuous positions and is more robust to environmental effects on the RSS than using the RSS-based trilateration algorithm. This is because the location fingerprinting algorithm constructs a searching space according to the previously-measured RSS distributions, which is called fingerprinting maps, for positioning. This process is called the training phase. The advantage of conducting the training phase searching space, or the training phase database, is that it can be used to consider a great number of detrimental effects from the surrounding environment, such as reflections and obstructions, into the fingerprinting maps and thus increases the accuracy for finding the best matching position based on RSS in the positioning phase. This is superior to the RSS-based trilateration algorithm, which uses either empirical or theoretical models to represent the relationship between the RSS and the distance, since the effects from environments are, sometimes, too complex to be modelled.

3.2.3.1 Training Phase

Construction of a fine fingerprinting map is essential for the location fingerprinting algorithms. However, this usually leads to tremendous workloads. Various devices and algorithms have been developed to simplify this procedure, such as the data logging device (Li *et al.*, 2009), which can automatically store the reference positions and the RSS, and the spatial interpolation methods (Lee *et al.*, 2008). This generates the fine-grid map based on a number of observations. Li (2006) stated that the interpolation was an important tool for constructing the fine fingerprinting maps based on the known RSS at a few points. This method for cell phone positions was also investigated and it was shown that the workloads for constructing training phase

maps can be reduced. Our research also investigated the interpolation methods and compared the differences of using the interpolation in different extents of areas.

Three interpolation algorithms were investigated in this research for generating a fine-grid RSS distribution (1m×1m grid) in the defined area, including:

(a) Kriging;

(b) Polynomial regression; and

(c) Nearest neighbour.

Kriging is an interpolation method which uses the regression method to improve the prediction based on the assumptions that the interpolated values are continuously changed and spatially correlated. The idea was first presented by D.G. Krige in his Master's thesis which approached this research in a mining context (Krige, 1951). The theory was later further developed by the French mathematician Matheron and named after the pioneering plotter, Kriging (Cressie, 1990).

The Kriging algorithm is a linear predictor used to predict $Z(p_0)$ at a known location p_0 based on the observations $Z \equiv \{Z(p_1),\ldots,Z(p_n)\}$ from a stochastic process (see Equation (3.88)).

$$Z(p) = \mu(p) + \delta(p),\ p \in D \qquad (3.88)$$

where,

D is the set of positions where the observations are conducted;

$Z(p)$ is the observation at position p;

$\mu(p)$ is the mean value of the observation at position p; and

$\delta(p)$ is a zero-mean stochastic process with known covariance function $C(p_i, p_j) \equiv \mathrm{cov}(Z(p_i), Z(p_j))$, $p_i, p_j \in D$.

There are three kinds of Kriging algorithms that can be used to solve different problems, including:

(a) Simple Kriging,

(b) Ordinary Kriging, and

(c) Universal Kriging.

In simple Kriging, the mean value of the data set is assumed to be a known constant, $\mu(p) = \mu$. Then the predictor is obtained as a linear predictor (see Equation (3.89)).

$$\hat{Z}(p_0) = \sum_{i=1}^{n} \alpha_i \cdot Z(p_i) + k \qquad (3.89)$$

where,

$\hat{Z}(p_0)$ is the estimated value at position p_0; and

α_i and k are the parameters in the linear predictor.

The parameters are determined by minimising the mean-squared prediction error, $E(Z(p_0) - \hat{Z}(p_0))^2$. It yields the optimal predictor as shown in Equation (3.90).

$$\hat{Z}(p_0) = c' \cdot \underset{\sim}{C}^{-1} \cdot Z + (1 - c' \cdot \underset{\sim}{C}^{-1} \cdot I) \cdot \mu \qquad (3.90)$$

where,

$$c \equiv \begin{bmatrix} C(p_0, p_1) \\ \vdots \\ C(p_0, p_n) \end{bmatrix}$$

$$\underset{\sim}{C} \equiv \begin{bmatrix} C(p_1, p_1) & \cdots & C(p_1, p_n) \\ \vdots & \ddots & \vdots \\ C(p_n, p_1) & \cdots & C(p_n, p_n) \end{bmatrix}_{n \times n}$$

$$I \equiv \begin{bmatrix} 1 \\ \vdots \\ 1 \end{bmatrix}_{n \times 1}$$

In universal Kriging, the mean is assumed to have been modelled by a function of the location (see Equation (3.91)). In ordinary Kriging, the mean of the data set is assumed to be unknown. Types of estimators, such as the best linear unbiased estimator, can be engaged to estimate the mean in the procedure of ordinary Kriging and this method can be treated as a subset of universal Kriging.

$$\mu(p) = \sum_{k=0}^{m} \beta_k \cdot f(p) \qquad (3.91)$$

where, β_k is the parameter in the model and $f(p)$ is a function of location p.

In Li's research (Li, 2006), universal Kriging was used to establish the RSS distributions of cell phone or WiFi in a large scale. It is assumed that those RSS distributions in the large scale (e.g. hundreds or thousands of metres) have significant trends since the RSS will decrease when the signal travels over a certain distance. However, this assumption may not be applicable when the RF signals are reflected and/or obstructed by the surrounding environments over a short distance (say, a few metres), for example in the RFID indoor positioning. Figure 3.8 shows the differences of the results between a simple Kriging and a universal Kriging interpolation for RFID indoor positioning. The experiments were conducted in an 8m×10m room with windows and whiteboards on the walls and a few hydraulic pipes on the ceiling. Twelve measurements were conducted on the nodes of a 1.4m×1.4m grid in the middle of the room as the reference points for interpolations. The rest of the measurements on the nodes of a 1m×1m grid in the room were used as the evaluation values. The experiments show that the simple Kriging interpolation provided 1dBm higher accuracy for generating the RSS distribution than using the universal Kriging interpolation. The major differences between these two interpolation methods appeared in the boundary areas where contains less reference points (see Figure 3.8). This is because in this case the trend of the RSS is disrupted by the reflections and obstructions of the surrounding environments and could not be easily modelled using simple mathematical models (e.g. high-order polynomials) in the universal Kriging interpolation. According to the experiments, simple Kriging interpolation is more efficient and accurate for generating the RSS distribution in small scale (e.g. a few metres) indoor environments than using the universal Kriging. The universal Kriging is used when the data has a strong trend and the trend can be modelled (e.g. large scale RSS propagations in a cell phone or WiFi system). Figure 3.9 shows the variation of the RSS in an 8m×10m room using a simple Kriging interpolation based on a 1.4m×1.4m observation grid.

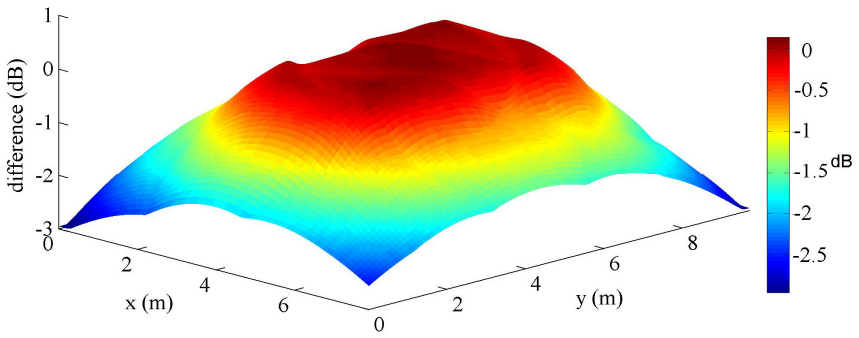

Figure 3.8 The differences between the simple Kriging and universal Kriging interpolations

(The comparison is based on the identical data sets of measured RSS in the middle of a closed room. Subtle differences of the interpolated values within the areas of reference points were found, but significant differences, up to 3dB, were found in the boundary areas that did not have reference points.)

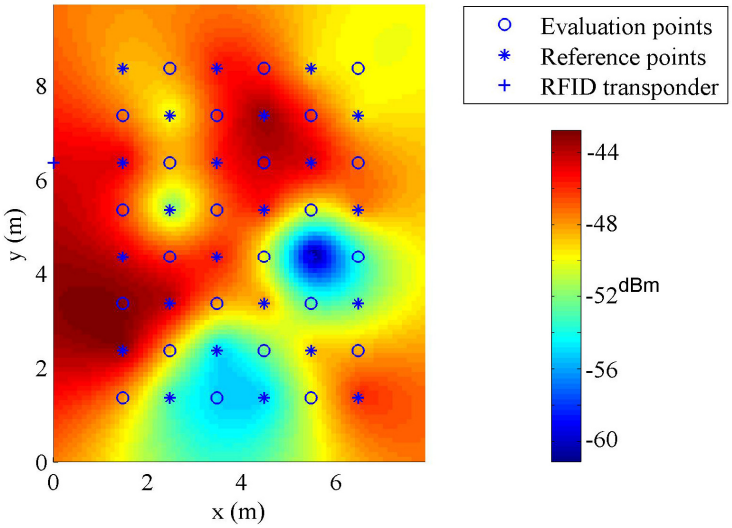

Figure 3.9 A sketch plot of RSS interpolation using a simple Kriging algorithm

(This experiment was conducted in an 8m×10m room with a ceiling height of 3.5m. There were windows with metal frames in the location where x=8m, a whiteboard on the wall where y=0m and pipes on the ceiling. A 1m×1m grid is set in the room. Half of the RSS values on the gird nodes were used for the interpolation and the rest were used for evaluations.)

Another method widely used in the interpolation is polynomial regression. It was first designed by Gergonne (1815; Stigler, 1974). This method uses a high-order

polynomial to model the relationship of variables. The interpolation algorithm can be expressed by the following function:

$$Z(p) = f(p, \beta) + \delta(p), \ p \in D \tag{3.92}$$

where,

$Z(p)$ is the RSS at position p in the defined area D;

$f(p, \beta)$ is the *n*th order polynomial with coefficient β; and

$\delta(p)$ is a higher order term or noise in the interpolation.

The goal is to obtain the optimised $\hat{\beta}$ to minimise the sum of squared residuals described by the following equation:

$$\sum_{i=1}^{n} (Z(p_i) - \hat{Z}(p_i))^2 \tag{3.93}$$

Then the interpolated value of the RSS, $\hat{Z}(p_0)$, at position p_0 is given by:

$$\hat{Z}(p_0) = f(p_0, \hat{\beta}) \tag{3.94}$$

The same dataset used for Kriging interpolation was used to evaluate the performance of polynomial regression interpolations. Considering the computational complexity, a third-order two-dimensional polynomial was applied (see Equation (3.95)).

$$Z(p) = \begin{bmatrix} \beta_0 & \beta_1 & \beta_2 & \beta_3 & \beta_4 & \beta_5 & \beta_6 & \beta_7 & \beta_8 & \beta_9 \end{bmatrix} \cdot \begin{bmatrix} 1 \\ p_x \\ p_y \\ p_x \cdot p_y \\ p_x^2 \\ p_y^2 \\ p_x \cdot p_y^2 \\ p_x^2 \cdot p_y \\ p_x^3 \\ p_y^3 \end{bmatrix} + \delta(p) \tag{3.95}$$

Figure 3.10 shows that the interpolation using the polynomial regression algorithm provides a similar RSS maximum and minimum location with the one using the Kriging algorithm, but the interpolated surface calculated by the polynomial regression is smoother and contains fewer details of variations. This is due to the

simplicity of the polynomial model used. Since the higher-order terms are discarded from the model, the higher-frequency variations are withdrawn.

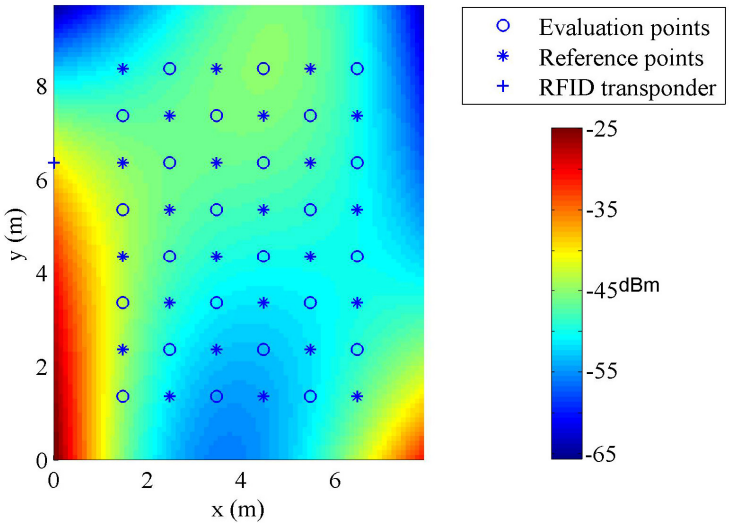

Figure 3.10 A sketch plot of RSS interpolation using a polynomial regression algorithm
(This experiment is conducted in an 8m×10m room with the ceiling height of 3.5m. There is a line of windows with metal frames in the location where x=8m, a whiteboard on the wall where y=0m and pipes on the ceiling. A 1m×1m grid is set in the room. Half of the RSS values on the gird nodes are used for interpolation and the rest are used for evaluations.)

Nearest neighbour interpolation is a simple method which originally comes from the Voronoi diagram (Voronoi, 1907). It is superior to the simplicity of implementations but not always as accurate as other algorithms. The goal of nearest neighbour interpolation is to find the point p_c in the defined area, D, which has the minimum distance from the interpolated point p_0 (see Equation (3.96)).

$$\|p_0 - p_c\| \leq \|p_0 - p_i\|, \ p_c \in D, \ \forall p_i \in D \tag{3.96}$$

Then the value of RSS at point p_c is assigned to the estimation (see Equation (3.97)).

$$\hat{Z}(p_0) = Z(p_c) \tag{3.97}$$

Figure 3.11 presents the RSS distribution using nearest neighbour interpolation based on the same reference dataset for Kriging and polynomial regression interpolations. This algorithm provides a discrete result of the RSS distribution instead of a smooth surface. The interpolated RSS changed suddenly in the

boundaries of the interpolating cells. Since the RSS is a continuous variant in the space without the obstacles, this interpolation method may lead to large errors in boundary areas of the interpolating cells.

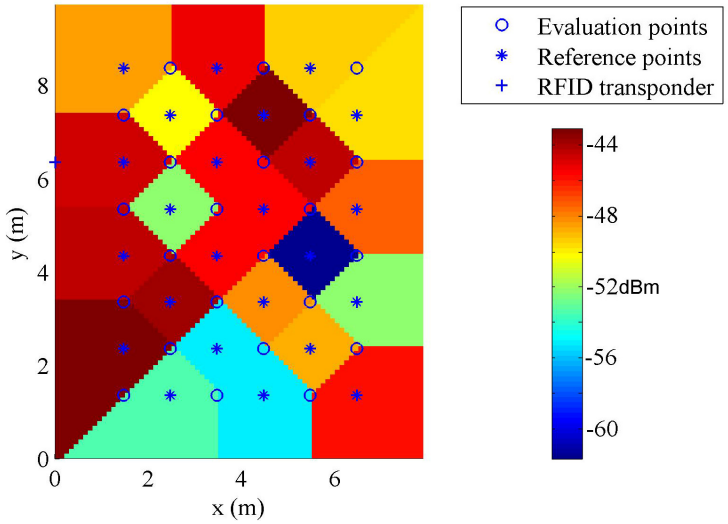

Figure 3.11 A sketch plot of RSS interpolation using the nearest neighbour algorithm

(This experiment is conducted in an 8m×10m room with a ceiling height of 3.5m. There is a line of windows with metal frames in the location where x=8m, a whiteboard on the wall where y=0m and pipes on the ceiling. A 1×1 grid is set in the room. Half of the RSS values on the gird nodes are used for interpolation and the rest are used for evaluations.)

Table 3.1 shows a performance comparison using different interpolation algorithms generating the RSS distributions. This evaluation is based on the observations in the 8m×10m room mentioned before. A 1m×1m grid is set in the room. Half of the RSS values on the gird nodes are used for interpolation and the rest are used for evaluations (see Figure 3.9, 3.10 and 3.11). The RSS measured from 16 RFID transponders around the room were included.

Table 3.1 The performance analysis of using different interpolation algorithms generating RSS distributions
(The values presented in this table are the errors of RSS in dB with 95% cumulative percentage. Interpolating results from 16 tags are validated using Kriging, polynomial regression and nearest neighbour algorithms respectively.)

Tag ID	Errors using Kriging (dB)	Errors using Polynomial Regression (dB)	Errors using Nearest Neighbour (dB)
Over all	10.4	10.3	13.7
Min	5.5	4.9	8.2
Max	13.7	14.1	17.3
200.168.200	8.5	6.6	9.2
200.168.201	7.2	5.3	10.8
200.168.202	7.5	7.5	13.2
200.168.203	8.6	10.2	12.7
200.168.204	12.2	12.9	17.3
200.168.205	5.5	4.9	8.2
200.168.206	11.8	9.1	13.9
200.168.207	13.7	14.1	10.4
200.168.208	7.5	6.6	12.1
200.168.209	8.1	7.9	14.9
200.168.210	8.3	10.8	15.0
200.168.211	10.4	10.3	12.1
200.168.212	9.4	10.2	14.8
200.168.213	13.6	13.7	13.7
200.168.218	8.8	9.3	14.5
200.168.220	9.7	8.2	14.1

In general, both simple Kriging and polynomial regression interpolations provide compatible results (see Figure 3.12), which are between 10.3dB and 10.4dB. In spite of the efficiency, the nearest neighbour interpolation algorithm provides less accurate results than the other two methods evaluated in this research. According to the comparison, the Kriging interpolation can provide more detailed variations than using the polynomial regression. This is due to the fact that the details are diminished with the removal of the higher-order terms in the polynomial regression and only the

large-scale trend can be represented. In location fingerprinting algorithms, the patterns of the detailed variations are essential to conduct the matchings in the positioning phase. In most cases, it relies more on the patterns of RSS variations but not the exact RSS values to find the best matching RSS vector. The Kriging interpolation is preferred for constructing the RSS distributions in the location fingerprinting's training phase even though the polynomial regression can provide a similar accuracy with the Kriging interpolation,

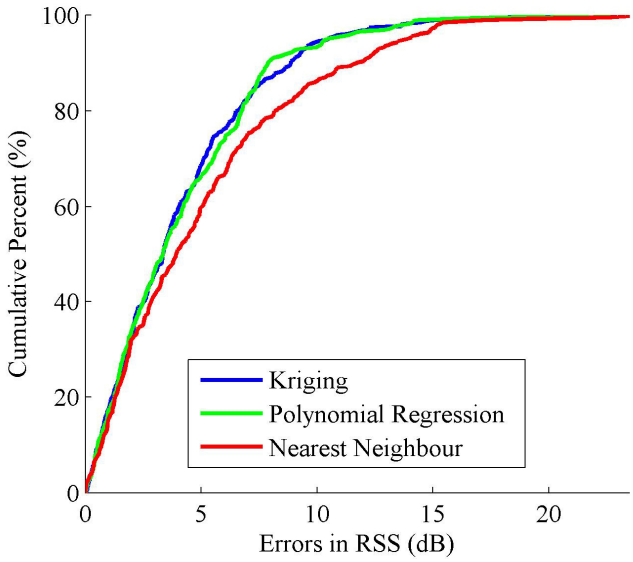

Figure 3.12 RSS interpolation accuracy using different algorithms (It is based on the RSS interpolation from 16 tags. The Kriging, polynomial regression and nearest neighbour are validated respectively.)

3.2.3.2 Positioning Phase

Based on the RSS distributions measured in the training phase, mobile users' positions can be estimated by either the deterministic approach or the probabilistic approach.

The deterministic approach was developed for the first RF-based location fingerprinting system, RADAR (Bahl and Padmanabhan, 2000). It is to find the point p_c in the defined area, D, which has the minimum distance between the vector of observations in positioning phase, $Z(p_0)$, and the vector of observations in training phase, $Z(p_i)$, $i=1,\ldots,n$ (see Equation (3.98)). The mobile user's position is assigned by the selected point, p_c (see Equation (3.101)).

$$\left\|Z(p_0)-Z(p_c)\right\| \le \left\|Z(p_0)-Z(p_i)\right\|,\ p_c \in D,\ \forall p_i \in D \tag{3.98}$$

$$D \equiv \{p_1,\ldots,p_n\} \tag{3.99}$$

$$Z \equiv \{Z(p_1),\ldots,Z(p_n)\} \tag{3.100}$$

$$\hat{p}_0 = p_c \tag{3.101}$$

where,

Z is a set of vectors with training phase observations;

D is a set of positions in the defined area;

$Z(p_0)$ is the RSS observed in positioning phase at position p_0;

$\hat{p}_0$ is the estimated position of the mobile user; and

$\|\bullet\|$ is the distance between two vectors.

The position can also be estimated by a weighted summary of positions in the defined area (see Equation (3.102)). The summary of weights equals to one and values are according to the distances between the vector of observations in positioning phase $Z(p_0)$, and the vector of observations in training phase, $Z(p_i)$, $i=1,\ldots,n$.

$$\hat{p}_0 = \sum_{i=1}^{n}(W_i \cdot p_i) \tag{3.102}$$

$$W_i = W(\left\|Z(p_0)-Z(p_i)\right\|),\ i=1,\ldots,n \tag{3.103}$$

$$\sum_{i=1}^{n} W_i = 1 \tag{3.104}$$

where, W_i is the weight at point p_i and $W(\bullet)$ is a function used to calculate the weight.

The error sources in the positioning phase of the deterministic approach has been discussed by Dempster *et al.* (2008) and they include the RSS directional patterns and the RSS variations. The former is mainly caused by the antenna gains and the obstacles of the mobile user who is always on one side of the antenna. In practice, the antenna gain problem can be partially resolved by matching the RSS with different orientations (e.g. 0˚, 90˚, 180˚ and 270˚). This matching method can also

minimise the effects caused by the obstacles in front of the mobile user. It is because of this that the mobile user can only block a small amount of the signals from a few transmitters which are behind the receiver. The rest of the detectable transmitters are not prone to this effect. By changing the orientation and increasing the number of observations, the number of unaffected RSS will be increased and eventually the positioning accuracy will be increased. The latter is due to the environmental dynamics (see Chapter 4). In contrast, effects are difficult to be minimised by increasing the number of observations since some changes of the environments can last for a long period of time (e.g. to keep the door open for a while or people to stay between the transmitter and receiver for a while) and, consequently, the RSS distribution will be changed and the positioning accuracy will be affected in this period. The solution of this problem for the deterministic approach is to resample the RSS for the training phase fingerprinting maps after the environments have changed. It makes the implementations of the deterministic approach difficult in the dynamic environments. In addition, the RSS errors in the training phase, which is up to 10dBm, is another major error source causing the uncertainties in matching.

Another approach of location fingerprinting, the probabilistic approach, was introduced by Castro *et al.* (2001) using a Bayesian network to find the most possible location according to the received WiFi signals. This approach was further developed by Roos *et al.* (2002). The statistical model, which includes the probabilities of RSS, was used instead of the empirical models. It is superior to the deterministic approach in dealing with the small amount of RSS variations caused by the environmental dynamics. The algorithm based on the Bayes' law is given by Equation (3.105).

$$P(p_i|Z) = \frac{P(p_i \cap Z)}{P(Z)} = \frac{P(p_i) \cdot P(Z|p_i)}{P(Z)}, \quad p_i \in D \tag{3.105}$$

where,

$P(p_i|Z)$ is a conditional probability of the mobile user at position p_i when he/she observes RSS Z;

$P(p_i)$ is a prior probability of the mobile user at location p_i;

$P(Z|p_i)$ is a conditional probability of the mobile user observing RSS Z when at position p_i; and

$P(Z)$ is a probability of the mobile user observing RSS Z.

In Equation (3.105), $P(Z)$ is independent of location, p, so $P(Z)$ can be treated as a constant. $P(p_i)$ can be assigned if the prior information of mobile user's location can be obtained. Otherwise, a uniform distribution can be assumed on $P(p_i)$. $P(Z|p_i)$ can be expressed as a joint probability of RSS at the mobile user's position, p_0, equalling to the RSS in the training phase at position, p_i (see Equation (3.106))

$$P(Z(p_0)|p_i) = P[(S_1(p_i) = S_1(p_0)) \cap \ldots \cap (S_n(p_i) = S_n(p_0))] \quad (3.106)$$

where,

$S_j(p_0)$ is the RSS from the tag j measured at user's position, p_0; and

$S_j(p_i)$ is the RSS from the tag j measured at position p_i in the training phase.

If the RSS from each transmitter measured is independent from each other, Equation (3.106) can be expressed as the marginal probability of $S_j(p_i) = S_j(p_0)$.

$$P(Z(p_0)|p_i) = \prod_{j=1}^{n} P[S_j(p_i) = S_j(p_0)] \quad (3.107)$$

The conditional probability of the mobile user at position p_i when receiving RSS $Z(p_0)$ can be simplified as the following Equation (3.108).

$$P(p_i|Z(p_0)) = c \cdot \prod_{j=1}^{n} P[S_j(p_i) = S_j(p_0)] \quad (3.108)$$

where, c is a constant.

The estimated position of the mobile user, $\hat{p}_0$, will be the most possible position, p_c, where $P(p_c|Z(p_0)) \geq P(p_i|Z(p_0))$, $p_c \in D$, $\forall p_i \in D$ or the conditional probability can be used as weights to calculate a weighted estimation.

The probabilistic approach enhances the reliability of using location fingerprinting algorithms in the dynamic environments by introducing the probabilities of RSS into the algorithms. However, it is still affected by the other two error sources in the deterministic approach, the directional patterns and the errors in training phase fingerprinting maps.

3.2.4 Comparison of RSS-Based Positioning Algorithms

According to the investigations, a comparison of the RSS-based positioning algorithms is provided in Table 3.2. The conventional CoO is the simplest method among all the algorithms investigated but it can not provide continuous positions. There is a trade-off between the accuracy and the number of the cells for covering an area. It can either provide accurate positions (metre-level) with small cell sizes and a large number of cells or provide approximate positions (tens or hundreds of metres) with large cell sizes and a small number of cells. The ZOI partially solves this problem by determine the positions based on the overlapped cells. Specific devices are required to avoid the conflictions of receiving the signals from multiple transmitters. Trilateration is another simple positioning algorithm and can provide continuous positions. However, to accurately estimate the distance according to the RSS is a challenge in complex and dynamic environments. The reflections and obstructions of the signals will significantly affect the relationship between the RSS and the transmitter to receiver distance. In a complex environment the location fingerprinting algorithm can provide more accurate positions than using trilateration by matching the RSS patterns in the searching space according to the measurements in the training phase (Mok and Retscher, 2007). The only benefit using trilateration instead of location fingerprinting is to avoid the tremendous workloads in the training phase. However, the interpolation methods can also reduce these workloads in the location fingerprinting training phase. The investigations of the Kriging, polynomial regression and nearest neighbour algorithms were carried out. It shows that the simple Kriging interpolation can provide better solutions for location fingerprinting in the small-scale indoor environments (a few hundred square metres) in which the RF signals are highly affected by the reflectors and obstacles.

In summary, every positioning algorithm investigated has its unique pros and cons. These are summarised in Table 3.2. The CoO is superior due to its simplicity and the probabilistic approach of the location fingerprinting is less affected by complex and dynamic environments. Detailed investigations and evaluations of these RSS-based positioning algorithms for RFID positioning are provided in the next chapter.

Table 3.2 A comparison of RSS-based positioning algorithms

Algorithm	Advantages	Disadvantages
CoO	• Simple algorithms	• Discrete positions • The accuracy and coverage areas depend on the size of cells
ZOI	• Simple algorithms • Higher accuracy than conventional CoO	• Specific devices are required to observe the overlapped ZOI
RSS-based trilateration	• Continuous positions • No training phase required	• Inaccurate distance estimations based on RSS caused by the environmental effects
Deterministic location fingerprinting	• Continuous positions • Considering the environmental effects in the training phase RSS distributions	• Inaccurate in a dynamic environment due to the RSS variations • Affected by the RSS directional patterns • Affected by the errors in the training phase
Probabilistic location fingerprinting	• Continuous positions • Considering the RSS variations caused by the environmental dynamics in the probabilistic distributions of RSS	• Affected by the RSS directional patterns • Affected by the errors in the training phase

3.3 Summary

The first part of this chapter provided an overview of KF and its related principles. It showed that KF is a superior tool for estimating the states by separating the signals from noise according to the uncertainties of the predictions and observations. Experiments and simulations were conducted to evaluate the KF's functionalities of state estimation and data fusion. The results indicated that KF can provide similar estimations to those from least square adjustment and is more efficient. KF is also considered to be an effective algorithm for multi-sensor integration, which weighs the observations according to covariance matrices. For the non-linear problems, EKF is superior to the linearised KF by only applying linear approximation over the ranges of state space.

The second part of this chapter focused on the algorithms for RSS-based positioning. An introduction and comparison of the algorithms, including the CoO, RSS-based trilateration and location fingerprinting, were first provided. The CoO can provide accurate and discrete positions on correction spots or the approximate positions in

large areas depending on the cell size. The RSS-based trilateration can provide continuous positions but the accuracy of the position is highly affected by the reflections and obstructions of the signals by the surrounding environments. The location fingerprinting algorithms on the other hand can provide more accurate and continuous positions than using RSS-based trilateration by considering the detrimental effects from surrounding environments in its training phase fingerprinting maps. In addition, the probabilistic approach is superior to the deterministic approach in dynamic environments by introducing the probabilities of RSS into the location fingerprinting model.

RSS-based positioning algorithms will be validated by RFID positioning technique in the next chapter. KF and its related principles for the multi-sensor integration will be investigated in Chapters 5 and 6.

Chapter 4 RFID Positioning

The RFID market has expanded quickly over the last two decades and the areas of applications have increased exponentially, particularly in everyday use. Positioning using RFID has recently become an attractive research topic due to its unique features, such as external-power-free tags, size and portability. In our research, the unique contributions in long-range RFID positioning include:

(a) A probabilistic CoO algorithm for integrated RFID/MEMS INS positioning (Zhu, 2008);

(b) A 3-D location fingerprinting algorithm for integrated RFID/MEMS INS positioning (Zhang *et al.*, 2008); and

(c) An Iterated Reduced Sigma Point Kalman Filter for RFID/low-cost GPS seamless positioning (Peng *et al.*, 2009).

4.1 Introduction to RFID Positioning Techniques

A typical RFID system has three components: a transponder or tag (located on the object to be tracked); an interrogator or reader (which receivers the information from tags); and a control unit (which operates the system and processes the information) (Finkenzeller, 2003). The basic idea of the RFID technique is to transfer the information of identification from an electronic data-carrying device - the RFID tag - to an RFID reader via a RF interface. The technique can be classified into two systems - passive and active - depending upon the signals transmitted and the tag structures. A passive RFID tag contains very simple components to respond with its information of identification to the signals triggered from a RFID reader. It does not contain an electronic power source itself. The energy for the RFID tag's circuit is transmitted from the RFID reader via magnetic or electromagnetic fields over a short range (less than 3m). Its reading range is limited by the range of energy transition. In contrast, active RFID tags have a longer reading range (over 15m) due to built-in batteries. In positioning applications, RSS is the major observation component in RFID systems. It is used to determine either the appearance of a mobile user in the reading range (Abowd *et al.*, 2004) or the distance between transmitters and receivers (Hightower *et al.*, 2000).

4.1.1 Historical development of RFID Positioning Techniques

RFID research for positioning began in the late 1990s through investigating position solutions using trilateration algorithms (Hightower *et al.*, 2000). It has quickly become an attractive system for location based services due to its unique features, such as its high penetratability of signals, low power consumption, simplicity of use and relatively low-cost.

The feasibility of using RFID for positioning was first investigated using a commercial long range active system in order to develop a new positioning system – *SpotON* (Hightower *et al.*, 2000). This was one of the early investigations of RFID positioning. The system used for evaluation claimed a reading range of 4.5m. A second-order polynomial regression method was used to model the RSS changes relative to distances in the system. It indicated a 3m accuracy. Also, an 0.05 to 0.1Hz update rate could be obtained by RFID trilateration algorithms, which was similar to the system's reading range. This was not suitable for personal indoor positioning applications in large areas (e.g. in a floor of a building). The RFID positioning performance was constrained by the technology as well as the nature of the trilateration algorithm at the time. Bekkali *et al*. (2007) improved RFID trilateration algorithms by indirectly measuring the tag-to-tag distances instead of tag-to-reader distances. The algorithm was called the inner-tag distance measurement. This algorithm calculates distances between tags having unknown positions and tags with known positions, according to tag-to-reader distances. It then determines the unknown positions by the tag-to-tag distances. The advantage of this algorithm is that many of the correlated errors in the tag-reader distance measurements can be removed. However, the main disadvantage of the method is that the signal directional patterns become a major error source that could not be reduced. An additional probabilistic mapping method was required to achieve better performance. Another effort to improve the performance of RFID trilateration algorithms was conducted by Retscher and Fu (2008). A calibration method was used according to the previous measurement method to increase the accuracy of distance estimation.

In summary, trilateration algorithms are highly dependent on the accuracy of distance measurements, but accuracy degrades significantly due to the inherent detrimental effects of the RFID indoor positioning technique, like environmental dynamics and signal directional patterns. Instead of minimising these detrimental effects, other

positioning algorithms have been investigated including CoO and location fingerprinting (Ni *et al.*, 2004; Tenmoku *et al.*, 2004).

The benefit of the CoO method is its simplicity of use, as active landmarks either provide approximate positions in large areas or accurate positions over an extremely small range (e.g. within a few metres). Tenmoku *et al.* (2003a; Tenmoku *et al.*, 2003b, 2003c) used a passive RFID system as outdoor landmarks to provide accurate positions in a wearable augmented reality system. Its RFID positioning algorithm also used the CoO method in a small cell size. It can provide accurate discrete positions. The benefit using passive RFID in their system was battery-free tags, which are easy to maintain outdoors. Chon *et al.* (2004) proposed a method using RFID to frequently provide sub-metre positions when there are no GPS signals available, for instance, a vehicle travelling in a tunnel. The CoO algorithm was again used and much work had been done on improving communication speeds in order to avoid the missing scans of RFID tags. Bohn (2006) introduced an accurate passive RFID positioning method using super-distributed tags (39 tags/m^2 on average) on a floor. The algorithm used was similar to CoO, which estimated the mobile user's position through the tags in the reading range. This method claimed 0.15m accuracy with 5Hz update rate, but the high-density tags that needed to be placed limited the use of this method in large areas. Fu and Retscher (2009b) introduced the RFID Time-Based CoO Positioning algorithm for the accurate determination of the time it took for a mobile user to pass through the centre of a cell.

One of the limitations in the CoO algorithm is the compromise between the cell size and accuracy. Some efforts have been made to overcome this limitation. For example, Vries (2005) introduced a positioning algorithm for a long range active RFID, *WeightedTracker*. This algorithm can be treated as the CoO that applies RSS-based weights on all observed cell center positions. A 4m positioning accuracy was achieved. A few other attempts have also been carried out using various integrations of sensors. For instance, Miller *et al.* (2006) proposed an integrated RFID/PDR method for locating first responders in indoor environments. This is pioneering research using RFID-based integration techniques for personal positioning. The RFID CoO algorithm was used to provide positioning corrections in order to constrain errors in PDR.

In addition, the location fingerprinting algorithms can also provide continuous and reliable positions using the RFID technique. One remarkable contribution in this area

of RFID positioning was made by Ni *et al.* (2004). They developed the *LANDMARC* system based on a deterministic location fingerprinting algorithm. Their invention used a dense RFID tag array to achieve a real-time training phase RSS distribution simultaneously with the measurements of mobile users' RSS. Therefore, this method alleviates the problems caused by environmental dynamics and reduces the workloads in training phase measurements. However, its limitation is the complexity for establishing the tag array in a large experimental area.

Table 4.1 below provides a brief overview of the major developments in the past decade (2000-2009). The systems and algorithms used and the performances of each development are listed.

Table 4.1 The historical development of the RFID positioning techniques – in brief.

Time	Authors	System used	Positioning algorithms for RFID-based system	Performance
2000	Hightower *et al.*	• Long range active RFID	• Trilateration • Regression model for path loss	3m accuracy and 0.1-0.05 Hz update rate
2003	Tenmoku *et al.*	• Passive RFID • Inertial sensor • Camera • Infrared system • Pedometer	• CoO	working as landmarks to provide accurate positions
	Ni *et al.*	• *LANDMARC* (active RFID)	• Deterministic location fingerprinting • Real-time measured training phase RSS	1m accuracy (50%) and 0.1Hz update rate; accommodate environmental dynamics
2004	Chon *et al*	• RFID • GPS	• CoO	seamless positioning for vehicle
	Abowd *et al.*	• Passive RFID • Camera	• CoO	working as landmarks to provide accurate positions
2005	Vries *et al.*	• Active RFID	• Weighted CoO	4m accuracy
2006	Miller *et al.*	• RFID • PDR	• CoO • Integration with PDR	Using RFID to constrain errors in PDR
	Bohn *et al.*	• Super-distributed passive RFID	• CoO	0.15m accuracy and 5Hz update rate
2007	Bekkali *et al.*	• RFID	• Trilateration based on inner-tag distances • Probabilistic RFID map	Sub-metre level accuracy
	Retscher *et al.*	• Long range active RFID • PDR, GPS	• CoO • Multi-sensor Integration	seamless positioning for pedestrian
2008	Fu *et al.*	• Long range active RFID	• Trilateration calibrated based on prior samples	Sub-metre level accuracy in static positioning
	Zhu *et al.*	• Long range active RFID • MEMS INS	• Probabilistic CoO • Integration with MEMS INS	Adjustable cell size for CoO algorithm

2008	Zhang *et al.*	• Long range active RFID • MEMS INS	• Location fingerprinting • Integration with MEMS INS • Probabilistic map matching	1.7m accuracy in real-time positioning
2009	Fu *et al.*	• Long range active RFID • MEMS INS	• Time-based CoO • Integration with MEMS INS	1m accuracy in post processing
	Peng *et al.*	• Long range active RFID • low-cost GPS	• Distance estimation • Integration with low-cost GPS	2.2m accuracy; seamless positioning for vehicle

4.1.2 Evaluation of the Long Range RFID Used

The RFID system used in this research was an intelligent long range system produced by *Identec Solutions*. It consists of an *i-Card III* interrogator (reader) and *i-Q* transponders (tags) (see Figure 4.1).

Figure 4.1 RFID interrogator and transponder used in the research (*i-Card III* interrogator (left) and *i-Q* transponder (right) of the *Identec Solutions* long range active RFID system)

The *i-Card III* interrogator is an RFID reader working on 915MHz frequency. It is the size of a PCMCIA card with a 6cm omni antenna (Identec Solutions, 2004b) and the *i-Q* transponders are the active tags with built-in batteries which can last up to six years under 1Hz scanning frequency (Identec Solutions, 2004a). The dimensions of the tags are 131mm×28mm×31mm. It is claimed that the reading range of this RFID system is up to 100m in free space and the reader can detect the RSS over -85dBm. In practice, the maximum reading range is about 30m due to the effects from the surrounding environments (reflections and obstructions). This system also contains an anti-collision multi-tag-handling algorithm to avoid the potential scanning collisions.

Figure 4.2 shows the instability of the RSS in static environments. The data is collected at 300 positions in different environments, including outdoor open areas, indoor large rooms (8m×10m), indoor corridors (2m×40m) and indoor stairways. There are 100 scans at each position. It indicates that the RSS in the static

environments are very stable. The average is approximately ± 0.8dBm at a 95% confidence interval. This value does not change much with different environments and different distances between the RFID reader and tags. This refers to a relatively stable transmitted power in the RFID system.

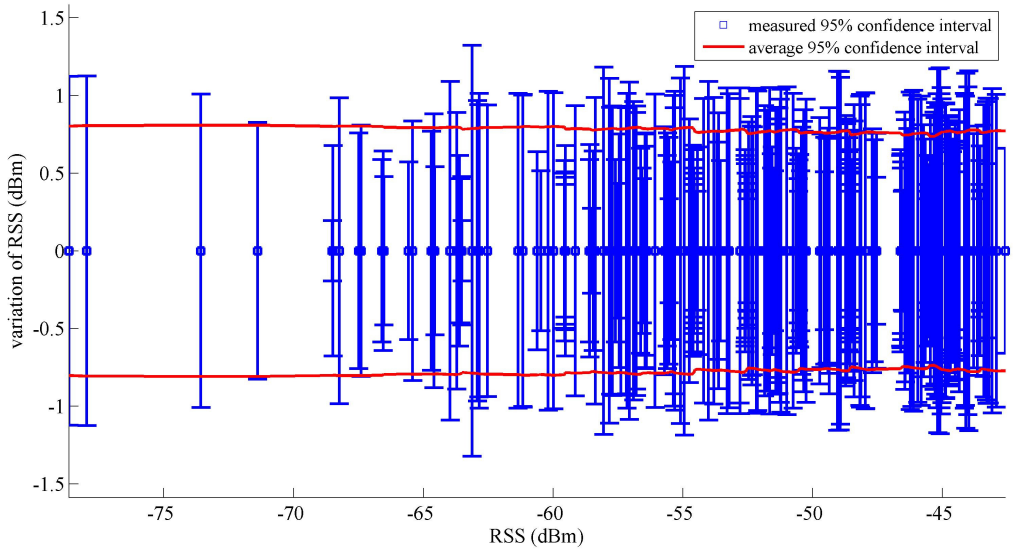

Figure 4.2 The instability of the RSS in static environments (The RSS were measured at 300 positions in different environments, including outdoor open areas, large indoor rooms (8m × 10m), indoor corridors (2m × 40m) and indoor stairways. There were 100 scans at each position. The error bars indicate the RSS instability at each position. The red lines indicate the average instability at all the positions.)

However, RSS can be dramatically changeable in dynamic environments. Figure 4.3 shows the RSS measured at the same position in different contexts (static environments and dynamic indoor environments). In the static environments, the distribution of RSS aligned well with the associated Gaussian distribution but in the dynamic environments, the distribution was disturbed and several peaks were observed. The mean RSS value also shifted away from the one measured in the static environment. This was caused by moving obstacles and reflectors, such as the people passing through the areas between the RFID reader and the tag scanned, during the surveying process. It indicates that RSS measurement is sensitive to the dynamics of surrounding environments.

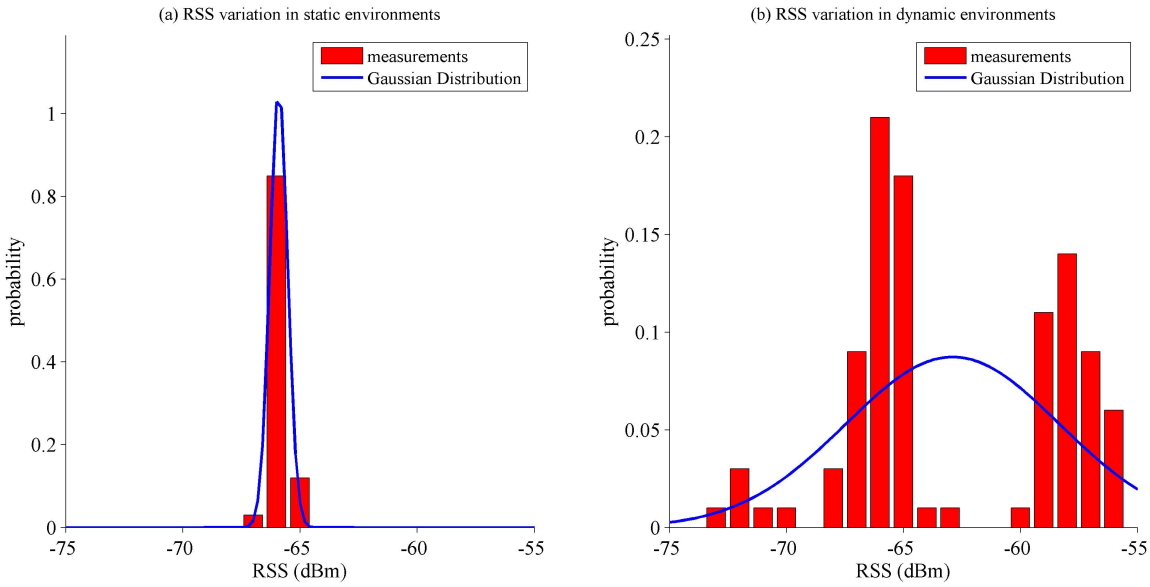

Figure 4.3 Comparisons of the RSS values in both static and the dynamic environments

(The bars show the probabilities of observing certain values of RSS and the lines are the associated Gaussian distributions with the same means and variations of the measurements.)

4.2 Characteristics of Radio Frequency Propagation In RFID System

The signals transmitted by RFID systems are done at radio frequencies. They are transmitted via an antenna into the space with different signal strengths in different directions. The signal is quite powerful and it can propagate through the space and penetrate through some obstacles, such as bricks, wooden walls and human bodies. It also has the property of being reflected by metal objects.

The characteristics of the signal propagation in the RFID system investigated in this research include:

(a) Path loss patterns;

(b) Directional patterns; and

(c) Reflectional patterns.

4.2.1 Path Loss

In general, the power of the RF signals decreases when it propagates into space (Rappaport, 1996). The trend of this process can be mathematically modelled. The

simplest model, which represents this process without reflections and obstructions, is called the free space propagation model. It is given by:

$$PL(d) = S_t - S_r(d) = -10 \cdot \lg(\frac{G_t \cdot G_r \cdot \lambda^2}{(4\pi)^2 \cdot d^2}) \quad (4.1)$$

where,

S_t is the strength of the signal transmitted;

$S_r(d)$ is the RSS from the distance d;

G_t is the antenna gain of the transmitter;

G_r is the antenna gain of the receiver;

λ is the wavelength of the transmitted signal; and

$PL(d)$ is the path loss at distance d.

This model is only valid in the far-field (Fraunhofer region) of the transmitting antenna. The Fraunhofer distance which defines the boundary of the region is given by:

$$d_f = \frac{2D_a^2}{\lambda} \quad (4.2)$$

where, d_f is the Fraunhofer distance and D_a is the largest physical linear dimension of the transmitting antenna.

For the free space propagation model, d_f must satisfy $d_f \gg D_a$ and $d_f \gg \lambda$. However, it is usually difficult to measure the transmitted signal strength. Hence the estimated RSS, $S_r(d)$, is calculated based on the RSS measured at the reference distance, $S_r(d_0)$, rather than the transmitted signal strength. This model is given by:

$$S_r(d) = S_r(d_0) + 20 \cdot \lg(\frac{d_0}{d}),\ d \geq d_0 \geq d_f \quad (4.3)$$

where, d_0 is the reference distance and $S_r(d_0)$ is the RSS at the reference distance.

In reality, the RF signal strength is affected significantly by the propagation media and the surrounding environments, and it may not exactly follow the trend described in the free space propagation model. Some efforts have been made to adjust the free space propagation model to reality, such as the log-distance path loss model (Rappaport, 1996). This model introduces a parameter, called the path loss exponent,

to adjust the trend of the model according to different kinds of propagation media and is given by Equation (4.4) below.

$$PL(d) = PL(d_0) + 10 \cdot \gamma \cdot \lg(\frac{d_0}{d}) \qquad (4.4)$$

where,

$PL(d_0)$ is the path loss at the reference distance; and

γ is the path loss exponent.

Some typical values of the path loss exponent are presented in the literature (Rappaport, 1996) (also see Table 4.2). In free space, the path loss exponent equals 2, which aligns the log-distance path loss model with the free space propagation model. In lossy environments, such as outdoor and indoor non-line-of-sight areas, the path loss exponent increases and its normal range is between 2 and 6. In the indoor line-of-sight area, especially in corridors, this value can fall to less than 2. This is caused by surrounding structures (waveguides) forcing the RF to propagate along the directions of the structures instead of propagating uniformly into the space.

Table 4.2 Typical values of the path loss exponent cited by Rappaport (1996)

Environment	**Path loss exponent**
Free space	2
Outdoor	2.7 to 5
Indoor line-of-sight	1.6 to 1.8
Indoor non-line-of-sight	4 to 6

Figure 4.4 shows a log-distance path loss model generated by outdoor observations of RFID RSS in which the path loss exponent equals 2.3. The 90% confidence level of the modelled path loss varies between 9.1dB and 10.1dB within 25m. These uncertainties may be due to the signals being reflected from the environment, the changes of the antenna orientation and the variations of the transmission power.

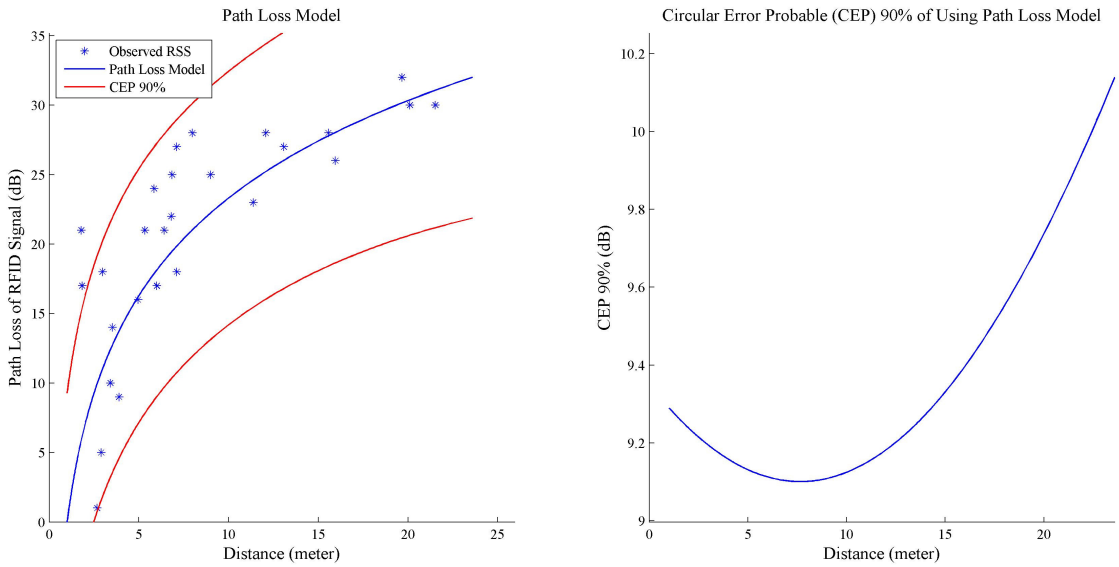

Figure 4.4 A log-distance path loss model and its 90% confidence level based on the observations in open areas

(The plot at left shows the path loss model (blue line) established based on the observations (blue dots) in open areas and its 90% confidence interval (red lines). The distances between the RFID reader and tag ranging from 0.9m to 21.5m which are measured by RTK GPS. The plot at right shows the size of the 90% confidence level changing with distance. The error varies between 9.1dB and 10.2dB.)

4.2.2 Directional Patterns

As noted from the observations, the RSS measured can be misaligned with empirical path loss models. One of the major causes is related to the relative directions between the transmitter and the receiver. Theoretically, it is due to the antenna gain patterns, obstructions and reflections between the transmitters and receivers in different directions.

In practice, the antenna gain patterns can be precisely measured in a laboratory, but the exact effects from the environment between the transmitters and receivers are not easy to be modelled and separated from the RSS directional patterns. In this research, a statistic model was used to investigate the effects on the directional patterns of RSS in combination, instead of modelling them separately.

A ratio was introduced to relate the RSS from one particular orientation to the mean value of the RSS from multiple directions (see Equation (4.5)). An ellipse was used to model the change of the ratio with the orientation (see Equation (4.6)).

$$\overline{S}_r(d) = r(d,\theta) \cdot S_r(d,\theta) \qquad (4.5)$$

$$r(d,\theta) = \frac{a(d)}{\sqrt{1 + e'^2(d) \cdot \cos^2\theta}} \qquad (4.6)$$

where,

$\overline{S}_r(d)$ is the average RSS value at distance d;

$S_r(d,\theta)$ is the RSS observed at distance d with the relative orientation θ;

$r(d,\theta)$ is the ratio between the average RSS and the RSS observed with the relative orientation θ at distance d. It is represented by an ellipse model (see Equation (4.6));

$a(d)$ is the semi-major axis of the ellipse model; and

$e'(d)$ is the second eccentricity of the ellipse model, which is $e' = \frac{\sqrt{a^2 - b^2}}{b}$.

A non-linear least square adjustment was used to estimate the parameters (see Equation (4.7)) based on the observations from different orientations (e.g. 0˚, 45˚, 90˚, 135˚, 180˚, 225˚, 270˚ and 315˚ respectively).

$$\begin{bmatrix} \Delta e'^2 \\ \Delta a \end{bmatrix} = (\underset{\sim}{J}^T \cdot \underset{\sim}{J})^{-1} \cdot \underset{\sim}{J}^T \cdot \Delta r \qquad (4.7)$$

$$\underset{\sim}{J} \equiv \begin{bmatrix} \left.\frac{\partial r(\theta_1)}{\partial e'^2}\right|_{e'^{2nom}, a^{nom}} & \left.\frac{\partial r(\theta_1)}{\partial a}\right|_{e'^{2nom}, a^{nom}} \\ \vdots & \vdots \\ \left.\frac{\partial r(\theta_n)}{\partial e'^2}\right|_{e'^{2nom}, a^{nom}} & \left.\frac{\partial r(\theta_n)}{\partial a}\right|_{e'^{2nom}, a^{nom}} \end{bmatrix} \qquad (4.8)$$

where,

$\underset{\sim}{J}$ is the Jacobian matrix of the ratio with respect to the second eccentricity's square and the semi-major axis;

e'^{2nom} is the nominated value of the second eccentricity's square; and

a^{nom} is the nominated value of the semi-major axis of the ellipse model.

The experiments were conducted outdoors and indoors with different distances between the RFID reader and tag (1.5m, 3.5m, 4.5m and 5.4m in outdoor

environments and 1.5m, 2.5m, 3.5m, 4.5m and 5.4m in indoor environments) respectively. Observations from eight orientations (0˚, 45˚, 90˚, 135˚, 180˚, 225˚, 270˚ and 315˚ in the arbitrary coordinates) were selected (see Figure 4.5 and Figure 4.6 respectively).

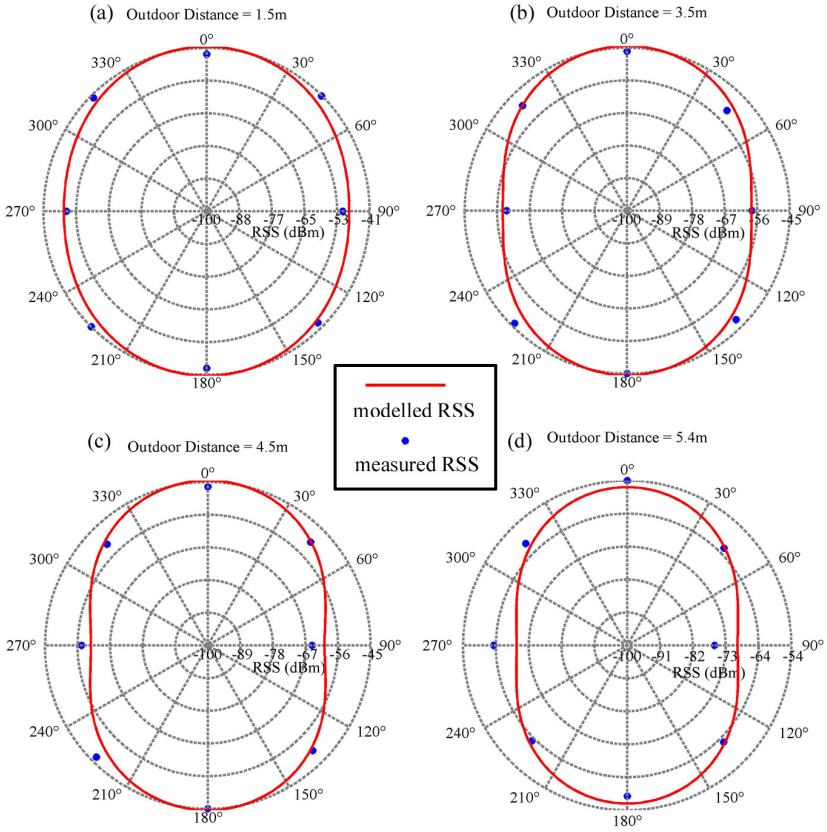

Figure 4.5 The directional patterns and the models used to represent the patterns of RSS in outdoor environments with different distances between the RFID reader and tag

(The RSS from eight relative directions (0˚, 45˚, 90˚, 135˚, 180˚, 225˚, 270˚ and 315˚) and four distances (1.5m, 3.5m, 4.5m and 5.4m) between the reader and tag were measured in outdoor environments.)

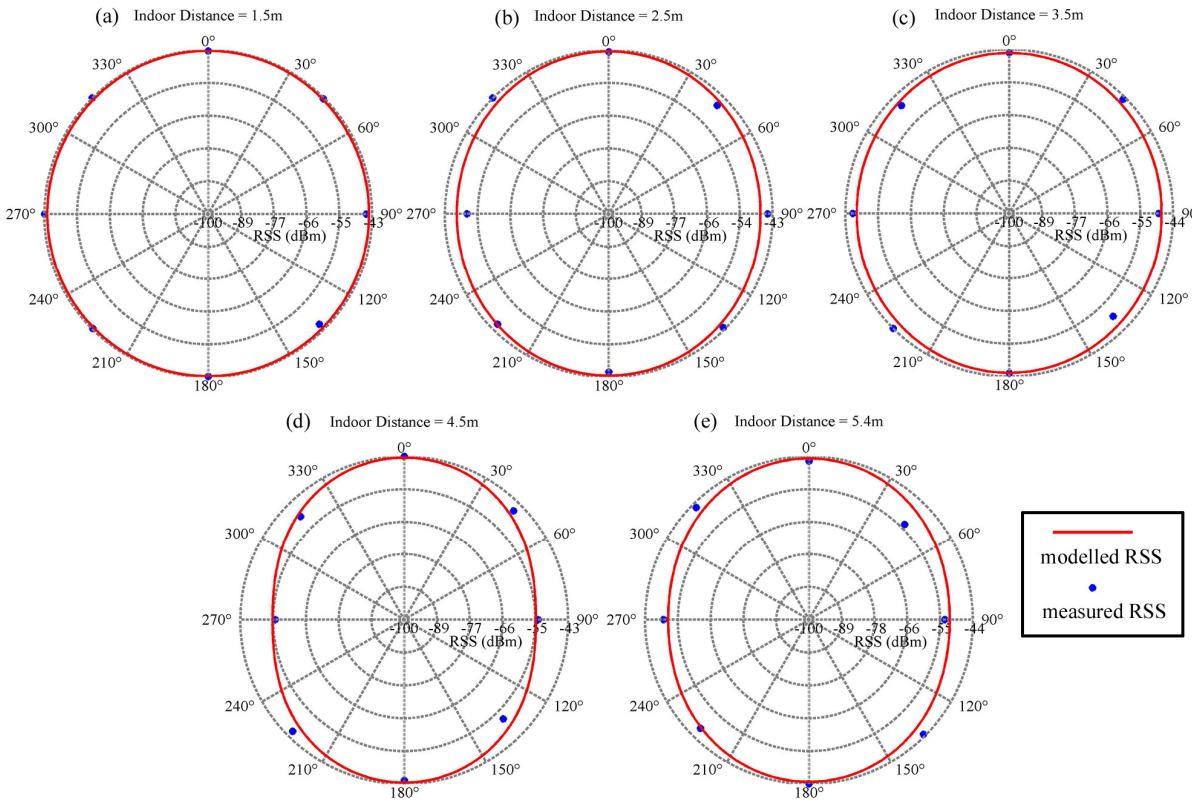

Figure 4.6 The directional patterns and the models used to represent the patterns of RSS in indoor environments with different distances between the RFID reader and tag

(The RSS from eight relative directions (0˚, 45˚, 90˚, 135˚, 180˚, 225˚, 270˚ and 315˚) and five distances (1.5m, 2.5m, 3.5m, 4.5m and 5.4m) between the reader and tag were measured in indoor environments.)

The experiments showed that RSS variations due to directional patterns can be up to 20dB. The ellipse model developed can be used to estimate the RSS directional patterns with the RMSE up to 3.4dB within 5.4m in both indoor and outdoor environments respectively (see Table 4.3). It is also shown that a trend exists between the accuracy of the models and the distances from transmitters to receivers. The shorter the distance, the more accurate the RSS estimation. This is due to the effects from the surrounding environments, since the longer the distance the more reflectors and obstacles between the transmitter and the receiver are needed. Apparently, the detrimental effects on the RF signals from those objects will disturb the RSS measurements dramatically in different orientations and the ellipse model cannot be used directly. It also indicates that the ellipse model developed is not applicable for estimations where there is a large distance between the transmitter and receiver. Another limitation of the ellipse model is that there are no significant trends of the estimated parameters with the increase of the distance in the models

(see Figure 4.7 and Figure 4.8). The parameters in the ellipse model vary with the distance and the context of the environments.

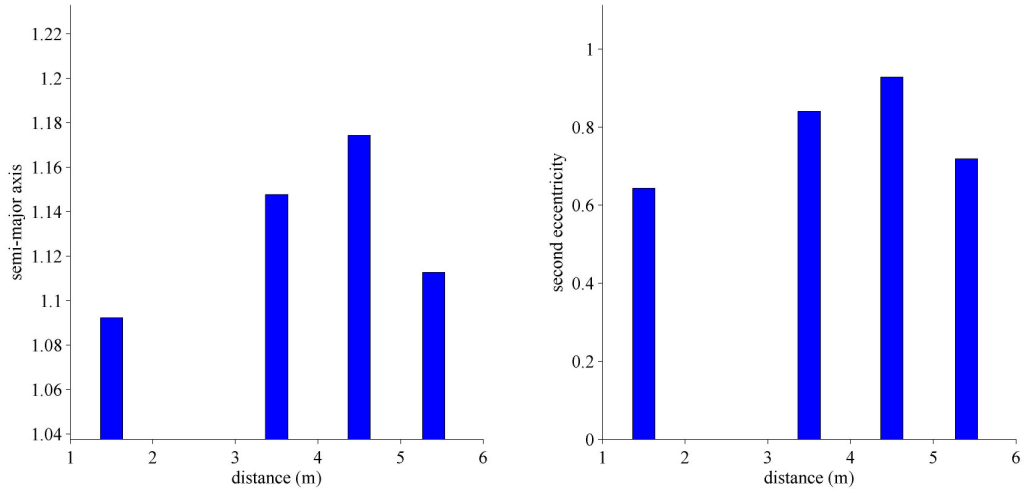

Figure 4.7 The estimated parameters of the ellipse models based on the observations in the outdoor observations

(left: semi-major axis; right: second eccentricity.)

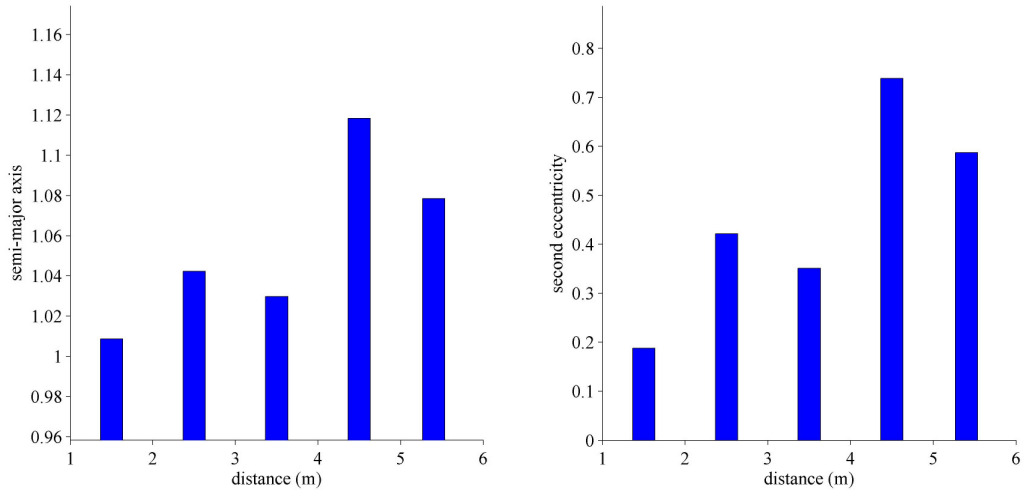

Figure 4.8 The estimated parameters of the ellipse models based on the observations in the indoor environments

(left: semi-major axis; right: second eccentricity.)

Table 4.3 The errors of the ellipse models

Distance between Tx and Rx (m)	1.5	2.5	3.5	4.5	5.4
Indoor RMSE (dB)	0.8	1.9	1.8	1.8	2.7
Outdoor RMSE (dB)	2.3	N/A	1.9	2.5	3.4

In summary, the ellipse model developed can be used to estimate RSS directional patterns with small RMSE (less than 3.4dB) in short distances (within 5.4m) both indoors and outdoors. However, the increase in errors with the increase in the distances between the transmitter and receiver makes the model inapplicable to large-distance observations. In addition, the unpredictable parameters in the model make it difficult to be applied to various positions and in the context of the particular environments of use. The directional patterns of the RSS are too difficult to be accurately modelled due to environmental complexities. One practical solution to minimize the detrimental effects from the RSS directional patterns is to include observations from different orientations for positioning. Nevertheless, in dynamic positioning, positions are resolved in real time. It is impracticable to let the mobile user collect RSS from different orientations at every point. Eventually, the positioning errors caused by RSS directional patters cannot be minimized. Therefore, using standalone RFID positioning for dynamic positioning cannot achieve high accuracy due to the directional patterns of RSS.

4.2.3 Multipath Effects

Another detrimental effect, which is difficult to be modelled, is multipath effect. This phenomenon is mainly caused by reflections of the RF signals, which make the received signals a combination of signals from both direct and indirect paths. Since the paths are site-specific and the signals are electromagnetic waves, the combination of the signals will lead to an unpredictable variation of strength in the space.

The ground reflection model is the simplest model for representing multipath effects caused by the ground surface only. The model simulated the combination of two rays from the transmitter (see Figure 4.9), one from the line-of-sight and the other from the single reflection of the ground surface (Feuerstein *et al.*, 1994). The transfer functions of the rays are given by Equations (4.9) and (4.10). This model can be used to simulate RFID propagation process in the outdoor open areas.

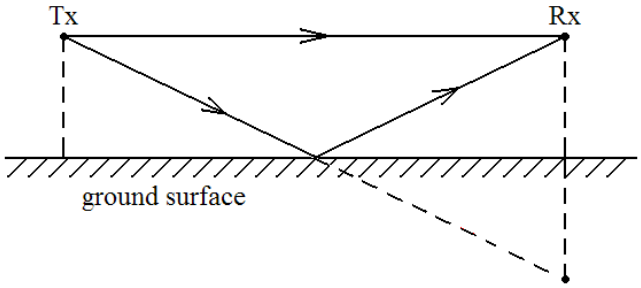

Figure 4.9 A schematic plot of the ground reflection model (Tx refers to the RFID tag; Rx refers to the RFID reader and the arrow lines refer to RF propagation paths.)

$$H(d) = \frac{\lambda}{4\pi \cdot d}(1 + \Gamma \cdot e^{-j2\pi\frac{\delta(d)}{\lambda}}) \qquad (4.9)$$

$$H(d_0) = \frac{\lambda}{4\pi \cdot d_0}(1 + \Gamma \cdot e^{-j2\pi\frac{\delta(d_0)}{\lambda}}) \qquad (4.10)$$

where,

j is the imaginary unit;

Γ is the reflection coefficient;

$\delta(d_0)$ is the path difference between the line-of-sight ray and the reflected ray at the reference distance d_0 (see Equation (4.11)); and

$\delta(d)$ is the path difference between the line-of-sight ray and the reflected ray at the distance d (see Equation (4.12)).

$$\delta(d_0) = \sqrt{(h_t + h_r)^2 + {d_0}^2} - \sqrt{(h_t - h_r)^2 + {d_0}^2} \qquad (4.11)$$

$$\delta(d) = \sqrt{(h_t + h_r)^2 + d^2} - \sqrt{(h_t - h_r)^2 + d^2} \qquad (4.12)$$

The path loss of the ground reflection model is given by:

$$PL(d) = PL(d_0) + 10 \cdot n \cdot \lg(\left|\frac{H(d)}{H(d_0)}\right|) \qquad (4.13)$$

Figure 4.10 shows a comparison of propagation models and outdoor observations in the open areas. The log-distance model and the ground reflected model are generated based on observations. It shows that the RSS observations are scattered around the estimated values of the log-distance model (red line) but have a significant drop between 2m and 3m. The variations of the RSS observations also

show a similarity with the ground reflected model since the conditions in the outdoor open areas are similar with that of the ground reflected model. However, in the metropolitan areas or indoors, the number of RF reflectors needed can be enormous and the conditions of the environments can be very complex. This will make the RSS estimation very difficult. Some techniques, such as using the site specific propagation model for simulating the RF reflections in complex environments, are discussed in Chapter 7.

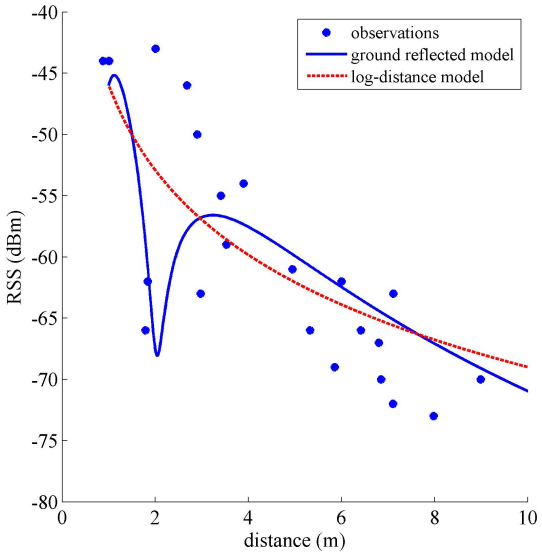

Figure 4.10 The comparison of the log-distance path loss model, the ground reflected model and the observations in outdoor environments

(The RSS is measured in the open areas outdoor within 10m from the transmitter. The log-distance path loss model (red line) and the ground reflected model (blue line) are generated based on the same dataset.)

4.3 CoO Positioning Algorithms in RFID Positioning

CoO positioning is one of the algorithms used in RFID systems. Passive RFID systems with less than a 3m reading range can be used as accurate landmarks, providing positioning references with conventional CoO algorithms. Active RFID systems with longer reading ranges provide approximate positions using large cell sizes (e.g. tens of metres) or positioning references like those available from passive RFID systems using small cell sizes.

4.3.1 Deterministic CoO Algorithm

The conventional CoO algorithm has been extensively studied by Fu and Retscher (2009b) using the identical RFID system that was used in this research. They placed seven tags along a 200-metre trajectory. The experiments showed that the deterministic CoO algorithm can achieve 20m accuracy by using the largest cell size in the RFID system (20m radius). This method is only suitable for application where high accuracy is not required. By setting the RSS threshold to -45dBm, metre-level reference positions can be achieved when the mobile user passes over certain tags. Fu and Retscher (2009b) also improved the continuity and accuracy of the RFID deterministic CoO algorithm by integrating it with INS and introducing the time-based CoO algorithm. In their time-based CoO algorithm, the exact time when the mobile user passes through the cell centre was determined by the mean time of the mobile user moving into the cell, rather than arbitrarily assigning the cell's central position to all of the epochs within the cell. By introducing this into deterministic CoO algorithms and using an RSS threshold of -45dBm, they claimed a 1m accuracy using the time-based CoO algorithm in the RFID positioning system. However, this algorithm is based on the assumption that the mobile user passes through a cell with a constant speed. It can only be applied in post processing since it requires all epochs of the mobile user in a certain cell to determine the exact time when the mobile user is at the cell centre. In addition, the compromise between the cell size and the accuracy is another problem in the deterministic CoO algorithms, as these values have to be fixed in a deterministic CoO positioning system.

4.3.2 Probabilistic CoO Algorithm

Rather than using a fixed solid cell in the deterministic CoO, an adjustable ring-shaped cell was developed using the probabilistic CoO (Zhu, 2008). The radius of the ring was determined by a RSS-based ranging model:

$$d_0 = \left\| p_0 - p_t \right\| = f(S_r(d_0)) + \varepsilon,\ \varepsilon \sim N(0, \sigma^2) \qquad (4.14)$$

where,

d_0 is the distance between the transmitter and the receiver;

p_0 is the position of the receiver;

p_t is the position of the transmitter;

$S_r(d_0)$ is the RSS at the distance, d_0, from the transmitter; and

ε is the zero-mean Gaussian noise in the ranging model with the variance, σ^2.

The probability of the mobile user's position is given by the joint probability of the mobile user at position p and the distance from the mobile user to the transmitter equals d_0,

$$P(p_0 = p) = P(p \cap (d_0 = d)) = P(p) \cdot P(d_0 = d) \quad (4.15)$$

$$P(d_0 = d) \sim N(d, \sigma^2) \quad (4.16)$$

where,

$P(p_0 = p)$ is the probability of the mobile user's position;

$P(p)$ is the probability of the mobile user at position p; and

$P(d_0 = d)$ is the probability of the distance from the mobile user to the transmitter equalling d_0.

Figure 4.11 shows a typical procedure of the probabilistic CoO algorithm. The result of this algorithm is given by the joint probabilities of the RFID-based and the external sensor based probabilities. The RFID-based probabilities, $P(d_0 = d)$, are calculated using the RSS-based ranging model. The probabilistic distribution is like a crater, where the centre is the position where the RFID tag is detected. The peak is a ring with the centre of the RFID tag and the radius of the estimated distance is determined according to the RSS-based ranging model. The probabilities decrease along both normal directions from the peak according to the uncertainties of the ranging model. External sensor based probabilities, $P(p)$, are determined by sensors, such as PDR, INS or GPS. Its peak is the position estimated by external sensors and the slope of the decrease depends on the measurement uncertainties of these sensors.

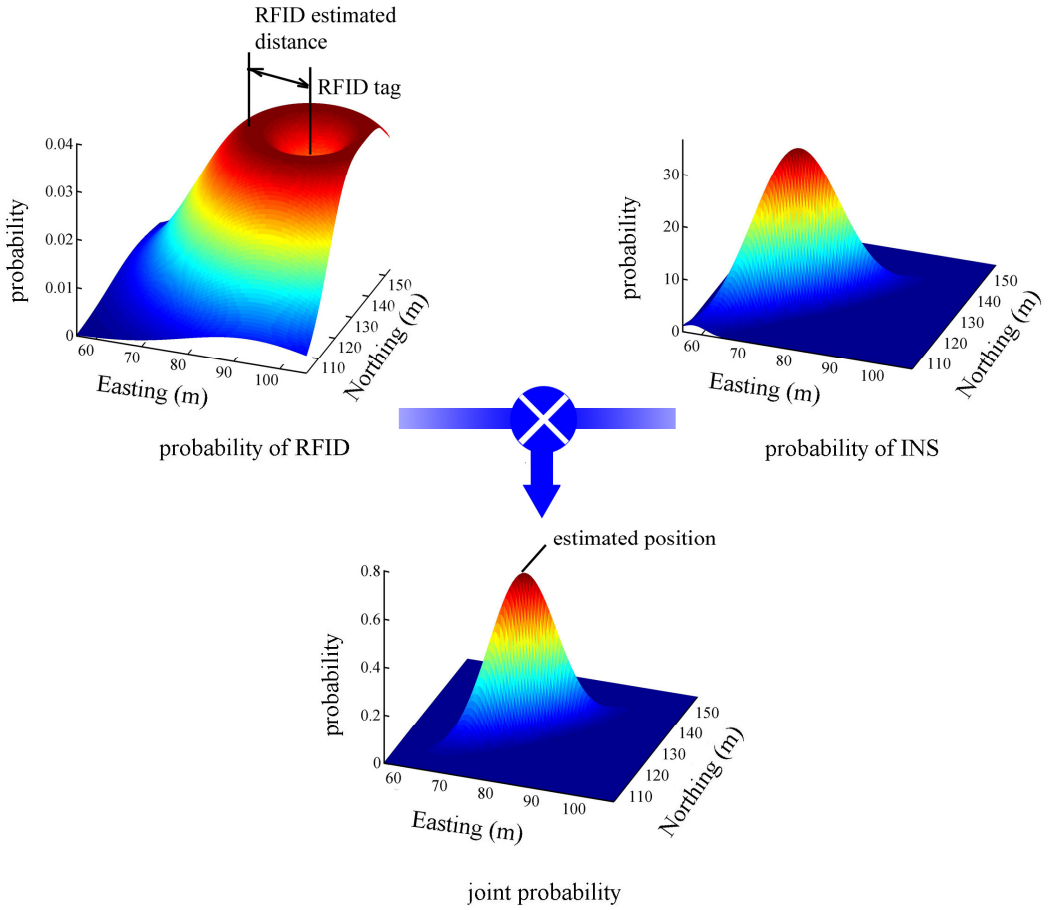

Figure 4.11 A schematic plot of the probabilistic CoO algorithm (The probability of RFID probabilistic CoO algorithm is a round-shape distribution with the radius of the distance estimated by RFID and centre of the RFID tag. The position is determined by the joint probability with the observations from other sensors, such as INS.)

The advantage using the probabilistic CoO is that this approach does not identify the mobile user's position as being at the centre of the cell. However, it estimates the probability of the distance between the rover and the centre of the cell based on RSS measurements (Zhu, 2008). The improvement provides an adjustable cell in real-time positioning. It solves the problem between the cell size and the accuracy in the deterministic CoO algorithm. However, it can not be implemented using RFID stand-alone, as some external sensors are required for generating joint probabilities.

4.3.3 Evaluations of RFID CoO Algorithms

An evaluation of RFID CoO algorithms was conducted in Yarra Bend Park, in Melbourne, Australia. Seven RFID tags were placed in an open area with different intervals. The positions of the tags were accurately measured using a *Trimble R8*

RTK system. This RTK system was also used as a reference to evaluate the RFID positioning algorithms (see Figure 4.12).

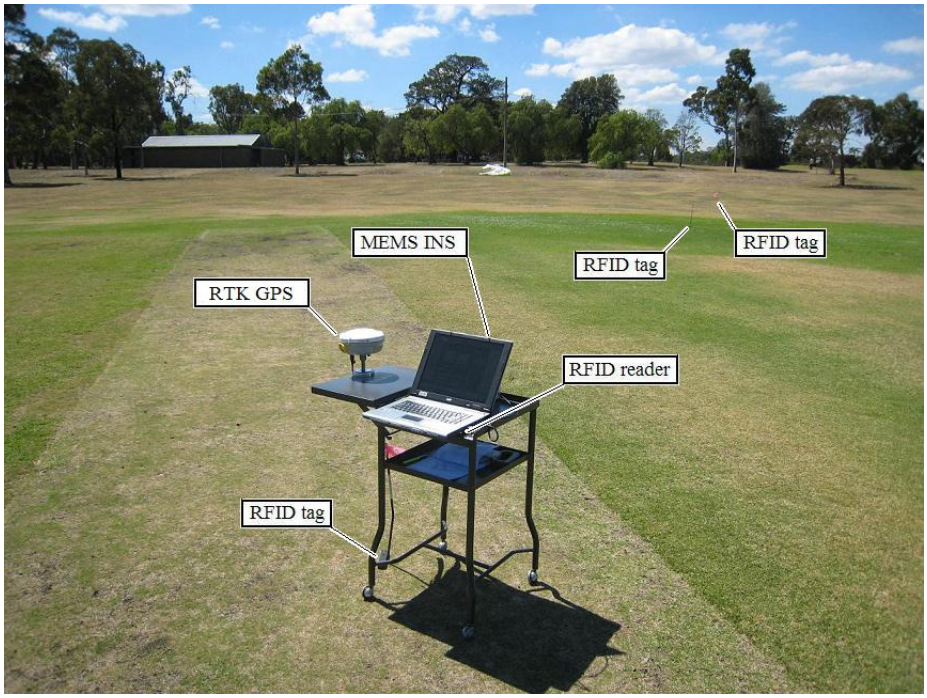

Figure 4.12 The experiments for RFID CoO positioning
(The experiments were conducted in open areas in Yarra Bend Park, in Melbourne, Australia. One MEMS INS, one RFID reader and seven RFID tags were used for the experiments and RTK GPS was used as a reference system.)

The comparison of the RFID deterministic CoO with different cell sizes and the comparison of the RFID deterministic CoO and the probabilistic CoO algorithms were conducted. The cell sizes were defined by RSS thresholds. Four thresholds (-50dBm, -60dBm, -70dBm and -80dBm) were selected with reference to small and large cells. The higher the threshold, the smaller the cell size. The results are provided in Table 4.4. It indicates that there is a compromise between the accuracy and the accessibility of using RFID deterministic CoO in an area having a fixed number of RFID tags. Where the cell size is biggest (threshold=-80dBm), the largest number of observations are accepted, but the RMSE is only 9.7m. With the smallest cell size (threshold=-50dBm), the accuracy is as high as 2.6m, but only six observations were possible. The comparison between the deterministic CoO and the probabilistic CoO shows that the probabilistic CoO improves the accessibility of the observations, which is as same as the largest number in deterministic approaches. However, the

probabilistic approach cannot provide standalone positions. Further analysis of the accuracy of the probabilistic approach is provided in the following chapter.

Table 4.4 Comparison of the stand-alone CoO
(The probabilistic CoO cannot provide the position determinations stand-alone. Its accuracy is analysed in Chapter 5.)

Method	RMSE (m)	Number of Observations
Deterministic CoO (threshold=-80dBm)	9.7	33
Deterministic CoO (threshold=-70dBm)	5.6	23
Deterministic CoO (threshold=-60dBm)	2.9	9
Deterministic CoO (threshold=-50dBm)	2.6	6
Probabilistic CoO	N/A	33

4.4 Trilateration Algorithms in RFID Positioning

The first continuous positioning algorithm investigated in the RFID positioning systems is trilateration. The mobile user's position is estimated according to known positions of the RFID tags and the distances between the tags and the reader. The accuracy of this algorithm is highly dependent on the accuracy of distance estimation. According to experiments (Fu and Retscher, 2009a), this accuracy in the RSS-based RFID positioning system is significantly affected by the ranging model and also the effects of the surrounding environment.

4.4.1 Ranging Models in RFID Positioning

The distance between the transmitter and receiver can be estimated using the RSS by inversing the path loss model (see Equation (4.17)), which represents the theoretical relationship between these two variables:

$$\hat{d} = d_0 \cdot 10^{\frac{S_r(d_0) - S_r(d)}{10 \cdot \gamma}} \qquad (4.17)$$

where,

$\hat{d}$ is the estimated distance from the transmitter to the receiver;

d_0 is the reference distance;

$S_r(d_0)$ is the RSS at the reference distance;

$S_r(d)$ is the observed RSS; and

γ is the path loss exponent.

Table 4.5 The values of the path loss exponent in different environments according to experiments undertaken.

Environments	Path Loss Exponent
Corridor	0.6992
Outdoor	2.3313

The experiments were conducted in both outdoor and indoor environments. The parameters of the inverse path loss model, such as d_0 and γ, were estimated using least square adjustments according to observations. The results showed that observations in outdoor environments present a clear logarithmic relationship with the path loss exponent 2.3313 (see Table 4.5). The 90% confidence level of distance estimation varies between 5.05m and 5.35m using the inverse path loss model in outdoor experiments (see Figure 4.13). In contrast, when using the inversed path loss model, the value varies between 32.15m and 32.26m in indoor experiments (see Figure 4.14).

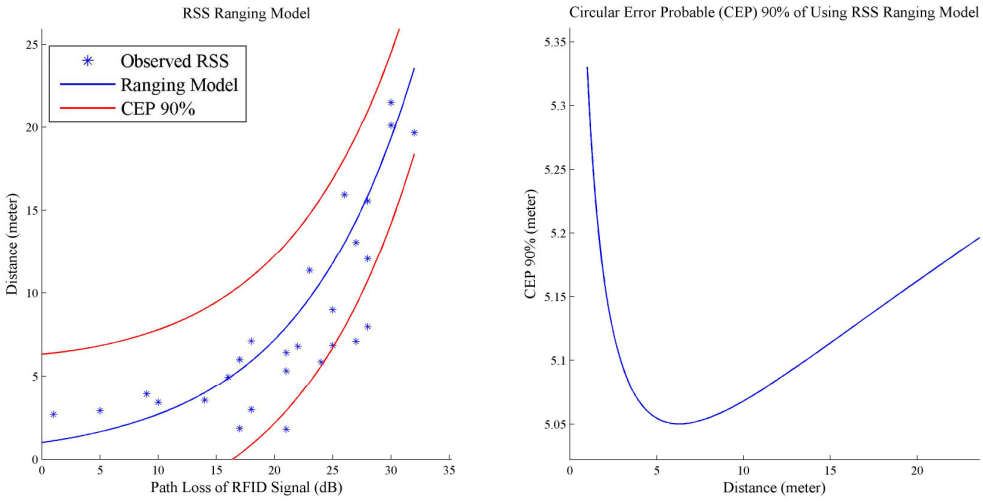

Figure 4.13 An inverse path loss ranging model based on observations in open areas and its 90% confidence level (The plot at left shows the inversed path loss ranging model (blue line), which was established based on observations (blue dots) in open areas and its 90% confidence interval (red lines). The plot at right shows the 90% confidence level of the estimated distance changing with distance. It varies between 5.05m and 5.35m.)

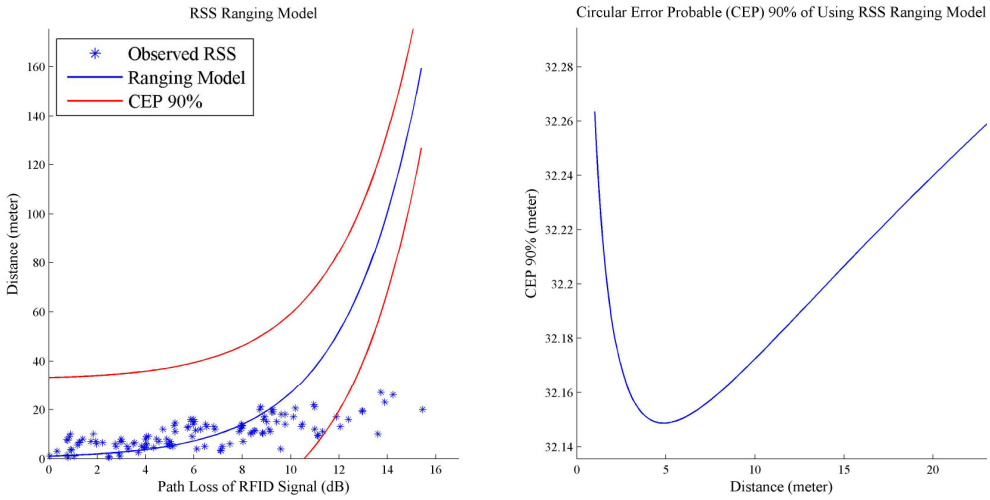

Figure 4.14 An inverse path loss ranging model based on indoor observations and its 90% confidence level.

(The plot at left shows the inverse path loss ranging model (blue line), which was established based on the observations (blue dots) in indoor corridors and its 90% confidence interval (red lines). The plot at right shows the 90% confidence level of the estimated distance changing with distance. It varies between 32.15m and 32.26m.)

The error analysis indicates that the inverse path loss model gives larger errors in indoor environments than in outdoor environments. This is mainly due to the reflections of RF signals from indoor walls, which form a structure called a waveguide. This structure forces the spherical RF signals to propagate in particular directions. For example, the signals will mainly propagate in the two directions along an indoor corridor. Path loss trends and RSS variations are both affected.

Regression models can sometimes provide more accurate estimations than inverse path loss models, since the presentation of the model can be specified according to environments. A general presentation of the regression model is shown in Equation (4.18):

$$\hat{d} = f(S_r(d)) \qquad (4.18)$$

where $f(\bullet)$ is the regression model to convert the path loss, $S_r(d)$, to the distance, d.

Figure 4.15 shows the regression model for indoor RSS-based distance estimation. A linear model is used to estimate the range between the transmitter and the receiver (see Equation (4.19)).

$$d = c \cdot S_r(d) + \varepsilon,\ \varepsilon \sim N(0, \sigma^2) \qquad (4.19)$$

where,

c is a coefficient of the linear model; and

ε is a zero-mean Gaussian noise with the variance, σ^2.

The results show that at a 90% confidence level the error of the estimated distance varies between 6.74m and 6.86m when using the linear regression model. This is about five times more accurate than using the inversed path loss model for the same dataset in indoor environments.

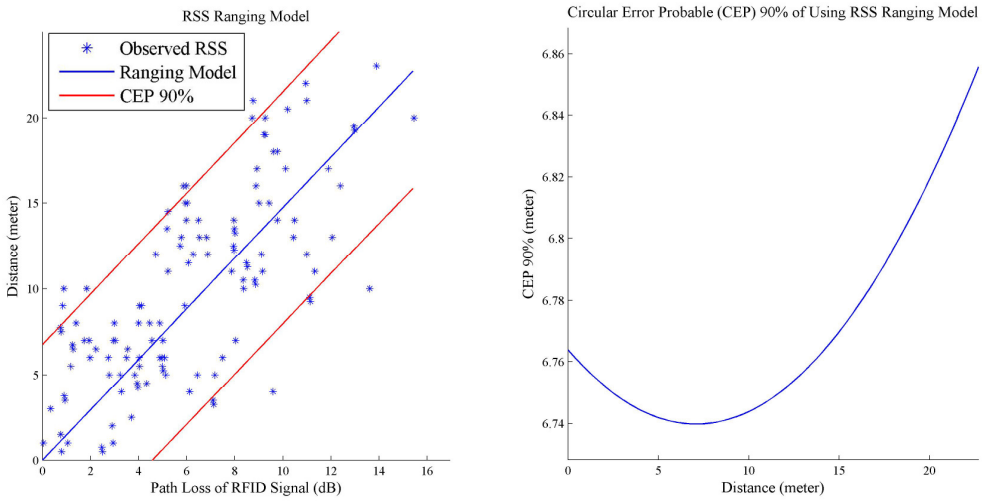

Figure 4.15 A regression ranging model based on the observations indoor and its 90% confidence interval

(The plot at left shows the regression ranging model (blue line) established based on observations (blue dots) in indoor corridors and its 90% confidence interval (red lines). The plot at right shows the size of the 90% confidence interval changing with distance. The errors change between 6.74m and 6.86m.)

4.4.2 Multipath Effects in RFID Positioning

Another detrimental effect on the RSS-based trilateration method is the variations of RSS caused by multipath effects. These effects can cause the non-monotonous of the relationship between the distance and the RSS and make trilateration impracticable for the RSS-based techniques. The effects can be significant in indoor environments where many reflectors are used. Even in open areas, it can also cause

fluctuations of RSS in areas near the transmitter. The range of affected areas in open areas can be simulated using the ground reflection model.

According to the simulations (see Figure 4.16), in open areas the variation of RSS caused by multipath effects only occurs in the areas near the transmitter. There is always a distance between the transmitter and the receiver after which the relationship between the distance and the RSS is monotonous. The range of the area, in which the RSS fluctuates, varies according to the different combinations of the transmitter and the receiver heights. Generally, the higher the device mounting, the larger the area of RSS fluctuation.

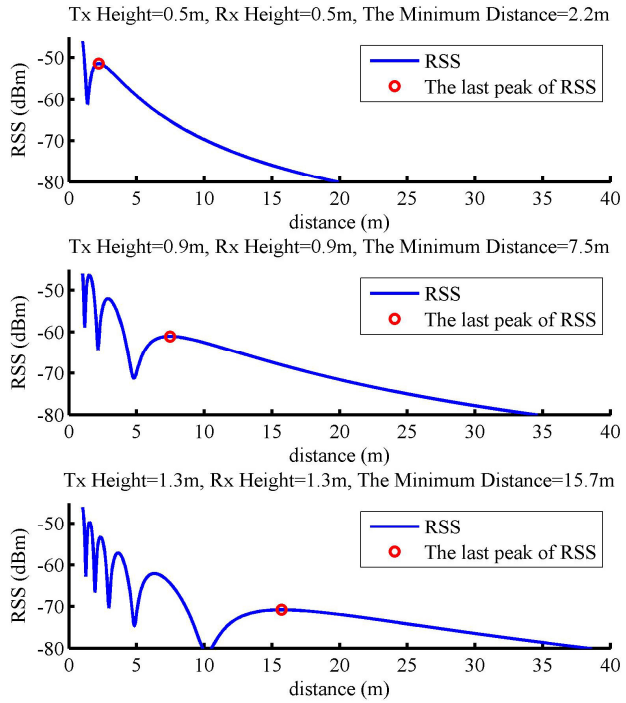

Figure 4.16 A schematic plot of the ground reflection model simulated RSS (This experiment simulated the RSS in the open area where the RF signal is only reflected by the ground. The RSS fluctuates in the areas near transmitters due to the RF signal reflections. The frequency of this fluctuation decreases with the increase of the distance from the transmitter, so there is a point after which the RSS decreases monotonously.)

Further calculations were delivered to represent the variation of this range outside which the trilateration can be applied in outdoor open areas. Figure 4.17 shows a corn-shaped surface of the value of this range according to the different combinations of the transmitter and receiver heights, which usually appear in personal positioning applications. In the RFID positioning system using 915MHz RF

signal, the range can be up to 37m when a transmitter and a receiver are both at 2m above the ground. The RSS fluctuation can theoretically be avoided if the transmitter and receiver are mounted lower than 0.3m above the ground. In normal cases, where transmitters and receivers are mounted at the waist level (e.g. 0.9m above the ground), the range is 7.5m. The simulations indicated that multipath effects can greatly affect the performance of RSS-based trilateration algorithm. Theoretically, this can be avoided in outdoor open areas if the devices are mounted very low. However, in practice, this causes some wiring and installation problems. In indoor environments this creates more serious problems, where the presence of more reflective objects, results in multipath being more detrimental to the accuracy of positioning, which cannot be completely avoided.

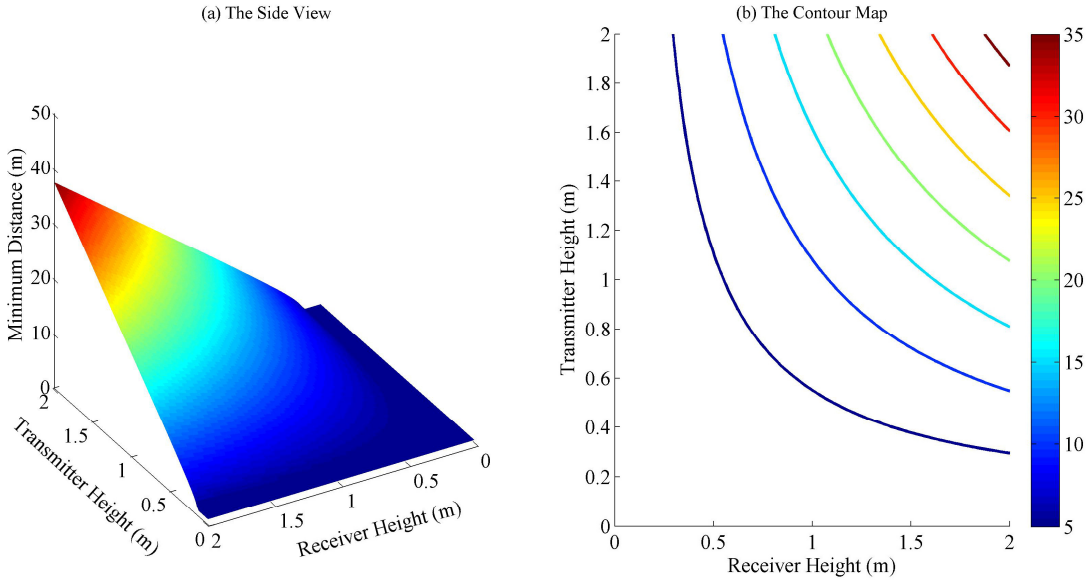

Figure 4.17 The minimum distances for the monotonous RSS-distance relationships in open areas simulated by the ground reflection model

(The surface (at left) refers to the distances after which there exist monotonous relationships between the RSS and the distance with different combinations of transmitter and receiver heights in a ground reflection context. The contour plot (at right) is the top view of this surface.)

4.4.3 Analysis of the Performance Using Trilateration in RFID Positioning

The experiments and simulations conducted indicate that selecting appropriate ranging models and minimising multipath effects are the two critical aspects in RFID trilateration. However, both of these aspects are challenging in practice.

Some research undertaken indicated that there is no universal model for the RSS-based distance estimation that can be readily applied (Fu and Retscher, 2009b). At times, the regression models will perform better than the inverse path loss models (Mok and Retscher, 2007). This is because RSS is affected significantly by an environment. The distribution of RSS is dependent on an environment. Regression models, according to RSS samples at a site, can include more specific environmental effects into the estimation than when theoretical models are used. Fu (2008) developed an RFID trilateration algorithm for static positioning. The regression ranging model and the calibration procedure are used to estimate distances between the RFID reader and tags. Four directional observations, each for one minute, are taken to determine positions. She claimed sub-metre level accuracy. However, in dynamic positioning, multi-directional observations associated with long observation times for every epoch, are not practical. Here, positioning accuracy will be lower. The study conducted in this research indicates that the variation of the RSS based on a single-directional short-term (1sec) observation is very large. Even using appropriate models, a 90% confidence interval can be around 6m, which is not suitable for trilateration algorithms.

Another detrimental effect is multipath. According to experiments (Fu, 2008; Li, 2006; Mok and Retscher, 2007; Zhang *et al.*, 2008) it is very significant and cannot be avoided. Simulations indicate that even on an ideal environment (e.g. open areas with no obstructions and only one significant reflection) this effect can still cause the non-monotonous relationships between the RSS and the distance. Simulations also indicate that with normal setups for personal positioning applications (waist mounted sensors) the distance estimation is better when implemented 7.5m away from the transmitter, so that effects caused by multipath can be minimised. In indoor environments, it is even harder to mitigate these effects.

In summary, the RFID trilateration algorithm can only be used for static positioning applications due to the limitations of ranging models and the effects of multipath, which are challenging in dynamic positioning applications.

4.5 Location Fingerprinting Algorithms in RFID Positioning

Another type of RSS-based continuous positioning algorithm, which is more robust against the effects from environments, is the location fingerprinting algorithm. This algorithm uses the match between prior RSS-distribution and real-time

measurements to determine the mobile user positions. The advantage of this algorithm is that it considers environmental effects prior to RSS-distribution. However, to generate the prior RSS-distribution always requires tremendous workload.

4.5.1 RFID Location Fingerprinting Algorithms for 2-D Indoor Positioning

RFID location fingerprinting experiments in 2-D indoor environments were conducted in an 8m×10m room at RMIT University. There are a number of windows with metal frames on the side walls, two whiteboards on the front wall and a few hydraulic pipes on the ceiling (see Figure 4.18). The RFID reader was connected to a laptop and placed on a trolley with the antenna height at 1.2m. 16 RFID tags were placed on the walls and ceiling of the room (see Figure 4.19).

In the training phase, both the means and variances of RSS were measured using 100 scans at each node on a 1m×1m grid (refer to Chapter 3) in static environments. The fingerprinting maps were constructed using observations and refined into the 0.1m×0.1m grid by the simple Kriging interpolation method.

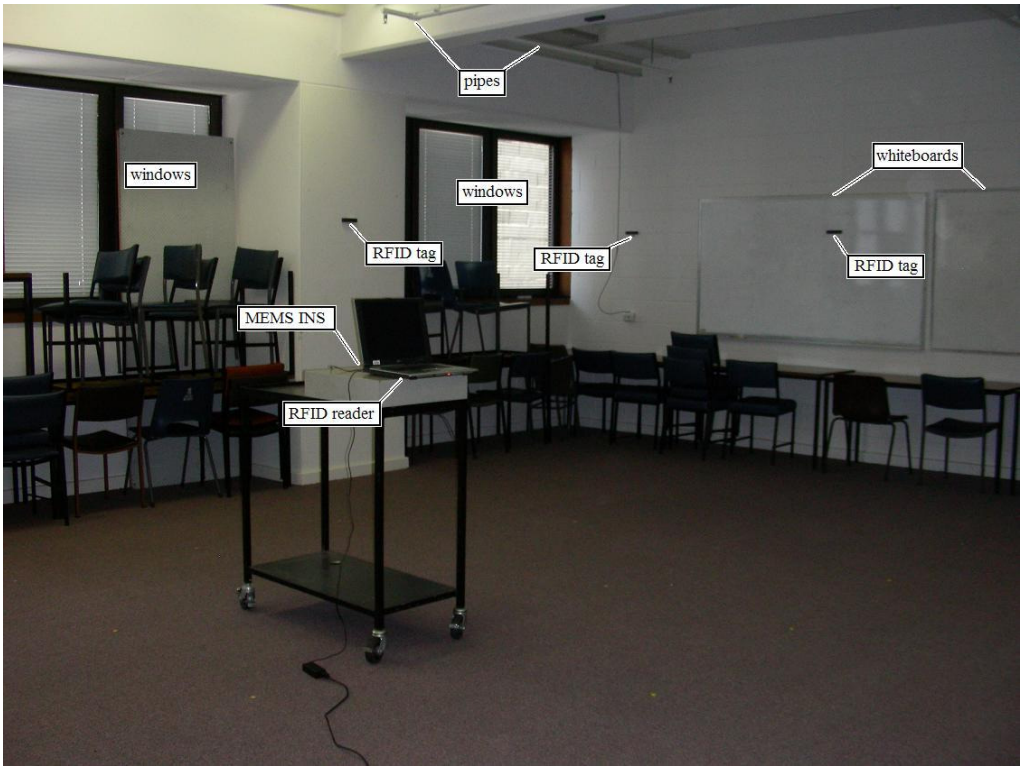

Figure 4.18 The experiments for RFID indoor positioning
(The experiments were conducted in an 8m × 10m classroom in the city campus of RMIT University, Melbourne, Australia. 16 RFID tags were mounted on the walls and ceiling.)

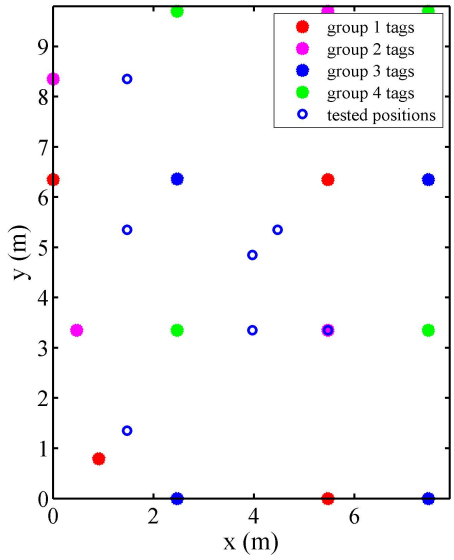

Figure 4.19 The site setup for the 2-D RFID indoor positioning experiments

(Sixteen RFID tags were used to cover the experimental room. They are divided into four groups (identified by colours) and scanned group by group to avoid conflictions. Eight tested positions in the centre, side and corner of the room are used for the evaluations respectively.)

Both the deterministic approach and the probabilistic approach were investigated in the experiments conducted. The RFID tags were separated into four groups for scanning. In every scan only one group of RFID tags were used so as to avoid scanning collisions and the time prolonged. The RSS were measured at eight positions in the room. Eight scans were taken at every point. The results of the experiments show that the positioning RMSE of the location fingerprinting algorithms in the room varies from 3.5m to 4.4m (see Figure 4.20). Positioning accuracy can be improved by increasing the observations obtained from different RFID tags. However, increasing the number of observations from the same tags does not significantly improve the accuracy. In addition, there is a minimal difference between the deterministic approach and the probabilistic approach in static environments.

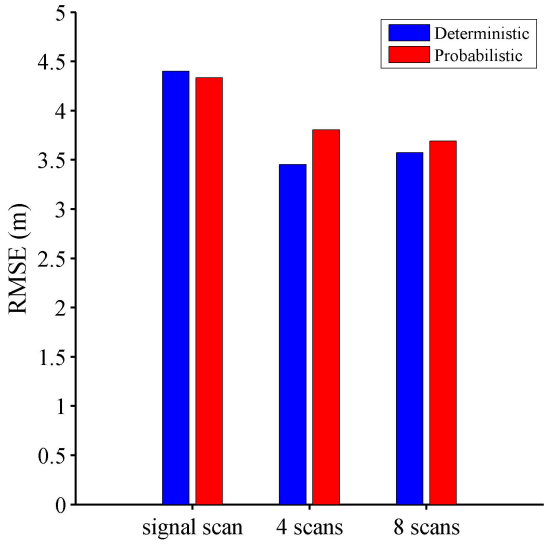

Figure 4.20 RMSE of the RFID 2-D static indoor positioning tests (Both the deterministic approach and the probabilistic approach of location fingerprinting algorithms were used. Single scan: RSS from tags in one group were used for each position determination; 4 scans: RSS from all the 16 tags (each tag scanned once) were used for each position determination; 8 scans: RSS from all the 16 tags (each tag scanned twice) were used for each position determination.)

4.5.2 RFID Location Fingerprinting Algorithm for 3-D Indoor Positioning

The experiments of RFID location fingerprinting algorithms for 3-D indoor positioning were conducted in a stairway between different levels in a building at RMIT University. Eight RFID tags are placed on the walls (see Figure 4.21) to cover the three levels of the experimental areas. Six tested positions on the level 10, level 11 and the intermedia level between 10 and 11 are used for evaluating the algorithms (Zhang *et al.*, 2008).

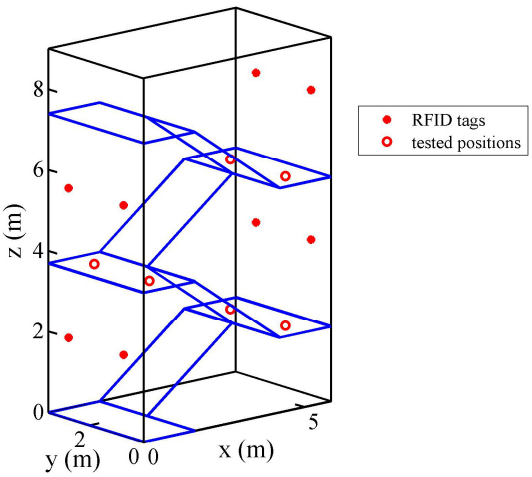

Figure 4.21 The site setup of the 3-D RFID indoor positioning experiments
(Eight RFID tags are used to cover two levels in the stairway. Six tested positions were used for the static positioning evaluations.)

The fingerprinting maps in the training phase were constructed using observations of RSS means and variances at twelve positions along the stairway. The maps were then interpolated into the $1\text{m} \times 1\text{m} \times 1\text{m}$ uniform grid using simple Kriging interpolations. In addition, the RSS was measured in four directions: 0˚, 90˚, 180˚ and 270˚, so as to evaluate the effects from directional patterns on the location fingerprinting algorithms (see Figure 4.22).

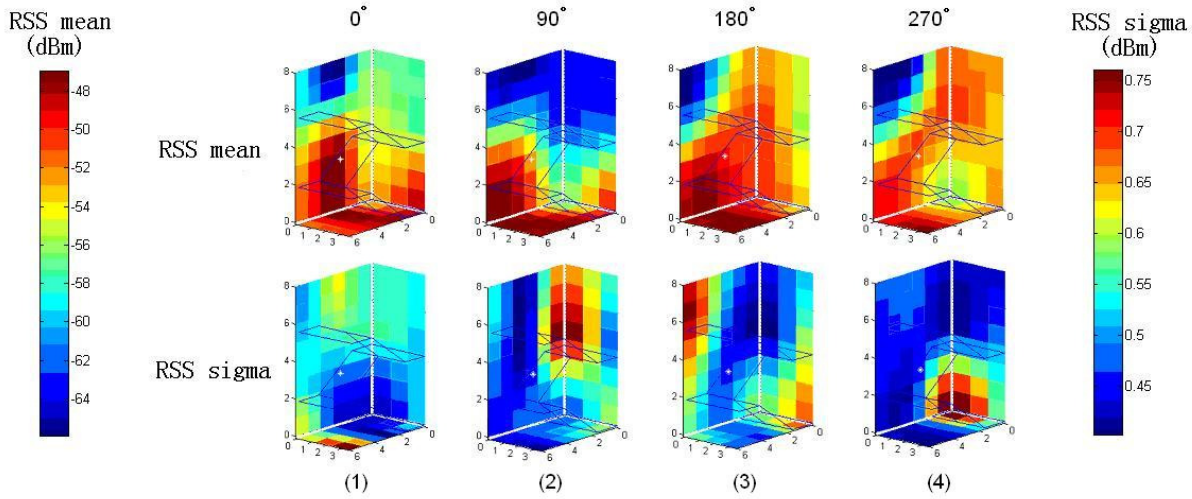

Figure 4.22 A schematic plot of the training phase measurements in the stairway
(The upper four plots show the RSS from tag 0.200.168.210 measured by a RFID reader with different orientations. The lower four plots show the sigma values of the RSS measured with different orientations respectively.)

The results (see Figure 4.23 and Figure 4.24) show that a positioning accuracy better than 2.5m can be achieved using 3-D location fingerprint algorithms. By using multiple scans both in number and in directions, accuracy can be improved to 0.8m. It also indicates that the accuracy can be improved significantly by using the deterministic approach rather than the probabilistic approach, with increased observation numbers in static environments. This is due to the lower sensitivity to the variations of the RSS measurements in the probabilistic approach than those in the deterministic approach. This low sensitivity in the probabilistic approach not only makes it less prone to dramatic RSS variations in dynamic environments, but also less sensitive to the subtle changes of RSS in multiple observations for static positioning.

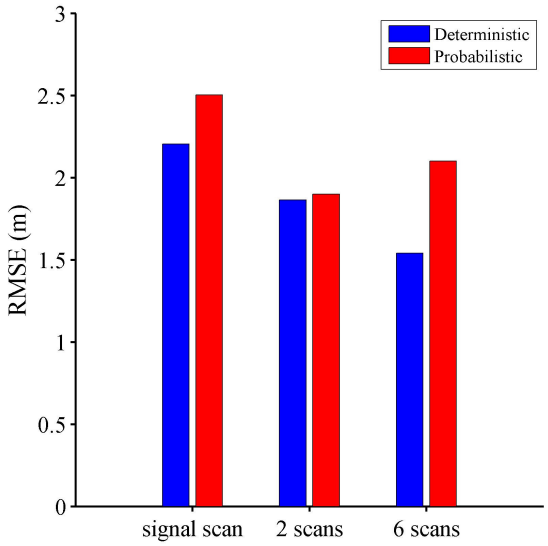

Figure 4.23 RMSE of the RFID 3-D static indoor positioning tests (Both deterministic and probabilistic approaches of location fingerprinting algorithms are used. Single scan: RSS from tags in one group (4 tags) are used for each position determination; 2 scans: RSS from all the 8 tags (each tag scanned once) are used for each position determination; 6 scans: RSS from all the 8 tags (each tag scanned three times) are used for each position determination.)

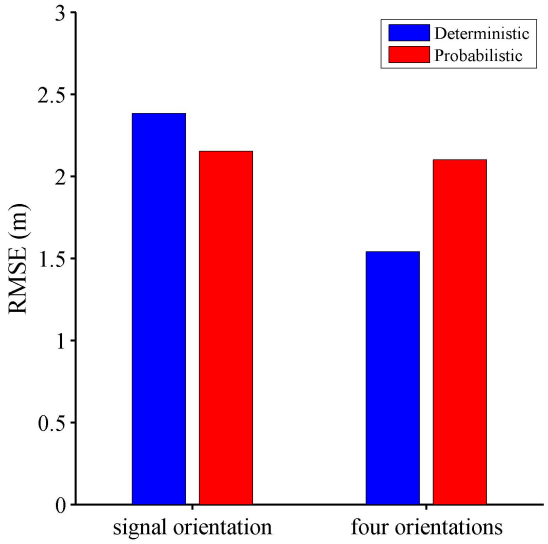

Figure 4.24 RMSE of the RFID static indoor positioning tests with multi-direction observations

(Both deterministic and probabilistic approaches of location fingerprinting algorithms are used. Single orientation: the observation from only one orientation is used for each position determination; four orientations: the observations from four orientations (0˚, 90˚, 180˚ and 270˚) in the arbitrary coordinates are used for each position determination.)

4.6 Comparison of RFID Positioning Algorithms

When comparing standalone RFID positioning algorithms, the deterministic CoO algorithm is the simplest positioning algorithm and less prone to environmental effects. However, the major limitations of this algorithm are the lack of capability to provide continuous positions and the compromise between the coverage size and positioning accuracy. In contrast, the probabilistic CoO algorithm developed overcomes the limitation of the conventional CoO by introducing an adjustable cell according to RSS-based distance estimation. However, it cannot be implemented on its own. External observations for generating the joint probabilities are required. The trilateration algorithm is one of the algorithms which can provide continuous positions with a stand-alone RFID system. However, it faces a number of detrimental effects, such as the accuracy of the path loss model, the effects from the signal directional patterns and the multipath effects. These detrimental effects make the trilateration algorithm site-specific. The regression path loss models based on RSS samples at

the site and on-line calibrations are required to achieve the metre-level accuracy (Fu, 2008). However, RSS is not stable in dynamic environments. This makes the regression path loss models and on-line calibrations unreliable in dynamic positioning. Consequently, it limits the use of RSS-based trilateration algorithms in practice. According to this research, the most practicable algorithm for standalone RFID positioning is the location fingerprinting algorithm. In contrast to the trilateration algorithm, the location fingerprinting algorithms tackles the problems by considering most environmental effects with previously measured RSS distributions (fingerprinting maps). Normally, a positioning accuracy better than 5m can be achieved using the standalone RFID location fingerprinting algorithm. But, the major limitation is the misalignment of RSS distributions between the training phase and the positioning phase caused by environmental dynamics. This research, as well as others (Fu and Retscher, 2009a), indicate that positioning accuracy can be improved by using the probabilistic approach, including observations from multiple directions and increasing the number of observations. However, collecting multiple observations is not practicable for dynamic positioning, as mobile user positions need to be estimated in real-time for dynamic positioning. There are no adequate epochs for collecting multiple observations at each position for the mobile user. Therefore, the probabilistic approach of the location fingerprinting algorithm is optimal for the RFID dynamic positioning.

4.7 Summary

This chapter provided a brief history of RFID positioning developments and reported investigations into the detrimental effects on RFID positioning (limitations of the RSS-based ranging models, RSS directional patterns and the multipath effects) and the development of standalone RFID positioning algorithms. From experimental results it shows that it is challenging to use trilateration algorithms based on tag-reader distances in RFID dynamic positioning due to the limitations of the RSS-based ranging models and the detrimental effects from the environments. In contrast, CoO algorithms are less prone to detrimental effects and can provide reliable discrete positions. The probabilistic CoO algorithm developed is superior to the deterministic CoO algorithms as it solves the problem between cell size and accuracy in the conventional CoO algorithms by using adjustable cells. For RFID continuous positioning, location fingerprinting algorithms can be used. A static positioning accuracy of 4.4m and 2.5m can be achieved in rooms and in stairways respectively.

The accuracy can be further improved by increasing the number of static positioning observations. The analysis showed that the probabilistic approach of the location fingerprinting algorithm is less prone to the noisy measurements in dynamic environments and it is optimal for RFID dynamic positioning.

The next chapter discussed the feasibility of improving positioning accuracy by using multi-sensor integrated techniques.

Chapter 5 Multi-sensor Integrated Positioning

The concepts of INS and DR have been used for centuries, from conventional gimballed INS to fiber-optic gyroscopes and resonating beam accelerometers, then to the MEMS sensors. As development occurred, the cost and size of the systems were dramatically reduced (Barbour and Schmidt, 2001). MEMS sensors in coin-sized chips, costing around AUD 10, can be widely used in personal positioning applications, for example, monitoring a human's daily activities for physiological research (Najafi *et al.*, 2003). The high noise level and fast drift in these sensors can be constrained by sensor integration (Eskin, 2006; Li D *et al.*, 2008), such as GPS.

This chapter introduces these techniques and the integrations with RFID positioning techniques for indoor personal positioning. In the first part of this chapter, the theoretical analyses and experiments covered include:

(a) stand-alone MEMS INS;

(b) stand-alone PDR;

(c) integrated GPS/INS; and

(d) integrated GPS/PDR.

These were conducted to enable the selection of a technique to integrate with an RFID system for multi-sensor integrated indoor personal positioning. In the remainder of the chapter, other experiments for testing RFID-based multi-sensor integrated positioning algorithms developed are covered. These are:

(a) integrated INS/RFID deterministic CoO positioning;

(b) integrated INS/RFID probabilistic CoO positioning;

(c) 2-D integrated INS/RFID location fingerprinting positioning; and

(d) 3-D integrated INS/RFID location fingerprinting positioning.

5.1 Existing Applications Using INS and PDR for Personal Tracking and Indoor Positioning

Early research using the MEMS sensors for personal tracking and indoor positioning were about PDR (Judd, 1997). In the early 2000s, a series of research activities were conducted related to foot-mounted PDR, due to its easy implementation and

relatively slower drift speed, compared to INS (Foxlin, 2005; Jirawimut *et al.*, 2003; Stirling *et al.*, 2005). In 2008, Tomé and Yalak (2008) significantly improved orientation estimations in PDR using an adaptive EKF developed. In the same year, Beauregard *et al.* (2008) decreased the post processing positioning error to the sub-metre level by using a backtracking particle filter, where a long-range geometrical constraint was applied according to the cooperation between maps and historical trajectories.

In contrast, MEMS INS is not widely used in personal tracking systems as the stand-alone MEMS INS drifts too quickly to be applied. However, with careful design and the application of frequent constraints, the performance of MEMS INS can be greatly improved. Krach and Roberston (2008) developed a foot-mounted INS which was constrained by the map matching method using particle filters. The technique achieved metre-level accuracy for personal positioning indoor, but the convergence procedure takes over 1 minute to perform. As well, Williams *et al.* (2009) developed another algorithm for personal positioning using INS. Their experiments showed that the algorithm that integrated the conventional INS and the gyroscope-free INS could provide better results than the stand-alone INS algorithm for personal positioning.

5.2 Introduction to INS and PDR

INS and PDR techniques for personal positioning are similar to conventional techniques that use inertial sensors, but they contain more significant noise generated by MEMS sensors and the general dynamics from mobile users. This section provides information on positioning principles and the error models related to MEMS INS and PDR respectively.

5.2.1 Principles and Error Models related to INS

The principles of INS navigation has been developed over many years. INS estimates relative position using acceleration and rotation rates measurements based on a series of physical principles.

5.2.1.1 Navigation

Acceleration measured by INS on the Earth's surface is a combination of the system's acceleration, gravity and the acceleration caused by the rotation of the

reference frame with respect to the inertial frame (Titterton and Weston, 2004). Accordingly, the navigation equation in the navigation frame is given by the following Equation (5.1).

$$\dot{v}^n = \underset{\sim}{C}_b^n \cdot f^b - (2 \cdot \omega_{ie}^n + \omega_{en}^n) \times v^n + g^n \qquad (5.1)$$

where,

$\dot{v}^n$ is the acceleration in the navigation frame;

$\underset{\sim}{C}_b^n$ is the Direction Cosine Matrix (DCM) transforming the vector from the body frame to the navigation frame;

f^b is the acceleration in the body frame;

ω_{ie}^n is the rotation rate vector of the Earth frame with respect to the inertial frame;

ω_{en}^n is the rotation rate vector of the navigation frame with respect to the Earth frame;

v^n is the velocity in the navigation frame; and

g^n is the gravity in the navigation frame.

For the short-term navigation, the effects from the Earth rotation are so small that these terms can be safely ignored. The navigation equation is simplified as Equation (5.2)

$$\dot{v}^n = \underset{\sim}{C}_b^n \cdot f^b + g^n \qquad (5.2)$$

For the attitude determination, the DCM is updated according to the rotations (see Equation (5.3)).

$$\underset{\sim}{C}_k = \underset{\sim}{C}_{k-1} \cdot \exp[\sigma\times] \qquad (5.3)$$

where,

$\underset{\sim}{C}_k$ is the DCM at epoch k;

$\underset{\sim}{C}_{k-1}$ is the DCM at the previous epoch;

$\exp[\bullet]$ is the exponential term of the matrix; and

$\sigma\times$ is the skew symmetric matrix (see Equation (5.4)).

$$\sigma\times = \begin{bmatrix} 0 & -\delta\psi & \delta\theta \\ \delta\psi & 0 & -\delta\phi \\ -\delta\theta & \delta\phi & 0 \end{bmatrix} \quad (5.4)$$

where,

$\delta\phi$ is the change of the pitch angle between two epochs;

$\delta\theta$ is the change of the roll angle between two epochs; and

$\delta\psi$ is the change of the yaw angle between two epochs.

5.2.1.2 Calibration

In this research the measurements of acceleration and rotation rates come from the MEMS sensors, including the *Kionix KXM52* tri-axes accelerometer (Kionix Inc., 2006), *Analog Devices ADXRS300* gyroscopes (Analog Devices Inc., 2004) and *Hitachi Metals HM55B* magnetometers (Hitachi Metals Ltd., n.d.). These sensors output the binary data from a serial port so that calibration is needed to enable the transformation of these data into appropriate units (see Equation (5.5)).

$$DN = \alpha \cdot REF + \beta \quad (5.5)$$

where,

DN is the digital outputs from the sensor;

REF is the reference value;

α is the scale factor of the linear transformation; and

β is the offset of the linear transformation.

A simplified calibration method was developed for MEMS INS sensors, based on the KF (see Chapter 3). Unlike the highly-accurate calibrations that can be done using accurate and costly equipment, such as rate table and vibration table in laboratory settings, a simplified method is based on gravity and the geomagnetic field (see Figure 5.1).

For accelerometers, the vertical component of gravity is used as a reference. The value is defined as being 9.8m/s^2 instead of the value obtained from the accurate gravity model, as Equations (5.6) and (5.7) (Titterton and Weston, 2004). This is because accelerometers used in this research have a resolution in the order of 10^{-1},

but the effects from latitude and height on gravity are both in the order of 10^{-3} for personal navigation near the Earth's surface. Therefore these subtle terms can be safely ignored.

$$g(0) = 9.780318 \cdot (1 + 5.3024 \times 10^{-3} \cdot \sin^2 L - 5.9 \times 10^{-6} \cdot \sin^2 2 \cdot L) \quad (5.6)$$

$$\frac{dg(0)}{dh} = -0.0000030877(1 - 1.39 \times 10^{-3} \sin^2 L) \quad (5.7)$$

where,

$g(0)$ is the gravity at the sea level;

L is the latitude;

$dg(0)$ is the change of the gravity from the sea level; and

dh is the change of the height from the sea level.

For magnetometers, the vertical component of the geomagnetic field can be used as a reference. This value is estimated by the Australian Geomagnetic Reference Field (AGRF) model, a mathematical model used to estimate the geomagnetic field according to position and time in Australia and some surrounding areas. This model has been improved and updated every five years since its deployment in 1985. This has been done to track as accurately as possible unpredicted variations of the geomagnetic field, caused by magnetic storms, the rotation of the Earth, the Moon and the Sun (Luyendyk, 1997) (Geoscience Australia, 2005). For implementations in other areas, the International Geomagnetic Reference Field (IGRF) model can be used (Maus, 2005). However, in practice, the measurements of magnetometers contain more errors emanating from sensors and the surrounding environment (Moafipoor et al., 2007). These error sources apparently cause some misalignment between the modelled values and the measured geomagnetic field component (see Figure 5.1).

For gyroscopes, first-order differentiations of the orientations estimated by magnetometers are used to reference the rotation rate. Due to the variation of the geomagnetic field and the noise in orientation determination, this rotation rate reference contains significant noise (see Figure 5.1). This leads to low accuracy estimations of gyroscope scale factors. Consequently, overestimated observation covariance is assigned to the KF in order to filter out part of significant noise.

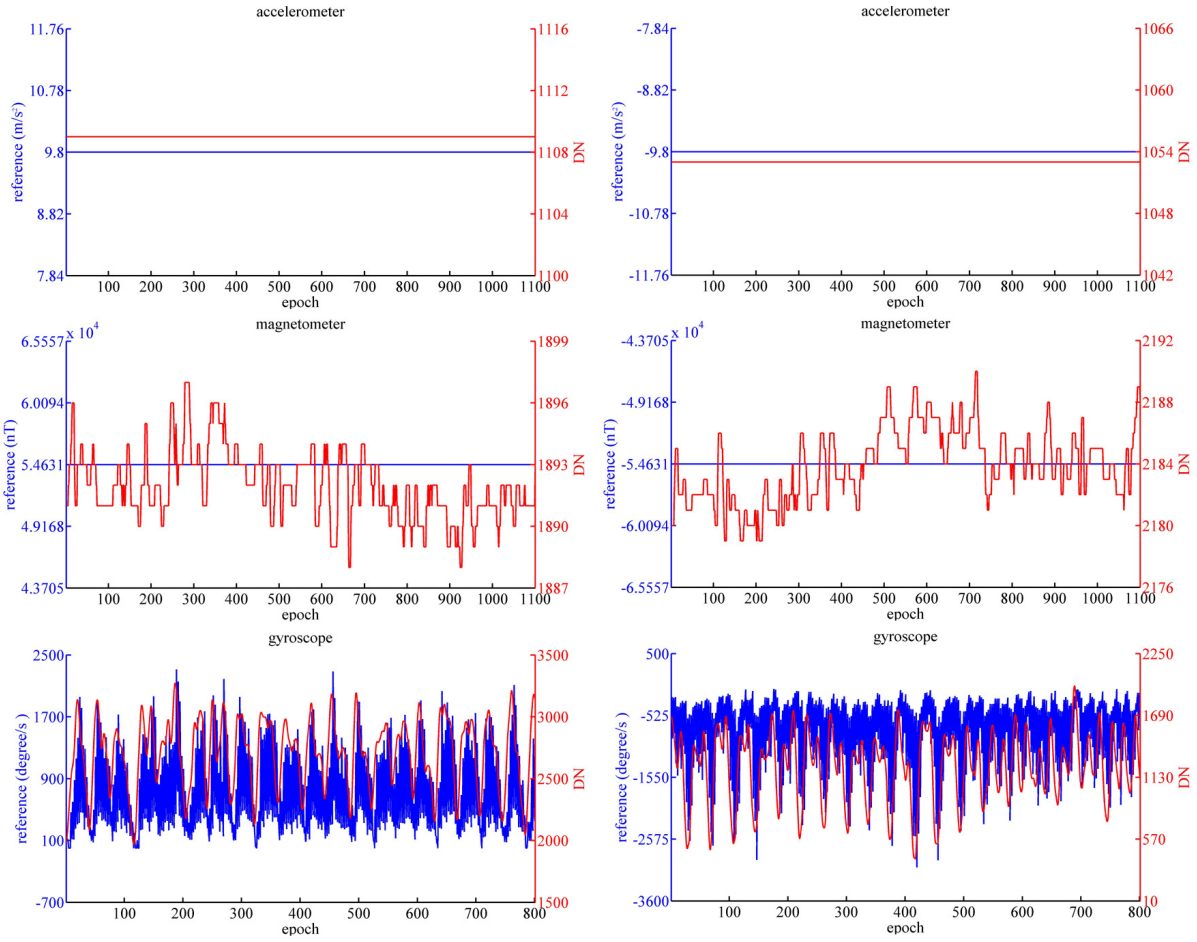

Figure 5.1 The calibration of the MEMS INS sensors
(The left axes (blue) show the references in the calibration, including the vertical components of gravity and the geomagnetic field vector and the rotation rates estimated by magnetometers. The right axes (red) show digital output from the sensors.)

5.2.1.3 Alignment

The purpose of alignment is to estimate the relationship between the body frame and the navigation frame in the initial state (Jiang, 1998). This relationship is represented by the DCM (see Equation (5.8)).

$$\underset{\sim}{C}_b^n = \begin{bmatrix} \underset{\sim}{c}_{11} & \underset{\sim}{c}_{12} & \underset{\sim}{c}_{13} \\ \underset{\sim}{c}_{21} & \underset{\sim}{c}_{22} & \underset{\sim}{c}_{23} \\ \underset{\sim}{c}_{31} & \underset{\sim}{c}_{32} & \underset{\sim}{c}_{33} \end{bmatrix} \tag{5.8}$$

where,

$\underset{\sim}{c}_{ij}$ is the component of the DCM in row i, column j.

The value of every component is listed in Equations (5.9) - (5.17).

$$\underset{\sim}{c}_{11} = \cos\theta \cdot \cos\psi \tag{5.9}$$

$$\underset{\sim}{c}_{12} = -\cos\theta \cdot \sin\psi + \sin\phi \cdot \sin\theta \cdot \cos\psi \tag{5.10}$$

$$\underset{\sim}{c}_{13} = -\sin\phi \cdot \sin\psi + \cos\phi \cdot \sin\theta \cdot \cos\psi \tag{5.11}$$

$$\underset{\sim}{c}_{21} = \cos\theta \cdot \sin\psi \tag{5.12}$$

$$\underset{\sim}{c}_{22} = \cos\phi \cdot \cos\psi + \sin\phi \cdot \sin\theta \cdot \sin\psi \tag{5.13}$$

$$\underset{\sim}{c}_{23} = -\sin\phi \cdot \cos\psi + \cos\phi \cdot \sin\theta \cdot \sin\psi \tag{5.14}$$

$$\underset{\sim}{c}_{31} = -\sin\theta \tag{5.15}$$

$$\underset{\sim}{c}_{32} = \sin\phi \cdot \cos\theta \tag{5.16}$$

$$\underset{\sim}{c}_{33} = \cos\phi \cdot \cos\theta \tag{5.17}$$

where,

ϕ is the pitch angle;

θ is the roll angle; and

ψ is the yaw angle.

Since the DCM is an orthogonal matrix, its inverse matrix is equal to its transpose (see Equation (5.18)).

$$\underset{\sim}{C}_{n}^{b} = \underset{\sim}{C}_{b}^{nT} \tag{5.18}$$

where,

$\underset{\sim}{C}_{b}^{n}$ is the DCM for transforming the vector from the navigation frame to the body frame;

Theoretically, the relationship between two coordinates can be determined by two non-parallel vectors. For high-accuracy INS, the vector of the gravity, sensed by accelerometers, and the vector of the Earth rotation rate, sensed by the gyroscope, are selected (Schimelevich and Naor, 1996). However, for the MEMS INS, the Earth rotation rate is too subtle to be detected by gyroscopes due to their high noise level. Instead, the vectors of the gravity and the geomagnetic fields are used.

The gravity measured by accelerometers in the stationary status is given by Equation (5.19). Accordingly, the three terms, $\tilde{c}_{31}$, $\tilde{c}_{32}$ and $\tilde{c}_{33}$, can be determined based on the accelerations measured and the vertical component of the gravity since the Easting and Northing components of the gravity are zero.

$$\begin{bmatrix} f_x^b \\ f_y^b \\ f_z^b \end{bmatrix} = \tilde{C}_n^b \cdot \begin{bmatrix} -g_E \\ -g_N \\ -g_U \end{bmatrix} = \begin{bmatrix} \tilde{c}_{31} \\ \tilde{c}_{32} \\ \tilde{c}_{33} \end{bmatrix} \cdot \left[-g_U\right] \tag{5.19}$$

where,

f_x^b, f_y^b and f_z^b are the measured accelerations of the x, y and z axis in the body frame respectively; and

g_E, g_N and g_U are the easting, northing and up components of the gravity respectively.

The geomagnetic field vector measured by magnetometers is given by the following Equation (5.20).

$$\begin{bmatrix} m_x^b \\ m_y^b \\ m_z^b \end{bmatrix} = \tilde{C}_n^b \cdot \begin{bmatrix} m_E^{AGRF} \\ m_N^{AGRF} \\ m_U^{AGRF} \end{bmatrix} \tag{5.20}$$

By rearranging the Equations (5.9) - (5.17) the following equations can be achieved.

$$\tilde{c}_{12} = \tilde{c}_{23} \cdot \tilde{c}_{31} - \tilde{c}_{33} \cdot \tilde{c}_{21} \tag{5.21}$$

$$\tilde{c}_{22} = \tilde{c}_{33} \cdot \tilde{c}_{11} - \tilde{c}_{13} \cdot \tilde{c}_{31} \tag{5.22}$$

$$\tilde{c}_{32} = \tilde{c}_{13} \cdot \tilde{c}_{21} - \tilde{c}_{23} \cdot \tilde{c}_{11} \tag{5.23}$$

Consequently, the Equation (5.20) can be rearranged as the Equation (5.24).

$$\begin{bmatrix} m_x^b - \tilde{c}_{31} \cdot m_U^{AGRF} \\ m_y^b - \tilde{c}_{32} \cdot m_U^{AGRF} \\ m_z^b - \tilde{c}_{33} \cdot m_U^{AGRF} \end{bmatrix} = \begin{bmatrix} m_E^{AGRF} & -m_N^{AGRF} \cdot \tilde{c}_{33} & m_N^{AGRF} \cdot \tilde{c}_{32} \\ m_N^{AGRF} \cdot \tilde{c}_{33} & m_E^{AGRF} & -m_N^{AGRF} \cdot \tilde{c}_{31} \\ -m_N^{AGRF} \cdot \tilde{c}_{32} & m_N^{AGRF} \cdot \tilde{c}_{31} & m_E^{AGRF} \end{bmatrix} \cdot \begin{bmatrix} \tilde{c}_{11} \\ \tilde{c}_{12} \\ \tilde{c}_{13} \end{bmatrix} \tag{5.24}$$

where,

m_x^b, m_y^b and m_z^b are the measured magnetic vector of the x, y and z axes in the body frame respectively; and

m_E^{AGRF}, m_N^{AGRF} and m_U^{AGRF} are the easting, northing and up components of the geomagnetic vector respectively.

Accordingly, the terms, $\underset{\sim}{c}_{11}$, $\underset{\sim}{c}_{12}$ and $\underset{\sim}{c}_{13}$, can be determined from the measured magnetic components and the geomagnetic field vector. In addition, the remainder of the terms in the DCM can be calculated using Equations (5.21), (5.22) and (5.23) respectively.

Figure 5.2 shows results of the alignment using this method. When compared to the estimations of the pitch angle and roll angle, there are significant variations of a few degrees in the yaw angle. This is mainly due to the uncertainties of the magnetic measurements. According to the accuracy required in personal positioning, this method can provide efficient and effective results for the MEMS INS alignment.

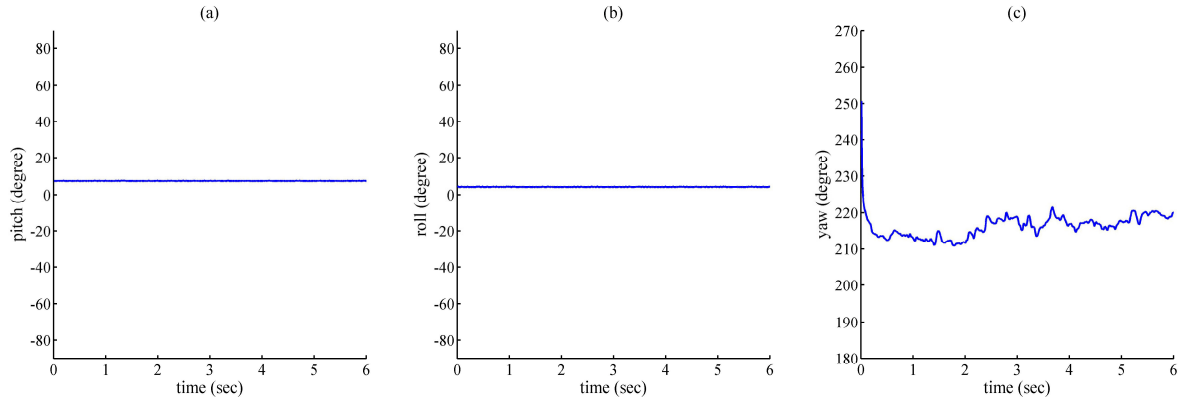

Figure 5.2 The schematic plots of the INS alignment results in three Euler angles respectively

(Plots (a), (b) and (c) are the pitch angle, roll angle and the yaw angle estimated by the simplified alignment respectively.)

5.2.1.4 INS Error Models

The positioning equations in INS are given by Equations (5.25), (5.26) and (5.27) (Titterton and Weston, 2004).

$$\hat{p} = (p_0 + \delta p) + \hat{v} \cdot t \tag{5.25}$$

$$\hat{v} = (v_0 + \delta v_0) + \hat{f}^n \cdot t \tag{5.26}$$

$$\hat{f}^n = \hat{\underset{\sim}{C}}_b^n \cdot (f^b + \delta f^b) \tag{5.27}$$

where,

v_0 is the initial velocity;

δv_0 is the error of the initial velocity;

$\hat{v}$ is the estimated velocity;

f^b is the acceleration in the body frame;

δf^b is the error of the acceleration in the body frame;

$\hat{f}^n$ is the estimated acceleration in the navigation frame;

$\hat{C}_b^n$ is the estimated DCM which is a function of Euler angles, $\begin{bmatrix} \phi \\ \theta \\ \psi \end{bmatrix}$; and

t is the time between the epoch of the initial state and the estimated epoch.

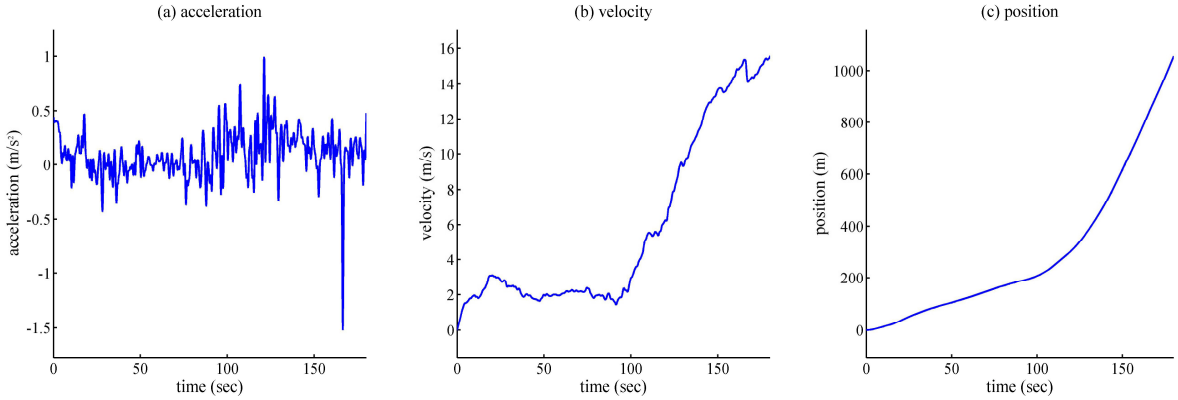

Figure 5.3 The schematic plots of the white noises in acceleration, the random walk noises in velocity and the significant drifts in position of INS

((a): the acceleration measured with white noise; (b): the velocity based on the integral of the acceleration; and (c): the position based on the double-integral of the acceleration.)

It indicates that the position can be calculated by the double-integral of the measured acceleration with respect to time, so the Gaussian noise in the acceleration becomes a random-walk noise in velocity and a significant drift in position (see Figure 5.3). In a two-dimensional strapdown INS that provides the horizontal positions like a PDR, the positioning error model can be written as:

$$\delta p_x = \delta p_{x0} + \delta v_{x0} \cdot t + \delta\psi_0 \cdot f_y^n \cdot \frac{t^2}{2} + \delta f_x^b \cdot \cos\psi \cdot \frac{t^2}{2} + \delta f_y^b \cdot \sin\psi \cdot \frac{t^2}{2} + \delta\dot{\psi} \cdot f_y^n \cdot \frac{t^3}{6} \qquad (5.28)$$

$$\delta p_y = \delta p_{y0} + \delta v_{y0} \cdot t - \delta\psi_0 \cdot f_x^n \cdot \frac{t^2}{2} - \delta f_x^b \cdot \sin\psi \cdot \frac{t^2}{2} + \delta f_y^b \cdot \cos\psi \cdot \frac{t^2}{2} - \delta\dot{\psi} \cdot f_x^n \cdot \frac{t^3}{6} \qquad (5.29)$$

where,

δv_{x0} and δv_{y0} are the errors of the initial velocity;

$\delta\psi_0$ is the error of the initial orientation; and

$\delta\dot{\psi}$ is the error of the rotation rate along the z-axis.

It is assumed that the variances of accelerometer bias are same, $\sigma^2_{f_x^b} = \sigma^2_{f_y^b}$. The positioning variance is given by:

$$\sigma_p^2 = \sigma_{p0}^2 + t^2 \cdot \sigma_{v0}^2 + f^{n2} \cdot \frac{t^4}{4} \cdot \sigma_{\psi 0}^2 + \frac{t^4}{2} \cdot \sigma_{f^b}^2 + f^{n2} \cdot \frac{t^6}{36} \cdot \sigma_{\dot{\psi}}^2 \qquad (5.30)$$

where,

σ_{v0}^2 is the variance of the initial velocity;

$\sigma_{\psi 0}^2$ is the variance of the initial orientation;

$\sigma_{f^b}^2$ is the variance of the acceleration in the body frame; and

$\sigma_{\dot{\psi}}^2$ is the variance of the rotation rate along the z-axis.

5.2.2 PDR Principles and Error models

5.2.2.1 Introduction to PDR

Another technique used for personal positioning applications based on MEMS sensors is PDR. This technique uses accelerometers mounted on the mobile users to detect the number of user steps. Relative positions are estimated by the step numbers detected combining with the orientations and the measured or modelled results of step lengths (see Figure 5.4).

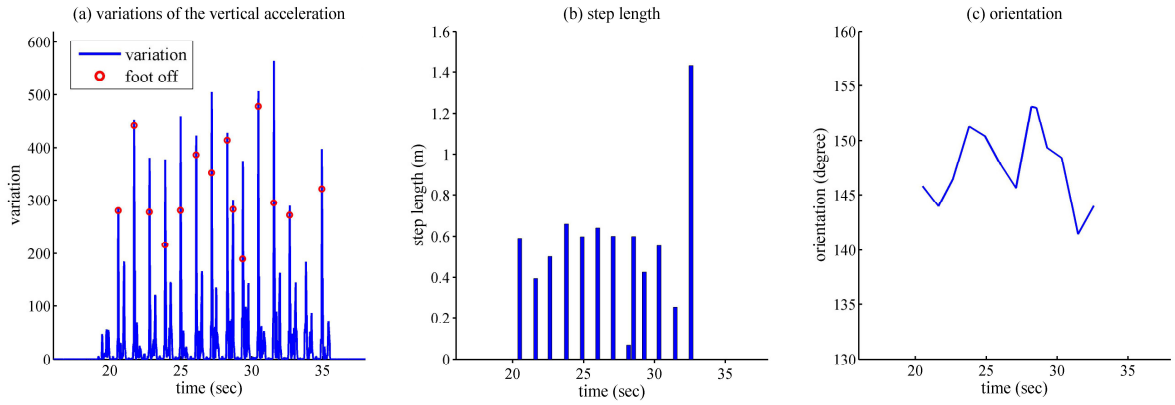

Figure 5.4 The schematic plots of the step detection, step length estimation and orientation estimation in PDR ((a): the mobile user's steps detected according to the variations of the vertical acceleration measured; (b): the mobile user's step lengths estimated; (c): the orientations of the mobile user.)

The most challenging elements in PDR are to correctly detect the user steps and estimate step length. For steps, these are usually detected according to the acceleration patterns collected from mobile users' moving body parts. The most common body parts for mounting the accelerometers are the feet and the waist (see Figure 5.5). The advantage of waist-mounted sensors is low noise, since many high-frequency shocks are absorbed by leg joints. However, the trade-off is the smooth and less detailed signals which will sometime cause underestimation of step numbers. In contrast, foot-mounted sensors can collect more detailed data, but with higher noise levels, which will lead to overestimation. For step length, there are mainly two kinds of estimating methods: to indirectly estimate the step length based on statistical models using certain parameters, such as the length of the mobile users' legs, step frequencies, and step patterns (Rose and Gamble, 2006); and to physically measure the step length according to distance measurements (e.g. from GPS), single integral of speed or double integral of acceleration (e.g. from accelerometers). Each method has its pros and cons. The statistical method contains less error in long-term estimation, but it cannot deal well with the anomalies of the mobile user movements. The direct measurement method can physically measure step lengths, but it has more noise associated with the measurement of each step, which accumulates in positioning estimations.

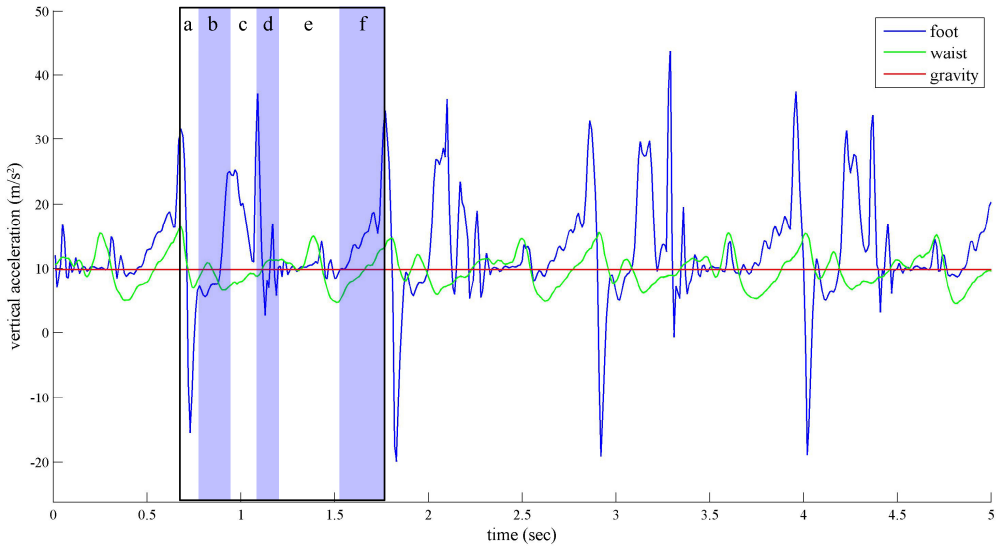

Figure 5.5 A schematic plot of the PDR data with the devices mounted on the waist and foot respectively

(The plot shows the vertical accelerations measured by the foot-mounted sensors (blue) and the waist-mounted sensors (green). Six stages of a walk circle can be detected by the foot mounted-sensors. (a): initial swing; (b): mid swing; (c): terminal swing; (d): initial double support; (e): single limb stance; (f): second double support.)

5.2.2.2 PDR Error Models

The observation model of the PDR is given by Equation (5.31).

$$\hat{p} = (p_0 + \delta p_0) + \hat{n} \cdot \hat{l} \qquad (5.31)$$

where,

$\hat{p}$ is the estimated position;

p_0 is the initial position;

δp_0 is the error of the initial position;

$\hat{n}$ is the estimated step number; and

$\hat{l}$ is the estimated step length.

In detail, the errors in step number determinations, step length calculations and orientation estimations are given by Equations (5.32), (5.33) and (5.34).

$$\hat{n} = n + \delta n \tag{5.32}$$

where,

n and δn are the true value and the error of the step number respectively.

$$\hat{l}^n = \hat{C}_b^n \cdot (l^b + \delta l^b) \tag{5.33}$$

where,

l^b and δl^b are the true value and the error of the step length in the body frame respectively; and

$\hat{C}_b^n$ is the DCM used to transform the measurements from the body frame to the navigation frame.

For simplicity, the step length is only measured in the forward and backward directions of the body frame (l_x^b) and the platform does not contain the rotations in roll and pitch angles. Eventually, The DCM, C_b^n, is simplified by a function of the horizontal orientation, ψ.

$$\hat{\psi} = \psi + \delta\psi \tag{5.34}$$

where,

$\hat{\psi}$ is the estimated orientation; and

$\delta\psi$ is the error of orientation.

The error models in the 2-D coordinates are given by the Equations (5.35) and (5.36) respectively.

$$\delta p_x = \delta p_{x0} + \delta n \cdot l_x^n + n \cdot \delta\psi \cdot l_y^n + n \cdot \delta l_y^b \cdot \cos\psi \tag{5.35}$$

$$\delta p_y = \delta p_{y0} + \delta n \cdot l_y^n + n \cdot \delta\psi \cdot l_x^n - n \cdot \delta l_x^b \cdot \sin\psi \tag{5.36}$$

where,

δp_x and δp_y are the positioning errors in x and y axes respectively;

δp_{x0} and δp_{y0} are the errors of the initial position;

l_x^n and l_y^n are the step length in the navigation frame; and

δl_y^b is the error of the step length in the forward axis of the body frame.

The positioning variance of PDR is given by:

$$\sigma_p^2 = \sigma_{p0}^2 + l^{n2} \cdot \sigma_n^2 + n^2 \cdot l^{n2} \cdot \sigma_\psi^2 + n^2 \cdot \sigma_{l^b}^2 \quad (5.37)$$

where,

σ_p^2 is the variance of the estimated position;

σ_{p0}^2 is the variance of the initial position estimated;

σ_n^2 is the variance of the step number estimated;

σ_ψ^2 is the variance of the orientation estimated; and

$\sigma_{l^b}^2$ is the variance of the step length estimated.

5.3 Evaluation of INS and PDR

According to the literature consulted (see Section 5.1), both MEMS INS and PDR are used in personal tracking and indoor positioning applications. Analyses and experiments are provided in the following section to provide support related to the selection of a proper technique for integrated personal positioning techniques in this research.

According to the error models (see Sections 5.1.1.4 and 5.1.2.2), positioning variance is a second-order polynomial of the step number in PDR and a sixth-order polynomial of the observation time in INS. This indicates that drifts in INS are generally faster than drifts in PDR, when the sensors with the same noise level are used. It also means even if the mobile user does not move, the INS will still drift over time, leading to large positioning errors. Field tests were conducted to compare MEMS INS, PDR and integrated methods with low-cost GPS so as to validate the above analysis. The selected site for the testing was an outdoor open area (see Figure 5.6). The device used was a *MinimaxX* (Wu et al., 2008), which contained a low-cost GPS receiver (Fastrax, 2007) and a MEMS INS.

The drift between the stand-alone MEMS INS and the stand-alone PDR were calculated and are shown in Figure 5.7. The figure shows that the INS started drifting from the beginning of the experiment, but the PDR only drifted after the mobile user started to move (80 seconds after the experiment began). At the end of the experiment, it was found that the INS drifted almost twelve times further than the

PDR. These empirical results agree well with the analysis according to theoretical error models.

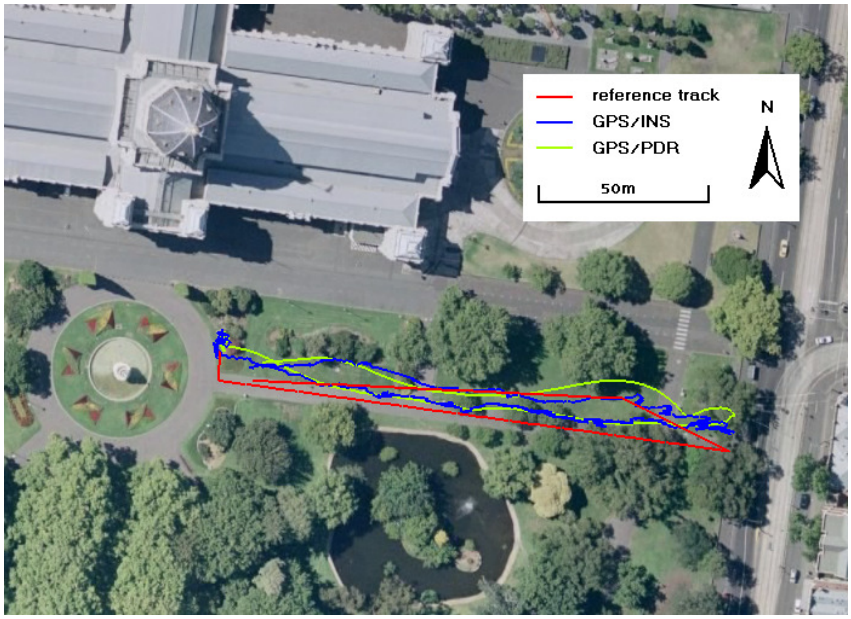

Figure 5.6 The reference track and the estimated positions by integrated GPS/INS and integrated GPS/PDR respectively
(The satellite image in the background is sourced from *GoogleEarth* (URL: http://www.google.com/earth/index.html Access date: 28 Jul 2010). The reference track is a pre-defined trajectory for the mobile user.)

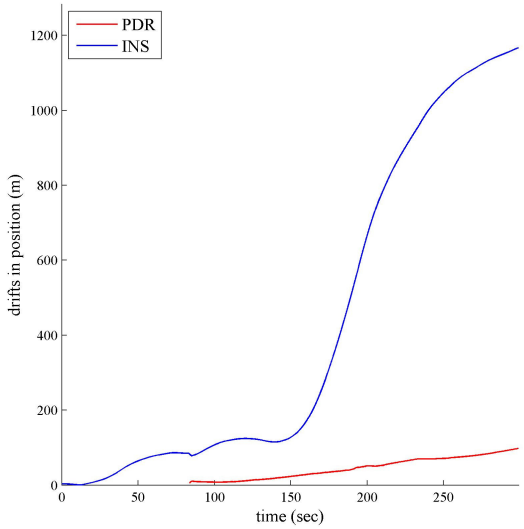

Figure 5.7 A comparison of the drifts in MEMS INS and PDR
(The blue line shows the positioning drifts in MEMS INS starting from the beginning of the experiment. The red line shows the positioning drifts in PDR starting from the beginning of the mobile user's movements.)

The differences between the positioning errors for integrated GPS/INS and integrated GPS/PDR were also calculated (see Figure 5.8). The figure below shows that by providing the frequent constraints from the external sensors, such as GPS, the large drifts in both INS and PDR can be constrained and integrated INS and integrated PDR can provide the equivalent positioning accuracy.

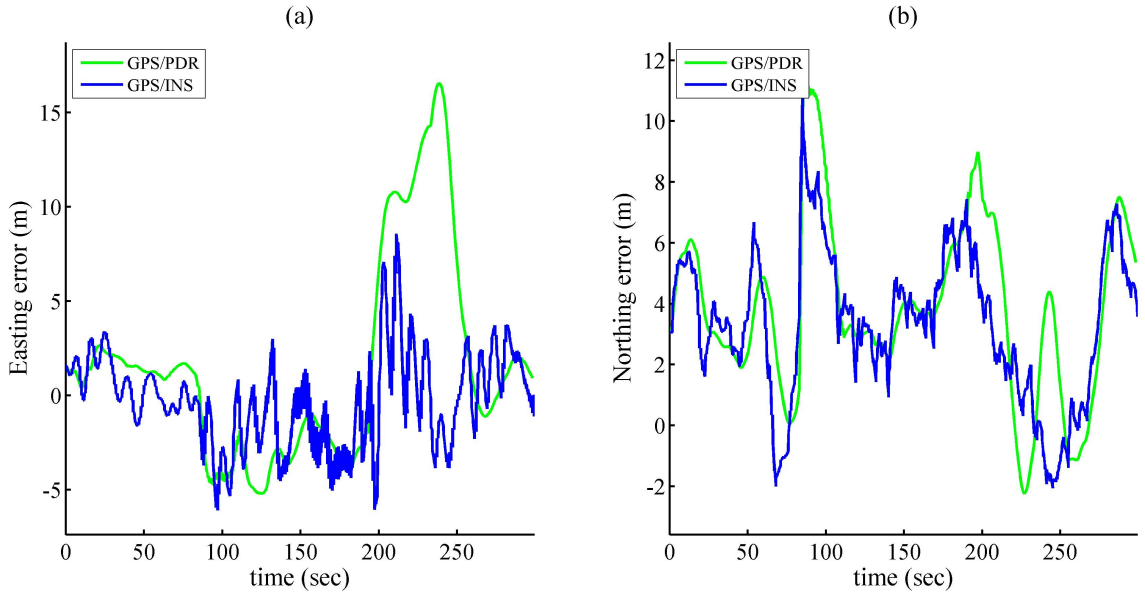

Figure 5.8 The error analysis of the integrated GPS/INS and integrated GPS/PDR methods

((a): Easting errors, (b) Northing errors)

In summary, both MEMS INS and PDR can provide better results for personal positioning by integrating with external sensors, like GPS, which can provide frequent constraints. According to positioning mechanisations, even though the PDR has a slower drift than MEMS INS, in the long-term, without any constraints, it contains a major limitation that is not sensitive to the smooth movements of the mobile users, such as a mobile user who may be moving on an escalator or in a lift. These results suggest that the integrated positioning method based on MEMS INS can provide more reliable estimations in a wider range of circumstances than that is based on PDR. As a result, the MEMS INS was selected for further testing in this research.

5.4 Integration of RFID and MEMS INS

According to current research (Grejner-Brzezinska *et al.*, 2007a, 2007b; Kim, 2004; Zhao *et al.*, 2009), multi-sensor integrations can provide more accurate and reliable estimations by constraining the results with redundent observations. It can also sigificantly reduce the cost and volume of the entire positioning system. For example,

integrated positioning algorithms based on INS and GPS have been extensively studied for vehicle navigation and robot positioning (Brown and Lu, 2004; Godha and Cannon, 2005a, 2005b; Godha *et al.*, 2006; Wang *et al.*, 2009a, 2009b; Zhou *et al.*, 2009) since INS is not prone to signal propagation problems (e.g. obstructions and multipath effects) and it can achieve frequent constraints when GPS is available. However, the results achieved from integrated MEMS INS algorithms for indoor personal positioning have not been extensively studied. As a consequence, RFID positioning techniques were integrated with MEMS INS and used for further testing of the algorithms developed in this research, so as to obtain reliable integrated positioning estimations. The algorithms tested include:

(a) Integrated INS/RFID CoO algorithms; and

(b) Integrated INS/RFID location fingerprinting algorithms.

5.4.1 Integrated INS/RFID CoO Algorithms

A unique advantage of INS is that it can provide high-frequency and continuous positions. Therefore, the integration of INS/RFID CoO can improve the continuity of the RFID CoO stand-alone. In this research a 2-D reduced INS algorithm was used and both the RFID deterministic CoO and the RFID probabilistic CoO algorithms were tested for multi-sensor integrated methods.

5.4.1.1 Reduced INS Algorithm for 2-D Personal Positioning

In order to reduce INS sensors' noise, a reduced INS, which includes one forward accelerometer, one gyroscope and two horizontal magnetometers, are often used for 2-D personal positioning. The measurement vector includes sensor outputs (see Equation (5.38)).

$$z = \begin{bmatrix} m_x^b & m_y^b & \dot{\psi}^b & f_y \end{bmatrix}^T \tag{5.38}$$

where,

$\dot{\psi}^b$ is the rotation rate along z axis; and

f_y is the acceleration in the forward axis.

The measurement model is given by:

$$m_{xk}^b = -m_N^{AGRF} \cdot \sin(\psi_k) + m_E^{AGRF} \cdot \cos(\psi_k) + v_{m_x,k} \tag{5.39}$$

$$m_{yk}^{b} = m_{N}^{AGRF} \cdot \cos(\psi_k) + m_{E}^{AGRF} \cdot \sin(\psi_k) + v_{m_y,k} \tag{5.40}$$

$$\dot{\psi}_k^{b} = \dot{\psi}_k + v_{\dot{\psi},k} \tag{5.41}$$

$$f_{y,k} = |f_k| + v_{f,k} \tag{5.42}$$

where,

$|f|$ is the magnitude of the acceleration; and

$v_{\bullet,k}$ are the zero-mean white Gaussian measurement uncertainties in the magnetic field components, rotation rate and acceleration respectively.

The state vector includes horizontal coordinates, velocities and accelerations in easting and northing respectively (see Equation (5.43)).

$$x = [\, p \quad v \quad f \quad \psi \quad \dot{\psi} \,]^T \tag{5.43}$$

where,

p is the position vector;

v is the velocity vector; and

f is the acceleration vector.

The constant acceleration model is used as the dynamic model.

$$p_k = p_{k-1} + v_{k-1} \cdot \Delta t + w_{p,k-1} \tag{5.44}$$

$$v_k = v_{k-1} + f_{k-1} \cdot \Delta t + w_{v,k-1} \tag{5.45}$$

$$f_k = f_{k-1} + w_{f,k-1} \tag{5.46}$$

$$\psi_k = \dot{\psi}_k \cdot \Delta t + w_{\psi,k-1} \tag{5.47}$$

$$\dot{\psi}_k = \dot{\psi}_{k-1} + w_{\dot{\psi},k-1} \tag{5.48}$$

where,

p_k, v_k, f_k, ψ_k and $\dot{\psi}_k$ are the position, velocity, acceleration vectors, orientation and rotation rate at epoch k respectively;

$w_{\bullet,k}$ is the zero-mean white Gaussian process noises in the position, velocity, acceleration and orientation; and

Δt is the time between the epoch $k-1$ and k.

5.4.1.2 Integrated INS/RFID Deterministic CoO Algorithm

For the integrated INS/RFID deterministic CoO algorithm, the identical dynamic model and measurement model of the reduced INS algorithm were used outside the RFID cells. Inside the cells, the positions of the cells' centres were used for correcting INS drifts. Eventually, the measurement vector and measurement model became:

$$z = [m_x^b \quad m_y^b \quad \dot{\psi} \quad f_y \quad p_{cell}]^T \tag{5.49}$$

$$p_{cell} = p_k + v_{p,k} \tag{5.50}$$

where,

p_{cell} is the position estimated by deterministic CoO algorithm; and

$v_{p,k}$ is the measurement uncertainty in the position.

5.4.1.3 Integrated INS/RFID Probabilistic CoO Algorithm

For the integrated INS/RFID probabilistic CoO algorithm, an EKF was used to integrate the observations from reduced INS and RFID (see Figure 5.9). The estimated positions using the RFID probabilistic CoO algorithm and the average velocity between two estimations were used as constraints (Zhu, 2008). The measurement vector and measurement model are given by:

$$z = \left[m_x^b \quad m_y^b \quad \dot{\psi} \quad f_y \quad p_{CoO} \quad \overline{v} \right]^T \tag{5.51}$$

$$p_{CoO} = p_k + v_{p,k} \tag{5.52}$$

$$\overline{v} = \dot{p}_k + v_{v,k} \tag{5.53}$$

where,

p_{CoO} is the position estimated by probabilistic CoO algorithm;

$\overline{v}$ is the average velocity; and

$\dot{p}_k$ is the true velocity.

The models of the Integrated INS and RFID Deterministic CoO Algorithm are used when the mobile user is close to the cell centre (i.e. the RSS is over -50dBm), as

distance estimation is not accurate within this range due to significant multipath effects (see Chapter 4). When an RFID signal is not available, identical models of reduced INS algorithm are used.

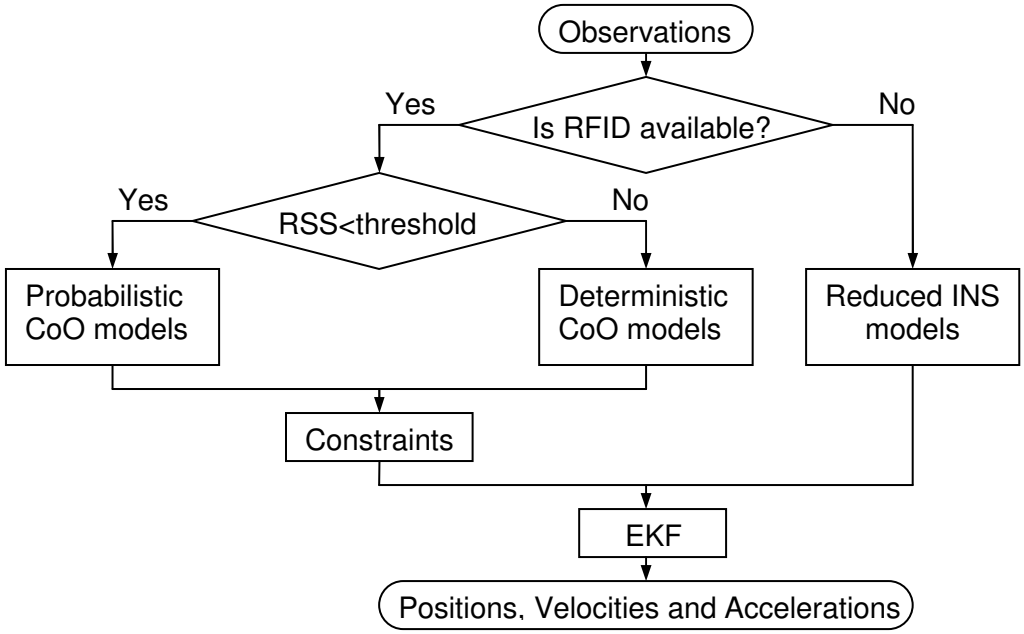

Figure 5.9 The flow chart of the Integrated INS and RFID Probabilistic CoO Algorithm

(When the RFID is available, the constraints generated from RFID CoO algorithms are used to constrain drifts in the reduced INS. Probabilistic CoO models are used in the far areas of the cell where there are less multipath effects from ground reflections. Deterministic CoO models are used in near areas affected more significantly by multipath effects.)

5.4.1.4 Evaluation of Integrated INS/RFID CoO Algorithms

Experiments to evaluate integrated INS/RFID CoO algorithms were conducted at Yarra Bend Park, Melbourne, Australia. Seven RFID tags were placed in a U-shape trajectory in outdoor open areas. The cell centres were placed with different intervals (20m intervals in the east part and 50m intervals in the west part of the trajectory). The MEMS INS and RFID integrated system was used to implement the algorithms (see Figure 5.10) including:

(a) the 2-D reduced INS algorithm;

(b) the integrated INS/deterministic CoO algorithms with the small cell size (RSS threshold = -50dBm);

(c) the integrated INS/deterministic CoO algorithms with the large cell size (RSS threshold = -80dBm); and

(d) the integrated INS/probabilistic CoO algorithm.

A GPS RTK system (*Trimble R8*) was mounted on the mobile user as well to provide the centimetre-level reference positions for comparison purpose.

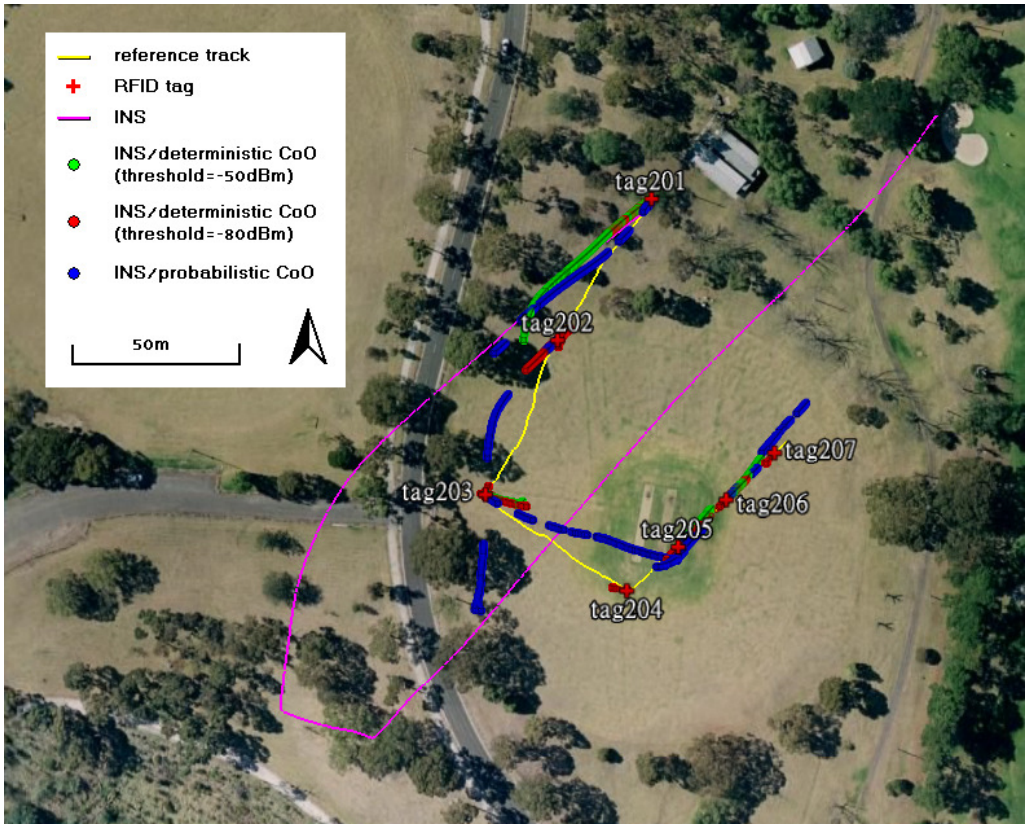

Figure 5.10 The experimental site for the evaluations of the integrated INS/RFID CoO algorithms

(The satellite image in the background comes from *GoogleEarth* (URL: http://www.google.com/earth/index.html Access date: 28 Jul 2010).)

The results show that all of the integrated INS/RFID CoO algorithms constrain INS drifts significantly. The accuracy of integrated INS/RFID deterministic CoO algorithms is highly dependent on the size and distribution of the cell. The accurate positions of the cell centres can be used to constrain INS drifts when using small cells (e.g. RSS threshold = -50dBm). However, the cells have to be densely distributed to provide frequent corrections (at least 0.2Hz) to the INS sensors. Otherwise, the dramatic drifts of INS can significantly degrade the positioning accuracy of the integrated algorithm within the large spacings between cells (see Figure 5.10). An alternative is

to use large cells (e.g. RSS threshold = -80dBm) to provide continuous cell coverage and, consequently, the frequent corrections to INS. However, the limitation of this approach is that large cells cannot provide corrections as accurately as the small cells. This is because it arbitrarily assigns the cell centre position to the mobile users' positions when they appear in the cell. As a result, when the cells become larger, this algorithm becomes more inaccurate. From experiment results, even though the integrated algorithm with large cells can better constrain INS drifts and provide more accurate positioning than the algorithm with small cells (see Table 5.1 and Figure 5.11), the former cannot provide reasonable and continuous trajectories. All estimations are highly constrained near cell centres when using the integrated algorithm with large cells (see Figure 5.10). This is a response to the nature of the deterministic CoO algorithm. It is a great challenge to the compromise between accuracy, continuity and the number of cells for deterministic CoO algorithms. In contrast, the INS/RFID probabilistic CoO algorithm overcomes this limitation and provides more accurate positions by introducing a flexible cell size according to the RSS. This provides continuous trajectories and it is more accurate than the integrated INS/RFID deterministic CoO algorithms. In spite of some occasional large errors, which are caused by RSS instabilities in areas where the mobile user is far from RFID tags, the INS/RFID probabilistic CoO can provide acceptable positioning accuracy and continuous trajectories with fewer RFID tags.

Table 5.1 The positioning errors of the integrated INS/RFID CoO algorithms

Method	RMSE (m)
INS/Probabilistic CoO	15.4
INS/Deterministic CoO (threshold=-80dBm)	19.6
INS/Deterministic CoO (threshold=-50dBm)	28.1
INS	67.7

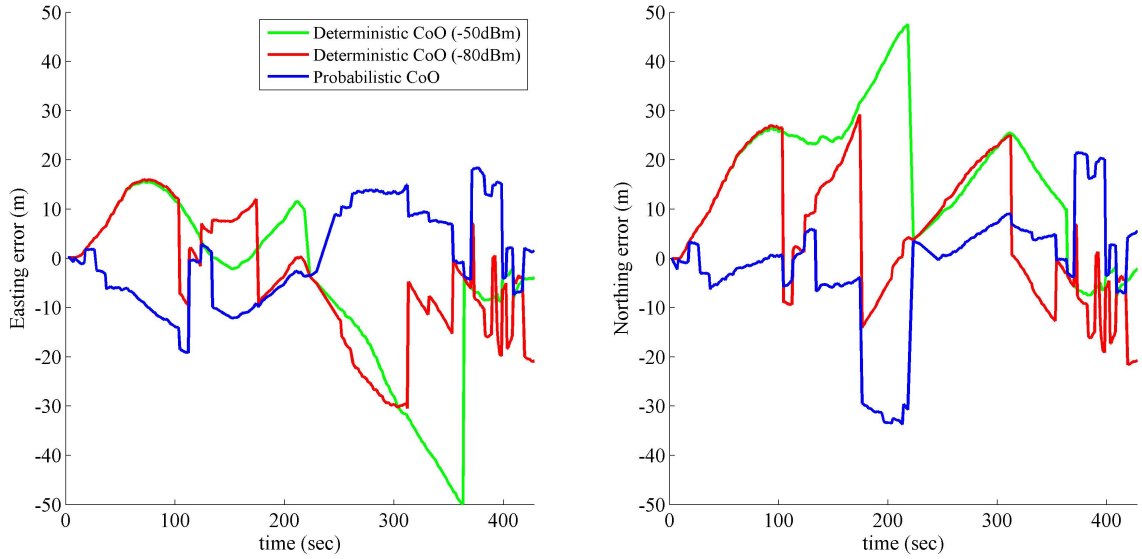

Figure 5.11 The error analysis of the integrated INS/RFID CoO algorithms

5.4.2 Integrated INS/RFID Location Fingerprinting Algorithms

For RFID location fingerprinting algorithms, the instability of RSS is a major error source. It is mainly caused by environmental dynamics. Due to significant effects from RSS instability in RFID, the probabilistic distribution can be disturbed from a single-peak into several peaks in the probabilistic approach of the location fingerprinting algorithm. A similar situation of disturbance caused by RSS instability happens to the deterministic approach as well. In most of the cases, the highest peak is not the one near the true position and it leads to large positioning errors. Consequently, a method using additional observations or constraints to select the correct peak in the disturbed context is required.

5.4.2.1 Prior Probability of the Mobile User in Probabilistic Location Fingerprinting Algorithm

Figure 5.12 is a schematic plot that shows distributions of positioning probabilities in free space (simulated) and dynamic environments (measured) respectively.

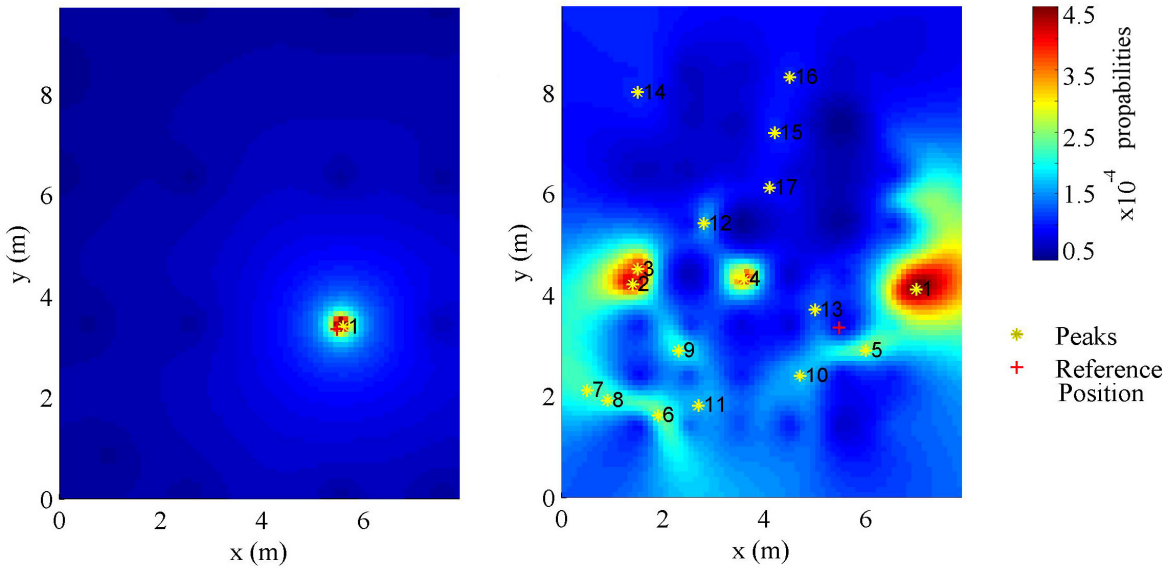

Figure 5.12 A schematic plot of the comparisons of the probabilistic distribution in the free space and the complex indoor environments

(The left plot shows the single-peak probabilistic distribution in free space. The right plot shows the multi-peak probabilistic distribution in complex indoor environments. The red cross (+) indicates the true position and the yellow stars show the position of the peaks.)

The left plot shows the distribution of probabilities in the free space which do not contain reflectors or obstacles. The probabilities peak is very close to the true position. The small error is due to the spatial resolution of RSS samples in the training phase and the noise of the transmission power source. In contrast, the plot at right shows the disturbance of the probabilities with a number of peaks in dynamic environments with reflectors and obstacles (e.g. people and furniture). There are 17 peaks and the highest (peak 1) is not the closest to the true position.

An integrated INS/RFID location fingerprinting algorithm is introduced here to amplify the probabilities around the predicted positions so as to increase the possibility of selecting the correct peak in disturbed distributions of the probabilities. This method is based on the assumption that the correct peak of the probabilities in RFID positioning is in the near areas of the INS predicted position. This can be true when the INS is frequently corrected and the positioning update interval is very small (e.g. a few seconds). The INS estimated positions can be constrained and will not significantly drift from the true position during this short period. Therefore, in this

research, the period was set to one second and the INS predictions were constrained by an EKF according to the values in the initial state and the positions determined (see Figure 5.13). Nine state variables were used for the dynamic models of the 3-D positioning algorithm, including the three orthogonal axes' position errors, velocity errors and tilts. The state transition matrix is given by the following Equation (5.54) (Rogers, 2000).

$$\underset{\sim}{\Phi} = \begin{bmatrix} 1 & \Delta t & 0 & 0 & 0 & 0 & 0 & 0 & 0 \\ 0 & 1 & -g \cdot \Delta t & 0 & 0 & 0 & 0 & 0 & 0 \\ 0 & \frac{\Delta t}{R} & 1 & 0 & 0 & 0 & 0 & 0 & \dot{\phi} \cdot \Delta t \\ 0 & 0 & 0 & 1 & \Delta t & 0 & 0 & 0 & 0 \\ 0 & 0 & 0 & 0 & 1 & -g \cdot \Delta t & 0 & 0 & 0 \\ 0 & 0 & 0 & 0 & \frac{\Delta t}{R} & 1 & 0 & 0 & \dot{\theta} \cdot \Delta t \\ 0 & 0 & 0 & 0 & 0 & 0 & 1 & \Delta t & 0 \\ 0 & 0 & 0 & 0 & 0 & 0 & \frac{-2g \cdot \Delta t}{R} & 1 & 0 \\ 0 & 0 & 0 & 0 & 0 & 0 & 0 & 0 & 1 \end{bmatrix} \qquad (5.54)$$

where,

R is the radius of the Earth;

g is the magnitude of the gravity;

$\dot{\phi}$ and $\dot{\theta}$ are the rotation rate of the x and y axes in the body frame respectively; and

Δt is the time interval between two adjacent epochs.

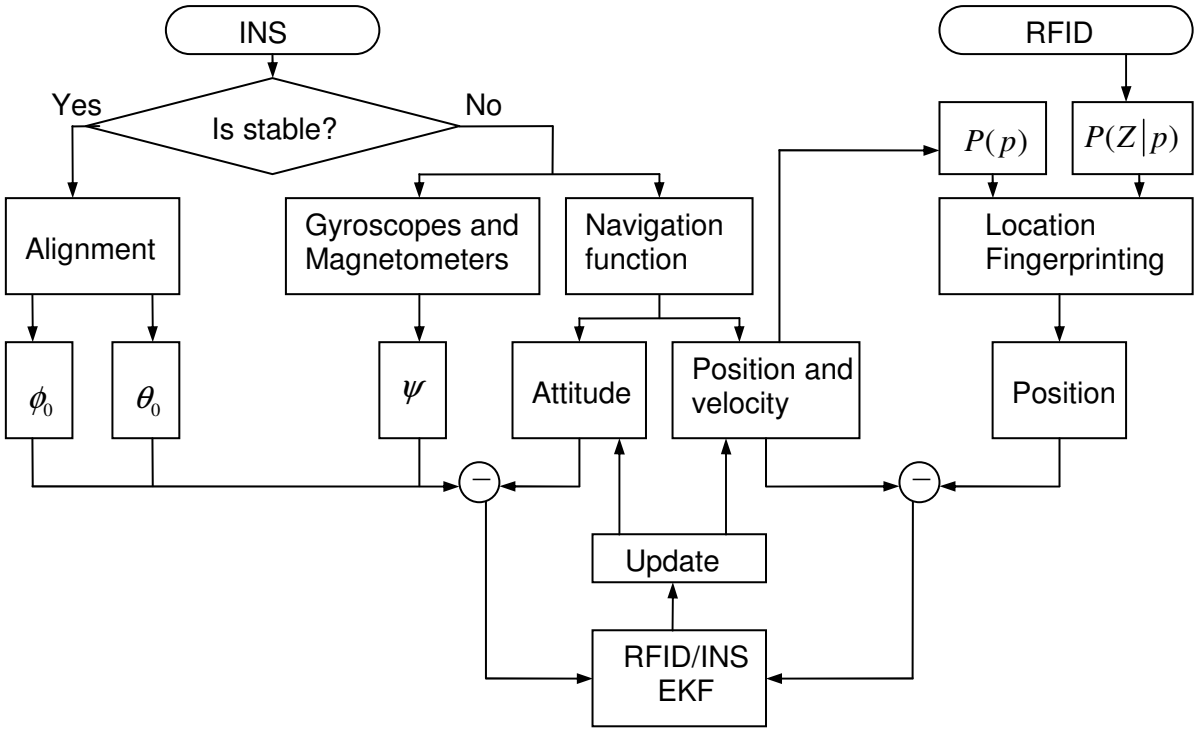

Figure 5.13 The flow chart of the Integrated INS and RFID location fingerprinting Algorithm

(The left part of this flow chart shows the data flow in the INS navigation. The Euler angles in the stable status and orientation estimated by the magnetometers are used as the constraints for attitude determination. The final estimated positions and velocities are used as the constraints of the INS estimated positions and velocities. The right part of the flow chart shows the data flow in the RFID location fingerprinting algorithm. The prior probabilities of a mobile user are calculated according to the INS estimated positions and velocities. Finally, the observations from the INS and RFID are integrated by an EKF.)

The amplification of the probabilities is completed according to Bayes' law (see Equation (5.55)). Unlike the uniform distribution of the prior probability of the mobile user's positioning in the RFID stand-alone techniques, a normal distribution is used with the mean of the predicted position and the variance according to the uncertainty of the INS positioning. These normal distributed probabilities, $P(p_i)$, are multiplied with the probabilities calculated based on the RFID observations, $P(Z|p_i)$, and amplifies the value of the probabilities near the predicted positions.

$$P(p_i|Z) = \frac{P(p_i \cap Z)}{P(Z)} = \frac{P(p_i) \cdot P(Z|p_i)}{P(Z)} \quad (5.55)$$

5.4.2.2 Evaluation of the Integrated INS/RFID Location Fingerprinting Algorithms

Two series of experiments were conducted in different sections of a building at RMIT University's City Campus to test integrated INS/RFID location fingerprinting algorithms in 2-D and 3-D contexts. Experiments for evaluating the performance of the 2-D integrated INS/RFID location fingerprinting algorithm were conducted in identical environments to the 2-D RFID stand-alone positioning experiments (see Chapter 4). The positions of the eight tested places were recalculated using the integrated INS/RFID location fingerprinting algorithm.

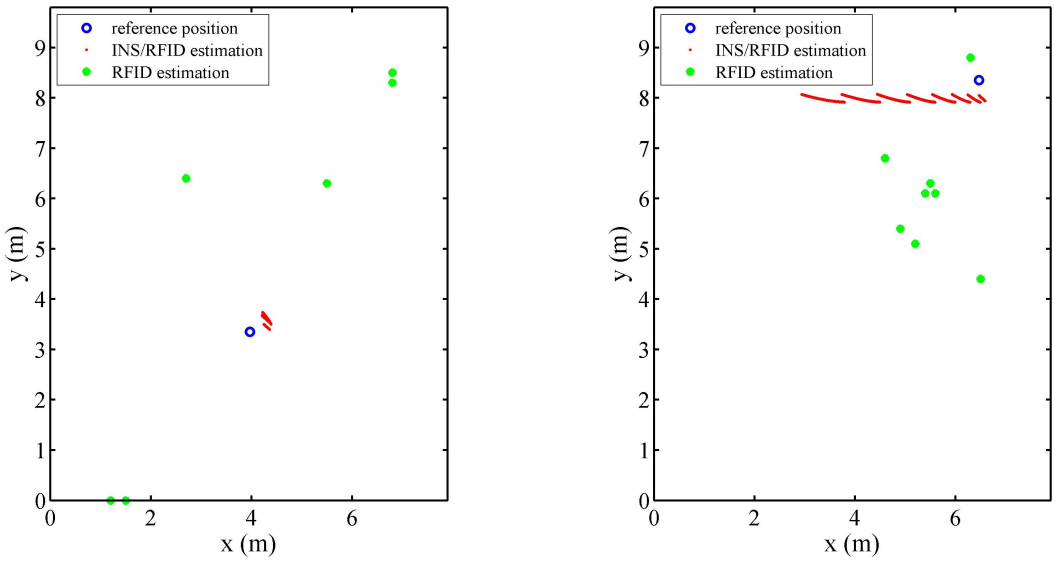

Figure 5.14 The schematic plots of two 2-D integrated INS/RFID location fingerprinting algorithm results
(The left plot shows the results of the test 4 at a middle point of the room. The right plot shows the results of the test 8 in a corner of the room. The red dots and the green dots are the results generated by the integrated INS/RFID algorithm and the RFID stand-alone positioning algorithm respectively.)

Figure 5.14 shows the results of two of the eight tests for the evaluation. One is at the middle of the room and the other is in the corner of the room. It shows that the uncertainties of the RFID stand-alone positioning algorithm can be minimised by

amplifying the probabilities according to the integrated INS observations and that INS drifts can be frequently constrained by RFID, especially at the centre of the room where the RSS distributions are less disturbed by environmental effects. In the boundary areas of the room, the signals reflected by objects may significantly affect RSS distributions and consequently make the INS to be constrained ineffectively. Figure 5.15 shows the positioning errors of all eight tests respectively. It shows that most of the errors are less than 1m except those from tests 1, 3 and 8, which are near the edges or corners of the room. The total RMSE is 1.07m. Despite some drifts in difficult environments, the integrated INS/RFID location fingerprinting algorithm can improve the positioning accuracy from 4m in RFID stand-alone techniques to about 1m in static positioning applications.

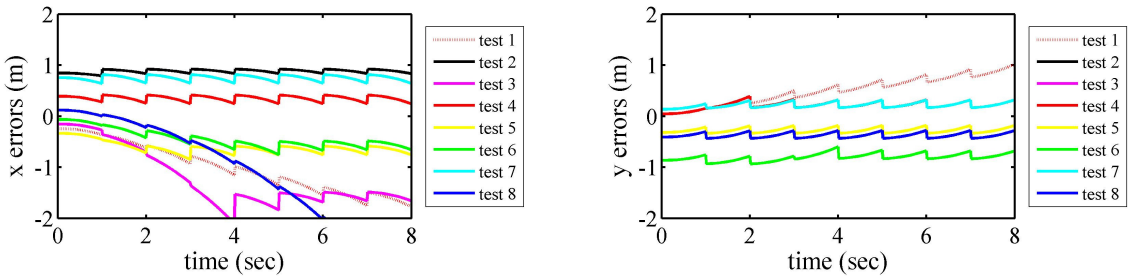

Figure 5.15 Positioning errors of the eight tests for evaluating the 2-D integrated INS/RFID location fingerprinting algorithm.

(The left plot shows the x-axis errors and the right plot shows the y-axis errors. The errors estimated from different tests are represented by different colours.)

Evaluations of the 3-D integrated INS/RFID location fingerprinting algorithm were conducted in the stairway of the same building at the RMIT University's City Campus (see Figure 5.16) which is identical to the environment for the 3-D RFID stand-alone positioning experiments (see Chapter 4).

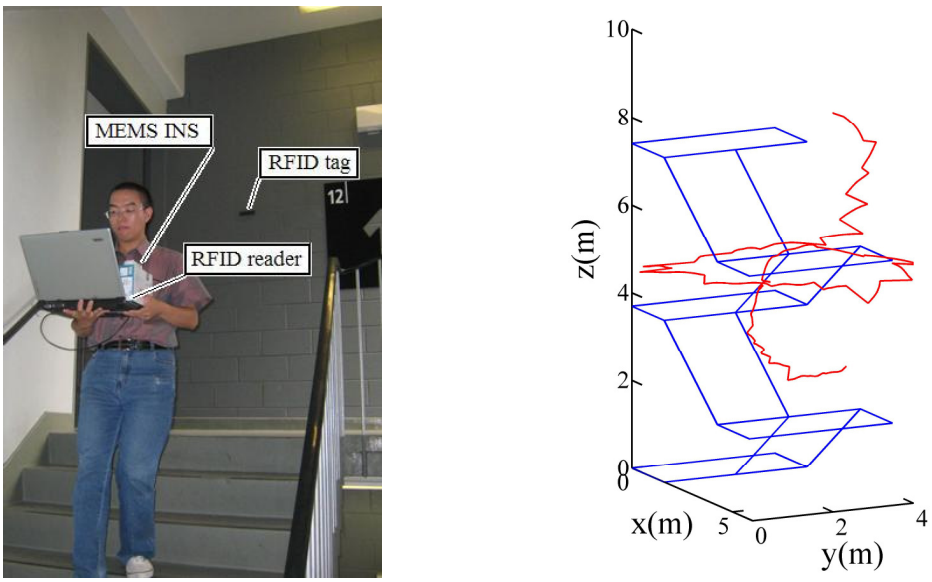

Figure 5.16 The experimental site for evaluating the 3-D integrated INS/RFID location fingerprinting and a schematic plot of the estimated trajectory

(Left side is a photo taken at the experiment site. The plot at right side illustrates the results of one of the estimated trajectories in the experiments.)

Four trajectories between levels 9 and 11 of the building were used for the evaluations. The results show that mobile user movements between the levels can be clearly mapped using the 3-D integrated INS/RFID location fingerprinting algorithm. The RMSE of the experiments were 3.7m, 3.4m, 4.2m and 4.0m respectively. The drifts in INS can be constrained and the integrated algorithm can provide a continuous trajectory for dynamic positioning (see Figure 5.17) (Zhu *et al.*, 2008).

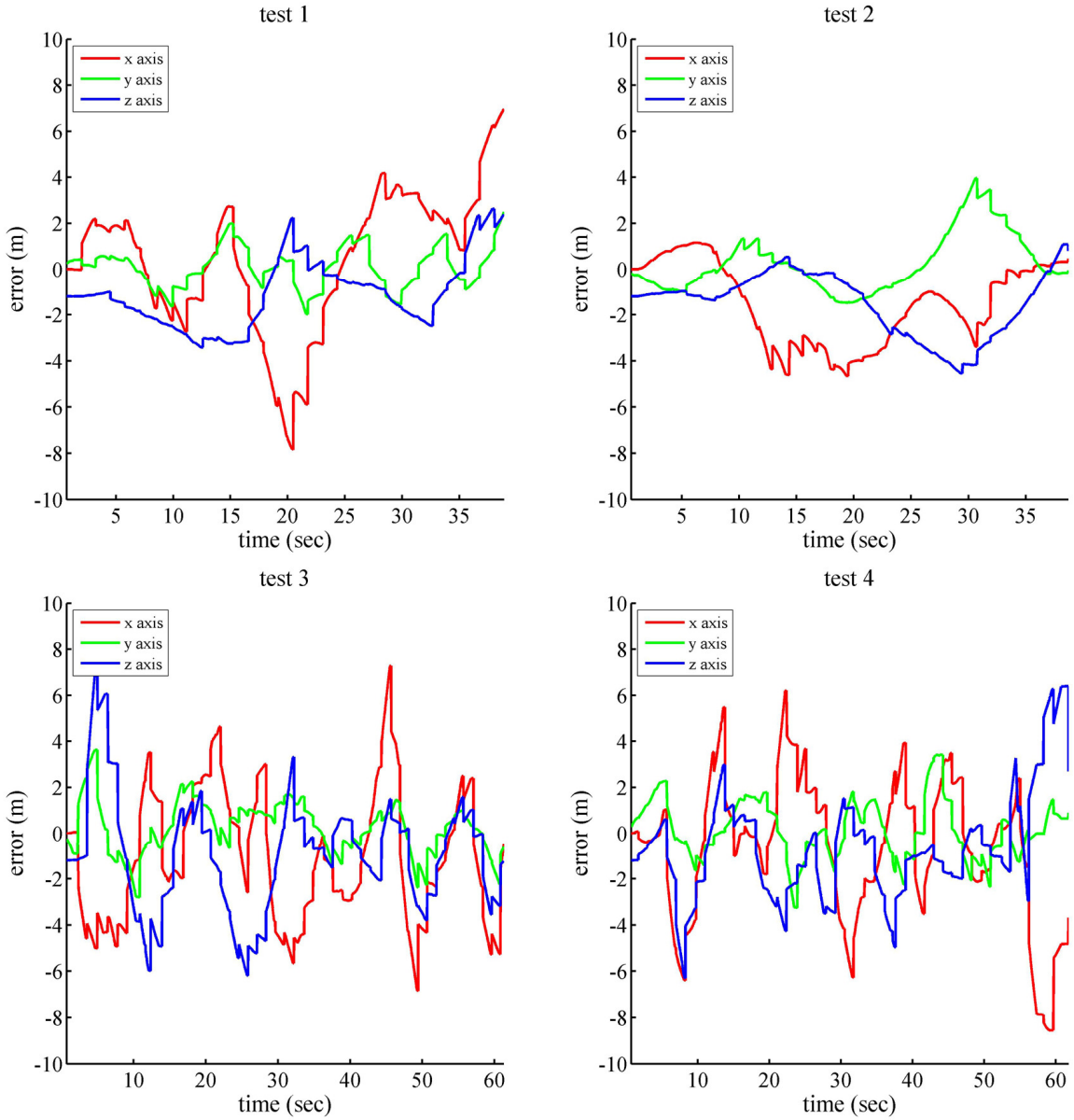

Figure 5.17 Positioning errors of the 3-D integrated INS/RFID location fingerprinting algorithms
(Test 1: the trajectory from levels 11 to 10. Test 2: the trajectory in test 1, travelling in the opposite direction. Test 3: the trajectory from the intermediate level between levels 10 and 11 to the intermediate part between levels 9 and 10. Test 4: the trajectory in test 3, travelling in the opposite direction.)

5.5 Summary

This chapter has presented an approach for improving the positioning accuracy through multi-sensor integration. Evaluations of MEMS INS and PDR were conducted to select an appropriate technique for integrating with RFID positioning

techniques. Based on subsequent experiments and analyses, MEMS INS was selected as the most effective technique. Developments of the integrated INS/RFID probabilistic CoO algorithm and the integrated INS/RFID location fingerprinting algorithms were provided. The experiments and comparisons of the reduced INS, the integrated INS/RFID deterministic CoO and the integrated INS/RFID probabilistic CoO at the Yarra Bend Park test site showed that the integrated INS method could improve the continuity when using RFID CoO techniques. The RFID CoO techniques could also effectively constrain the positioning drifts in INS, especially using the probabilistic CoO approach. The other experiments conducted in a building of the RMIT University City Campus showed that the integrated INS/RFID location fingerprinting algorithm developed could provide metre-level accuracy in dynamic indoor positioning without the need for multiple observations at every position. This is a superior method to the stand-alone RFID location fingerprinting algorithm, which has the difficulties in providing metre-level accuracy for dynamic indoor positioning (see Chapter 4).

The algorithms for extended usage of RFID-based multi-sensor integrated positioning techniques in indoor/outdoor seamless positioning applications are discussed in the following chapter.

Chapter 6 Seamless Positioning Using RFID-Based Techniques

The demand for seamless positioning has significantly increased since the introduction of 'ubiquitous computing' (Weiser, 1991) in the late 1980s. In this technology revolution, people, instead of computational devices, became the focus of the system. Consequently, locating people in indoor/outdoor contexts seamlessly has become a core component of ubiquitous computing. This chapter describes the investigation of the use of the RFID-based multi-sensor techniques for seamless positioning and introduces the algorithms that were developed for these applications.

6.1 Introduction of Seamless Positioning

Positional information is very important. It is needed almost everywhere all the time and this has been possible since the introduction of the concept of 'ubiquitous computing'. This concept is termed the 'third wave' of computing. The core of this concept is to consider the user instead of the computational devices as being the centre of the system (Dodson *et al.*, 2007). Knowing the user's position is an essential component for implementing this concept. By knowing positional information, the system can automatically detect the context and provide the most appropriate services to the user. Consequently, having a technique that can provide continuous indoor and outdoor positional information is an essential element (Mok, 2007). The methods of providing continuous indoor/outdoor positions seamlessly and the algorithms for smoothly transferring the estimation from one outdoor system, like GPS, to another indoor system, like RFID, has attracted a great interest in the LBS research community (Hightower and Borriello, 2001; Retscher and Kealy, 2005). This type of technique is called 'ubiquitous positioning' or 'seamless positioning'.

6.2 Low-cost GPS/RFID Integration Method

Most seamless positioning techniques are based on integration methods. Multiple sensors are used to provide adequate observations for resolving position. In this research, low-cost GPS and RFID were used. Reliable positioning algorithms were developed to deal with the significant nonlinearity of a seamless positioning system.

6.2.1 GPS-based Integration

One kind of seamless GPS-based indoor/outdoor positioning technique is to use integrated RF-based techniques to provide additional observations when the GPS signals are blocked. These RF-based techniques can be WiFi, UWB and other pseudo systems, such as *LOCATA* (Barnes *et al.*, 2003; Mok *et al.*, 2006; Retscher *et al.*, 2007). RFID can also be used as a radio-based ranging technique for low-accuracy dynamic positioning (see Chapter 4). Its measurements can be used to compensate for the inadequate observations obtained from low-cost GPS and in areas where the GPS signal is blocked. The algorithms for integrating low-cost GPS and RFID were developed in cooperation with the National University of Defence Technology, China.

6.2.2 Iterated Reduced Sigma Point Kalman Filter

EKF is the preferred algorithm for integrating the measurements in nonlinear systems (see Chapter 3). In theory, the ultimate goal of KF is to determine the optimal values of Equations (6.1), (6.2) and (6.3). A priori estimate of the state is the expectation of the state transition according to posterior estimates and the process noise in the previous epoch. A priori estimate of the measurement is the expectation according to a priori estimation of the state and the measurement uncertainty. The Kalman gain is the ratio of the error covariance matrices.

$$\hat{x}_k^- = E(f(\hat{x}_{k-1}^+, w_{k-1})) \qquad (6.1)$$

where,

$\hat{x}_k^-$ is the a priori estimates of the state vector;

$\hat{x}_{k-1}^+$ is the posterior estimates of the state vector in the previous epoch;

w_{k-1} is the zero-mean white Gaussian process noise in the previous epoch;

$f(\bullet)$ is the state transition function; and

$E(\bullet)$ is the expectation.

$$\hat{z}_k^- = E(h(\hat{x}_k^-, v_k)) \qquad (6.2)$$

where,

$\hat{z}_k^-$ is the a priori estimates of the measurement;

v_k is the zero-mean white Gaussian measurement uncertainty; and

$h(\bullet)$ is the measurement function.

$$\begin{aligned}\underset{\sim}{\overline{K}}_k &= \underset{\sim}{P}_{x_k z_k} \cdot \underset{\sim}{P}_{\tilde{z}_k}^{-1} \\ &= E[(x_k - \hat{x}_k^-) \cdot (z_k - \hat{z}_k^-)^T] \cdot E[(z_k - \hat{z}_k^-) \cdot (z_k - \hat{z}_k^-)^T]^{-1}\end{aligned} \qquad (6.3)$$

$\underset{\sim}{\overline{K}}_k$ is the Kalman gain;

$\underset{\sim}{P}_{x_k z_k}$ is the error covariance matrix of the state vector and measurements;

$\underset{\sim}{P}_{\tilde{z}_k}$ is the error covariance matrix of the measurements; and

x_k and z_k are the true values of the state vector and measurements respectively.

In an EKF (see Chapter 3), it approximates the Equations (6.1), (6.2) and (6.3) by the following equations (see Equations (6.4), (6.5) and (6.6)).

$$\hat{x}_k^- \approx f(\hat{x}_{k-1}^+) \qquad (6.4)$$

$$\hat{z}_k^- \approx h(\hat{x}_k^-) \qquad (6.5)$$

$$\underset{\sim}{\overline{K}}_k \approx \underset{\sim}{\hat{P}}_{x_k z_k} \cdot \underset{\sim}{\hat{P}}_{\tilde{z}_k}^{-1} \qquad (6.6)$$

where,

$\underset{\sim}{\hat{P}}_{x_k z_k}$ and $\underset{\sim}{\hat{P}}_{\tilde{z}_k}$ are the estimated error covariance matrices.

Apparently, noises are ignored in Equations (6.4) and (6.5). In addition, the error covariance matrices are determined by linear models. These approximations may cause divergence of the filter in the complex nonlinear systems.

In order to compensate for the limitations in the EKF, the SPKF was introduced in the mid-1990's (Julier and Uhlmann, 1997). This algorithm transforms a set of sample points nonlinearly, which are cited as sigma-points, instead of using the linearised functions in the EKF. The sigma-points are determined by the following equations (see Equations (6.7), (6.8) and (6.9)).

$$\mathbf{X}_i^x = \begin{cases} \overline{x} & i = 0 \\ \overline{x} + \zeta \cdot (\sqrt{\underset{\sim}{P}})_i & i = 1,...,N \\ \overline{x} - \zeta \cdot (\sqrt{\underset{\sim}{P}})_i & i = N+1,...,2N \end{cases} \quad (6.7)$$

where,

$\mathbf{X}_i^x$ is the i th sigma-point of the state;

$\overline{x}$ is the mean of the state;

$\underset{\sim}{P}$ is the error covariance matrix of the state;

ζ is a scalar scaling factor that determines the spread of the sigma-points; and

N is the dimension.

$$\mathbf{X}_i^w = \begin{cases} \overline{w} & i = 0 \\ \overline{w} + \zeta \cdot (\sqrt{\underset{\sim}{Q}})_i & i = 1,...,N \\ \overline{w} - \zeta \cdot (\sqrt{\underset{\sim}{Q}})_i & i = N+1,...,2N \end{cases} \quad (6.8)$$

where,

$\mathbf{X}_i^w$ is the i th sigma-point of the state;

$\overline{w}$ is the mean of the process noise; and

$\underset{\sim}{Q}$ is the covariance matrix of the process noise.

$$\mathbf{X}_i^v = \begin{cases} \overline{v} & i = 0 \\ \overline{v} + \zeta \cdot (\sqrt{\underset{\sim}{R}})_i & i = 1,...,N \\ \overline{v} - \zeta \cdot (\sqrt{\underset{\sim}{R}})_i & i = N+1,...,2N \end{cases} \quad (6.9)$$

where,

$\mathbf{X}_i^v$ is the i th sigma-point of the state;

$\overline{v}$ is the mean of the measurement uncertainty; and

$\underset{\sim}{R}$ is the covariance matrix of the measurement uncertainty.

The scalar scaling factor is determined by the dimension of the state and the scaling factors (see Equation (6.10)).

$$\zeta = \alpha \cdot \sqrt{(N + \kappa)} \tag{6.10}$$

where,

α is the primary scaling factor determining the extent of the spread of the sigma-points around the prior mean value; and

κ is the tertiary scaling factor.

The weights to transform the sigma-points back into the state space are determined according to the dimension of the state and the scaling factors (see Equations (6.11), (6.12) and (6.13)).

$$w_0^m = \frac{\alpha^2 (N + \kappa) - N}{\alpha^2 (N + \kappa)} \tag{6.11}$$

$$w_0^c = w_0^m + (1 - \alpha^2) + \beta \tag{6.12}$$

$$w_i^c = w_i^m = \frac{1}{2\alpha^2 \cdot (N + \kappa)}, \; i = 1, ..., 2N \tag{6.13}$$

where,

w_0^m is the weight for the sigma-point of the measurement;

w^c is the weight for the sigma-point of the covariance; and

β is the secondary scaling factor used to emphasize the weighting on the zero-th sigma-point for the posterior covariance calculation.

According to the theory and the definitions, the time update equations of the SPKF are:

$$\mathbf{X}_{i,k|k-1}^x = f(\mathbf{X}_{i,k-1}^x, \mathbf{X}_{i,k-1}^w) \tag{6.14}$$

$$\hat{x}_k^- = \sum_{i=0}^{2N} w_i^m \cdot \mathbf{X}_{i,k|k-1}^x \tag{6.15}$$

$$\underset{\sim}{P}_{x_k}^- = \sum_{i=0}^{2N} \sum_{j=0}^{2N} w_{ij}^c \cdot (\mathbf{X}_{i,k|k-1}^x) \cdot (\mathbf{X}_{i,k|k-1}^x)^T \tag{6.16}$$

The measurement update equations of the SPKF are:

$$\mathbf{Z}_{i,k|k-1} = h(\mathbf{X}_{i,k|k-1}^x, \mathbf{X}_{i,k}^v) \tag{6.17}$$

$$\hat{z}_k^- = \sum_{i=0}^{2N} w_i^m \cdot \mathbf{Z}_{i,k|k-1} \tag{6.18}$$

$$\underset{\sim}{P}_{\tilde{z}_k} = \sum_{i=0}^{2N}\sum_{j=0}^{2N} w_{ij}^c \cdot (\mathbf{Z}_{i,k|k-1}) \cdot (\mathbf{Z}_{i,k|k-1})^T \tag{6.19}$$

$$\underset{\sim}{P}_{x_k z_k} = \sum_{i=0}^{2N}\sum_{j=0}^{2N} w_{ij}^c \cdot (\mathbf{X}_{i,k|k-1}^x) \cdot (\mathbf{Z}_{i,k|k-1})^T \tag{6.20}$$

$$\underset{\sim}{\overline{K}}_k = \underset{\sim}{P}_{x_k z_k} \cdot \underset{\sim}{P}_{\tilde{z}_k}^{-1} \tag{6.21}$$

$$\hat{x}_k^+ = \hat{x}_k^- + \underset{\sim}{\overline{K}}_k \cdot (z_k - \hat{z}_k^-) \tag{6.22}$$

$$\underset{\sim}{P}_{x_k}^+ = \underset{\sim}{P}_{x_k}^- - \underset{\sim}{\overline{K}}_k \cdot \underset{\sim}{P}_{\tilde{z}_k} \cdot \underset{\sim}{\overline{K}}_k^T \tag{6.23}$$

By implementing the SPKF, the major limitations in the EKF, including the complicities and the instabilities of the linearised Jacobian approximations, can be satisfactorily resolved. In addition, this algorithm can be made more robust by using the iterative method (Zhan and Wan, 2007). However, computational burden can be a limitation for implementation (Sugimoto *et al.*, 2009).

The reduced SPKF is based on the theory that the number of points used for constructing the largest possible affinely independent set is $N+1$. For example, the two dimensional (2-D) three points as a triangle can be used instead of a four-point rhomboid. A 3-D four-point tetrahedron can be used instead of a six-point octahedron (see Figure 6.1). Accordingly, the Reduced SPKF (RSPKF) reduces the number of sigma-points required from $2N+1$ in standard SPKF to $N+2$. (Julier, 2003)

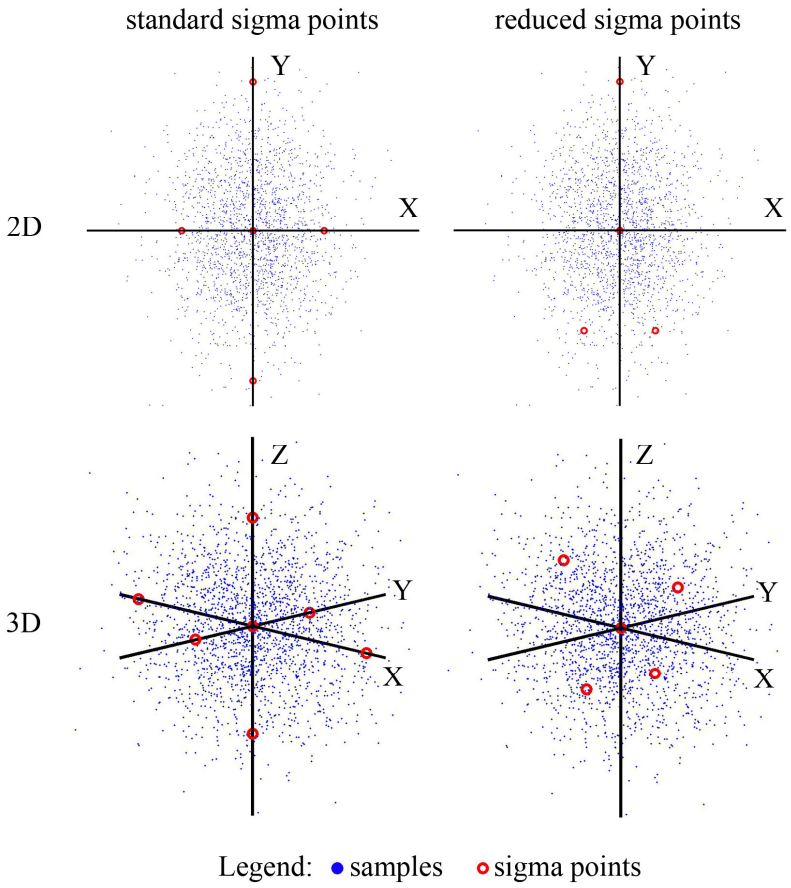

Figure 6.1 A schematic plot of the fundamentals in the reduced sigma points theory

(The top two plots show the standard sigma points (5 points) and reduced sigma points (4 points) in 2-D and the bottom two plots show the standard sigma points (7 points) and reduced sigma points (5 points) in 3-D)

In the RSPKF, the weight sequence is given by the following Equation (6.24).

$$w_i^c = \begin{cases} 1 - w_0^c & i = 1 \\ w_1^c & i = 2 \\ 2^{i-1} w_1^c & i = 3, \ldots, n+1 \end{cases} \tag{6.24}$$

The scalar scaling factor sequence for 1-D problems is:

$$\zeta_0^1 = [0] \tag{6.25}$$

$$\zeta_1^1 = \left[-\frac{1}{\sqrt{2w_1^c}} \right] \tag{6.26}$$

$$\zeta_2^1 = \left[\frac{1}{\sqrt{2w_1^c}} \right] \tag{6.27}$$

The scalar scaling factor sequence for higher dimensional problems is:

$$\zeta_i^N = \begin{cases} \begin{bmatrix} \zeta_0^{N-1} \\ 0 \end{bmatrix} & i = 0 \\ \begin{bmatrix} \zeta_i^{N-1} \\ -\dfrac{1}{\sqrt{2w_N^c}} \end{bmatrix} & i = 1,...,N \\ \begin{bmatrix} O \\ \dfrac{1}{\sqrt{2w_N^c}} \end{bmatrix} & i = N+1 \end{cases} \tag{6.28}$$

In addition, the square-root unscented KF is used to improve the efficiency (see Equation (6.29)).

$$\underset{\sim}{S} \equiv \sqrt{\underset{\sim}{P}} \tag{6.29}$$

where, $\underset{\sim}{S}$ is the square-root of the error covariance matrix.

The simplex sigma-points (the sigma-points of the set with the minimum number of sigma-points) are given by the following Equations (6.30), (6.31) and (6.32).

$$\mathbf{X}_i^x = \overline{x} + \zeta_i \cdot (\underset{\sim}{S})_i \tag{6.30}$$

$$\mathbf{X}_i^w = \overline{w} + \zeta_i \cdot (\sqrt{\underset{\sim}{Q}})_i \tag{6.31}$$

$$\mathbf{X}_i^v = \overline{v} + \zeta_i \cdot (\sqrt{\underset{\sim}{R}})_i \tag{6.32}$$

The time update equations are:

$$\underset{\sim}{S}_{x_k}^- = \mathrm{qr}\{[\sqrt{w_{1:N+1}^c} \cdot (\mathbf{X}_{1:N+1,k|k-1}^x - \hat{x}_k^-)]\} \tag{6.33}$$

$$\underset{\sim}{S}_{x_k}^- = \mathrm{cholupdate}\{\underset{\sim}{S}_{x_k}^-, \mathbf{X}_{0,k|k-1}^x - \hat{x}_k^-, w_0^c\} \tag{6.34}$$

where,

$\mathrm{qr}\{\bullet\}$ is the lower-triangular part resulted from a QR decomposition of the matrix; and

$\mathrm{cholupdate}\{\bullet\}$ is the N consecutive rank-1 Cholesky updates.

The measurement update equations are:

$$\underset{\sim}{S}_{\tilde{z}_k} = \mathrm{qr}\{[\sqrt{w_{1:N+1}^c} \cdot (\mathbf{Z}_{1:N+1,k|k-1} - \hat{z}_k^-)]\} \tag{6.35}$$

$$\underset{\sim}{S}_{\tilde{z}_k} = \text{cholupdate}\{\underset{\sim}{S}_{\tilde{z}_k}, \mathbf{Z}_{0,k|k-1} - \hat{z}_k^-, w_0^c\} \tag{6.36}$$

$$\underset{\sim}{P}_{x_k z_k} = \sum_{i=0}^{N+1} w_i^c \cdot (\mathbf{X}_{i,k|k-1}^x - \hat{x}_k^-) \cdot (\mathbf{Z}_{i,k|k-1} - \hat{z}_k^-)^T \tag{6.37}$$

$$\overline{\underset{\sim}{K}}_k = (\underset{\sim}{P}_{x_k z_k} / \underset{\sim}{S}_{\tilde{z}_k}^T) / \underset{\sim}{S}_{\tilde{z}_k} \tag{6.38}$$

$$\underset{\sim}{S}_{x_k}^+ = \text{cholupdate}\{\underset{\sim}{S}_{x_k}^-, \overline{\underset{\sim}{K}}_k \cdot \underset{\sim}{S}_{\tilde{z}_k}, -1\} \tag{6.39}$$

Using a similar idea of the iterated SPKF, further developments of the RSPKF was provided by Peng *et al.* (2009). The objective was to obtain an updated measurement as an approximate maximum of a posterior estimate via the Gauss-Newton iterative method (Bar-Shalom *et al.*, 2001). The algorithm repeats the process of the RSPKF at every epoch until the results meet the terminal conditions using the Gauss-Newton iterative method (see Equation (6.40)).

$$\left\| \hat{x}_{k(i+1)}^+ - \hat{x}_{k(i)}^+ \right\| \leq \varepsilon \text{ or } i \leq M \tag{6.40}$$

6.2.3 Dynamic Model

In the developed algorithm, the dynamic model for the epochs with the low-cost GPS observations is given by a constant acceleration model (see Equations (6.41) - (6.45)).

$$c \cdot \dot{\delta t}_k = c \cdot \dot{\delta t}_{k-1} + w_{k-1}^{c \cdot \dot{\delta t}} \tag{6.41}$$

$$c \cdot \delta t_k = c \cdot \delta t_{k-1} + c \cdot \dot{\delta t}_{k-1} \cdot t + w_{k-1}^{c \cdot \delta t} \tag{6.42}$$

$$f_k = f_{k-1} + w_{k-1}^f \tag{6.43}$$

$$v_k = v_{k-1} + f_{k-1} \cdot t + w_{k-1}^v \tag{6.44}$$

$$p_k = p_{k-1} + v_{k-1} \cdot t + w_{k-1}^p \tag{6.45}$$

where,

c is the speed of light;

δt_k and $\dot{\delta t}_k$ are the clock bias and drift respectively;

f_k, v_k and p_k are the acceleration, velocity and position respectively;

w_k is the Gaussian noise in the states; and

t is the time interval between the epochs.

Since only the distances can be measured by an RFID system, the dynamic model for the epochs with the RFID observations is given by a constant velocity model (see Equations (6.46) - (6.47)).

$$v_k = v_{k-1} + f_{k-1} \cdot t + w_{k-1}^v \tag{6.46}$$

$$p_k = p_{k-1} + v_{k-1} \cdot t + w_{k-1}^p \tag{6.47}$$

6.2.4 Measurement Model

The measurement models are defined by the pseudorange observation equations and the distance equations for low-cost GPS measurements and RFID measurements respectively.

$$\rho_j = \sqrt{(p_x^j - p_x^{user})^2 + (p_y^j - p_y^{user})^2 + (p_z^j - p_z^{user})^2} + c \cdot \delta t + v^\rho \tag{6.48}$$

where,

ρ_j is the pseudorange from the j th satellite to the user;

p_x^j, p_y^j and p_z^j is the position of the j th satellite in three axes respectively;

p_x^{user}, p_y^{user} and p_z^{user} are the user's position in three axes respectively; and

v^ρ is the pseudorange measurement noise.

$$d_i = \sqrt{(p_x^i - p_x^{user})^2 + (p_y^i - p_y^{user})^2 + (p_z^i - p_z^{user})^2} + v^d \tag{6.49}$$

where,

d_i is the distance from the i th RFID tag to the user;

p_x^i, p_y^i and p_z^i is the position of the i th RFID tag in three axes respectively; and

v^d is the distance measurement noise.

6.2.5 Experiments and Analyses

Experiments for evaluating the iterated RSPKF were conducted at the Formula 1 Grand Prix circuit in Albert Park, Melbourne (see Figure 6.2). In the open areas, the pseudorange measurements from a low-cost GPS were used for positioning. In the GPS blocked areas, which are in the north-east corner of the circuit, an RFID tag array was placed along the roads in order to provide additional distance observations (see Figure 6.3). The iterated RSPKF was used to integrate the measurements for seamless positioning. The positions measured by the RTK GPS technique were used as the references for evaluations.

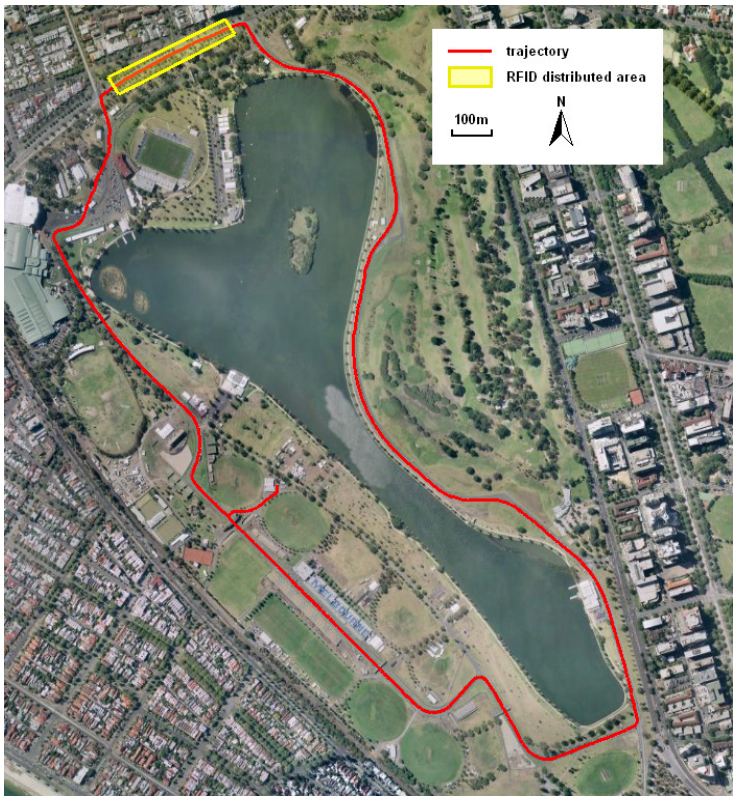

Figure 6.2 The experimental site and the trajectory for evaluating the iterated reduced SPKF for the GPS/RFID integrated seamless positioning technique

(The tested trajectory is along the Formula 1 Grand Prix circuit in Albert Park, Melbourne, Australia. In the north-east corner some of the GPS signals were blocked by the buildings nearby the roads. The RFID tags were placed in those areas to provide additional distance measurements. The satellite image in the background is taken from *GoogleEarth*.)

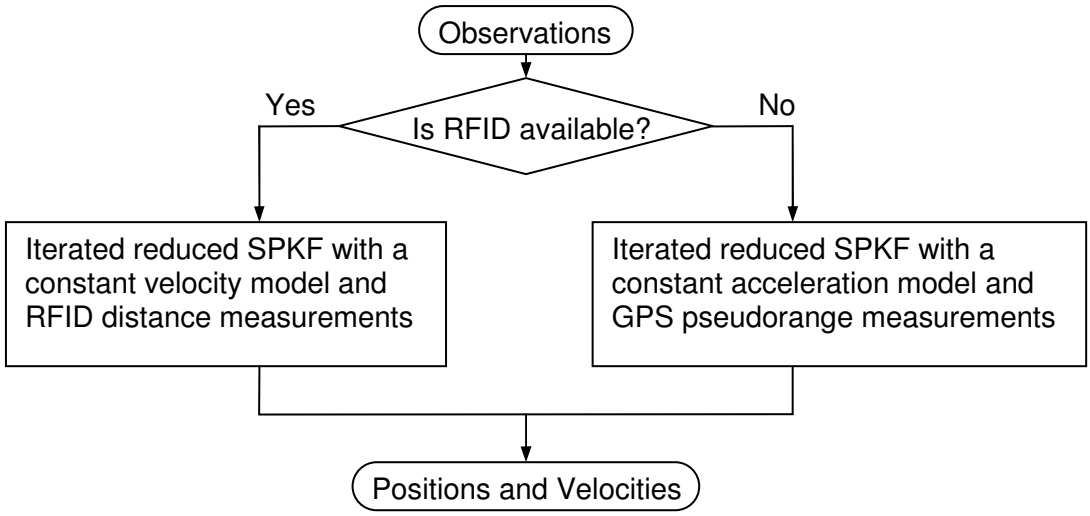

Figure 6.3 The flow chart of the GPS RFID integration method (The algorithm shifts to the module for RFID positioning when the RFID tags are detected.)

From the experiments, the comparisons of the low-cost GPS stand-alone using conventional SPKF, the integrated low-cost GPS/RFID using conventional SPKF and the iterated RSPKF are shown in Table 6.1. Results show that the positioning accuracy can be increased by 69.5% by using the integrated low-cost GPS/RFID technique since the RFID system provides the additional observations in the areas with limited GPS visibility. It also indicates that iterated RSPKF can further improve the performance by 28.8% (Peng *et al.*, 2009).

Table 6.1 The experimental results for low-cost GPS/RFID integrations

Method	Positioning RMSE (m)	Maximum positioning errors in the GPS visibility constraint areas (m)
GPS using SPKF	7.4	90.9
GPS/RFID using SPKF	3.2	37.3
GPS/RFID using iterated RSPKF	2.2	20.9

6.3 GPS/RFID/INS Integration Method

The integrated low-cost GPS/RFID method evaluated in the previous section provides satisfactory results of this low-cost seamless positioning technique. However, for personal positioning applications in large areas with limited GPS visibility such as in metropolitan areas or in forests, placing RFID tags in all the GPS low-visibility areas would involve a tremendous workload. An alternative method is to

include the self-contained INS into the integrated system to provide short-term relative positions in the GPS blockage areas without the need to establish a dense network of RFID tags. One similar method that uses GPS/UWB/INS integration has been published by Tanigawa et al. (2008). Their results showed that an indoor accuracy of 0.2m could be achieved by using UWB/INS and an outdoor accuracy of 3.6m was possible using GPS/INS. Nevertheless, this method comes with associated high costs. The expensive UWB positioning system usually costs tens of thousands Australian dollars. In this research, the low-cost RFID system was used instead of the more expensive UWB system. The objective was to achieve metre-level seamless positioning accuracy using cost-effective devices in order to make the technique practical for personal positioning applications.

6.3.1 Integration with INS

In an open area with a good visibility of GPS satellites, integrated GPS/INS algorithms are used for positioning. In the literature (e.g. Groves, 2008; Titterton and Weston, 2004) these algorithms have been well studied. Generally, there are three types of GPS/INS integrated algorithms, according to the different levels of GPS data used for integration. Examples are the loose, tight and ultra-tight integrations (see Figure 6.4). The tighter the integration, the more robust the performance. However, there are two major limitations when using the tighter integrations with low-cost GPS/MEMS INS integration. Firstly, large noises and drifts in the MEMS sensors make the tuning of the KF difficult for tighter integrations. Secondly, most commercial low-cost GPS can only provide position and velocity measurements. There is no lower level observations accessible, such as pseudoranges and delta ranges (Fastrax, 2007). Consequently, the loose integration method was used for the GPS/INS integration in this research.

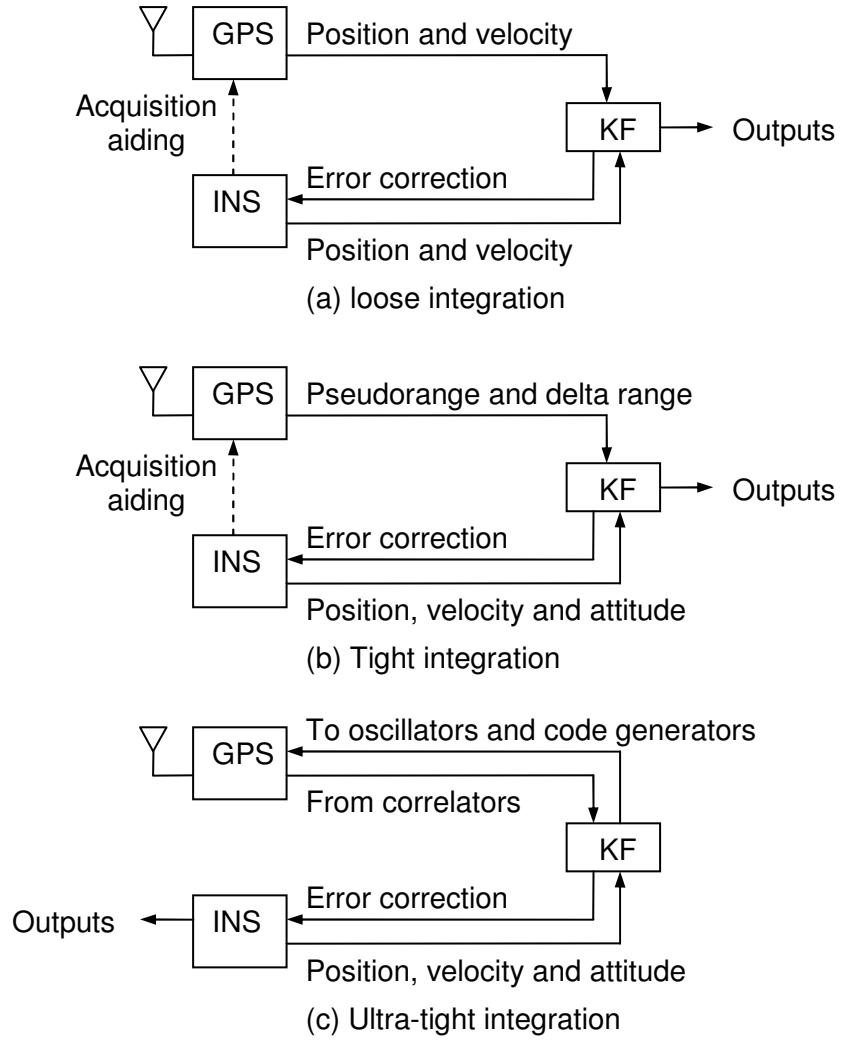

Figure 6.4 The schematic plots of typical GPS/INS integrated algorithms (Groves, 2008; Titterton and Weston, 2004)
((a) loose integration: the solutions of position and velocity from GPS are used for the integration.
(b) Tight integration: the pseudorange and delta range measurements from GPS are used for the integration.
(c) Ultra-tight integration: the raw measurements in the correlators are directly used for the integration.)

In the GPS blockage areas, the integrated RFID/INS algorithms, as discussed in Chapter 5, were used. An algorithm was developed to assist in choosing the appropriate integrated RFID/INS algorithm, according to the number of detected tags and the achievable knowledge (see Figure 6.5).

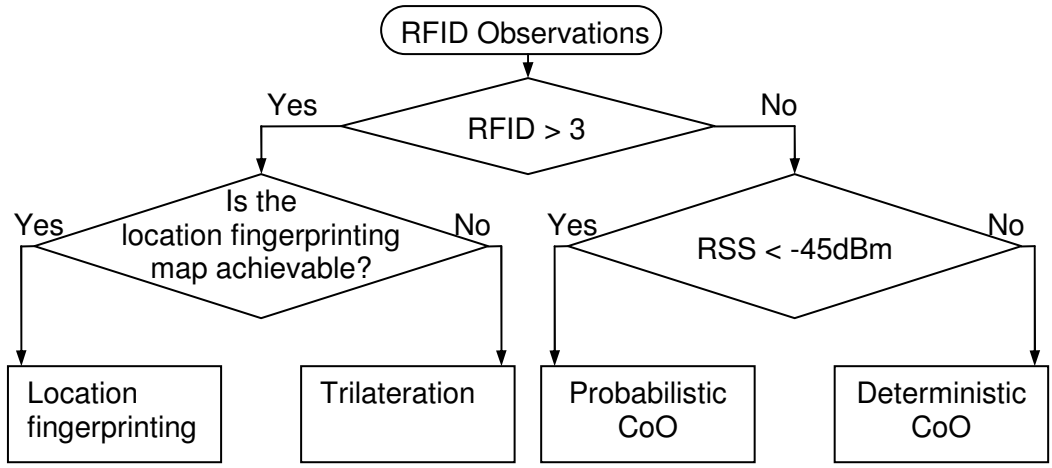

Figure 6.5 A schematic plot of the strategy for choosing the appropriate RFID/INS algorithm

(The CoO algorithms will be used if less than three RFID tags are detected. The deterministic CoO will be applied if the mobile user is near the cell centre. Otherwise, the probabilistic CoO is used. If the number of the detected tags is over three, the trilateration or the location fingerprinting will be applied depending on the accessibility of the RSS distributions.)

6.3.2 Dynamic and Measurement Models

Nine state variables were used for the dynamic models of the seamless positioning system, including the three orthogonal axes' position errors, velocity errors and tilts (Zhu, Zhang, Wu, Cartwright *et al.*, 2007). The state transition matrix is given by Equation (6.50) (Rogers, 2000). The measurement models are selected according to the combinations of the available measurements (see Chapter 5).

$$\underset{\sim}{\Phi} = \begin{bmatrix} 1 & \Delta t & 0 & 0 & 0 & 0 & 0 & 0 & 0 \\ 0 & 1 & -g\cdot\Delta t & 0 & 0 & 0 & 0 & 0 & 0 \\ 0 & \frac{\Delta t}{R} & 1 & 0 & 0 & 0 & 0 & 0 & \dot{\phi}\cdot\Delta t \\ 0 & 0 & 0 & 1 & \Delta t & 0 & 0 & 0 & 0 \\ 0 & 0 & 0 & 0 & 1 & -g\cdot\Delta t & 0 & 0 & 0 \\ 0 & 0 & 0 & 0 & \frac{\Delta t}{R} & 1 & 0 & 0 & \dot{\theta}\cdot\Delta t \\ 0 & 0 & 0 & 0 & 0 & 0 & 1 & \Delta t & 0 \\ 0 & 0 & 0 & 0 & 0 & 0 & \frac{-2g\cdot\Delta t}{R} & 1 & 0 \\ 0 & 0 & 0 & 0 & 0 & 0 & 0 & 0 & 1 \end{bmatrix} \quad (6.50)$$

where,

R is the radius of the Earth;

g is the magnitude of the gravity;

$\dot{\phi}$ and $\dot{\theta}$ are the rotation rate of the x and y axes in the body frame respectively; and

Δt is the time interval between two adjacent epochs.

6.3.3 Experiments and Analysis

The experiments were conducted at Yarra Bend Park, Melbourne, Australia. A complicated environment setting was chosen for the seamless positioning experiments. This included the indoor areas experiments in a house that was mainly constructed of timber, the canopy covered areas outside the house and outdoor open areas (see Figure 6.6). Figure 6.7 shows the Position Dilution of Precision (PDOP) observed along the trajectory, which extended from the outside to the inside of the house. The average PDOP value was 3.85. A small number of peaks were caused by trees and the house itself, which blocked the GPS signals. Since the dimension of the house was relatively small and it was mainly built of timber, the GPS signals were always available during the experiments, even inside the house. However, some GPS signals were arbitrarily withdrawn in order to evaluate the algorithms developed. Eleven RFID tags were placed outdoors to provide additional observations in the blocked GPS signal areas. Another four RFID tags were placed along the corridor in the house for indoor positioning experiments. The GPS RTK system was used to provide outdoor reference positions. Building plans provided the indoor positioning reference.

(a) (b)

Figure 6.6 The experimental site
(Plot (a) shows the house and the trees in the experimental site and plot (b) shows the indoor setups in the house.)

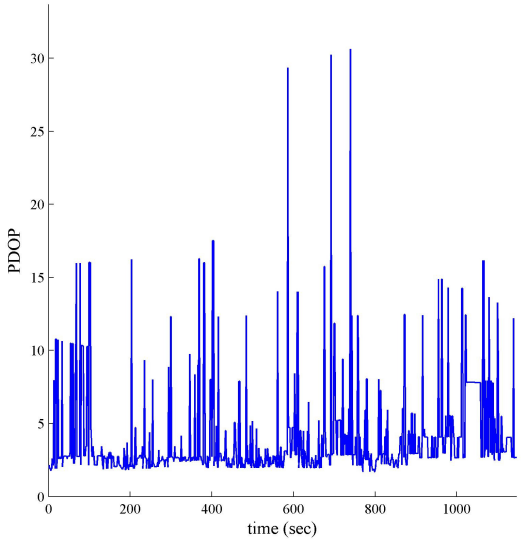

Figure 6.7 The PDOP values observed along the experimental trajectory
(The average PDOP value is 3.85. the peaks, which are up to 30, are mainly caused by the blockage of the GPS signals from the trees and the house.)

The experiments showed that the seamless positioning technique, based on low-cost GPS, MEMS INS and RFID, can provide metre-level and continuous positions both outdoors and indoors. In the outdoor areas, the horizontal RMSE was 4.0m (see Figure 6.8). In the blocked GPS signal areas, the integrated RFID/MEMS INS technique can decrease the horizontal RMSE from 8.2m to 3.0m (see Figure 6.9 and Figure 6.10).

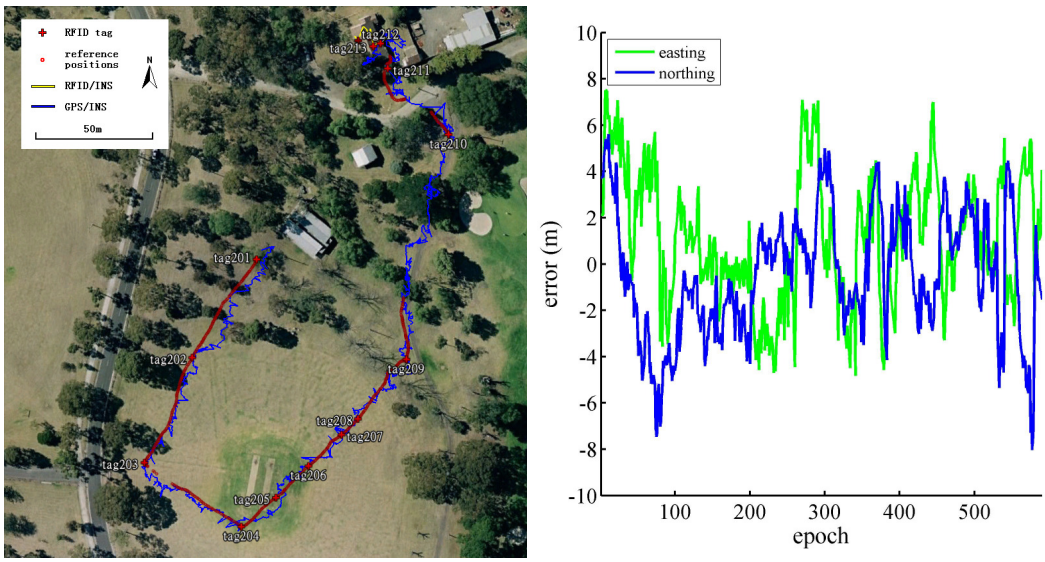

(a) (b)

Figure 6.8 The experimental results and the errors of the seamless positioning

(Plot (a) shows the experimental results of the seamless positioning at Yarra Bend Park, Melbourne. Plot (b) shows the easting and northing errors according to the GPS RTK measurements in the open areas. The satellite image in the background is taken from *GoogleEarth*.)

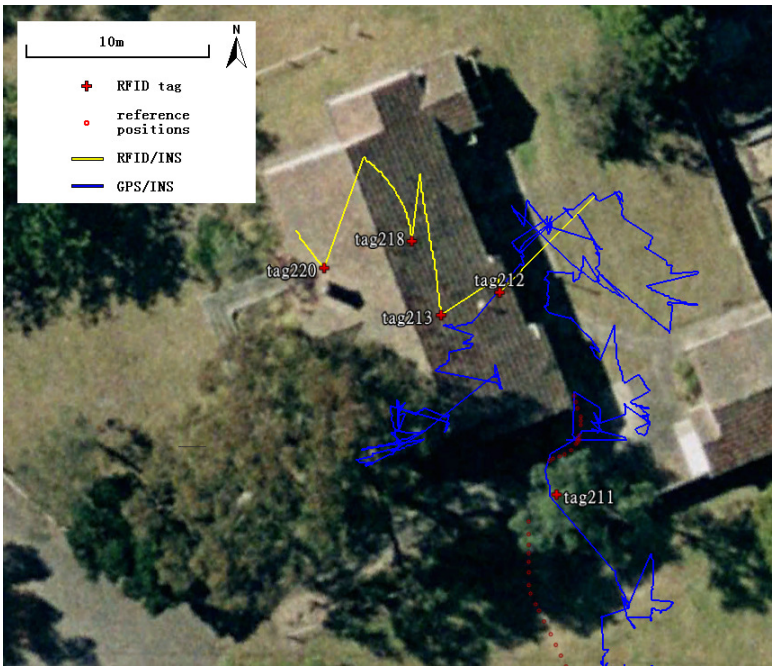

Figure 6.9 The enlarged plot of the positioning results in the indoor and GPS visibility limited areas

(The RFID tags 212, 213, 218 and 220 were placed along the corridor in the house. The satellite image in the background is from *GoogleEarth*.)

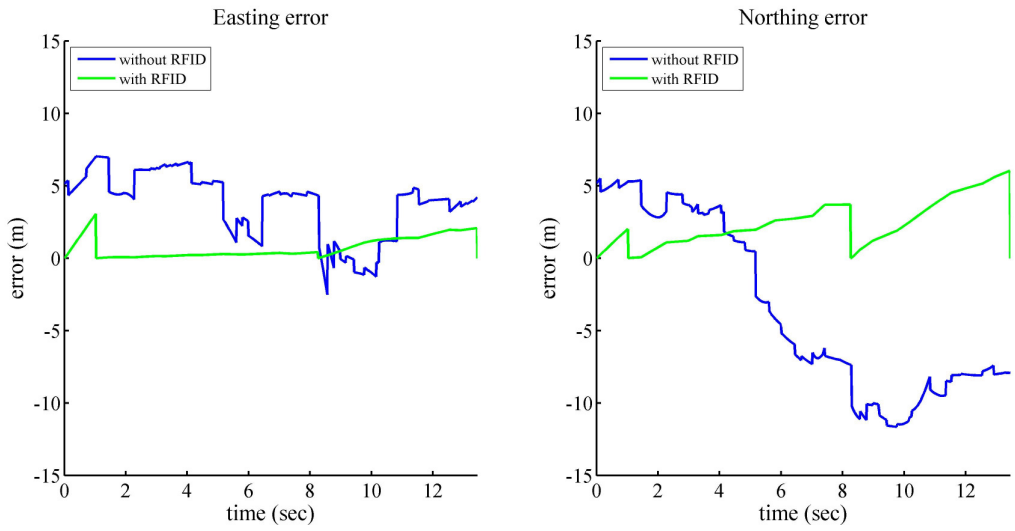

Figure 6.10 The indoor positioning errors in the experiments with and without using RFID respectively

6.4 Summary

This chapter has presented the development of algorithms for RFID-based multi-sensor integrated positioning techniques in seamless indoor/outdoor positioning applications. The experiments at the Albert Park Formula 1 circuit show that an integrated GPS/RFID system can provide additional range observations with RFID in the blocked GPS signals areas, so that seamless positions can be provided. The experiments also indicate that the iterated RSPKF algorithm developed for this integrated positioning system is superior to the conventional SPKF. It can increase the positioning accuracy by 28.8%. The other experiments conducted in Yarra Bend Park show that the iterated RSPKF algorithm developed can also be applied to other integrated positioning systems effectively. It indicates that the integrated low-cost GPS/RFID/INS technique with the algorithm developed can efficiently provide metre-level accuracy for personal indoor/outdoor seamless positioning. In conclusion, the RFID positioning techniques can provide additional observations in blocked GPS signal areas and can also provide seamless indoor/outdoor positions by integrating with other positioning sensors. The iterated RSPKF algorithm developed is more efficient and effective than the conventional SPKF for the multi-sensor integrated seamless positioning systems.

The utilization of geospatial information to improve the accuracy of RFID-based multi-sensor integrated positioning techniques for personal navigation is investigated in the next chapter.

Chapter 7 GIS Assisted RFID Positioning

With the rapid development of computer-based geospatial techniques and virtual reality techniques, position-related environmental information can be systematically collected, analysed, storied and represented. The geospatial information can be used to:

(a) represent the geometrical environments of the positioning operation;

(b) increase positioning precision; and

(c) build SISP propagation models for estimating RSS distributions.

7.1 Indoor GIS Database

The fundamental requirement of implementing GIS-assisted indoor positioning algorithms is a 3-D indoor GIS database. One pioneer work in this area was conducted by Koninger and Bartel (1997). A 3-D GIS urban model was developed for visualisation purposes without internal structures of the buildings being used. Meijers *et al.* (2005) investigated this further and an indoor path database was developed for the purpose of emergency evacuation. Path finding methods in multi-story buildings were further developed by Musliman *et al.* (2006). Lee (2007) combined these and developed a 3-D navigable data model based on a 3-D geometric network. In this model both the path connectivity and the geospatial database of the physical and environmental factors were included. This idea was implemented by Sinha *et al.* (2009) through the developments of a 3-D indoor GIS model. It provided an interesting new opportunity for assisting positioning and navigation services indoors.

As mentioned previously, a typical 3-D indoor GIS usually contains two types of information (see Figure 7.1). One is the structure model which consists of the structure of the building and the other is a route map which provides possible connectivity to the positions of interest inside the building. These two types of information can be used for different purposes with indoor positioning techniques. For example, the route map can be used as constraining factors in pedestrian movement models (Khider *et al*., 2009). For RFID-based positioning techniques, these maps can be used for 3-D map matching in order to increase positioning accuracy and reference for sensor calibration. The structural model of the buildings can be used to

generate the environmental parameters for SISP propagation models in order to provide an efficient method for estimating RSS distributions in specific environments.

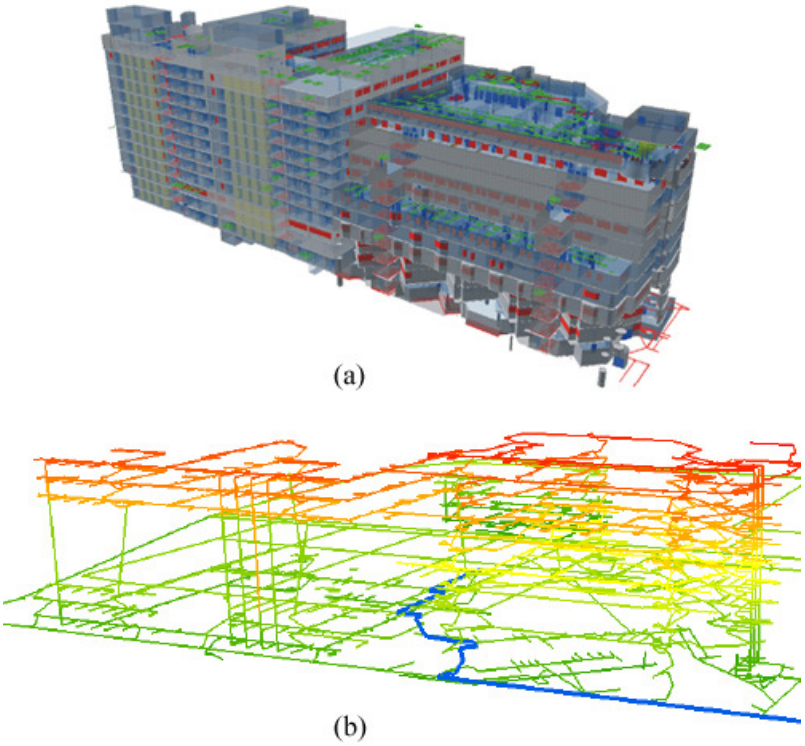

Figure 7.1 The schematic plots of the 3-D indoor GIS model of the buildings at RMIT University city campus
(Plot (a) is the structural model of the buildings and plot (b) is the route map of the multi-story buildings (Sinha *et al.*, 2009).)

7.2 Map Matching

The map matching algorithm was first developed in the Automatic Route Control System (ARCS) for land vehicle positioning (French and Lang, 1973). Map matching was used to improve the positioning accuracy of an automated vehicle based on the DR measurements from a differential odometer. 1.15m positioning accuracy was achieved in their experiments (French, 1989). The basic concept of the map matching algorithms was to constrain the positions onto road segments based on the assumption that the vehicle always travels along the road. These algorithms are widely used in the land vehicle positioning applications (Quddus *et al.*, 2007; Stephen, 2000; Zhao, 1997). Typical examples of the map matching algorithms include using landmarks as positional constraints (Krakiwsky *et al.*, 1988) and road maps as constraints in the pathways (Bullock, 1995) of the land vehicles.

7.2.1 Map Matching Methods

A typical map matching method can be divided into three steps (see Figure 7.2). This includes calculating raw positions according to observations, extracting and evaluating the road segment candidates from maps and updating the mobile user's positions.

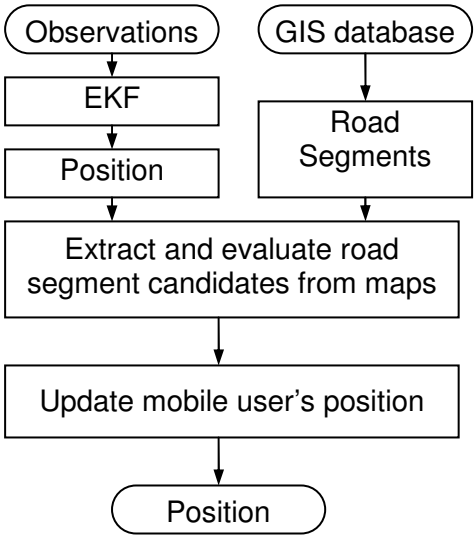

Figure 7.2 Typical steps in a map matching algorithm

Different methods can be used when extracting and evaluating road segment candidates. For example, this includes semi-deterministic algorithms, probabilistic algorithms and fuzzy-logic-based algorithms (Zhao, 1997). The semi-deterministic algorithms find the matched road segment directly according to the distribution of the road networks and land vehicle behaviour. A key limitation of this algorithm is the possibility of mismatching the vehicle to the adjacent parallel road segments. It is because the behaviours of the vehicle travelling on the adjacent parallel road are similar to the behaviour on the road where the vehicle is actually travelling. The probabilistic algorithm was developed by Honey *et al.* (1989). It introduced a searching space for the matched road segment according to the uncertainty of the determined position. This algorithm minimises the possibility of mismatching by including more adjacent road segments into the searching space (Andersson and FjellstrÄom, 2004). However, there are still some difficult situations in which the exact road segment can not be selected confidently. Some advanced algorithms were recently developed to solve this problem using fuzzy-logic (Zadeh, 1965) and a likelihood of the mobile user's positions instead of a deterministic solution is provided (Syed and Cannon, 2004).

In the position updating step, two approaches can be used for the updates using either a geometric model or a probabilistic model. With the geometric model, the updated position is defined as the nearest point in the extracted road segment. In the Euclidian space, this point is the projection of the mobile user's position on the extracted road segment. In the probabilistic model, the updated position is defined as the most possible position in the road segment. The probability is calculated based on the uncertainty of the mobile user's position. The updated position will tend towards the direction of the road segment in which the positioning uncertainty is low. In particular, when the positioning uncertainty is symmetric, the updated positions from the probabilistic model will be identical to the results from the geometric model. It indicates that the probabilistic model is more generic and the geometric model can be treated as a special case of it with the symmetric uncertainty distributions.

7.2.2 Map-aided Calibration

The concept of the map-aided calibration is to use the map matched positions as references to detect and correct the errors in the sensors' raw measurements (see Figure 7.3). According to the map matched and raw positions, an additional feedback to the conventional data flows in map matching is provided to the EFK for corrections.

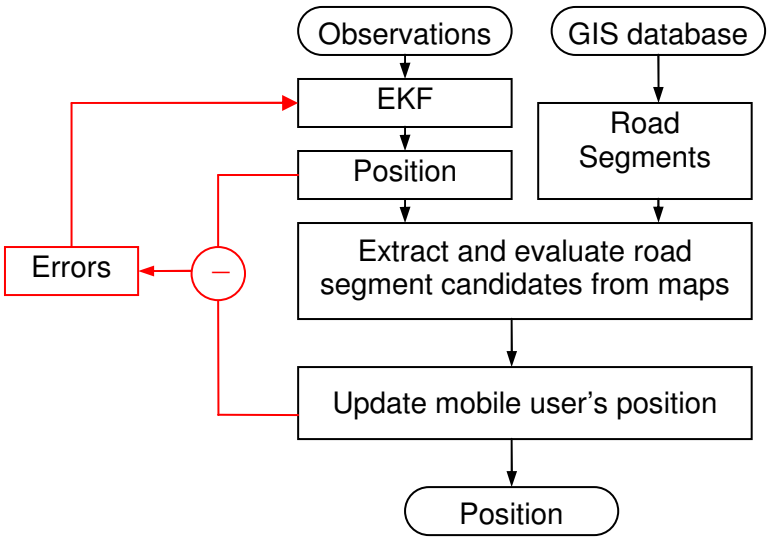

Figure 7.3 A flow chart of the typical map-aided calibration algorithm (The major difference between the map-aided calibration algorithms and the map matching algorithms is the feedback of the errors according to the map matching algorithms to the raw measurements.)

Typical examples using this technique in land vehicle positioning include using the length of the road segment to calibrate the DR and/or using the direction of the road segment to calibrate the orientation sensors such as the compass and gyroscopes (Zhao *et al.*, 1996). Theoretically, this method can also be implemented in other map matching applications such as personal positions.

7.2.3 Theoretical Analysis of Map Matching Method

Theoretically, map matching can be considered as a positioning process with constraints applied. The mathematical presentation and theoretical approvements of this method are listed below.

In map matching techniques, the pathway selected from a GIS database can be treated as a constraint with respect to the state of the retrieved mobile user's position from a KF (see Chapter 3). The constraints can be applied by projecting the unconstrained state estimation into the constrained surface. The constraints can be expressed by the following Equation (7.1):

$$\underset{\sim}{C} \cdot \hat{x}_k^+ = b \qquad (7.1)$$

where, $\hat{x}_k^+$ is the unconstrained state estimation; and $\underset{\sim}{C}$ and b are the matrix and vector with respect to the constraints respectively.

The constraints can be applied to KF by the following equations (see Equations (7.2) and (7.3)). (Williams, 2001)

$$\hat{x}_{kc}^+ = \hat{x}_k^+ + \underset{\sim}{W}_{kc} \cdot (b - \underset{\sim}{C} \cdot \hat{x}_k^+) \qquad (7.2)$$

$$\underset{\sim}{P}_{kc}^+ = \underset{\sim}{P}_k^+ - \underset{\sim}{W}_{kc} \cdot \underset{\sim}{S}_{kc} \cdot \underset{\sim}{W}_{kc}^T \qquad (7.3)$$

where,

$$\underset{\sim}{W}_{kc} = \underset{\sim}{P}_k^+ \cdot \underset{\sim}{C}^T \cdot \underset{\sim}{S}_{kc}^{-1} \qquad (7.4)$$

$$\underset{\sim}{S}_{kc} = \underset{\sim}{C} \cdot \underset{\sim}{P}_k^+ \cdot \underset{\sim}{C}^T \qquad (7.5)$$

$\hat{x}_{kc}^+$ is the constrained state vector;

$\underset{\sim}{P}_k^+$ is the error covariance matrix of state vector x_k; and

$\underset{\sim}{P}_{kc}^+$ is the error covariance matrix of the constrained state vector $\hat{x}_{kc}^+$.

Simon and Chia (2002) theoretically proved the benefits of applying constraints on the state estimation in KF. Their conclusions include:

(a) The constrained state estimation is unbiased; and

(b) The constrained state estimation has a smaller error covariance than unconstrained state estimation.

According to Equation (7.2), the error in the constrained state can be written as:

$$\begin{aligned} x_k - \hat{x}_{kc}^{+} &= x_k - \hat{x}_k^{+} + \underset{\sim}{W}_{kc} \cdot [(b - \underset{\sim}{C} \cdot x_k) - (b - \underset{\sim}{C} \cdot \hat{x}_k^{+})] \\ &= [I - \underset{\sim}{W}_{kc} \cdot \underset{\sim}{C}] \cdot (x_k - \hat{x}_k^{+}) \end{aligned} \qquad (7.6)$$

where, x_k is the true value of the state.

The average of the errors in the constrained state is:

$$E(x - \hat{x}_c^{+}) = [I - \underset{\sim}{W}_c \cdot \underset{\sim}{C}] \cdot E(x - \hat{x}^{+}) \qquad (7.7)$$

Since the unconstrained state estimation in KF is unbiased (see Equation (7.8)).

$$E(\hat{x}^{+}) = E(x) \qquad (7.8)$$

The right side of Equation (7.7) is zero and, eventually, the average of the errors in a constrained state becomes zero. Therefore, the constrained state estimation is unbiased.

According to Equation (7.3), the covariance of the constrained state estimation is equal to the covariance of the unconstrained state estimation minus a term with respect to the constraints. The covariance of the constrained state estimation is always smaller than the covariance of the unconstrained state estimation due to the positive term, $\underset{\sim}{W}_c \cdot \underset{\sim}{S}_c \cdot \underset{\sim}{W}_c^{T}$, by definition.

These features of the constrained KF indicate that the precision of positioning can be improved and the accuracy will not be degraded by using a correct pathway in a GIS database as a mathematical constraint surface for positioning solutions. By projecting the mobile user's position into the constraint surface, 3-D or 2-D positioning problems can be simplified into a 1-D problem (i.e. locating mobile user on a point of the pathway).

7.2.4 Probabilistic Map for Personal Navigation

The concept of map matching has already been applied into personal navigation applications. Conventional map matching algorithms for personal navigation have been introduced using both 2-D and 3-D routes maps to constrain mobile users along routes (Bernstein and Kornhauser, 1998; Gilliéron *et al.*, 2004). These were similar to the methods for land vehicle map matching.

However, the conventional map matching algorithms were originally developed for land vehicle navigation. These algorithms are based on the assumption that the vehicle is restricted to move in either direction along a road. However, for personal positioning applications, this assumption is not always true. Pedestrians may have more freedom to move in the space. Their trajectories may approximate to one of the pathways, but some significant manoeuvres may occur during the movement period.

Accordingly, Widyawan et al. (2007) used structure models in the GIS database instead of route maps to generate the prior probabilities of the mobile user's position at every epoch. This method did not constrain the positioning results in the 1-D paths, but it provided greater degrees of freedom for estimating the mobile user's position. Therefore, the mobile user's occasional movements outside the route paths could be correctly calculated and the positioning accuracy could be improved.

This research has increased the degrees of freedom to the mobile user's movements via another approach. Instead of generating the probabilities epoch by epoch, a probabilistic distribution, which represents the greatest number of possible positions of a mobile user, is established according to the structure of the building before the positioning stage is undertaken. The probability is based on the Gaussian distribution using the greatest number of possible positions and the 90% confidence interval with the dimensions of specific structures, such as the width of the corridor or the size of a room (see Figure 7.4). This method can reduce the computational burden in the positioning stage since the probabilities can be pre-calculated prior to the positioning stage. The experimental site chosen was identical to the one used for evaluating the 3-D RFID positioning algorithms (see Chapters 4 and 5). A probabilistic map, generated instead of the conventional map extracted from a 3-D indoor GIS database, was used in the positioning procedures (see Figure 7.4). An accuracy of 1.7m was achieved (see Figure 7.5) (Zhang *et al.*, 2008).

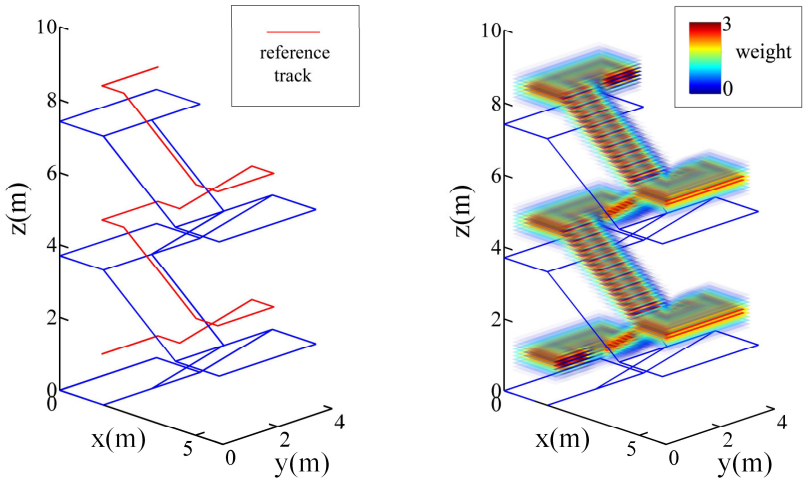

Figure 7.4 The schematic plots of the conventional map and the probabilistic map for the stairway

(The conventional map (left) consists of the line segments of the routes. The probabilistic map (right) represents the probabilities of the mobile users' positions.)

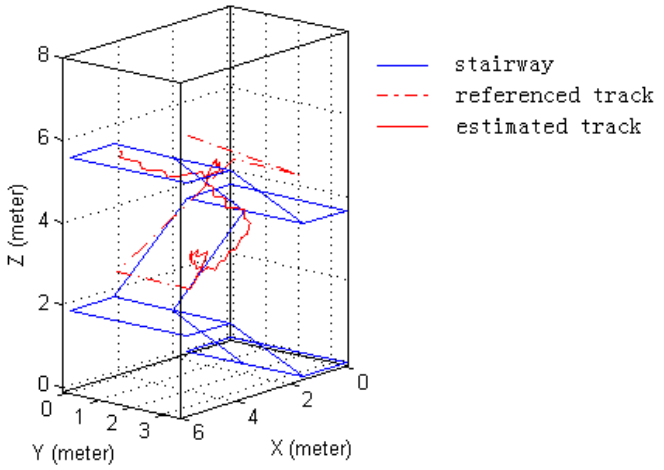

Figure 7.5 The positioning results using the probabilistic map

(The experimental track: level 10 to level 11 in RMIT Building 12, Swanston Street, Melbourne.)

7.3 Site Specific Model

As well as being used to understand the surrounding environments from a geospatial database, the SISP model can be used to estimate the radio frequency signal strength. This model can be used to increase the accuracy of interpolations and reduce the sampling number needed for establishing the training phase database.

The SISP model is based on the theory of radio wave propagation behaviour and it relies on having detailed information of the environments (McKown and Hamilton, 1991). In practice, approximate numerical methods, such as ray tracing algorithms, are preferred instead of setting the boundary conditions to Maxwell's equations according to the geometry of the surrounding environments. These preferred methods are more computationally efficient (Tam and Tran, 1995). The concept of using ray tracing algorithms is that high-frequency radio waves contain similar behaviours in a ray-like fashion. Since the model estimates the RF propagation process according to the information regarding the environments' setup, an up-to-date geospatial database is essential to the accuracy of the SISP propagation models (Rappaport, 1996). In addition, due to the propagation of RF signals in 3-D space instead of a 2-D surface, the 3-D geospatial database is essential to the performances rather than conventional maps or a 2-D database.

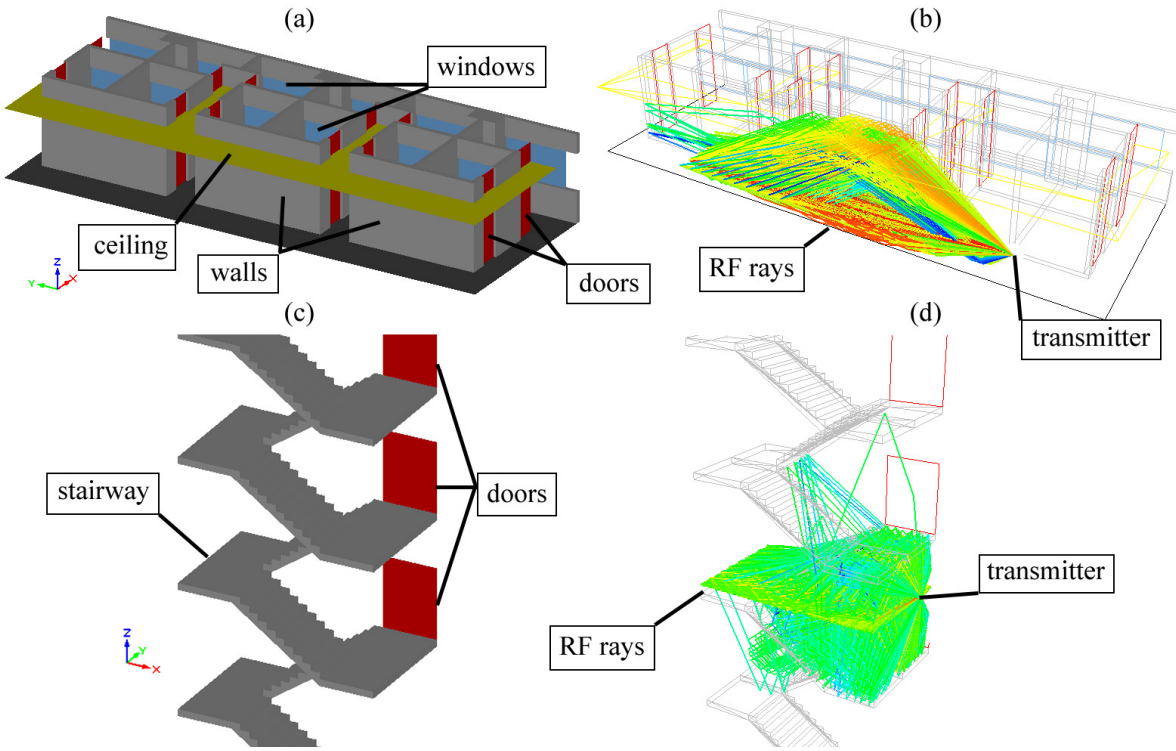

Figure 7.6 The schematic plots using SISP models according to the 3-D GIS database for estimating RSS indoor distributions
(The plots (a) and (c) are the 3-D GIS model for the building structures at the corridor and stairway respectively. The plots (b) and (d) are the ray tracing results in the corresponding environments.)

Experiments to evaluate the 3-D GIS-based SISP propagation model for estimating the RSS distributions were conducted both in a stairway and a corridor at RMIT University, Australia (Building 12, city campus (see Figure 7.6)). Plots (a) and (c) show the layout of the segment of the corridor and the segment of the stairway respectively where the experiments were conducted. In the corridor areas, offices are separated by concrete block walls and glass. The ceiling consists of plaster boards attached to the underside of a concrete ceiling. In the stairway the major structures are constructed from concrete and a wooden door is at one side of the stairway at each level. Plots (b) and (d) are the simulated RF rays in the experimental areas.

The results were compared with the interpolated methods of achieving RSS distributions (see Chapter 3). The measured RSS in the experimental areas were used as references. It indicated that the SISP propagation model can accurately provide the trends of the RSS variations, which are caused by the surrounding environments without overelaborating sampling procedures in the location fingerprinting training phase. However, the accuracy of the estimated RSS values cannot be compared to the accuracy of the interpolation method. The errors of the SISP propagation model in some areas can be as large as 20dB. It is mainly caused by two limitations in the SISP model (the limited accuracy of the 3-D structure model and the difficulty of estimating the transmitted RF power). Firstly, the paths of the simulated rays are very sensitive to the 3-D structure model. (For example, a curved edge and a sharp edge of the walls may lead to totally different directions of the reflected rays and cause large errors in the RSS estimation.) Secondly, it is difficult to estimate the transmitted power from the RFID tags, which can lead to wrongly estimating the RSS, even with an accurate path loss. In summary, the SISP model has the potential to reduce the workload at the location fingerprinting training phase when generating the RSS distributions. This provides more accurate variations, caused by the obstacles in the surrounding environment. However, due to the limitations of the SISP model, it cannot provide adequate accuracy in estimating the value of the RSS for the RFID location fingerprinting. A solution combining the interpolation method to estimate the RSS values and the SISP model to estimate the RSS variation trends may provide more reliable results with reduced workloads.

7.4 Summary

This chapter has presented a new approach that uses geospatial information to improve the accuracy in RFID-based multi-sensor integrated positioning techniques for personal navigation. Both the probabilistic map based map matching algorithm and the SISP propagation model were evaluated. Firstly, a positioning accuracy of 1.7m can be achieved by using the probabilistic map based map matching algorithm developed as part of this research. The results indicate that it is superior to conventional map matching algorithms since it provides a greater degree of freedom to pedestrian movement. Secondly, the SISP propagation model can provide accurate trends of the variations of RSS distribution since it considers the specific environmental effects according to the 3-D indoor GIS database. However, the limitations of the sensitivity of the 3-D GIS models and the accuracy in estimating the RFID transmission power degrades the accuracy when using SISP model in RSS value estimations. It is less accurate than the interpolation method, which is based on a large number of real measurements. This research has also found that a combination of the SISP model and the interpolation method may be a solution for providing accurate RSS distribution with reduced workloads for the RFID location fingerprinting training phase.

Chapter 8 Conclusions and Recommendations

The goal of this research was to investigate and develop innovative algorithms for low-cost indoor/outdoor personal positioning techniques. This goal has been accomplished through the use of a low-cost RFID-based multi-sensor personal positioning platform developed by the SPAN Laboratory within the School of Mathematical and Geospatial Sciences at RMIT University, Melbourne, Australia.

8.1 Results and Contributions

The major work in this research includes the review and comparisons of existing indoor and personal positioning techniques, developments of new algorithms and integrated techniques for personal tracking indoor. The algorithms investigated include RFID stand-alone and RFID-based multi-sensor integrated positioning algorithms and utilizations of 3-D GIS databases in RFID-based personal positioning applications.

8.1.1 Sensors Selections

The integrated techniques are capable of providing reliable and accurate positions using low-cost and portable devices for indoor personal positioning. According to the intensive review and comparisons of existing indoor and personal positioning techniques, all the existing techniques have their own strengths and weaknesses. For example, inertial sensors are less prone to the effects from the surrounding environment, but contain significant drifts. Radio-based techniques provide a relatively large coverage area using a small number of devices, but they have serious multipath effects. One emerging solution for developing a low-cost and reliable positioning system is to use a hybrid system - integrating multiple sensors to compensate for the limitations in each single technique. Consequently, the integrated techniques based on RFID and MEMS INS were selected as the platform upon which to develop low-cost personal indoor positioning services.

8.1.2 RFID Positioning Algorithms

RFID stand-alone positioning algorithms were evaluated and three major detrimental effects in RFID positioning were investigated, including the limitations of RSS-based

ranging models, RSS directional patterns and multipath effects. as well. Results have shown that there is a compromise between the accuracy and the continuity in RFID deterministic CoO positioning algorithms. It can either provide accurate, but discrete, positions using a small cell size or approximations, but continuous positions using a large cell size. The trilateration algorithm, which can provide continuous positions, is highly affected by detrimental effects in RFID positioning. The most reliable continuous positioning algorithm in RFID positioning is the location fingerprinting algorithm. In experiments undertaken in buildings at the RMIT University city campus indicated that the RFID location fingerprinting algorithm can provide at least 4.4m positioning accuracy in static positioning. Duplicated observations and observations from different directions can further improve positioning performance in static positioning.

8.1.3 RFID/MEMS INS Integrated Positioning Algorithms

RFID/MEMS INS integrated positioning algorithms were developed, including the probabilistic CoO algorithm and INS/RFID location fingerprinting integrated positioning algorithms. The experiments conducted at Yarra Bend Park, Melbourne showed that the probabilistic CoO algorithm can provide continuous trajectories at an accuracy of 15.4m, which is higher than other integrated algorithms that are based on MEMS INS and the conventional RFID CoO. It also indicated that the probabilistic CoO algorithm developed can both improve the continuity and the accuracy in CoO algorithms by using flexible cell sizes. The other experiments conducted at the RMIT University city campus demonstrated that by integrating MEMS INS with RFID location fingerprinting algorithms, probabilities near the INS predicted positions can be amplified. This can minimise some effects that disturb RSS distributions due to environmental dynamics. In static experiments, the positioning accuracy was increased from 4.4m to 1.07m. In dynamic experiments, a 4m positioning accuracy was achieved.

8.1.4 RFID-Based Seamless Positioning Algorithms

The integration of RFID, MEMS INS and low-cost GPS was introduced to provide metre-level indoor/outdoor seamless positioning services. An iterated RSPKF was developed in cooperation with the National University of Defence Technology, China in order to effectively and efficiently deliver results. Generally, 4m positioning

accuracy can be achieved seamlessly indoors/outdoors using the algorithm developed for the Yarra Bend Park experiments. The RFID observations in the GPS signal-obstructed areas significantly increased positioning accuracy from 8m to approximately 3m.

8.1.5 GIS-Assisted Positioning Algorithms for Personal Positioning

More accurate and efficient positioning algorithms can be developed by utilising 3-D GIS databases. The utilisation of a route map in the 3-D GIS database provided a map matching algorithm based on the probabilistic maps for personal positioning. The experiments showed that, by using this constraint, positioning accuracy can be improved from 4m to 1.7m. As well, some detailed movements of the mobile user can still be retained. This is superior to the conventional map matching algorithms, which simply projected the positions to the road segments. The SISP propagation model was also investigated based on the structure model in the 3-D GIS database. The results from this investigation indicated that the SISP propagation model can efficiently provide accurate trends of the variations of RSS distribution, but the accuracy of the RSS values was highly dependent on the accuracy of the structure model in the 3-D GIS and the accuracy of the estimated transmission powers.

8.1.6 Contributions

The major contributions of this study include:

(a) Intensive reviews and comparisons of current indoor and personal positioning techniques and the selection of techniques (e.g. RFID, MEMS INS and low-cost GPS) for providing a low-cost personal positioning system;

(b) Developments of the RFID probabilistic CoO algorithm, which is superior to the conventional CoO positioning algorithm in its positioning accuracy and continuity;

(c) Developments of the integration algorithms for RFID-based multi-sensor positioning techniques, which can provide metre-level positioning accuracy for dynamic personal positioning indoors;

(d) Developments of the indoor/outdoor seamless positioning algorithm based on the iterated RSPKF for RFID/MEMS INS/low-cost GPS integrated

technique, which can provide metre-level positioning accuracy indoor/outdoor seamlessly for personal positioning; and

(e) Developments of the 3-D GIS database for personal positioning and its integration with positioning technique. This includes the map matching algorithm based on the probabilistic maps for personal positioning and the SISP propagation model for efficiently generating the RFID signal strength distributions in location fingerprinting algorithms.

8.2 Recommendations

This research has demonstrated that metre-level positioning accuracy can be achieved by RFID-based multi-sensor integrated techniques using the algorithms developed. According to the research outcomes, the thesis proposes the following:

(a) The RFID location fingerprinting algorithm is superior to the CoO and the RSS-based trilateration algorithms in providing reliable and continuous positions for indoor positioning;

(b) Accurate and up-to-date RSS fingerprinting maps are essential for positioning accuracy in RFID location fingerprinting algorithms;

(c) RFID positioning techniques can be used for personal positioning services. However, it is not accurate enough to be used stand-alone for dynamic positioning applications due to the significant effects on the RSS from the surrounding environment; and

(d) Integrated techniques are ideal solutions for providing low-cost and accurate personal positioning services, as the independent errors from multiple sensors can be compensated for by integration;

8.3 Future Work

The following sections outline a number of issues that warrant further investigation in the area of low-cost personal positioning techniques, based on RFID systems.

8.3.1 Directional Patterns of RFID Signal Strength

Firstly, accurately estimating directional patterns of RFID signal strength is essential to RSS-based positioning accuracy, but this is still a challenge, especially in complex

environments. In reality, these patterns are not only affected by antenna gain patterns which can be accurately measured in the laboratory, but also affected by obstacles and reflectors in surrounding environments. In this research (see Chapter 4), a statistical model was introduced to estimate these patterns in areas near RFID tags (within 5m), but in remote areas there is no accurate model for estimating these patterns. Developing accurate models for RSS directional patterns may greatly increase positioning accuracy.

8.3.2 Updating Methods of Signal Strength Database for Location Fingerprinting Algorithms

Secondly, there are still problems in generating accurate RSS distributions (fingerprinting maps) in the location fingerprinting training phase. On one hand, the conventional methods require tremendous workloads for collecting adequate RSS samples in the experimental site in order to represent RSS distributions correctly (see Chapter 3). On the other hand, alternative methods based on geospatial information and SISP propagation model are very sensitive to the accuracy of the structure models in the GIS database and the estimated transmission powers (see Chapter 7). A method which can efficiently and accurately update the RSS distributions in the dynamic environments is essential.

8.3.3 Sensor Selection for Integration

From this research (see Chapter 2), it was found that multi-sensor integration is an ideal solution for providing accurate position with low-cost devices, since some significant error from one sensor can be compensated by the redundant observations from other integrated sensors. However, selecting the sensors to optimise the positioning performance and the cost of the system is still a challenge. This research selected the RFID, MEMS INS and low-cost GPS, but with technical developments some novel techniques, such as the INS using atomic sensors, may be more appropriate for use in the near future.

8.3.4 Intelligent Algorithms for Integration

For integration, intelligent algorithms, which can select the combination of observations efficiently, are required. This research only selected observations according to their accessibility. However, some observations selected may contain

large errors and thus degrade positioning accuracy. An intelligent algorithm which can reject these noisy observations may further increase positioning accuracy.

8.4 Summary

This thesis has made significant contributions to the development of algorithms for low-cost personal positioning techniques. It has shown that RFID is a low-cost and portable technique, which can satisfy indoor personal positioning requirements. Using the new algorithms developed in the study, metre-level accuracy (e.g. 3.5m in rooms and 1.5m in stairways) can be achieved using RFID stand-alone in static indoor positioning. With dynamic positioning, environmental effects and system dynamics significantly degrade the positional accuracy of RFID stand-alone techniques. Multi-sensor integrated algorithms developed as part of this research (e.g. the probabilistic CoO algorithm and the INS/RFID location fingerprinting algorithm) can be used to improve performance. Approximately, 4m positioning accuracy can be achieved using INS/RFID location fingerprinting algorithms in dynamic indoor positioning. The experiments also indicated that the techniques selected in this study, integrated with low-cost GPS, can be used to provide seamless indoor/outdoor positions at approximately 4m accuracy, with iterated RSPKF. In addition, the utilization of a 3-D GIS database shows the potential for increasing the accuracy by minimizing the search space in positioning and efficiently generating RSS fingerprinting maps based on geospatial information for RFID-based personal indoor positioning. In summary, the RFID-based multi-sensor personal positioning techniques using the algorithms developed can provide seamless positions in metre-level accuracy using low-cost and portable devices. However, there are still a number of significant research issues that need further investigation.

References

1 Abowd G, Battestini A and O'Connell T (2004) The Location Service: a Framework for Handling Multiple Location Sensing Technologies*, Proceedings of the 2nd International Workshop on Middleware for Pervasive and Ad-Hoc Computing*, Toronto, Ontario, Canada, Oct 18-22.

2 Analog Devices Inc. (2004) ADXRS300, *Data Sheet,* Analog Devices Inc.

3 Andersson D and FjellstrÄom J (2004) Vehicle Positioning with Map Matching Using Integration of a Dead Reckoning System and GPS, *Thesis*, Institutionen för Systemteknik, Linköpings Universitet, LinkÄoping.

4 Arc Second (2004) Indoor GPS Error Budget and Specifications, *White Paper,* Arc Second Inc.

5 Arc Second (2002) Indoor GPS Technology for Metrology, *White Paper,* Arc Second Inc.

6 Bahl P and Padmanabhan V (2000) RADAR: An In-Building RF-Based User Location and Tracking System*, Proceedings of the 19th Annual Joint Conference of the IEEE Computer and Communications Societies*, Tel Aviv, Israel, Mar 26-30.

7 Bar-Shalom Y, Li XR and Kirubarajan T (2001) *Estimation with Applications to Tracking and Navigation: Theory Algorithms and Software*, John Wiley & Sons, Inc., New York.

8 Barbour N and Schmidt G (2001) Inertial Sensor Technology Trends, *IEEE Sensors Journal 1*(4), 332-339.

9 Barnes J, Rizos C, Wang J, Small D, Voigt G and Gambale N (2003) Locata: A New Positioning Technology for High Precision Indoor and Outdoor Positioning*, Proceedings of the 16th International Technical Meeting of the Satellite Division of the Institute of Navigation (ION GNSS)*, Portland, Oregon, USA, Sep 9-12, 1119-1128.

10 Beauregard S, Widyawan and Klepal M (2008) Indoor PDR Performance Enhancement Using Minimal Map Information and Particle Filters*, Proceedings of the IEEE/ION Position, Location and Navigation Symposium (PLANS)*, Monterey, California, USA, May 5-8, 141-147.

11 Bekkali A, Sanson H and Matsumoto M (2007) RFID Indoor Positioning Based on Probabilistic RFID Map and Kalman Filtering*, Proceedings of the 3rd IEEE International Conference on Wireless and Mobile Computing, Networking and Communications (WiMob)*, White Plains, New York, USA, Oct 8-10.

12 Bellusci G, Janssen GJM, Yan J and Tiberius CCJM (2009) A Sub-Sampling Receiver Architecture for Ultra-Wideband Time of Arrival Based Ranging*,*

Proceedings of the 22nd International Technical Meeting of the Satellite Division of the Institute of Navigation (ION GNSS), Savannah, Georgia, USA, Sep 22-25, 471-480.

13 Bernstein D and Kornhauser A (1998) Map Matching for Personal Navigation Assistant*, Proceedings of the 77th Annual Meeting of the Transport Research Board*, Washington D.C., USA, Jan 11-15, 561-569.

14 Bohn J (2006) Prototypical Implementation of Location-Aware Services Based on Super-Distributed RFID Tags*, Proceedings of the 19th International Conference on Architecture of Computing Systems (ARCS)*, Frankfurt, Germany, Mar 13-16, 69-83.

15 Brown AK and Lu Y (2004) Performance Test Results of an Integrated GPS/MEMS Inertial Navigation Package*, Proceedings of the 17th International Technical Meeting of the Satellite Division of the Institute of Navigation (ION GNSS)*, Long Beach, California, USA, Sep 21-24.

16 Brown RG and Hwang PYC (1992) *Introduction to Random Signals and Applied Kalman Filtering*, John Wiley & Sons, Inc., New York, 502pp.

17 Bullock JB (1995) A Prototype Portable Vehicle Navigation System Utilizing Map Aided GPS, *Master Thesis*, Department of Geomatics Engineering, University of Calgary, Calgary, Canada.

18 Castro P, Chiu P, Kremenek T and Muntz R (2001) A Probabilistic Room Location Service for Wireless Networked Environments*, Proceedings of the 3rd International Conference on Ubiquitous Computing (ubiComp)*, Atlanta, Georgia, USA, Sep 30-Oct 2.

19 Chen R, Hyyppä J, Zhang J, Takala J, Kuittinen R, Chen Y, Pei L, Liu Z, Zhu L, Kuusniemi H, Liu J, Qin Y, Leppäkoski H and Wang J (2009) Development of a 3D Personal Navigation and LBS System with Demonstration in Shanghai EXPO in 2010*, Proceedings of the 22nd International Technical Meeting of the Satellite Division of the Institute of Navigation (ION GNSS)*, Savannah, Georgia, USA, Sep 22-25, 2124-2129.

20 Chiu DS and O'Keefe KP (2008) Seamless Outdoor-to-Indoor Pedestrian Navigation Using GPS and UWB*, Proceedings of the 21st International Technical Meeting of the Satellite Division of the Institute of Navigation (ION GNSS)*, Savannah, Georgia, USA, Sep 16-19, 2626-2637.

21 Chon H, Jun S, Jung H and An S (2004) Using RFID for Accurate Positioning, *Journal of Global Positioning Systems 3*(1-2), 32-39.

22 Christ R and Lavigne R (2000) Radio Frequency-Based Personnel Location Systems*, Proceedings of the IEEE 34th Annual 2000 International Carnahan Conference on Security Technology*, Ottawa, Ontario, Canada, Oct 23 - 25, 141-150.

23 Cobb H (1997) GPS Pseudolites: Theory, Design, and Applications, *PhD Thesis*, Department of Aeronautics and Astronautics, Stanford University.

24 Cressie N (1990) The Origins of Kriging, *Mathematical Geology 22*, 239-252.

25 Dafesh P, Hanson P, Yowell R, Stansell T and Alcocer D (2004) A Portable UWB to GPS Emission Simulator*, Proceedings of the IEEE Position, Location and Navigation Symposium (PLANS)*, Monterey, USA, Apr 26-29, 405-413.

26 Dedes G and Dempster A (2005) Indoor GPS Positioning Challenges and Opportunities*, Proceedings of the IEEE 62nd Semiannual Vehicular Technology Conference*, Dallas, USA, Sep 25-28.

27 Dempster AG, Li B and Quader I (2008) Error in Deterministic Wireless Fingerprinting Systems for Localisation*, Proceedings of the International Symposium on Wireless Pervasive Computing (ISWPC)*, Santorini, Greece, May 7-9.

28 Diggelen Fv (2009) *A-GPS: Assisted GPS, GNSS, and SBAS*, Artech House, Boston, USA.

29 Dodson A, Roberts GW, Moore T and Meng X (2007) Innovation: Ubiquitous Positioning, *GPS World*.

30 Drane C, Macnaughtan M and Scott C (1998) Positioning GSM Telephones, *IEEE Communications Magazine*, 46-59.

31 Eskin M (2006) Design of an Inertial Navigation Unit Using MEMS Sensors, *Master Thesis*, Engineering Division of the Graduate School, Cornell University.

32 Fastrax (2007) iTrax03 OEM GPS Receiver Module, *Data Sheet,* Fastrax.

33 Feuerstein MJ, Blackard KL, Rappaport TS, Seidel SY and Xia HH (1994) Path Loss, Delay Spread, and Outage Models as Functions of Antenna Height for Microcellular System Design, *IEEE Transactions on Vehicular Technology 43*(3), 487-498.

34 Finkenzeller K (2003) *RFID Handbook: Fundamentals and Applications in Contactless Smart Cards and Identification* (2nd edition), Chichester, Hoboken, USA.

35 Fontana R (2002) Experimental Results From an Ultra Wideband Precision Geolocation System, in: Smith PD and Cloude SR (Eds.), *Ultra-Wideband, Short-Pulse Electromagnetics*, Kluwer Academic/Plenum Publishers.

36 Ford T, Neumann J, Toso N, Petersen W, Anderson C, Fenton P, Holden T and Barltrop K (1996) HAPPI – a High Accuracy Pseudolite/GPS Positioning Integration*, Proceedings of the 9th International Technical Meeting of the Satellite Division of the Institute of Navigation (ION GPS)*, Kansas City, Missouri, USA, Sep 17-20, 1719-1728.

37 Foxlin E (2005) Pedestrian Tracking with Shoe-Mounted Inertial Sensors, *IEEE Computer Graphics and Applications 25*(6), 38-46.

38 Frank K, Krach B, Catterall N and Robertson P (2009) Development and Evaluation of a Combined WLAN & Inertial Indoor Pedestrian Positioning System*, Proceedings of the 22nd International Technical Meeting of the Satellite Division of the Institute of Navigation (ION GNSS)*, Savannah, Georgia, USA, Sep 22-25, 538-546.

39 French RL (1989) Map Matching Origins, Approaches and Applications*, Proceedings of the 2nd International Symposium on Land Vehicle Navigation*, Münster, Federal Republic of Germany, Jul 4-7, 91-116.

40 French RL and Lang GM (1973) Automatic Route Control System, *IEEE Transactions on Vehicular Technology 22*(2), 36-41.

41 Fu Q (2008) Active RFID for Positioning Using Trilateration and Location Fingerprinting Based on RSSI*, Proceedings of the 21st International Technical Meeting of the Satellite Division of the Institute of Navigation (ION GNSS)*, Savannah, Georgia, USA, Sep 16-19, 2613-2625.

42 Fu Q and Retscher G (2009a) Active RFID Trilateration and Location Fingerprinting Based on RSSI for Pedestrian Navigation, *Journal of Navigation 62*(2), 323-340.

43 Fu Q and Retscher G (2009b) Integration of a RFID Time-Based CoO Positioning with INS Using a Time Data Capture Tool for Verification*, Proceedings of the 22nd International Technical Meeting of the Satellite Division of the Institute of Navigation (ION GNSS)*, Savannah, Georgia, USA, Sep 22-25, 845-852.

44 Gallagher T, Li B, Kealy A and Dempster AG (2009) Trials of Commercial Wi-Fi Positioning Systems for Indoor and Urban Canyons*, Proceedings of the International Global Navigation Satellite Systems (IGNSS) Symposium*, Gold Coast, Australia, Dec 1-3.

45 Gallagher T, Tan YK, Li B and Dempster AG (2009) Wi-Fi + GPS for Urban Canyon Positioning*, Proceedings of the International Global Navigation Satellite Systems (IGNSS) Symposium*, Gold Coast, Australia, Dec 1-3.

46 Geoscience Australia (2005) New Geomagnetic Field Models Released, *AusGeo News 55*.

47 Gergonne JD (1815) The Application of the Method of Least Squares to the Interpolation of Sequences.

48 Ghilani CD and Wolf PR (2006) *Adjustment Computations: Spatial Data Analysis*, John Wiley & Sons, Inc., Hoboken, United States, 611pp.

49 Gilliéron P, Büchel D, Spassov I and Merminod B (2004) Indoor Navigation Performance Analysis*, Proceedings of the European Navigation Conference (ENC GNSS)*, Rotterdam, the Netherlands, May 17-19.

50 Godha S and Cannon ME (2005a) Development of a DGPS/MEMS IMU Integrated system for Navigation in Urban Canyon Conditions*, Proceedings of the International Symposium on GPS/GNSS*, Hong Kong, China, Dec 8-10.

51 Godha S and Cannon ME (2005b) Integration of DGPS with a Low Cost MEMS-Based Inertial Measurement Unit (IMU) for Land Vehicle Navigation Application*, Proceedings of the 18th International Technical Meeting of the Satellite Division of the Institute of Navigation (ION GNSS)*, Long Beach, California, USA, Sep 13-16.

52 Godha S, Lachapelle G and Cannon ME (2006) Integrated GPS/INS System for Pedestrian Navigation in a Signal Degraded Environment*, Proceedings of the 19th International Technical Meeting of the Satellite Division of the Institute of Navigation (ION GNSS)*, Fort Worth, Texas, USA, Sep 26-29.

53 Grejner-Brzezinska DA, Toth C and Moafipoor S (2007a) Adaptive Knowledge Based System Based on Artificial Neural Networks and Fuzzy Logic for Pedestrian Navigation*, Proceedings of the International Global Navigation Satellite Systems (IGNSS) Symposium*, Sydney, Australia, Dec 4-6.

54 Grejner-Brzezinska DA, Toth C and Moafipoor S (2007b) Pedestrian Tracking and Navigation Using an Adaptive Knowledge System Based on Neural Networks, *Journal of Applied Geodesy 1*(3), 111-123.

55 Grewal MS and Andrews AP (2001) *Kalman Filtering: Theory and Practice Using MATLAB*, John Wiley & Sons, Inc., New York, United States, 401pp.

56 Groves PD (2008) *Principles of GNSS, Inertial, and Multisensor Integrated Navigation Systems*, Artech House, Boston, 518pp.

57 Hallaway D, Höllerer T and Feiner S (2003) Coarse, Inexpensive, Infrared Tracking for Wearable Computing*, Proceedings of the 7th IEEE International Symposium on Wearable Computers (ISWC)*, White Plains, New York, USA, Oct 21-23.

58 Harter A, Hopper A, Steggles P, Ward A and Webster P (1999) The Anatomy of a Context-Aware Application*, Proceedings of the 5th Annual ACM/IEEE International Conference on Mobile Computing and Networking (MOBICOM)*, Seattle, Washington, USA, Aug 15-19, 59-68.

59 Hightower J and Borriello G (2001) Location Systems for Ubiquitous Computing, *Computer*, 57-66.

60 Hightower J, Borriello G and Want R (2000) SpotON: An Indoor 3D Location Sensing Technology Based on RF Signal Strength, *Technical Report,* Computer Science and Engineering, University of Washington.

61 Hitachi Metals Ltd. (n.d.) Magnetic Compass Sensor HM55B, *Data Sheet,* Hitachi Metals Ltd.

62 Honey SK, Zavoli WB, Milnes KA, Phillips AC, White MS and Loughmiller GE (1989) *Vehicle Navigational System and Method*, Patent No. 4796191, USA.

63 Identec Solutions (2004a) Active UHF Tag i-Q Line, *Data Sheet,* Identec Solutions.

64 Identec Solutions (2004b) PC Card UHF Interrogator i-CARD III, *Data Sheet,* Identec Solutions.

65 Jiang YF (1998) Error Analysis of Analytic Coarse Alignment Methods, *IEEE Transactions on Aerospace and Electronic Systems 34*(1), 334-337.

66 Jirawimut R, Ptasinski P, Garaj V, Cecelja F and Balachandran W (2003) A Method for Dead Reckoning Parameter Correction in Pedestrian Navigation System, *IEEE Transactions on Instrumentation and Measurement 52*(1), 209-215.

67 Judd C (1997) A Personal Dead Reckoning Module*, Proceedings of the 10th International Technical Meeting of the Satellite Division of the Institute of Navigation (ION GPS)*, Kansas City, Missouri, USA, Sep 16-19.

68 Julier S (2003) The Spherical Simplex Unscented Transformation*, Proceedings of the American Control Conference*, Denver, USA, Jun 4-6.

69 Julier S and Uhlmann J (1997) A New Extension of the Kalman Filter to Nonlinear Systems*, Proceedings of the 11th International Symposium on Aerospace/Defence Sensing, Simulation and Controls*, Orlando, Florida, USA, Apr 20-25.

70 Jung S and Woo W (2004) UbiTrack: Infrared-Based User Tracking System for Indoor Environment*, Proceedings of the 14th International Conference on Artificial Reality and Telexistence (ICAT)*, Coex, Seoul, Korea, Nov 30-Dec 2, 181-184.

71 Jung W and Woo W (2005a) Indoor Orientation Tracking Method Using ubiTrack*, Proceedings of the 1st Korea/Japan Joint Workshop on Ubiquitous Computing and Networking Systems (ubiCNS)*, Jeju, Korea, Jun 9-10.

72 Jung W and Woo W (2005b) Orientation Tracking Exploiting ubiTrack*, Proceedings of the 7th International Conference on Ubiquitous Computing (ubiComp)*, Tokyo, Japan, Sep 11-14.

73 Kalman RE (1960) A New Approach to Linear Filtering and Prediction Problems, *Journal of Basic Engineering 82*(1), 35-45.

74 Khider M, Kaiser S, Robertson P and Angermann M (2009) Maps and Floor Plans Enhanced 3D Movement Model for Pedestrian Navigation*, Proceedings of the 22nd International Technical Meeting of the Satellite Division of the Institute of Navigation (ION GNSS)*, Savannah, Georgia, USA, Sep 22-25, 790-802.

75 Kim A (2004) Development of Sensor Fusion Algorithms for MEMS-Based Strapdown Inertial Navigation Systems, *Master Thesis*, Mechanical Engineering, University of Waterloo, Waterloo, Ontario, Canada.

76 Kim M, Takeuchi T and Chong NY (2004) A 3-Axis Orthogonal Antenna for Indoor Localization*, Proceedings of the 1st International Workshop on Networked Sensing Systems*, Tokyo, Japan, Jun 22-23, 59-62.

77 King A (1998) Inertial Navigation – Forty Years of Evolution, *GEC Review 13*(3), 140-149.

78 Kionix Inc. (2006) KXM52 Series Accelerometers and Inclinometers, *Data Sheet,* Kionix Inc.

79 Koninger A and Bartel S (1997) *3D-GIS for urban purposes, GeoInformatica 2*, Kluwer Academic Publishers, Boston, USA.

80 Krach B and Roberston P (2008) Cascaded Estimation Architecture for Integration of Foot-Mounted Inertial Sensors*, Proceedings of the IEEE/ION Position, Location and Navigation Symposium (PLANS)*, Monterey, USA, May 6-8.

81 Krakiwsky EJ, Harris CB and Wong RVC (1988) A Kalman Filter for Integration Dead Reckoning, Map Matching and GPS Positioning*, Proceedings of the IEEE Position, Location and Navigation Symposium (PLANS)*, Orlando, Florida, USA, Nov 29-Dec 2, 39-46.

82 Krasner NF, Marshall G and Riley W (2002) Position Determination Using Hybrid GPS/Cellphone Ranging*, Proceedings of the 15th International Technical Meeting of the Satellite Division of the Institute of Navigation (ION GPS)*, Portland, Oregon, USA, Sep 24-27.

83 Krige DG (1951) A Statistical Approach to Some Mine Valuations and Allied Problems at the Witwatersrand, *Master Thesis*, the University of Witwatersrand.

84 Krumm J, Harris S, Meyers B, Brumitt B, Hale M and Shafer S (2000) Multi-Camera Multi-Person Tracking for EasyLiving*, Proceedings of the 3rd IEEE International Workshop on Visual Surveillance*, Dublin, Ireland, Jul 1.

85 Larson K, Akos D and Marti L (2008) Characterizing Multipath from Satellite Navigation Measurements in Urban Environments*, Proceedings of the 5th IEEE Consumer Communications and Networking Conference (CCNC)*, Las Vegas, Nevada, USA, Jan 10-12.

86 Lee HK, Shim J-Y, Kim H-S, Li B and Rizos C (2008) Feature Extraction and Spatial Interpolation for Improved Wireless Location Sensing, *IEEE Sensors Journal 8*, 2865-2885.

87 Lee J (2007) A Three-Dimensional Navigable Data Model to Support Emergency, *Annuals of the Association of American Geographers 97*(2), 512-529.

88 Lee S and Mase K (2001) A Personal Indoor Navigation System Using Wearable Sensors*, Proceedings of the 2nd International Symposium on Mixed Reality (ISMR)*, Yokohama, Japan, Mar 14-15, 147-148.

89 Lehner A and Steingaß A (2003) The Influence of Multipath on the Positioning Error*, Proceedings of the European Navigation Conference (ENC GNSS)*, Graz, Austria, Apr 22-25.

90 Li B (2006) Terrestrial Mobile User Positioning Using TDOA and Fingerprinting Techniques, *PhD Thesis*, School of Surveying and Spatial Information Systems, the University of New South Wales, Sydney, Australia.

91 Li B, Dempster A, Rizos C and Barnes J (2005) Hybrid Method for Localization Using WLAN*, Proceedings of the Spatial Sciences Institute Biennial International Conference (SSC)*, Melbourne, Australia, Sep 12-16.

92 Li B, Kam J, Lui J and Dempster AG (2007) Using Directional Information in Wireless LAN Based Indoor Positioning*, Proceedings of the International Global Navigation Satellite Systems (IGNSS) Symposium*, Sydney, Australia, Dec 4-6.

93 Li B, Quader IJ and Dempster AG (2008) On Outdoor Positioning with Wi-Fi, *Journal of Global Positioning Systems 7*(1), 18-26.

94 Li B, Salter J, Dempster AG and Rizos C (2006) Indoor Positioning Techniques Based on Wireless LAN*, Proceedings of the 1st IEEE International Conference on Wireless Broadband and Ultra Wideband Communications (AusWireless)*, Sydney, Australia, Mar 13-16.

95 Li B, Zhang J and Rizos C (2009) fLogger – a WiFi and GSM Information Logging System for Positioning Purposes*, Proceedings of the International Global Navigation Satellite Systems (IGNSS) Symposium*, Gold Coast, Australia, Dec 1-3.

96 Li D, Landry RJ and Lavoie P (2008) Low-Cost MEMS Sensor-Based Attitude Determination System by Integration of Magnetometers and GPS: A Real-Data Test and Performance Evaluation*, Proceedings of the IEEE/ION Position, Location and Navigation Symposium (PLANS)*, Monterey, California, USA, May 5-8, 1190-1198.

97 Luyendyk APJ (1997) Processing of Airborne Magnetic Data, *AGSO Journal of Australian Geology & Geophysics 17*(2), 31-38.

98 MacGougan GD and Klukas R (2009) Method and Apparatus for High Precision GNSS/UWB Surveying*, Proceedings of the 22nd International Technical Meeting of the Satellite Division of the Institute of Navigation (ION GNSS)*, Savannah, Georgia, USA, Sep 22-25, 853-863.

99 Maus S (2005) The 10th Generation International Geomagnetic Reference Field, *Geophysical Journal International 161*, 561-565.

100 McKown JW and Hamilton RL (1991) Ray Tracing as a Design Tool for Radio Networks, *IEEE Network Magazine*, 27-30.

101 Meijers M, Zlatanova S and Preifer N (2005) 3D Geoinformation Indoors: Structuring for Evacuation*, Proceedings of the Next Generation 3D City Models*, Bonn, Germany, Jun 21-22.

102 Mezentsev O, Lachapelle G and Collin J (2005) Pedestrian Dead Reckoning – a Solution to Navigation in GPS Signal Degraded Areas, *Geomatica 59*(2), 175-182.

103 Miller L, Wilson P, Bryner N, Francis M, Guerrieri J, Stroup D and Klein-Berndt L (2006) RFID-Assisted Indoor Localization and Communication for First Responders*, Proceedings of the International Symposium on Advance Radio Technologies (ISART)*, Boulder, Colorado, USA, Mar 7-9.

104 Misra P and Enge P (2006) *GPS Signals, Measurements and Performance* (2nd edition), Ganga-Jamuna Press, Lincoln, Massachusetts, USA.

105 Moafipoor S, Grejner-Brzezinska DA and Toth C (2007) Adaptive Calibration of a Magnetometer Compass for a Personal Navigation System*, Proceedings of the International Global Navigation Satellite Systems (IGNSS) Symposium*, Sydney, Australia, Dec 4-6.

106 Moeglein M and Krasner N (1998) An Introduction to SnapTrack Server-Aided GPS Technology*, Proceedings of the 11th International Technical Meeting of the Satellite Division of the Institute of Navigation (ION GPS)*, Nashville, Tennessee, USA, Sep 15-18.

107 Mok E (2007) Ubiquitous Positioning Technologies and LBS, *Location 2*(4), 36-40.

108 Mok E, Hui T, Lau F and Xia L (2007) Positioning Performance of Ultra-Wide Band and ZigBee Technologies*, Proceedings of the International Global Navigation Satellite Systems (IGNSS) Symposium*, Sydney, Australia, Dec 4-6.

109 Mok E and Retscher G (2007) Location Determination Using WiFi Fingerprinting Versus WiFi Trilateration, *Journal of Location Based Service 1*(2), 145-159.

110 Mok E and Retscher G (2008) Navigation Support for Wayfinding in Smart Environments Using ZigBee Positioning Technology, in: Gartner G and Rehrl K (Eds.), *Location Based Services and TeleCartography II – From Sensor Fusion to Context Models, Lecture Notes in Geoinformation and Cartography*, Springer Verlag, Berlin-Heidelberg.

111 Mok E, Retscher G and Xia L (2006) Investigation of Seamless Indoor and Outdoor Positioning Integrating WiFi and GNSS*, Proceedings of the XXIII International FIG Congress*, Munich, Germany, Oct 8-13.

112 Musliman I, Rahman A and Coors V (2006) 3D Navigation for 3D-GIS – Initial Requirements, in: Cartwright W, Gartner G, Meng L and Peterson M (Eds.), *Innovations in 3D Geo Information Systems*, Springer, Berlin, Germany.

113 Najafi B, Aminian K, Paraschiv-Ionescu A, Loew F, Büla CJ and Robert P (2003) Ambulatory System for Human Motion Analysis Using a Kinematic Sensor: Monitoring of Daily Physical Activity in the Elderly, *IEEE Transactions on Biomedical Engineering 50*(6), 711-723.

114 Ni L, Liu Y, Lau Y and Patil A (2004) LANDMARC: Indoor Location Sensing Using Active RFID, *Wireless Networks 10*, 701-710.

115 Olesk A and Wang J (2009) Geometric and Error Analysis for 3D Map-Matching*, Proceedings of the International Global Navigation Satellite Systems (IGNSS) Symposium*, Gold Coast, Australia, Dec 1-3.

116 Opshaug G and Enge P (2001) GPS and UWB for Indoor Navigation*, Proceedings of the 14th International Technical Meeting of the Satellite Division of the Institute of Navigation (ION GPS)*, Salt Lake City, Utah, USA, Sep 11-14.

117 Parikh HK and Michalson WR (2008) Impulse Radio UWB or Multicarrier UWB for Non-GPS Based Indoor Precise Positioning Systems, *Navigation: Journal of the Institute of Navigation 55*(1), 29-37.

118 Peng J, Wu F, Zhu M, Zhang K and Wang F (2009) A New GPS/RFID Integration Algorithm Based on Iterated Reduced Sigma Point Kalman Filter for Vehicle Navigation*, Proceedings of the 22nd International Technical Meeting of the Satellite*

Division of the Institute of Navigation (ION GNSS), Savannah, Georgia, USA, Sep 22-25, 803-810.

119 Priyantha N (2005) The Cricket Indoor Location System, *PhD Thesis*, Department of Electrical Engineering and Computer, Massachusetts Institute of Technology (MIT).

120 Quddus MA, Ochieng WY and Noland RB (2007) Current Map-Matching Algorithms for Transport Applications: State-of-the-Art and Future Research Directions, *Transportation Research Part C 15*, 312-328.

121 Rapp RH (1991) Geometric Geodesy Part 1, *Lecture Notes,* Department of Geodetic Science and Surveying, The Ohio State University, Columbus, Ohio, USA.

122 Rappaport TS (1996) *Wireless Communications: Principles and Practice*, Prentice Hall PTR, Upper Saddle River, USA, 641pp.

123 Retscher G (2009) Multi-Sensor Fusion Using a Kalman Filter and Knowledge-Based Systems*, Proceedings of the 22nd International Technical Meeting of the Satellite Division of the Institute of Navigation (ION GNSS)*, Savannah, Georgia, USA, Sep 22-25, 728-735.

124 Retscher G (2007a) Selected Systems for Indoor and Pedestrian Navigation*, Proceedings of the International Global Navigation Satellite Systems (IGNSS) Symposium*, Sydney, Australia, Dec 4-6.

125 Retscher G (2007b) Test and Integration of Location Sensors for a Multi-Sensor Personal Navigator, *Journal of Navigation 60*(1), 107-117.

126 Retscher G and Fu Q (2008) Active RFID Trilateration for Indoor Positioning, *Coordinates 4*(5), 10-15.

127 Retscher G and Kealy A (2005) Ubiquitous Positioning Technologies for Intelligent Navigation Systems*, Proceedings of the 2nd Workshop on Positioning, Navigation and Communication (WPNC) and 1st Ultra-Wideband Expert Talk (UET)*, Hannover, Germany, Mar 17, 99-108.

128 Retscher G, Mok E and Xia LY (2007) UWB, RFID and GNSS Integration for Navigation and Tracking*, Proceedings of the 4th International Symposium on LBS and Telecartography*, Hong Kong, China, Nov 8-10.

129 Retscher G, Mok E and Yan WY (2005) Performance Test of Location-Based Services, *European Journal of Navigation 3*(3), 22-27.

130 Retscher G and Thienelt M (2004) NAVIO – A Navigation and Guidance Service for Pedestrians, *Journal of Global Positioning Systems 3*(1-2), 208-217.

131 Retscher G, Zhang K, Zhang S and Wang Y (2006) RFID and GNSS for Indoor and Outdoor Positioning – Two Different Case Studies, *European Journal of Navigation 4*(5), 49-54.

132 Rogers R (2000) *Applied Mathematics in Integrated Navigation Systems*, American Institute of Aeronautics and Astronautics, Inc., Reston, Virginia, 408pp.

133 Roos T, Myllymäki P and Tirri H (2002) A Statistical Modeling Approach to Location Estimation, *IEEE Transactions on Mobile Computing 1*(1), 59-69.

134 Rose J and Gamble JG (2006) *Human Walking*, Lippincott Williams & Wilkins, Philadelphia, USA, 234pp.

135 Sathyan T, Humphrey D, Hedley M and Johnson M (2009) A Wireless Indoor Localization Network System Introduction and Trial Results*, Proceedings of the International Global Navigation Satellite Systems (IGNSS) Symposium*, Gold Coast, Australia, Dec 1-3.

136 Schimelevich L and Naor R (1996) New Approach to Coarse Alignment*, Proceedings of the IEEE Position, Location and Navigation Symposium (PLANS)*, Atlanta, Georgia, USA, Apr 22-26, 324-327.

137 Schmidt GT (2009) INS/GPS Technology Trends, *IEEE Aerospace and Electronic Systems Magzine*.

138 Schmidt SF (1970) Computational Techniques in Kalman Filtering, in: *Theory and Applications of Kalman Filtering*, NATO Advisory Group for Aerospace Research and Development, London, UK.

139 Siebel NT (2003) Design and Implementation for People Tracking Algorithms for Visual Surveillance Applications, *PhD Thesis*, Computational Vision Group, Department of Computer Science, The University of Reading.

140 Simon D and Chia TL (2002) Kalman Filtering with State Equality Constraints, *IEEE Transactions on Aerospace and Electronic Systems 39*, 128-136.

141 Sinha A, Yu D and Khaouli J (2009) The Development of a Queryable and Navigable 3D Geodatabase, *Bachelor Thesis*, School of Mathematical and Geospatial Sciences, RMIT University, Melbourne, Australia.

142 Sorenson HW (1970) Least-Squares Estimation: from Gauss to Kalman, *IEEE Spectrum 7*, 63-68.

143 Stephen J (2000) Development of a Multi-Sensor GNSS Based Vehicle Navigation System, *Master Thesis*, Department of Geomatics Engineering, University of Calgary, Calgary, Alberta, Canada.

144 Stigler SM (1974) Gergonne's 1985 Paper on the Design and Analysis of Polynomial Regression Experiments, *Historia Mathematica 1*(4), 431-439.

145 Stirling R, Fyfe K and Lachapelle G (2005) Evaluation of a New Method of Heading Estimation for Pedestrian Dead Reckoning Using Shoe Mounted Sensors, *Journal of Navigation 58*, 31-45.

146 Sugimoto S, Kubo Y and Tanikawara M (2009) A Review and Applications of the Nonlinear Filters to GNSS/INS Integrated Algorithms*, Proceedings of the 22nd International Technical Meeting of the Satellite Division of the Institute of Navigation (ION GNSS)*, Savannah, Georgia, USA, Sep 22-25, 3101-3113.

147 Syed S and Cannon M (2004) Fuzzy Logic Based-Map Matching Algorithm for Vehicle Navigation System in Urban Canyons*, Proceedings of the Institute of Navigation (ION) National Technical Meeting*, San Diego, USA, Jan 26-28.

148 Tam WK and Tran VN (1995) Propagation Modelling for Indoor Wireless Communication, *Electronics and Communication Engineering Journal*, 221-228.

149 Tanigawa M, Hol JD, Dijkstra F, Luinge H and Slycke P (2008) Augmentation of Low-Cost GPS/MEMS INS with UWB Positioning System for Seamless Outdoor/Indoor Positioning*, Proceedings of the 21st International Technical Meeting of the Satellite Division of the Institute of Navigation (ION GNSS)*, Savannah, Georgia, USA, Sep 16-19, 1804-1811.

150 Tenmoku R, Kanbara M and Yokoya N (2003a) Geometric Registration Using Positioning Infrastructures and a Pedometer for Wearable Augmented Reality*, Proceedings of the 2nd CREST Workshop on Advanced Computing and Communicating Techniques for Wearable Information Playing*, Nara, Japan, May 23-24, 14-22.

151 Tenmoku R, Kanbara M and Yokoya N (2004) A Positioning Method Combining Specification of User's Absolute Position and Dead Reckoning for Wearable Augmented Reality Systems*, Proceedings of the 3rd CREST Workshop on Advanced Computing and Communicating Techniques for Wearable Information Playing*, Arlington, USA, Oct 31-Nov 4, 19-22.

152 Tenmoku R, Kanbara M and Yokoya N (2003b) A Wearable Augmented Reality System for Navigation Using Positioning Infrastructures and a Pedometer*, Proceedings of the IEEE/ACM International Symposium on Mixed and Augmented Reality (ISMAR)*, Tokyo, Japan, Oct 7-10, 344-345.

153 Tenmoku R, Kanbara M and Yokoya N (2003c) A Wearable Augmented Reality System Using Positioning Infrastructures and a Pedometer*, Proceedings of the 2nd International Semantic Web Conference (ISWC)*, Sanibel Island, Florida, USA, Oct 20-23, 110-117.

154 Titterton D and Weston J (2004) *Strapdown Inertial Navigation Technology* (2nd edition), The Institution of Electrical Engineers, Herts, 558pp.

155 Tomé P and Yalak O (2008) Improvement of Orientation Estimation in Pedestrian Navigation by Compensation of Magnetic Disturbances, *Navigation: Journal of the Institute of Navigation 55*(3), 179-190.

156 Trevisani E and Vitaletti A (2004) Cell-ID Location Technique, Limits and Benefits: an Experimental Study*, Proceedings of the 6th IEEE Workshop on Mobile Computing Systems and Applications (WMCSA)*, English Lake District, UK, Dec 2-3.

157 Voronoi G (1907) Nouvelles Applications des Paramètres Continus à la Théorie des Formes Quadratiques, *Journal für die Reine und Angewandte Mathematik 133*, 97-178.

158 Vries Ad (2005) RFID Positioning, *Bachelor Assignment,* University of Twente, The Netherlands.

159 Wang K, Li Y and Rizos C (2009a) The Effect of the Temperature-Correlated Error of Inertial MEMS Sensors on the Integration of GPS/INS*, Proceedings of the International Global Navigation Satellite Systems (IGNSS) Symposium*, Gold Coast, Australia, Dec 1-3.

160 Wang K, Li Y and Rizos C (2009b) The Feasibility of MEMS Inertial Sensors for Deep Integration of GPS and INS*, Proceedings of the 22nd International Technical Meeting of the Satellite Division of the Institute of Navigation (ION GNSS)*, Savannah, Georgia, USA, Sep 22-25, 3122-3127.

161 Want R, Hopper A, Falcão V and Gibbons J (1992) The Active Badge Location System, *ACM Transactions on Information Systems 10*(1), 91-102.

162 Wayn CJ, Li B, Dempster AG and Rizos C (2009) GPS/WiFi Real-Time Positioning Device: An Initial Outcome, in: Gartner G and Rehrl K (Eds.), *Location Based Services and TeleCartography II – From Sensor Fusion to Context Models, Lecture Notes in Geoinformation and Cartography*, Springer Verlag, Berlin-Heidelberg.

163 Weiser M (1991) The Computer for the 21st Century, *Scientific American 265*(3), 66-75.

164 Welch G and Bishop G (2006) An Introduction to the Kalman Filter, *Course Material,* Department of Computer Science, University of North Carolina.

165 Widyawan, Klepal M and Pesch D (2007) Influence of Predicted and Measured Fingerprint on the Accuracy of RSSI-Based Indoor Location Systems*, Proceedings of the 4th Workshop on Positioning, Navigation and Communication*, Hannover, Germany, Mar 22, 145-151.

166 Williams SB (2001) Efficient Solutions to Autonomous Mapping and Navigation Problems, *PhD Thesis*, Department of Mechanical and Mechatronic Engineering, University of Sydney, Sydney, Australia.

167 Williams T, Pahadia A, Petovello M and Lachapelle G (2009) Using an Accelerometer Configuration to Improve the Performance of a MEMS IMU: Feasibility Study with a Pedestrian Navigation Application*, Proceedings of the 22nd International Technical Meeting of the Satellite Division of the Institute of Navigation (ION GNSS)*, Savannah, Georgia, USA, Sep 22-25, 3049-3063.

168 Wren CR, Azarbayejani A, Darrell T and Pentland AP (1997) Pfinder: Real-Time Tracking of the Human Body, *IEEE Transactions on Pattern Analysis and Machine Intelligence 19*(7), 780-785.

169 Wu F, Zhang K, Zhu M, Mackintosh C, Rice T, Gore C, Hahn A and Holthouse S (2008) An Integrated Low-Cost GPS, IMU and Magnetometer System for Sport

Applications*, Proceedings of the 2nd International Association of Chinese Professionals in Global Positioning Systems (CPGPS) Forum on The Next Generation GNSS – Opportunities and Challenges*, Guangzhou, China, Jan 5-7.

170 Wu F, Zhang K, Zhu M, Mackintosh C, Rice T, Gore C, Hahn A and Holthouse S (2007) An Investigation of an Integrated Low-Cost GPS, INS and Magnetometer System for Sport Applications*, Proceedings of the 20th International Technical Meeting of the Satellite Division of the Institute of Navigation (ION GNSS)*, Fort Worth, Texas, USA, Sep 25-28.

171 Wu F, Zhu M, Zhang K, Mackintosh C, Rice T, Gore C, Hahn A and Holthouse S (2007) Position and Velocity Determination for Sport Applications Using an Integrated Low-Cost GPS, INS and Magnetometer System*, Proceedings of the International Global Navigation Satellite Systems (IGNSS) Symposium*, Sydney, Australia, Dec 4-6.

172 Yan J and Bellusci G (2009) Low-Complexity Ultra-WideBand Indoor Positioning*, Proceedings of the 22nd International Technical Meeting of the Satellite Division of the Institute of Navigation (ION GNSS)*, Savannah, Georgia, USA, Sep 22-25, 1013-1024.

173 Yun D and Kee C (2002) Centimeter Accuracy Stand-Alone Indoor Navigation System by Synchronized Pesudolite Constellation*, Proceedings of the 15th International Technical Meeting of the Satellite Division of the Institute of Navigation (ION GPS)*, Portland, Oregon, USA, Sep 24-27.

174 Zadeh LA (1965) Fuzzy Sets, *Information and Control 8*(3), 338-353.

175 Zhan R and Wan J (2007) Iterated Unscented Kalman Filter for Passive Target Tracking, *IEEE Transactions on Aerospace and Electronic Systems 43*, 1155-1163.

176 Zhang K, Zhu M, Retscher G, Wu F and Cartwright WE (2008) Three-Dimension Indoor Positioning Algorithms Using an Integrated RFID/INS System in Multi-storey Buildings, in: Gartner G and Rehrl K (Eds.), *Location Based Services and TeleCartography II – From Sensor Fusion to Context Models, Lecture Notes in Geoinformation and Cartography*, Springer Verlag, Berlin-Heidelberg, 373-386.

177 Zhang K, Zhu M, Wang Y, Fu E and Cartwright W (2009) Underground Mining Intelligent Response and Rescue Systems*, Proceedings of the 6th International Conference on Mining Science and Technology*, Xuzhou, China, Oct 18-20.

178 Zhao X, Syed Z, Wright DB and El-Sheimy N (2009) An Economical and Effective Multi-Sensor Integration for Portable Navigation System*, Proceedings of the 22nd International Technical Meeting of the Satellite Division of the Institute of Navigation (ION GNSS)*, Savannah, Georgia, USA, Sep 22-25, 2088-2095.

179 Zhao Y (1997) *Vehicle Location and Navigation Systems*, Artech House, Inc, Norwood, USA, 345pp.

180 Zhao Y, Seymour LG and Kozikaro EM (1996) Absolute Heading Sensor Blunder Detection Using Relative Heading Sensor and Road Segment, *Technical Developments, Motorola 29*, 104-107.

181 Zhou J, Knedlik S and Loffeld O (2009) Tightly-Coupled MEMS-INS/GPS Integration Using Sequential Processing Method*, Proceedings of the 22nd International Technical Meeting of the Satellite Division of the Institute of Navigation (ION GNSS)*, Savannah, Georgia, USA, Sep 22-25, 3075-3086.

182 Zhu J (2006) Indoor/Outdoor Location of Cellular Handsets Based on Received Signal Strength, *PhD Thesis*, School of Electrical and Computer Engineering, Georgia Institute of Technology, Atlanta, Georgia, USA.

183 Zhu M (2008) Novel Positioning Algorithms for RFID Assisted 2D MEMS INS System*, Proceedings of the 21st International Technical Meeting of the Satellite Division of the Institute of Navigation (ION GNSS)*, Savannah, Georgia, USA, Sep 16-19.

184 Zhu M, Zhang K, Cartwright W, Retscher G and Fu Q (2009) Possibility Studies of Integrated INS/RFID Positioning Methods for Personal Positioning Applications*, Proceedings of the International Global Navigation Satellite Systems (IGNSS) Symposium*, Gold Coast, Australia, Dec 1-3.

185 Zhu M, Zhang K, Wu F and Cartwright WE (2007) An Integrated System of Dead Reckoning and RFID for Indoor Positioning*, Proceedings of the Spatial Sciences Institute Biennial International Conference (SSC)*, Hobart, Australia, May 14-18.

186 Zhu M, Zhang K, Wu F, Cartwright WE and Retscher G (2007) An Investigation of Pedestrian Positioning Algorithms Based on Integrated Low-Cost INS, GPS and Magnetometer*, Proceedings of the International Global Navigation Satellite Systems (IGNSS) Symposium*, Sydney, Australia, Dec 4-6.

187 Zhu M, Zhang K, Wu F, Cartwright WE, Retscher G and Fu Q (2008) Possibility Studies of RFID Positioning Techniques for Personal Positioning Applications*, Proceedings of the China Technical Application Association for Global Positioning System 2008*, Beijing, China, Dec 18-20.